

ACTIVE CONTROLLER IN ENERGY STORAGE  
SYSTEM FOR PEAK DEMAND REDUCTION WITH  
LIMITED CAPACITY

HAU LEE CHEUN

MASTER OF ENGINEERING SCIENCE

LEE KONG CHIAN  
FACULTY OF ENGINEERING AND SCIENCE  
UNIVERSITI TUNKU ABDUL RAHMAN  
APRIL 2017

**ACTIVE CONTROLLER IN ENERGY STORAGE SYSTEM FOR  
PEAK DEMAND REDUCTION WITH LIMITED CAPACITY**

By

**HAU LEE CHEUN**

A dissertation submitted to  
the Department of Electrical and Electronic Engineering,  
Lee Kong Chian Faculty of Engineering and Science,  
Universiti Tunku Abdul Rahman,  
in partial fulfillment of the requirements for the degree of  
Master of Engineering Science  
April 2017



## **ABSTRACT**

### **ACTIVE CONTROLLER IN ENERGY STORAGE SYSTEM FOR PEAK DEMAND REDUCTION WITH LIMITED CAPACITY**

**Hau Lee Cheun**

Commercial and industrial customers are subjected to the monthly maximum demand charges in addition to the electricity usage in Malaysia. The monthly maximum demand charges can be as high as 30% of the total electricity bills. To reduce the electricity bills, battery-based energy storage system (BESS) can be used to reduce the monthly maximum demand charges by reducing the overall peak demands in a month. A number of control strategies have been developed for the BESS to reduce the daily peak demands. However, the majority of the control strategies are only evaluated in simulation. It is, therefore, an unknown whether the demonstrated efficacy in the semi-idealized form is transferable to an operational scheme or not. Apart from that, the majority of the control strategies are also not tested when the capacity of the energy storage is limited, which is often the case in the actual setup due to financial constraint. Not only that, the control strategies have also been used so far to observe the reductions of the daily peak demands instead of the monthly maximum demand. The minimization of the daily peak demands does not necessarily correspond to a reduction in the electricity bills because the monthly maximum demand charges over the period of a month are not

investigated. If the energy storage is not able to sustain its energy throughout its operations, the monthly maximum demands may not be reduced as it may fail to reduce some of the daily peak demand of the month. Hence, a new control strategy is proposed for the BESS such that it can sustain throughout in order to cut down every daily peak demands. The proposed controller with a short-term load forecasting method, a persistent threshold adjuster and a real-time refinement of the BESS supplies is also extended to consider the situation where the capacity of the energy storage is limited to 39.23% of the required capacity. Tested and evaluated experimentally on a BESS setup, the proposed controller have demonstrated efficacy over the fundamental controller as well as the other controllers that are used in the literature of the similar topic of research interest. The proposed controller is also able to reduce the maximum demand charge by 9.07% as compared to 0.79% by the fundamental controller. Not only that, the proposed controller also reflected feasible financial yield as compared to the fundamental controller. Other than that, this research is also one of the first kind in Malaysia. The technical innovations thus are not only the peak reductions outcome which yields from the proposed controller but also the successful setup and integration of the BESS onto an actual electrical network at a commercial building in Malaysia.

## ACKNOWLEDGMENTS

First and foremost, praises and thanks to God, for providing me this opportunity and granting me the capability to proceed and complete the research successfully. I would also like to thank my beloved mom, Ng Poh Goik for her encouragement and support throughout the research.

Next, I would like to express my deep and sincere gratitude to my research supervisor, Prof. Ir. Dr. Lim Yun Seng for his invaluable advice, guidance and enormous patience throughout the development of the research. He teaches me not only academic skills but also help me to develop self-discipline, responsibility, and honesty. His ongoing support, ideas and professional assistance were central to the success in the research.

Besides that, I would like to extend my gratitude to my research co-supervisor, Assoc. Prof. Dr. Stella Morris for her guidance, encouragement and constructive suggestions. I would also like to thank Assistant Prof. Dr. Chua Kein Huat who have worked together in setting up the measuring meters, as well as given me valuable insights throughout the research.

Last but not least, I would like to thank the Collaborative Research in Engineering, Science and Technology Centre (CREST) and ERS Energy Sdn Bhd for their financial and technical supports. Without whom I would not have the chance to be involved in such meaningful project.

## APPROVAL SHEET

This dissertation entitled “**ACTIVE CONTROLLER IN ENERGY STORAGE SYSTEM FOR PEAK DEMAND REDUCTION WITH LIMITED CAPACITY**” was prepared by HAU LEE CHEUN and submitted as partial fulfillment of the requirements for the degree of Master of Engineering Science at Universiti Tunku Abdul Rahman.

Approved by:

\_\_\_\_\_  
(Prof. Ir. Dr. Lim Yun Seng)

Date:.....

Supervisor

Department of Electrical and Electronic Engineering  
Lee Kong Chian Faculty of Engineering and Science  
Universiti Tunku Abdul Rahman

\_\_\_\_\_  
(Assoc. Prof. Dr. Stella Morris)

Date:.....

Co-supervisor

Department of Electrical and Electronic Engineering  
Lee Kong Chian Faculty of Engineering and Science  
Universiti Tunku Abdul Rahman

**LEE KONG CHIAN FACULTY OF ENGINEERING AND SCIENCE**  
**UNIVERSITI TUNKU ABDUL RAHMAN**

Date: \_\_\_\_\_

**SUBMISSION OF DISSERTATION**

It is hereby certified that **HAU LEE CHEUN** (ID No: **15UEM01262**) has completed this dissertation entitled “ACTIVE CONTROLLER IN ENERGY STORAGE SYSTEM FOR PEAK DEMAND REDUCTION WITH LIMITED CAPACITY” under the supervision of Prof. Ir. Dr. Lim Yun Seng (Supervisor) from the Department of Electrical and Electronic Engineering, Lee Kong Chian Faculty of Engineering and Science, and Assoc. Prof. Dr. Stella Morris (Co-Supervisor) from the Department of Electrical and Electronic Engineering, Lee Kong Chian Faculty of Engineering and Science.

I understand that University will upload softcopy of my dissertation in pdf format into UTAR Institutional Repository, which may be made accessible to UTAR community and public.

Yours truly,

\_\_\_\_\_  
(*HAU LEE CHEUN*)

## DECLARATION

I (HAU LEE CHEUN) hereby declare that the dissertation is based on my original work except for quotations and citations which have been duly acknowledged. I also declare that it has not been previously or concurrently submitted for any other degree at Universiti Tunku Abdul Rahman (UTAR) or other institutions.

Name \_\_\_\_\_

Date \_\_\_\_\_

## TABLE OF CONTENTS

	<b>Page</b>
<b>ABSTRACT</b>	<b>iv</b>
<b>ACKNOWLEDGEMENTS</b>	<b>vi</b>
<b>APPROVAL SHEET</b>	<b>vii</b>
<b>SUBMISSION SHEET</b>	<b>viii</b>
<b>DECLARATION</b>	<b>ix</b>
<b>LIST OF TABLES</b>	<b>xv</b>
<b>LIST OF FIGURES</b>	<b>xviii</b>
<b>LIST OF PUBLICATIONS</b>	<b>xxi</b>
<b>LIST OF APPENDICES</b>	<b>xxii</b>
<b>LIST OF ABBREVIATIONS/NOTATIONS</b>	<b>xxiii</b>
<b>CHAPTER</b>	
<b>1.0 INTRODUCTION</b>	<b>1</b>
1.1 Research Background	1
1.2 Research Objectives	7
1.3 Research Work Plan	7
1.4 Structure of Dissertation	9
<b>2.0 LITERATURE REVIEW</b>	<b>11</b>
2.1 Challenges of High Peak Demands	11
2.2 Current Methods of Peak Demand Reductions	14
2.3 Peak Demand Reduction with Energy Storage System	17
2.3.1 Energy Storage Technologies	17
2.3.1.1 Mechanical Energy Storage	18
2.3.1.2 Electrical Energy Storage	19
2.3.1.3 Electrochemical Energy Storage	19
2.3.2 Applications of Energy Storage System	20
2.3.3 Battery-based Energy Storage Technologies	23
2.3.3.1 Valve-Regulated Lead Acid (VRLA)	24
2.3.3.2 Lithium-ion (Li-ion)	25
2.3.3.3 Nickel Cadmium (NiCd)	25
2.3.3.4 Nickel Metal-Hydride (NiMH)	26
2.3.3.5 Sodium Sulfur (NaS)	26

	2.3.3.6	VRLA Battery-based Energy Storage System	27
2.4		Peak Demand Reductions with Battery-based Energy Storage System	28
	2.4.1	Sizing of Battery-based Energy Storage System	29
	2.4.2	Control Techniques for Battery-based Energy Storage in the Application of Peak Demand Reductions	31
2.5		Summary	36
<b>3.0</b>		<b>SYSTEM ARCHITECTURE OF THE BATTERY-BASED ENERGY STORAGE SYSTEM</b>	<b>37</b>
3.1		Hardware Components	37
	3.1.1	SI8.0H Bi-directional Power Converter	39
	3.1.2	Valve-Regulated Lead Acid Battery Bank	39
	3.1.3	Star3 Measurement Meter	40
	3.1.4	Control Unit	41
	3.1.5	The Set-up of the Battery-based Energy Storage System	42
3.2		Modbus	43
	3.2.1	Modbus RTU	44
		3.2.1.1 Slave Address (SA)	46
		3.2.1.2 Function Code (FC)	46
		3.2.1.3 Data Field	46
		3.2.1.4 Error Check	47
		3.2.1.5 Modbus Events	48
	3.2.2	Modbus TCP	50
		3.2.2.1 Transaction Identifier (TI)	51
		3.2.2.2 Protocol Identifier (PI)	52
		3.2.2.3 Length Field	52
		3.2.2.4 Unit Identifier (UI)	52
		3.2.2.5 Modbus Events	53
	3.2.3	Modbus Profile	54
	3.2.4	Modbus Functions and Registers	56
		3.2.4.1 Read Coils	56
		3.2.4.2 Read Holding Registers	58
		3.2.4.3 Write Single Coil	60
		3.2.4.4 Write Single Register	61
		3.2.4.5 Write Multiple Coils	61
		3.2.4.6 Write Multiple Registers	63
		3.2.4.7 Read/Write Multiple Registers	64
	3.2.5	Modbus Exception Response	66
3.3		Star3 Communication System	69

3.3.1	Star3 Modbus Function and Data	69
3.3.1.1	Read Input Register	69
3.3.1.2	Read Holding Register	71
3.3.1.3	Read Output Status	72
3.3.1.4	Preset Single Register	73
3.3.1.5	Force Single Coil	74
3.3.2	Star3 Communication System in LabVIEW	74
3.3.2.1	The Read Function VI	76
3.3.2.2	The Write Function VI	77
3.3.2.3	The Error Check VI	78
3.4	SI8.0H Communication System	81
3.4.1	SI8.0H SMA Data Type and Format	82
3.4.1.1	Data with format of 'Duration'	82
3.4.1.2	Data with format of 'DT'	83
3.4.1.3	Data with format of 'ENUM' or 'FUNCTION_SEC'	84
3.4.1.4	Data with format of 'FIX'	85
3.4.1.5	Data with format of 'FW' or 'HW'	85
3.4.1.6	Data with format of 'IP4' or 'UTF8'	86
3.4.1.7	Data with format of 'REV'	87
3.4.1.8	Data with format of 'RAW'	87
3.4.1.9	Data with format of 'TEMP'	88
3.4.1.10	Data with format of 'TM'	88
3.4.2	SI8.0H Communication System in LabVIEW	89
3.4.2.1	The Grid Guard Mode	90
3.4.2.2	The System Control	91
3.4.2.3	The Feed-in Limits	92
3.4.2.4	The 'Read' State	93
3.4.2.5	The 'Update' State	93
3.4.2.6	The 'Write' State	94
3.4.2.7	The 'Reinitialize' State	95
3.4.2.8	The Read Function VI	95
3.4.2.9	The Write Function VI	97
3.4.2.10	The Error Check VI	98
3.5	Summary	102
<b>4.0</b>	<b>ACTIVE CONTROL ALGORITHM IN ENERGY STORAGE FOR PEAK REDUCTION</b>	<b>103</b>
4.1	Challenges of Reducing the Peak Demand with Battery-based Energy Storage System	103
4.2	Active Control Strategy	105
4.2.1	Activities before the Actual Peak Reduction: Calculating the Threshold Using the Forecasted	108

	Load Profile	
4.2.2	Activities during the Day of Peak Reduction: Actively Adjusting the Threshold and Updating the Operating Schedule of the BESS using the Latest Load Demand	111
4.2.2.1	Charging mode during off-peak periods	114
4.2.2.2	Charging mode during on-peak periods	115
4.2.2.3	Constant discharging mode	117
4.2.2.4	Discharging mode over the rising demand	118
4.2.2.5	Discharging mode over the decreasing demand	119
4.2.2.6	Standby mode	120
4.2.3	Implementation of the Active Control Strategy in LabVIEW	122
4.3	Fundamental Control Strategy	124
4.4	Simulation Analysis: Ideal Peak Demand Reductions	127
4.5	Summary	128
<b>5.0</b>	<b>RESULTS AND DISCUSSIONS</b>	<b>129</b>
5.1	Experimental Site	129
5.2	Technical Evaluations	132
5.2.1	Results of the Peak Reductions using the Fundamental Controller	134
5.2.2	Results of the Peak Reductions using the Active Controller	139
5.2.3	Evaluation Indexes – $R$ and $A$	145
5.2.4	Comparison with the Other Literature Experimental Results	148
5.3	Economic Evaluations	151
5.3.1	Evaluation Indexes – $T_{payback}$ and $NPV$	152
5.3.2	Results of the Monthly Maximum Demand Reductions	156
5.4	Summary	160
<b>6.0</b>	<b>CONCLUSIONS AND FUTURE WORKS</b>	<b>162</b>
6.1	Conclusions	162
6.2	Future Works	165

<b>LIST OF PUBLICATIONS</b>	<b>167</b>
<b>LIST OF REFERENCES</b>	<b>187</b>
<b>APPENDICES</b>	<b>198</b>

## LIST OF TABLES

<b>Table</b>		<b>Page</b>
2.1	Tariff C2 for medium voltage peak and off-peak commercial customers	13
2.2	Energy storage technologies and the applications	22
2.3	Technical characteristic and costs of various energy storage technologies	23
2.4	Summary of some commonly used battery technology in the ESS	24
3.1	The Modbus messaging mode for RTU and TCP	44
3.2	Three possible types of event in a Modbus RTU transaction	47
3.3	The common type of Modbus profile	54
3.4	List of function code in Modbus with data access and the respective data type that is involved	55
3.5	Breakdown of the data field in the responded frame in Figure 3.12	58
3.6	Breakdown of the data field in the responded frame in Figure 3.14	59
3.7	Breakdown of the data field in the requested frame in Figure 3.17	63
3.8	Breakdown of the data field in the requested frame in Figure 3.18	64
3.9	Breakdown of the data field in the requested frame in Figure 3.19	65
3.10	Breakdown of the data field in the responded frame in Figure 3.19	65
3.11	A list of exception codes	68
3.12	An example of Star3's measurements	70
3.13	An example of Star3's counters	71
3.14	An example of Star3's digital output	72

3.15	List of Star3 communication systems' main VIs	79
3.16	List of Star3 communication systems' subVIs	80
3.17	An example of SI8.0H data with format of 'Duration'	83
3.18	An example of SI8.0H data with format of 'DT'	84
3.19	An example of SI8.0H data with format of 'ENUM'	84
3.20	An example of SI8.0H data with format of 'FIX'	85
3.21	An example of SI8.0H data with format of 'FW'	86
3.22	An example of SI8.0H data with format of 'IP4'	87
3.23	The SI8.0H grid guard mode Modbus register	91
3.24	The SI8.0H system control Modbus registers	92
3.25	The SI8.0H feed-in limits Modbus registers	92
3.26	The SI8.0H Modbus registers which are used in the 'Read' state	93
3.27	The SI8.0H Modbus registers which are used in the 'Update' state	94
3.28	The SI8.0H Modbus registers which are used in the 'Write' state	95
3.29	The SI8.0H Modbus registers which are used in the 'Reinitialize' state	95
3.30	List of SI8.0H communication systems' main VIs	99
3.31	List of SI8.0H communication systems' subVIs	101
4.1	Activation conditions for the charging mode during off-peak periods	115
4.2	Activation conditions for the charging mode during on-peak periods	116
4.3	Activation conditions for the constant discharging mode	117
4.4	Activation conditions for the discharging mode over the rising demand	119

4.5	Activation conditions for the discharging mode over the decreasing demand	120
4.6	List of VIs associated to the activities before the actual peak reduction	122
4.7	List of VIs associated to the activities during the day of peak reduction	123
5.1	The controller's input parameters	133
5.2	The experimental peak demand reductions from different literature	149
5.3	The electricity tariff rate from 2006 to 2034	154
5.4	The input parameters for the economical analysis	156
5.5	Results of the financial analysis if the maximum demand reduction per month is improved by 5%–step of the present active controller's performance	159
5.6	Results of the financial analysis if the total investment cost of the BESS is reduced by 5%–step of the current BESS price	160

## LIST OF FIGURES

<b>Figures</b>		<b>Page</b>
1.1	Power flow diagram when BESS supplies power to the load	4
2.1	(a) Load shifting, (b) Peak clipping, (c) Strategic load conservation, (d) Strategic load growth, (e) Valley filling and (f) Flexible load shape	15
2.2	Type of energy storage system technology	18
2.3	Highest peak demand reduction for scenario of BESS (a) Constrained by the power rating (kW) and (b) Limited by the energy storage capacity (kWh)	30
3.1	Single-line diagram of the experimental BESS set-up	38
3.2	Grid-tied set-up configuration of the BESS	40
3.3	3PH-N set-up configuration of the measurement meter	41
3.4	The battery-based energy storage system and the control unit	42
3.5	The measurement meters installed at G and M floor	43
3.6	Modbus RTU application data unit	45
3.7	An example of a normal Modbus RTU transaction	48
3.8	An example of Modbus RTU transaction without a response	49
3.9	An example of Modbus RTU transaction with an exception response	49
3.10	Modbus TCP application data unit	51
3.11	An example of a normal Modbus TCP transaction	53
3.12	An example of 'Read Coils' Modbus Function	57
3.13	An example of 'Read Holding Registers' Modbus Function	59
3.14	An example of 'Write Single Coil' Modbus Function	60
3.15	An example of 'Write Single Register' Modbus Function	61
3.16	An example of 'Write Multiple Coils' Modbus Function	62

3.17	An example of ‘Write Multiple Registers’ Modbus Function	63
3.18	An example of ‘Read/Write Multiple Registers’ Modbus Function	65
3.19	An example of Modbus exception response	67
3.20	Flow diagram of the Star3 communication system	75
3.21	Flow diagram of the Star3 read function	77
3.22	Flow diagram of the Star3 write function	78
3.23	Flow diagram of the SI8.0H communication system	90
3.24	Flow diagram of the SI8.0H read function	96
3.25	Flow diagram of the SI8.0H write function	97
4.1	(a) Forecasted load profile with the scheduled threshold, (b) Unsatisfactory peak reduction in the actual load profile with a broad peak and (c) Peak reduction achieved with the active adjustment of the threshold	105
4.2	The flow chart of the active control strategy	107
4.3	The threshold level for scenario of (a) Narrow peak load demand and (b) Wide peak load demand	110
4.4	The graphical representation of the six operating modes of the BESS	114
4.5	The flowchart of the fundamental control strategy	125
5.1	The peak demands on the test site over a period of 156 weekdays	130
5.2	A sample historical load profiles on the experimental site from Monday to Sunday	131
5.3	The estimated energy required for peak demand reductions from 1kW to 21kW	132
5.4	The experimental result of a sample day without peak reduction by the fundamental controller due to the peak is lower than the threshold	135
5.5	(a) The experimental result and (b) the simulated result of a sample day with the unsuccessful peak reduction by the fundamental controller	137

5.6	(a) The experimental result and (b) the simulated result of a sample day with the peak reduction achieved by the fundamental controller	139
5.7	(a) The experimental result and (b) the simulated result of a sample day with the peak reduction achieved by the active controller	141
5.8	(a) The experimental result and (b) the simulated result of a sample day with the peak reduction achieved by the active controller without adjusting the threshold	143
5.9	Three consecutive days of peak reduction carried out by (a) the active controller and (b) the fundamental controller	144
5.10	The box plot of $R$ achieved by the fundamental controller and the active controller from experiment and in simulation	147
5.11	The box plot of $A$ achieved by the fundamental controller and the active controller	148
5.12	The breakdown of the net presence value achieved by the fundamental controller and the active controller	158

## LIST OF PUBLICATIONS

<b>Publication</b>	<b>Page</b>
A A Real-Time Active Peak Demand Reduction for Battery Energy Storage with Limited Capacity	168
B Active Control Strategy of Energy Storage System for Reducing Maximum Demand Charges under Limited Storage Capacity	175

## LIST OF APPENDICES

<b>Appendix</b>		<b>Page</b>
A	List of (some) electricity tariffs around the world	198
B	Summary of the size of BESS and its controller from various literatures	201
C	The experimental and simulation results of a month of peak reductions with the fundamental control strategy	203
D	The experimental and simulation results of a month of peak reductions with the active control strategy	205

## LIST OF ABBREVIATIONS / NOTATIONS

ADU	Modbus Application data unit
ASCII	American standard code for information interchange
$A$ or $K_{ps}$	Peak reduction factor, %
BESS	Battery based energy storage system
BatFuse	Battery fuse
BMS	Battery management system
BCD	Binary coded decimal
CAES	Compressed air energy storage
CB	Circuit breaker
CRC	Cyclical redundancy check
CT	Current transformer
CTratio	Current transformer ratio
$Cost$	Cost of BESS, RM
$C_{Replacement}$	Replacement cost of BESS, RM
$C_{O\&M}$	Operating and maintenance cost of BESS, RM
$C_{PCU}$	Cost of BESS's power conversion unit, RM
$C_{ESC}$	Cost of BESS's energy storage capacity, RM
DSM	Demand side management
DR	Demand response
DG	Distributed generation
$DoD$	Battery depth-of-discharge, %

ESS	Energy storage system
EV	Electric vehicles
$E_{\text{BESS}}^{\text{max}}$ or $E_{\text{BESS}}$	Battery storage capacity of the BESS, kWh
$E_{\text{BESS}}^{\text{Act}}$	Real-time energy capacity remaining in the BESS, kWh
$E_{\text{BESS}}^{\text{Sim}}$	Simulated energy capacity remaining in the BESS, kWh
FES	Flywheel energy storage
FC	Modbus function code
G	Ground floor
GGC	Grid guard code
GUI	Graphical user interfaces
IP	Internet protocol
LFC	Load frequency control
Li-ion	Lithium ion battery
LG	Lower ground floor
LV	Low-voltage network
LAN	Local area network
LSB	Least significant bit
MD	Maximum demand
M	Mezzanine floor
MSB	Most significant bit
MBAP	Modbus application protocol

MDU	Modbus data unit
MDR	Maximum Demand Reduction
<i>MAPE</i>	Mean absolute percentage error, %
NiCd	Nickel cadmium
NiMH	Nickel-metal hydride
NaS	Sodium sulphur
<i>NPV</i>	Net present value, RM
PHES	Pumped hydro energy storage
PV	Photovoltaic systems
PDU	Modbus Protocol data unit
PI	Protocol identifier in Modbus TCP
$P_{Grid}^{Act}$ or $P_{Grid}$	Real-time supply from the utility, kW
$P_{Load}^{For}$	Forecasted load profile, kW
$P_{Load}^{For(max)}$	Forecasted peak demand, kW
$P_{Load}^{For(*)}$	Forecasted load profile with the least discrepancy, kW
$P_{Load}^{Act}$ or $P_{Load}$	Real-time load profile, kW
$P_{Load}^{His}$	Historical load profile, kW
$P_{Load}^{His(max)}$	Maximum historical load profile, kW
$P_{Load}^{His(min)}$	Minimum historical load profile, kW
$P_{BESS}^{Sch}$	Scheduled BESS supply, kW
$P_{BESS}^{Act}$ or $P_{BESS}$	Real-time BESS supply, kW
$P_{Th}$ or $P_{Th}$	Peak reduction threshold, kW

$P_{Th}^{max}$	Maximum peak reduction threshold, kW
$P_{Th}^{opt}$	Optimum peak reduction threshold, kW
$P_{Load}^{Act(max)}$	Peak demand for the metered load, kW
$P_{Grid}^{Act(max)}$	Net load after peak reduction, kW
$P_{Reduction}^{Act}$	Post peak demand reductions, kW
$P_{Reduction}^{Sim}$	Simulated peak demand reductions, kW
$P_{Th}^{Act}$	Real-time peak reduction threshold, kW
$P_{Th}^{Sim}$	Simulated peak reduction threshold, kW
$P_{Grid}^{Sim}$	Simulated supply from the utility, kW
$P_{BESS}^{Sim}$	Simulated BESS supply, kW
$P_{Reduc.}^{Act(max)}$	Highest real-time peak reduction, kW
$P_{Reduc.}^{Act(Eff.)}$	Effective real-time peak reduction, kW
$P_{BESS}^{max}$ or $P_{BESS}$	Power rating of the BESS, kW
$P_{Reduction}$	Peak reduction achieved after the remaining energy in the BESS has been delivered, kW
$P_{BESS}^{Act(min+)}$	Specified minimum positive output supply for the BESS, kW
RE	Renewable energies
RTP	real-time pricing structure
RTU	Remote terminal unit
R	Demand reduction, %
SMES	Superconductive magnetic energy storage

SA	Slave address in Modbus RTU
<i>SOC</i>	Battery state-of-charge, %
$S_{MD}$	Saving from the reduction of the monthly maximum demand charge, RM
$S_{TR}$	Saving in the electricity bill from utilizing the on and off-peak tariff difference, RM
<i>Saving</i>	Savings from peak reductions, RM
$SoC^{max}$	Maximum BESS's battery state-of-charge, %
$SoC^{min}$	Minimum BESS's battery state-of-charge, %
TOU	Time-of-use pricing structure
TNB	Tenaga Nasional Berhad
TT	Terre – Terre grounding system
TCP	Transmission control protocol
TI	Transaction identifier in Modbus TCP
<i>T</i>	Temporary variable to store up the computation results
$T_{payback}$	Payback period, year
UPS	Uninterruptable power supply
UI	Unit identifier in Modbus TCP
$U_{MD}$	Unit price for the monthly maximum demand charge, RM/kW
$U_{off}$	Unit price for energy consumption during the off-peak period, RM/kWh
$U_{on}$	Unit price for energy consumption during the on-peak period, RM/kWh

VRLA	Valve-regulated lead-acid battery
VI	Virtual instrument
VTratio	Voltage transformer ratio
WAN	Wide area network
$Y_{\text{service}}$	Projected service life of the BESS, year
$d$	Date with subsets of $\{0, 1, 2, \dots, \text{End of month}\}$ , day
$f_{Th}$	Frequency of occurrence of the optimum peak reduction threshold
$g$	Increment rate of tariff, %
$i$	Year with subsets of $\{1, 2, 3, \dots, Y_{\text{service}}\}$ , year
$k$	Computation regions of the peak reduction threshold, kW
$n$	Number of historical load profiles
$r$	Discount rate, %
$t$	Time, minute
$t_s$ or $t_e$	The peak periods demand, minute
$t_{Q1}$ or $t_{Q2}$	Charging periods for the BESS, minute
$t_{\text{peak}}$	Peak period, minute
$\alpha$	Discrepancy between the actual and the forecasted load demands
$\mu$	Mean of the historical load profile envelopes
$\Delta P_{Th}$	Specified permitted fluctuation margin, kW

# CHAPTER 1

## INTRODUCTION

### 1.1. Research Background

In tandem with the economic growth in Malaysia, the electricity generation in the Peninsular Malaysia has increased from 112,841GWh to 116,813GWh in 2015 and it is expected to increase by 3.4% per annum. The peak demand has also reached a new record of 17,461MW in 2015 and it is expected to rise by 3.1% per annum (Energy Commission, 2016). Sufficient capacity of power generation is therefore required to provide a balance between the supply and demand at all times in order to maintain the stability of the electrical network (Benetti et al., 2016).

The capacity of the power generation is made up of the base-load, the intermediate-load and the peaking power plants. The base-load and the intermediate-load power plants operate throughout the day to supply power to the demand at all time, whereas the peaking power plants are only operated during the peak period to meet the increase in the demand. The peaking power plants make up about 20% of the total generation capacity and on average only 55% of the installed capacity are used (Lawder et al., 2014). The amount of electricity delivered to the customers by the peaking power plant is therefore

less than the base-load and the intermediate-load power plants. The electricity of the peaking power plants hence has to be sold at a relatively high price in order to recover the investment costs as well as the expenses within the lifespan of the power plants. As a result, several forms of billing mechanisms are used to charge the customers for the use of the peaking power plants. In Malaysia, the maximum demand charging structure is used to account for the use of the peaking power plants, whereby the customers are not only responsible for the amount of electricity (kWh) consumed by them but also the maximum demand (kW) contributed by them within a month. The monthly maximum demand charges can be as high as 30% of the total electricity bills (Chua et al., 2015).

The monthly maximum demand charges can be reduced through the minimisation of all the daily peak demands of the month. There are a number of methods being used to reduce the daily peak demands. These methods can be classified into the demand side management (DSM), the demand response (DR), the distributed generation (DG) and the energy storage system (ESS). Recent advancement in the power electronics and energy storage technology however has made the ESS a viable and potential solution for reducing the peak demands (Han et al., 2015; Whittingham, 2012; Yang et al., 2014). Unlike the DSM and DR, ESS can achieve peak demand reductions without interfering the consumers' activities. In contrast to DG, ESS is also able to meet the increase in demand and reduce the peak demands with the ability of adjustable supply.

Various ESS technologies have been used to store the electrical energy in the form of kinetic, potential, electromagnetic or electrochemical energy. Battery-based energy storage system (BESS), a type of energy storage based on electrochemical reactions, have seen a great growth and interest due to its versatility, wide range of power system applications, low initial investment as well as acceptable cycle efficiency. More grid applications have become suitable for BESS as battery costs have reduced while the performance and its' service life continued to improve. BESS is also scalable and modular for higher power rating and capacity. The setup is also simpler and shorter in developing time compared to the other ESS technologies (Han et al., 2015; Lawder et al., 2014). BESS is therefore selected for this research.

BESS reduces the daily peak demands for the customers if it is placed after the utility's meter to supply the power to the load over the peak hours. The power demand from the utility grid is reduced during the peak hours as shown in Figure 1.1. The BESS is then charged during the off-peak hours to replenish the energy. Numerous research efforts have been conducted to derive the optimum sizes of BESS designed based on the largest daily peak demands from the historical load data (Chauhan and Saini, 2014; ElNozahy et al., 2015; Lu et al., 2014; Oudalov et al., 2007). The storage capacity is however often limited due to the financial constraints. The peak also often happens at the wrong time with the unexpected width. The energy of the BESS thus can run out quickly during the process of peak reductions. As a result, the ESS may fail to reduce the daily peak demands and so the monthly maximum

demand. To reduce the peak demands, a control technique is therefore required to be incorporated with the BESS.

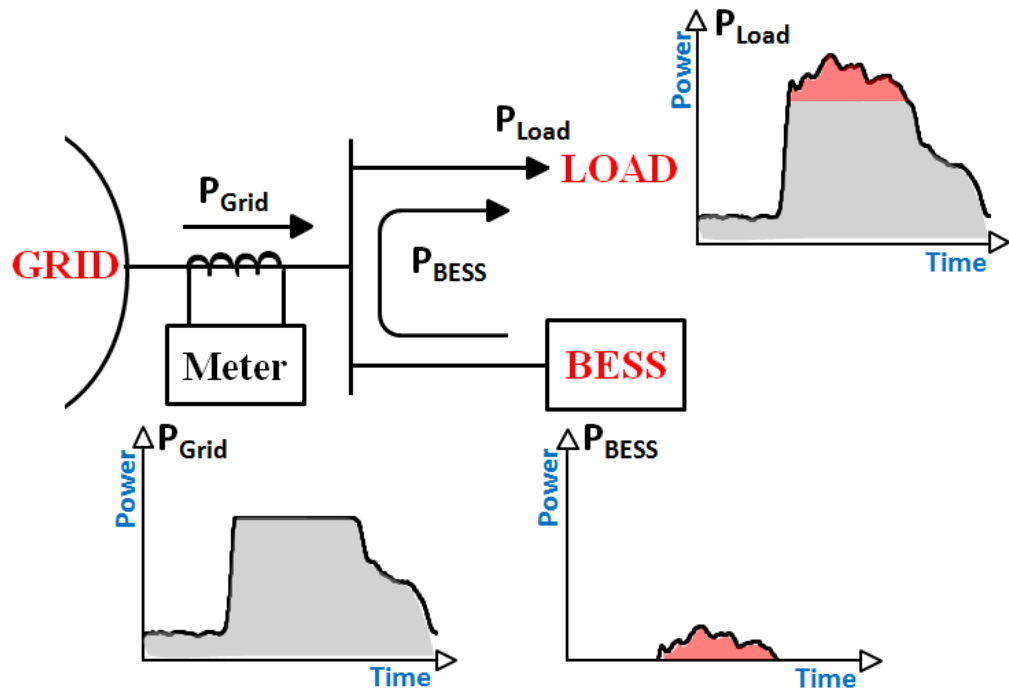


**Figure 1.1: Power flow diagram when BESS supplies power to the load**

At present, there are two fundamental control strategies for the BESS. The first is known as the fixed scheduled pattern whereby historical load data is used to determine the times and dates for the BESS to deliver power as well as to charge the batteries (Joshi and Pindoriya, 2015; Mattern et al., 2008; Purvins et al., 2013). The second strategy is a load following approach whereby a threshold is determined based on the historical load data. The BESS deliver power when the actual load demand exceeds the threshold and charges during the off-peak periods (Leadbetter and Swan, 2012; Levron and Shmilovitz, 2012; Rowe et al., 2013).

The first control strategy has the advantage of performing the peak demand reductions without any monitoring system. However, the daily peak demand reduction is unreliable and often not successful. This is because it does not optimize the reductions and the load demand is reduced uniformly. The real-time load profile is often not the same as the predicted profile, the peak therefore does not coincide with the power delivery from BESS and load spikes persist. The second control strategy on the other hand has the ability to control the power supply of BESS based on the real-time load demand. This method however is inconsistent when the battery does not have sufficient energy to cut down the whole peak. Moreover, once the threshold is determined, it will not be adjusted anymore. As a result, BESS can often fail to reduce the peak.

Both the fundamental control strategies are thus simple and easy to implement, however due to the inherently stochastic nature of the load demand, the discrepancy between the real-time and the forecasted load demand is unavoidable. Both the control strategies do not use forecasts and hence lack the dynamics foresight and consequently lacks the ability to reduce the peak demand optimally. Therefore, a need exists for a control strategy that can forecast the demand and reliably optimize the demand reduction. A number of control strategies, coupled with the forecasting and optimization techniques have thus been proposed (Bao et al., 2012; Bennett et al., 2015; Reihani et al., 2016a; Rowe et al., 2014a). The analyses are however confined to simulation evaluation only. An accurate estimate of the BESS's response in real-time is not comprehensively considered. The performance of the algorithm is also

often iterated to converge to have an outcome that is desirable. It is therefore an unknown of whether the demonstrated efficacy of the proposed strategies, in its semi-idealized form can be transferred to an operational scheme, and, further, whether such efficacy can be maintained.

In the recent year, only a few literature have shown their experimental works (Chua, 2016; Koller et al., 2015; Reihani et al., 2016b) but the evaluation is only based on a handful of experimental results. The majority of the control strategies are also not tested when the capacity of the BESS is limited, which is often the case in the actual BESS setup due to the financial constraint. The reduction of the maximum demand charge is also not assessed in all the literature. The minimization of the daily peak demands recorded in the literature does not necessarily mean an economic benefit because the charges of maximum demand over the period of a month are not investigated. It is, therefore, unknown whether the demonstrated experimental results can be maintained or has economical value.

## **1.2. Research Objectives**

The objectives of this research thus are as listed:

1. To design and set up a BESS for peak demand reduction at a commercial building.
2. To develop a control strategy for the BESS to cut down the daily peak demands as well as reduce the monthly maximum demand charges when the energy capacity of the BESS is limited.
3. To thoroughly investigate the performance of the control strategy in reducing the peak demands over a month.
4. To also investigate the economical value of the control strategy in reducing the monthly maximum demand charges.

## **1.3. Research Work Plan**

The research work plan is divided into four stages. The first stage is to conduct a thorough background study and literature review on the research topic. The challenges associated with the high peak demands will be investigated. The various existing methods for peak demand reductions as well as the strengths and potentials of the ESS in peak demand reductions will be explored. The various types of energy storage technologies will be studied as well. The existing state-of-arts peak demand reduction methodology using the BESS will also be reviewed.

Next, the second stage is to design and set up the BESS for peak demand reduction. The commercial building and the place of installation will be identified. A number of bi-directional inverters and batteries will be integrated to form the BESS and installed at the identified site. Multiple measuring meters will also be set up on the site to measure the demands as well as the inflow of supplies from the utility to the consumer. The communication system between the bi-directional inverters and the measuring meters will also be established with a control unit. The control features of the BESS will be studied as well and a user interface with the BESS will be developed.

Moving on, the third stage is to formulate and develop the peak reduction control strategy for the BESS. Various peak reductions control methodology will be studied and reviewed. The control strategy will be formulated to address the research challenges in the semi-idealized simulation environment. The control strategy will also be developed into the processing system of the BESS and experimentation will be carried out to collect data from the BESS over a period of time to study the performance of the control strategy.

Finally, the last stage is to investigate the performance and benefits of the proposed peak reduction controller. The technical and financial aspects of the control strategy will be evaluated. The implications of the proposed control strategy will be drawn. The limitations as well as the opportunities for future improvement of the proposed control strategy will also be elaborated.

## **1.4. Structure of Dissertation**

The structure of this dissertation lays out as follows: Firstly, the literature reviews are summarized in Chapter 2. In this chapter, the challenges associated with the high peak demands are first being investigated to understand the significance and importance of the peak demand reductions. Next, the various types of peak demand reductions methods are explored to point up the strength and potential of the ESS in the application of peak demand reductions. Followed by, the different types of energy storage technologies are discussed to provide evidence of support for selecting the BESS in this research. Besides that, the current methodologies of peak demand reductions using BESS are also reviewed to understand the limitations and weaknesses in the existing literature on the similar topic.

Next, the system architectures of the BESS are discussed in Chapter 3. In this chapter, the hardware components of the BESS are first being elaborated to provide an overview of the modules as well as the set up of the BESS in this research. The Modbus messaging protocol is then provided to bring about a preliminary understanding of the communication systems of the BESS before the communication frameworks and the implementation of the communication system are introduced.

The proposed peak reduction control strategy is then presented in Chapter 4. In this chapter, the challenges associated with the BESS in reducing the peak demands are first being introduced. The framework of the active

control algorithm is then discussed to bring about an understanding of the formulation process and the implementation of the active controller. Besides that, the fundamental set-point control strategy as well as the semi-idealized simulation environment is also presented to provide an overview of its frameworks.

Moving on, the experimental results are reviewed in Chapter 5. The load profiles are first being studied to analyze the load demands, the load characteristics as well as the energy consumptions on the experimental site. Next, the experimental results of the peak demand reductions are then technically evaluated to examine the strength and ability of the proposed active control strategy. The experimental results of the active controller are then compared to the fundamental control strategy and benchmarked with the simulation results. The experimental results of the active control strategy are also compared to the other literature experimental results. Besides that, the active controller is also financially evaluated to review the potential savings of the controller. A financial analysis is also included to provide a financial foresight of what would have been achieved if the savings by the active controller is improved or the price of the BESS is reduced.

Finally, the conclusions are drawn in Chapter 6. The key findings of the research and the implications of the active control strategy are summarized. The contributions of the research as well as the opportunities for future improvement of the active control strategy are also elaborated.

## CHAPTER 2

### LITERATURE REVIEW

The challenges associated with the high peak demands are presented in this chapter, followed by the various existing methods for peak demand reductions as well as the strengths and potentials of the energy storage systems in peak demand reductions. Next, the different types of energy storage technologies are discussed before the current methodologies of peak reduction using the battery-based energy storage system are reviewed.

#### **2.1. Challenges of High Peak Demands**

In order to maintain the stability of the electrical network, sufficient capacity of power generation is a necessity to ensure the supply and demand are balanced at all times (Benetti et al., 2016). The capacity of the generation is made up of the base-load, the intermediate-load and the peaking power plants. The base-load power plants serve as the base supply, delivering power near to its plant's capacities, providing a consistent supply for the load demand throughout the day. The intermediate-load and the peaking power plants on the other hand, provide power to meet the rest of the load demands that is not covered by the base-load power plants. The intermediate-load and the peaking power plants provide their power output with the profile matching closely to the load demand profile of the day (Chua et al., 2015). However, the peaking

power plants are only switched on for few hours per day to meet the sudden increase in the load demand.

The peaking power plants make up about 20% of the total generation capacity and on average only 55% of the installed capacity are used (Lawder et al., 2014). The amount of electricity delivered to the customers by the peaking power plant is therefore less than that of the base-load and the intermediate-load power plants. To recover the investment cost as well as the operational cost within the lifespan of the plants, the electricity of the peaking power plants hence has to be sold at a relatively high price. As a result, several forms of billing mechanisms are used in different countries to charge the customers for the use of the peak demand power plants. Some utility companies use the maximum demand charging mechanism whereby the customers are not only responsible for the amount of electricity (kWh) consumed by them but also the maximum demand (kW) created by the customers within a particular month. Other utilities use the time-of-use (TOU) pricing structure whereby the electricity prices become high during peak hours and low during off-peak periods. A real-time pricing (RTP) structure is another form of mechanisms whereby the electricity prices will vary depending on the demand for electricity. The electricity tariffs established by different countries around the world are listed in Appendix A.

In Malaysia, the maximum demand charging structure is used to account for the use of the peak power plants. The monthly maximum demand (MD) is the highest load demand of a particular month recorded by the

customers' power meters with the resolution of a 30-minute interval. Any customers who use the supply on the voltage level of 6.6kV and above are subjected to the maximum demand charges. The amount charged to the customers are calculated on the recorded peak demand in kilowatt (kW) multiplied by the respective maximum demand rate (RM/kW). Table 2.1 shows the electricity rates established by the utility company, Tenaga Nasional Berhad (TNB), for medium voltage peak and off-peak commercial customers.

**Table 2.1: Tariff C2 for medium voltage peak and off-peak commercial customers**

<b>Year</b>	<b>Maximum demand charge (RM/kW)</b>	<b>Energy charge during peak period (RM/kWh)<sup>d</sup></b>	<b>Energy charge during off-peak period (RM/kWh)<sup>d</sup></b>
2006 – 2008 <sup>a</sup>	29.0	0.234	0.144
2008 – 2009 <sup>b</sup>	36.6	0.296	0.182
2009 – 2011 <sup>b</sup>	35.6	0.288	0.177
2011 – 2014 <sup>c</sup>	38.6	0.312	0.192
2014 – 2016 <sup>c</sup>	45.1	0.365	0.224

a. Retrieved from [https://www.tnb.com.my/assets/files/Tariff\\_booklet.pdf](https://www.tnb.com.my/assets/files/Tariff_booklet.pdf)

b. Retrieved from [https://www.tnb.com.my/assets/files/Tariff\\_Rate\\_Final\\_1.March.2009.pdf](https://www.tnb.com.my/assets/files/Tariff_Rate_Final_1.March.2009.pdf)

c. Retrieved from [https://www.tnb.com.my/assets/files/Tariff\\_Rate\\_Final\\_01.Jan.2014.pdf](https://www.tnb.com.my/assets/files/Tariff_Rate_Final_01.Jan.2014.pdf)

d. Peak periods are between 8am to 10pm and off-peak periods are from 10pm to 8am.

Over the years, the electricity rates have increased by approximately 1.5 times and are expected to increase as the year goes (Chua et al., 2015). The maximum demand charge is also about tenfold the TOU charge during the peak period. According to Chua et al. (2015), the monthly maximum demand

charges can be as high as 30% of the total electricity bills. Hence, commercial and industrial customers have the urge to reduce their monthly maximum demand charges for their electricity bills.

## **2.2. Current Methods of Peak Demand Reductions**

The monthly maximum demand charges can be reduced through the minimisation of all the daily peak demands of the month. There are a number of methods being used to reduce the daily peak demands. These methods can be classified into the demand side management (DSM), demand response (DR), distributed generation (DG) and energy storage system (ESS).

DSM is a long-term program aimed to encourage the customers to be energy efficient. DSM generally focuses on curtailing or shifting the load demand away from the high electricity price during peak periods. Programs ranging from investment on energy saving devices (Luo et al., 2010) up to the installation of sophisticated dynamic load management system to schedule the usage of loads (Palensky and Dietrich, 2011) are some of the DSM methods. The latter method alters the patterns of the customers' electricity consumption to achieve peak demands reductions. As shown in Figure 2.1, the load shapes can be altered by the means of (i) load shifting; (ii) peak clipping; (iii) strategic conservation; (iv) strategic load growth; (v) valley filling; and (vi) flexible load shape (Logenthiran et al., 2012). Peak clipping and valley filling mitigate the peak demand by reducing the differences between the peak and valley levels, whereas load shifting makes use of the time independence loads,

and shifts the loads from the peak periods to the off-peak periods. Strategic conservation and strategic load growth then aim at achieving the load shape optimization through demand reduction at the customer premises. And the flexible load shape allows the utilities to controls the loads during critical periods.

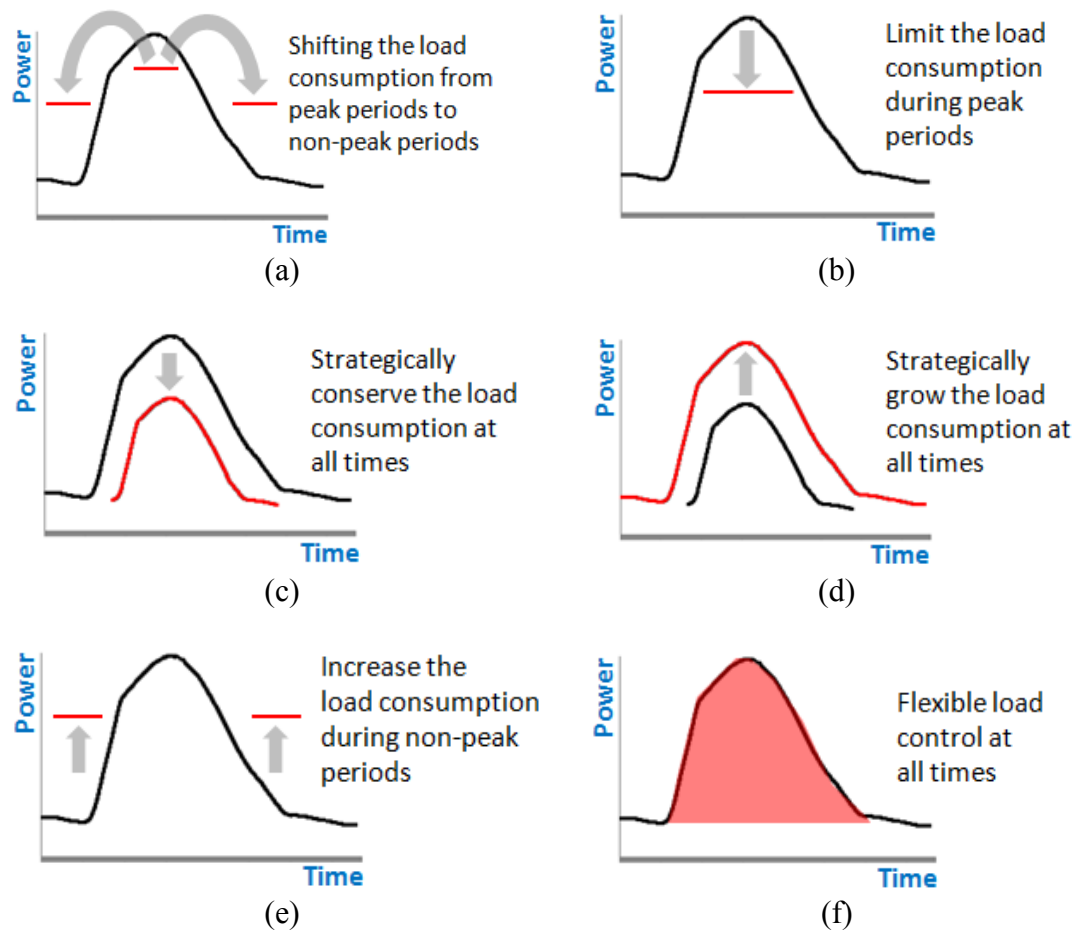


**Figure 2.1: (a) Load shifting, (b) Peak clipping, (c) Strategic load conservation, (d) Strategic load growth, (e) Valley filling and (f) Flexible load shape**

DR on the other hand is a short-term program, designed to encourage customers to make short-term reduction or deferral of load consumptions in response to the instructions sent by the grid operator or the online electricity

tariffs, which is dynamically changed over time by the energy provider (He and Zhang, 2015; Salies, 2013). DR includes the emergency-based or the economic-based programs. The emergency-based program, which responds to the instructions from the grid operator, reduces the load demand momentarily in response to the emergency power grid condition initiated by a request from the energy provider. The energy provider gets access to the customer loads, manages the loads to the required level and in exchange, the customers get rewarded with incentives.

On the other hand, the economic-based program reduces the hourly consumption voluntarily by the customers in response to the dynamic price of electricity, which is varied with time and location (Khodaei et al., 2011). Specific programs such as (i) time-of-use (TOU) pricing structure, wherein the price of electricity varies with the load demand, (ii) critical peak pricing based on a less predetermined variant of TOU, and (iii) real-time pricing (RTP), where a wholesale market prices are forwarded directly to the customers (Benetti et al., 2016) are some of the economic-based DR initiatives. Both DSM and DR thus required the voluntary participation of the customers to cut down the daily peak demands. However, load curtailments are usually undesirable. Most of the customers may not be willing to participate because such program hinders the productivity and reduce the profits.

Apart from DSM and DR, DG such as diesel generators and renewable energy sources can also be used to reduce the daily peak demands (Hanna et al., 2014; Pandiaraj et al., 2002; R  ther et al., 2008). Recent advancement in

the power electronics and energy storage technology has made the energy storage system (ESS) a viable and potential solution for reducing the monthly maximum demand charges for the customers (Han et al., 2015; Yang et al., 2014). Unlike the DSM and DR, ESS can achieve peak demand reductions without interfering or limiting the consumers' activities. Compared to DG, ESS is also able to meet the increase in demand and reduce the peak demands with the ability of adjustable supply. Not only that, ESS capabilities in conjunction with the smart grid are also expected to see a leap forward over the next 25 years (Whittingham, 2012).

### **2.3. Peak Demand Reduction with Energy Storage System**

#### **2.3.1. Energy Storage Technologies**

In the application of peak demand reductions, ESS provides the power to the loads during on-peak periods and stores the power from the grid during off-peak hours in order to reserve the energy for the following power delivery. Numerous ESS technologies have been developed over the years to store up energy in the form of kinetic, potential, electromagnetic or electrochemical energy (Bhuiyan and Yazdani, 2012; Chauhan and Saini, 2014; Fathima and Palanisamy, 2015; Hussein et al., 2012; Oudalov et al., 2006). Figure 2.2 shows the energy storage technology in the classification of mechanical energy storage, electrical energy storage and electrochemical energy storage.

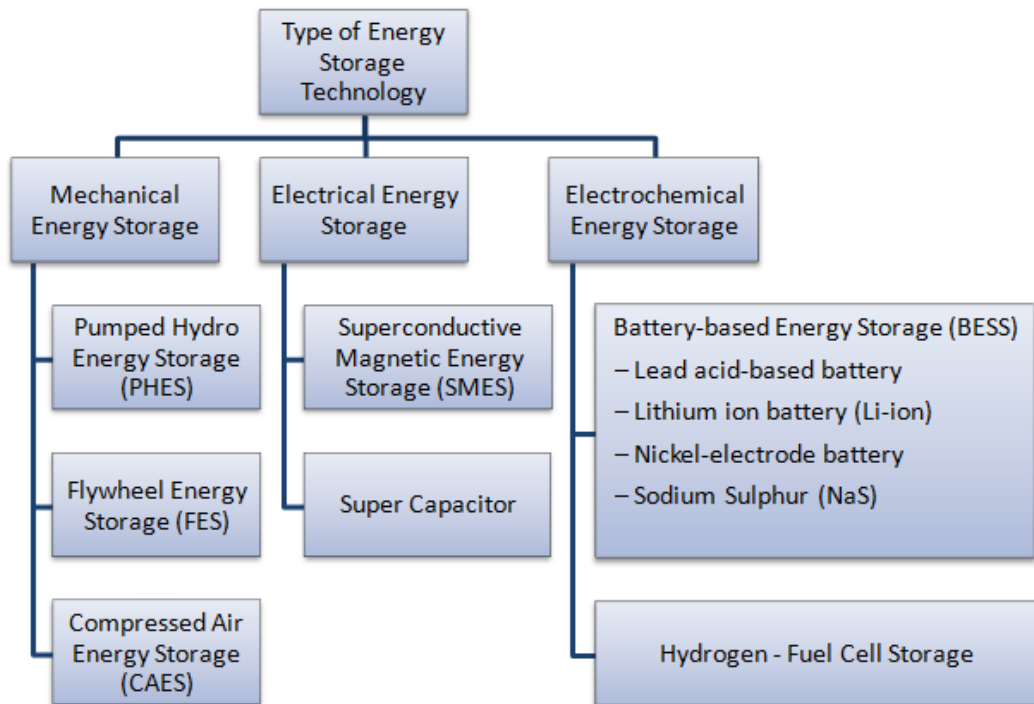


**Figure 2.2: Type of energy storage system technology**

### 2.3.1.1. Mechanical Energy Storage

Mechanical energy storage is such as pumped hydro energy storage (PHES), flywheel energy storage (FES) and compressed air energy storage (CAES). PHES stores the potential energy as water is pumped from a low-lying level reservoir to an elevated height. Electricity is generated when the water is released to drives a water turbine generator set. On the other hand, FES uses the mechanical inertia of a rotating flywheel coupled with an electrical machine to store energy. Energy is stored in the form of rotating kinetic energy when the electrical machine behaves as a motor and accelerate the flywheel to a high speed. When energy is needed, the motor then acts as a brake and extract energy from the rotating flywheel. Apart from that, CAES stores up energy by compressing the air in the form of pneumatic energy to a

specially designed cavern, and electricity is produced when the pressurized air is released to spin a gas turbine generator set.

### **2.3.1.2. Electrical Energy Storage**

Electrical energy storage such as superconductive magnetic energy storage (SMES) stores the energy from the electromagnetic field across a coil and advanced capacitor stores the energy from the electrostatic field across a parallel plate. SMES employs the electromagnetic in the coil to store the electromagnetic energy generated by a direct flow of current through a superconducting coil. Conversely, super capacitors stores electric energy using the potential phenomenon to store the electrostatic charges accumulated on a parallel plate contained in an insulating dielectric.

### **2.3.1.3. Electrochemical Energy Storage**

Electrochemical energy storage such as battery-based energy storage (BESS) and hydrogen-fuel cell storage stores energy as a form of charge in the electrochemical cells. BESS stores energy through the chemical reaction in the battery when DC voltage is supplied across the battery's terminals. Fuel cell stores the electrical energy in the form of hydrogen. When electrical power is required, the hydrogen is released to run through the fuel cell to produce electricity from the chemical reaction between hydrogen and the fuel cells. Fuel cells are however non-rechargeable, and cannot be used for the cyclic storage of energy.

### **2.3.2. Applications of Energy Storage System**

ESS covers a broad range of power system applications, ranging from energy management to power quality control. Apart from the peak demand reductions, ESS are also used in other grid applications such as unbalance load compensation (Lim et al., 2015), frequency regulation (Shankar et al., 2016), voltage support (Wong et al., 2014) and other ancillary services.

Lim et al. (2015) developed a fuzzy controller for ESS to correct the voltage unbalance and power factor caused by the intermittency of renewable energies (RE) and electrical vehicles (EV). The correction was performed by manipulating the real and reactive power between the ESS and the distributed network with RE and EV. Shankar et al. (2016) presented an opposition-based harmonic search technique incorporates with economic load dispatch mechanism for load frequency control with ESS in a deregulated power environment. Wong et al. (2014) formulated a fuzzy control algorithm for ESS to mitigate the voltage unbalance and fluctuations caused by the large number of clouds passing over the photovoltaic (PV) systems on the distribution network. The operation of ESS ensures the effective operation of the PV systems without wasting any excess production from the solar energy.

Gathered from the various literatures (Bhuiyan and Yazdani, 2012; Chauhan and Saini, 2014; Fathima and Palanisamy, 2015; Han et al., 2015; Hussein et al., 2012; Lawder et al., 2014; Oudalov et al., 2006), Table 2.2 lists the corresponding grid applications of the ESS technology and Table 2.3

summarizes the technical-cost characteristics of the ESS technology. Short discharge times and high power ratings make the SMES, the Super Capacitor and the FES suitable for applications of power quality regulation that require high power in short burst of energy. However, they are currently not available for large capacity and long duration of more than an hour. PHES and CAES on the other hand are suitable for the application of energy management that requires a longer duration of supply. However, they have high initial investment costs and the cycle-efficiency is lower than the SMES, Super Capacitor and FES.

BESS in particular have been seen in a great growth and interest due to its versatility, wide range of power system applications, low initial investment and acceptable cycle efficiency. More grid applications have become suitable for BESS as the costs of the battery have decreased while the performance and service life continued to increase. BESS is also scalable and modular for higher power rating and capacity. The setup time is also short and simpler compared to other ESS technologies (Lawder et al., 2014; Han et al., 2015).

**Table 2.2: Energy storage technologies and the applications**

<b>Application type</b>	<b>Example</b>	<b>Mechanical</b>	<b>Electrical</b>	<b>Electrochemical</b>
<b>(Response Time)</b>	<b>application</b>	<b>Energy Storage</b>	<b>Energy Storage</b>	<b>Energy Storage</b>
Power Quality (Seconds)	Voltage Support	FES	SMES,	BESS (Lead Acid-),
	Frequency Regulation		Super Capacitor	BESS (Li-ion)
	Flicker Compensation			
	Transient Stability			
Energy Management (Minutes – Hours)	Spinning Reserve	–	–	BESS (Lead Acid),
	Unbalanced Load			BESS (Li-ion),
	Compensation			BESS (Nickel-),
	UPS			Hydrogen-Fuel Cell
	Peak Reduction	PHES,	–	BESS (NaS),
	Increase Renewable	CAES		Hydrogen-Fuel Cell
	Power Penetration			
Islanded Operation				

**Table 2.3: Technical characteristics and costs of various energy storage technologies**

	<b>PHES</b>	<b>CAES</b>	<b>FES</b>	<b>BESS</b>	<b>Super Cap.</b>	<b>SMES</b>
<b>Energy density</b>	0.3 to	10 to	5 to	20 to	5 to	1 to
<b>(Wh/kg)</b>	1.5 <sup>a</sup>	30	70	2,000	25	11
<b>Power density</b>	–	–	1,000 to	25 to	> 1,000	> 10,000
<b>(W/kg)</b>			5,000	220		
<b>Life time<sup>b</sup></b>	10,000 to	< 15,000	> 20,000	100 to	> 20,000	7,500
<b>(cycles)</b>	20,000			16,000		
<b>Discharge</b>	20 to	5 to	10 s to	10 min to	1 s to	1 s
<b>time</b>	100 hrs	50 hrs	40 min	15 hrs	10 s	to 40s
<b>Cost<sup>c</sup></b>	> 4,000	1,600 to	> 2,400	> 800	–	1,200
<b>(RM/kW)</b>		4,000				
<b>Cost<sup>c</sup></b>	15 to	10 to	800 to	>300	> 10,000	> 20,000
<b>(RM/kWh)</b>	150	100	2,200			
<b>Efficiency</b>	65 to	40 to	< 90	50 to	80 to	< 90
<b>(%)</b>	75	60		95	90	

a. Not limited to, but depends on the reservoir volumes and the elevated height

b. Assuming the expected operations a year is 365 cycles

c. Conversion rate of 1USD (\$) to 4 MYR (RM)

### 2.3.3. Battery-based Energy Storage Technologies

Nowadays, there are a variety of batteries being used in BESS. The battery technologies vary widely in its energy densities, power densities, life cycles, costs and cycle efficiency. Obtained from the various literatures (Akinyele and Rayudu, 2014; Bhuiyan and Yazdani, 2012; Hussein et al., 2012; Yan et al., 2014; Zakeri and Syri, 2015), Table 2.4 summarizes the technical

characteristics and costs for some commonly used BESS technologies in the modern power industries such as valve-regulated lead acid (VRLA), lithium-ion (Li-ion), nickel cadmium (NiCd), nickel-metal hydride (NiMH) and sodium sulfur (NaS).

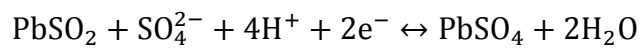
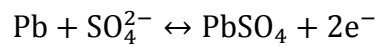
**Table 2.4: Summary of some commonly used battery technology in the ESS**

	VRLA	Li-ion	NiCd	NiMH	NaS
<b>Energy density (Wh/kg)</b>	20 to 50	100 to 200	40 to 75	60 to 80	120 to 240
<b>Power density (W/kg)</b>	25 to 100	360	140 to 180	220	120 to 220
<b>Life cycle (cycles)</b>	200 to 2,500	500 to 4,000	500 to 2,000	< 3,000	3,000 to 9,000
<b>Life time (years)</b>	5 to 15	5 to 15	10 to 20	10 to 20	10 to 15
<b>Discharge time (hours)</b>	1 to 6	1 to 3	1 to 6	2	6 to 12
<b>Self discharge</b>	low	low	low	medium	medium
<b>Overcharge tolerance</b>	high	very low	moderate	moderate	moderate
<b>Cost (RM/kW)</b>	> 800	> 1,200	> 800	> 1,200	> 4,000
<b>Cost (RM/kWh)</b>	< 1,200	> 4,800	1,600 to 2,400	2,400 to 6,400	1,200 to 3,200
<b>Operating temp. (°C)</b>	-5 to 40	-30 to 60	-40 to 50	-30 to 50	270 to 350
<b>Efficiency (%)</b>	70 to 80	70 to 95	60 to 75	50 to 80	75 to 85

### 2.3.3.1. Valve-Regulated Lead Acid (VRLA)

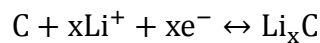
A cell of VRLA contains a cathode made of lead dioxide [PbO<sub>2</sub>] and an anode made of lead [Pb]. Both the electrodes are submerged in an aqueous sulphuric acid [H<sub>2</sub>SO<sub>4</sub>] electrolyte, separated by a micro-porous material to prevent

contacts. It is closed with a pressure regulating valve, sealed and the acid electrolyte is held immobilized. During discharge, the electrodes turn into lead-sulphate [PbSO<sub>4</sub>] and the electrolyte converts from sulphuric acid to water [H<sub>2</sub>O]. The reverse takes place when the battery is charged. The following describes the chemical reaction in a VRLA battery.



### 2.3.3.2. Lithium-ion (Li-ion)

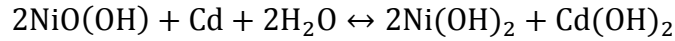
A cell of Li-ion contains a cathode made of graphite [C], an anode made from lithiated metal dioxide [LiMO<sub>2</sub>] of different lithium compounds, and an electrolyte made up of the lithium salt dissolved in organic carbonate solvents. Intercalation of lithium into graphite happens when the battery is charged and the reverse takes place when the battery is discharged. The following shows the reversible reactions involved in Li-ion battery.



### 2.3.3.3. Nickel Cadmium (NiCd)

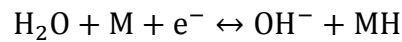
A cell of NiCd contains a nickel oxyhydroxide [NiO(OH)] cathode and a negative electrode of cadmium hydroxide [Cd(OH)<sub>2</sub>] which is converted from

metallic cadmium [Cd] by oxidation. The electrodes are separated and put in an electrolyte of potassium hydroxide [KOH]. The chemical reaction is involved in the charged or discharged states of the NiCd are as listed.



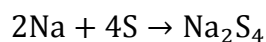
#### 2.3.3.4. Nickel Metal-Hydride (NiMH)

Similar to NiCd, NiMH uses a negative electrode of intermetallic compound [M] instead of cadmium. The chemical reactions at the negative electrode and positive electrode take places as followed.



#### 2.3.3.5. Sodium Sulfur (NaS)

A cell of NaS has an anode constructed from molten sulfur [S], and the cathode built from molten sodium [Na]. The electrodes are separated by solid beta alumina ceramic electrolyte [ $\beta$ -Al<sub>2</sub>O<sub>3</sub>]. As the battery discharge, positive sodium ions [Na<sup>+</sup>] transport through the electrolyte and combine with the sulfur [S] to form sodium polysulfide [Na<sub>2</sub>S<sub>4</sub>]. The external heat source is needed for its operation and the structure of the battery requires a special treat to minimize heat loss.



### **2.3.3.6. VRLA Battery-based Energy Storage System**

VRLA batteries are the most mature and widely used BESS technology. Despite low energy density, VRLA has reasonable cycle efficiency and life cycles. VRLA also has a much lower initial cost of investments compare to the other battery technologies. Li-ion on the other hand has high energy density, cycle efficiency and relatively high life cycles. However, Li-ion is expensive and requires complex circuitry to protect the cells during charging (Bhuiyan and Yazdani, 2012; Yan et al., 2014).

A balance between VRLA and Li-ion is NiCd. At a lower price compared to Li-ion, NiCd offers high energy density and long cycle-life in contrasts to VRLA. NiCd has good cost-to-cycles ratio as well. However, (1) it has the “memory effect” of the battery degradation from its maximum energy capacity when it is repeatedly recharged after being discharged partially, and (2) it is also not environmental friendly because of its toxic composition cadmium (Hussein et al., 2012). Similar to NiCd, NiMH has higher power density and longer cycle-life. NaS on the other hand, exhibit high power and energy densities with good cycle efficiencies as well as longer life cycles. NaS however, require an external heat source to operate and the initial investments for NaS are high due to the special construction needed to sustain the high temperature.

Each battery technology therefore has its own advantages and limitations. None of the battery technology is favorable for all the grid

application. Nonetheless, after taking into consideration of the cost, energy density, life cycles and other technical characteristics, VRLA battery is selected for this project. This is because VRLA provides a low-cost, simpler set-up and scalable solution for the application of peak demand reductions. VRLA also has the technical characteristic of bulk energy storage with rapid charge and discharge feature.

#### **2.4. Peak Demand Reductions with Battery-based Energy Storage System**

BESS reduces the daily peak demands for the customers if it is placed after the utility's meter to supply the power to the load over the peak hours. The power demand from the utility grid is reduced during the peak hours and its energy is replenished during the off-peak hours. A BESS generally consists of the battery units, a power conversion unit, a battery management unit and a central control unit. The battery units serve as the electrochemical energy storage device, arranged in series or parallel to achieve the desired electrical configuration of voltage and ampere-hour (Ah) capacity. A power conversion unit is required to interface the batteries with the utility grid. The power conversion unit functions bi-directionally, inverts the batteries DC supply to AC supply when the BESS is supplying power to the grid to reduce the peak demands and rectify the grid AC supply to DC supply when the BESS is absorbing power from the grid to charge the batteries.

The battery management unit maintains safe and optimal operation of the batteries. It functions (1) to ensures the temperature gradients across the

batteries is within tolerance, (2) to protect the batteries from internal degradation and capacity fade, (3) to balance the cells voltage throughout the string, and (4) to provide optimal charging patterns based on present state of the batteries (Lawder et al., 2014). The central control unit then governs the entire operation of the system, collects the measurements of the power line from various meters connected to the electrical network, performs the appropriate grid power application computations and accordingly manages the supplies of the batteries.

#### **2.4.1. Sizing of Battery-based Energy Storage System**

The power rating (kW) and the storage capacity of the energy storage system (kWh) play an important role in the effective minimisation of the daily peak demands. The power rating (kW) of any power conversion unit determines the highest power demand that can be reduced from the grid as shown in Figure 2.3(a). However, the peak demand can only be effectively reduced if the BESS has sufficient energy storage capacity (kWh) to supply the power to the load across the specified width of the peak as shown in Figure 2.3(b). Over sizing the BESS can increase the overall system cost while under sizing leads to the failure of minimizing the daily peak demands. Undersized BESS cannot satisfy the peak demand reductions and unable to minimize the peak to bring enough financial benefits to the customers.

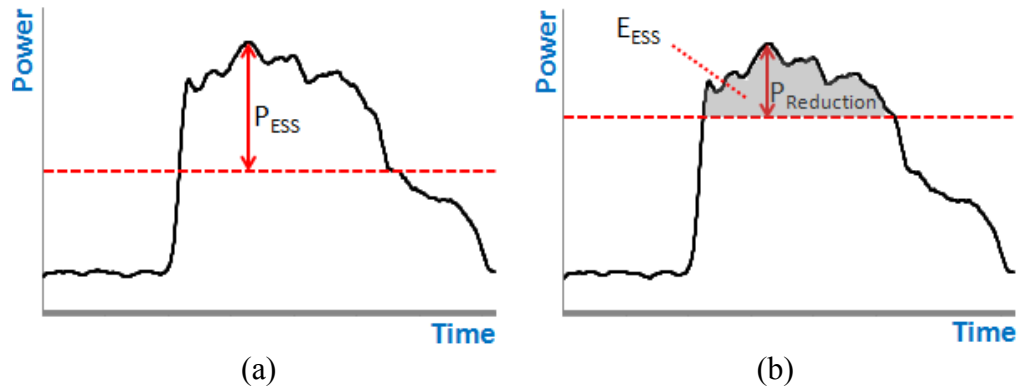


**Figure 2.3: Highest peak demand reduction for scenario of BESS (a) Constrained by the power rating (kW) and (b) Limited by the energy storage capacity (kWh)**

Numerous research efforts have been conducted to derive the optimum sizes of BESS. Yan et al. (2014) provide a variety of models to determine the optimal size of BESS through techno-economic assessment. Chauhan and Saini (2014) evaluated the systems' economics criteria and also its power reliability to determine the optimum size of the energy storage. Leadbetter and Swan (2012) determined the BESS size through a parametric study of the failure events such as energy depletion, limited by the energy storage capacity and undersized of power conversion unit, constrained by the power rating. ElNozahy et al. (2015) presented a Monte Carlo based probabilistic method to determine the appropriate size of BESS to enable the facilitating and integration of PVs and EVs in distribution networks. Lu et al. (2014) discussed a BESS capacity planning model for peak load reduction with optimization objective to reduce the difference between the peak and valley load. Dupont and Baltus (2009) and Hussein et al. (2012) provided a BESS dimensioning method based on empirical analysis of load profile to estimate the maximum BESS capacity for the application of full system load leveling.

Although many works of literature have been conducted to derive the optimum sizing of BESS, the storage capacity is often limited due to the financial constraints. Also, the peak often happens at the wrong time with the unexpected width. The energy of the BESS can run out quickly during the process of peak reductions. As a result, the ESS may fail to reduce the daily peak demands and so the monthly maximum demand. Therefore, a control strategy has to be used together with a load forecasting technique in order to establish the schedule of power supply from the BESS for improving the success rate of peak reductions.

#### **2.4.2. Control Techniques for Battery-based Energy Storage in the Application of Peak Demand Reductions**

At present, there are two fundamental control strategies for the BESS. The first is known as the fixed scheduled patterns whereby historical load data is used to determine the times and dates for the BESS to deliver power as well as to charge the batteries (Mattern et al., 2008; Purvins et al., 2013; Joshi and Pindoriya, 2015). The second strategy is a load following approach whereby a threshold is determined based on the historical load data so that the BESS deliver the power when the actual load demand exceeds the threshold and charges the batteries during off-peak periods (Leadbetter and Swan, 2012; Levron and Shmilovitz, 2012; Rowe et al., 2013).

The first control strategy has the advantage of performing the peak demand reductions without any monitoring system. However, the daily peak

demand reduction is unreliable and often not successful. This is because it does not optimize the reductions and the load demand is reduced uniformly. The real-time load profile is often not the same as the predicted profile, the peak therefore does not coincide with the power delivery from BESS and load spikes persist. On the other hand, the second control strategy has the ability to control the power supply of BESS based on the real-time load demand. This method however is inconsistent when the battery does not have sufficient energy to cut down the whole peak. Moreover, once the threshold is determined, it will not be adjusted anymore. As a result, BESS can often fail to reduce the peak.

Both the fundamental control strategies are simple and easy to implement, however due to the inherently stochastic nature of load demand, the discrepancy between the real-time and the forecasted load demands are unavoidable. Both the control strategies do not use forecasts and thus lack the dynamics foresight and consequently lacks the ability to reduce the peak demand optimally. Hence, a need exists for a control strategy that can reliably optimize the demand reduction. A number of control strategies, coupled with the forecasting and optimization techniques have therefore been developed. The summary of the controllers from the various literature is tabulated in Appendix B.

Bao et al. (2012) developed a real-time BESS load shifting control strategy based on short-term load forecasting and dynamic programming. A day-ahead load profile is predicted using linear regression by averaging the

historical load profile. On the day of operation, when new load demands are obtained, the predicted load profile is updated through regression. The control strategy carries out load shifting by discharging the BESS during the peak periods and charges the BESS during the off-peak periods. The control strategy is then optimized using dynamic programming techniques.

Rowe et al. (2014b) employed a low voltage distribution network load forecasting technique developed by Haben et al. (2014). The forecast undergoes a pre-processing stage to capture the regular but different timed behaviour of the peak demand. A scheduler then receives the forecast and iteratively determines the best charge and discharge set-points for a given predefined energy storage size, in which above the set-point the storage system will be set to discharge and below the storage system is set to charge. Rowe et al. (2014a) then extended the scheduling system to include an online optimisation based on model predictive control and stochastic receding horizon controller that operates by predicting the demands using a load scenario tree.

Lu et al. (2014) presented a BESS capacity planning model for peak shaving. Two BESS scheduling model are proposed, the first minimize the gap between the peak and the valley, whereas the second mitigate the variance of the daily load. The load forecasting is performed prior to shaving the peak. Two forecasting methods based on regression statistical method is proposed namely the one-shot prediction and rolling prediction.

Bennett et al. (2015) developed a low voltage BESS scheduling system composed of (1) a load forecast system based on artificial intelligent to predict the next-day load profile, (2) a BESS scheduler to obtain the initial charge and discharge set-point based on the forecasted load profile and (3) a real-time operator, an online control algorithm to minimize the forecast error through continuous adjustment of the BESS schedule.

The analyses of the stated literature are somehow confined to simulation evaluation only. An accurate estimate of the BESS's response in real-time is not comprehensively considered. Advanced modelling is required to accurately estimate the response of the BESS to adapt to the nonlinearity constraints of the batteries such as the ageing effects. The performance of the algorithm is also often iterated to converge to have an outcome that is desirable. Hence, it is unknown whether the demonstrated efficacy of the proposed strategies, in its semi-idealized form, is transferrable to an operational scheme, and, further, whether such efficacy can be maintained. At present, only a few works of literature have shown their experimental works.

Koller et al. (2015) implemented a predictive power dispatch optimization for peak shaving on a grid-connected Zurich BESS with 1 MW power rating and 580kWh energy capacity. The proposed peak shaving strategy is based on a continuation work presented in Arnold and Andersson (2011), where the framework calculates the peak shaving set-points determined by (1) the battery degradation cost function described in Koller et

al. (2013) and (2) a day-ahead demand forecast obtained from auto-regression artificial neural network with exogenous inputs.

Reihani et al. (2016a) demonstrated a peak shaving and power smoothing control strategy on a Microgrid system at the island of Maui in Hawaii with BESS size of 1MW power rating and 1.1MWh of battery capacity. The work is based on a continuation work from Reihani et al. (2016b). A parallel forecasting method is proposed using complex-valued neural networks. A state-of-charge (SOC) trajectory then obtained the forecasted load profile to schedule the BESS charge and discharge supplies. During operation of peak shaving, an optimization algorithm finds the optimal active power set-point of the BESS based on objective functions of minimizing the SOC cost and load cost.

Chua (2016) presented a novel fuzzy-based control algorithm for peak reductions with a BESS size of 15kW power rating and 64kWh of battery capacity. Tested at a low voltage network, the proposed controller demonstrated higher peak reduction compared to the fundamental controllers. The fuzzy-based control algorithm with the adaptive-threshold adjustment takes into account the battery state-of-charge or the useable energy of the battery storage during the time of operation to determine the amount of power to be delivered to the grid during the peak shaving process.

Besides the limited number of literature with supports of experimental work, the majority of the control strategies review thus far are also not tested

when the capacity of the BESS is limited, which is often the limitation in the actual BESS setup due to the economic constraint. Furthermore, the control strategies are only evaluated based on a few experimental results and the reduction of the monthly maximum demand charge has never been assessed. It is therefore unknown whether the demonstrated efficacy can be maintained. The minimization of the daily peak demands does not necessarily reflect an economic benefit because the maximum demand charge over the period of a month is not investigated. This dissertation hence presents a new control strategy for the BESS to sustain its energy throughout to cut down every daily peak demands and reduce the monthly MD charge. This new strategy is also extended to consider the situation where the capacity of the energy storage is limited.

## **2.5. Summary**

The significance and importance of the peak demand reductions have been elaborated in this chapter. The strengths and potentials of the energy storage system (ESS) over other types of peak demand reduction methods have been explored as well. The selection of the battery-based energy storage system (BESS) over the other ESS technologies has also been discussed. Besides that, the limitations and weaknesses of the current literature in the topic of peak demand reductions using BESS have also been reviewed.

## **CHAPTER 3**

### **SYSTEM ARCHITECTURE OF THE BATTERY-BASED ENERGY STORAGE SYSTEM**

The hardware components of the battery-based energy storage system (BESS) are elaborated in this chapter, followed by the set-up of the BESS. Next, the Modbus messaging protocol is presented to bring about a preliminary understanding of the BESS communication systems before the frameworks as well as the implementation of the communication systems are discussed.

#### **3.1. Hardware Components**

Similar hardware set up has been carried out previously by other researchers who are involved with the other grid application. The work carried out previously were however based on an older version of battery inverter (SI 5048) and compared to this research, the newer versions of battery inverter (SI 8.0H) is used. Not only that, the previous work was also carried out at a different site. The work that has been carried out previously is therefore not suitable for this research. All the hardware set up as well as the communication systems are hence re-established at the new site. Shown in Figure 3.1, the BESS is connected to the low-voltage (LV) electrical network setup at the Universiti Tunku Abdul Rahman (UTAR) campus in Sungai Long KA Block.

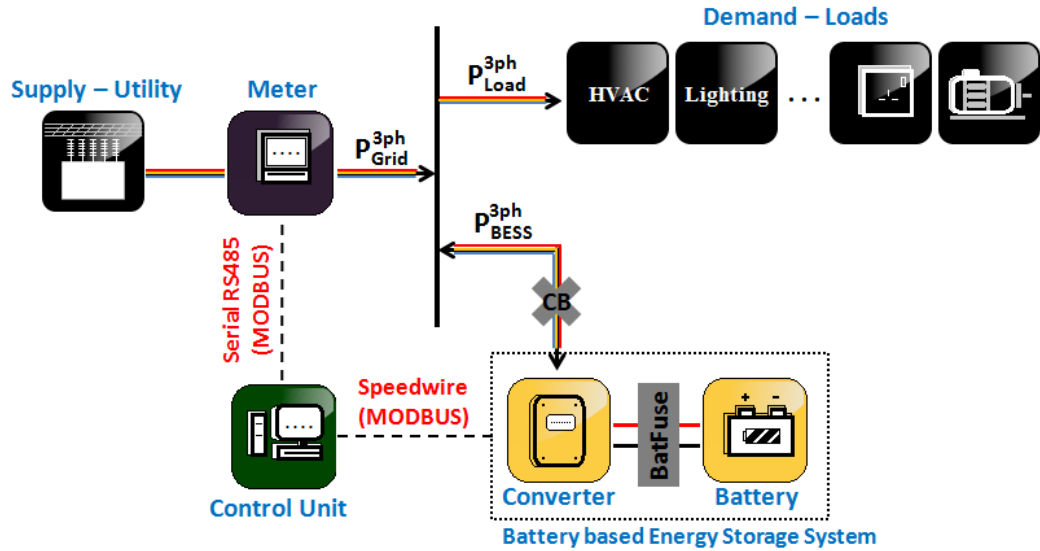


**Figure 3.1: Single-line diagram of the experimental BESS set-up**

The BESS have a total power rating ( $P_{\text{BESS}}$ ) of 18kW. It consists of three units of 6kW bi-directional power converter. Each of the power converters is connected to a bank of batteries formed by 16 pieces of 12V<sub>dc</sub>, 111Ah, valve-regulated lead-acid (VRLA) batteries, connected in a 4 × 4 matrix configuration. Forming the total energy capacity of up to 64kWh, each string of batteries carried an energy capacity of about 21.32kWh. To prolong the lifespan of the batteries, the amount of energy ( $E_{\text{BESS}}$ ) that can be used is however only about 27kWh or the depth-of-discharge (DOD) of up to 50%.

Furthermore, circuit breakers (CB) are connected in between the BESS and the LV network to provide AC protection against overcurrent and leakage current that flows through the BESS. On the DC side, battery fuses (BatFuse) are also attached in between the bi-directional power converter and the batteries to provide DC overcurrent protection. The bi-directional power converters are supervised by a control unit that communicates with each other

through the TCP/IP network. The power flow of the LV network is measured using the meter. The acquired measurements are then transmitted to the control unit through the RS485 medium. And the control unit stores the data, performs the necessary computations and take the appropriate actions to control the BESS remotely.

### **3.1.1. SI8.0H Bi-directional Power Converter**

Three units of single-phase, SMA Solar Technology, SI8.0H bi-directional power converters are used in this research, to perform conversion of the AC-DC supplies between the LV network and the batteries. Each of the SI8.0H has rated power rating of 6kW at the battery temperature of 25°C and its efficiency is about 92% for output per rated power ratio of 1. Shown in Figure 3.2, the SI8.0H is setup and configured as grid-tied to the LV network. Each of the SI8.0H served as a master by itself and it comes with a battery management system (BMS). The BMS estimates the battery's state-of-charge (SOC) and manage the utilization of the battery capacity. The BMS has a charge control as specified in SMA (2014). The BMS also has a deep discharge protection to prevent the batteries from premature aging caused by inadequate charging or frequent deep-discharge of the batteries.

### **3.1.2. Valve-Regulated Lead Acid Battery Bank**

Three sets of 4 × 4 strings of HOPPECKE solar.bloc 12V 135 VRLA batteries with round-trip efficiency of about 85% are used in this research. Each battery

has rated DC voltage of 12V and C10 rating of 111Ah battery capacity. The battery has a lifetime of about 1,500 to 4,000 cycles for DOD of 20% to 50%. The battery is maintenance-free and has higher external short-circuit safety. The battery also has an integrated backfire protection and central degassing system for optimum operational safety.

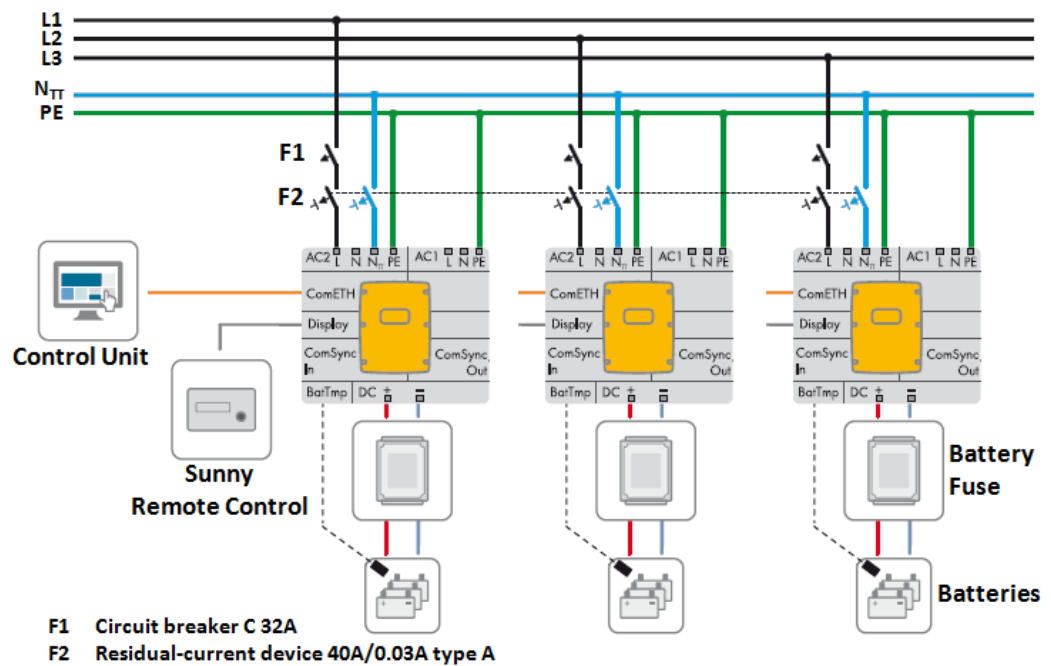
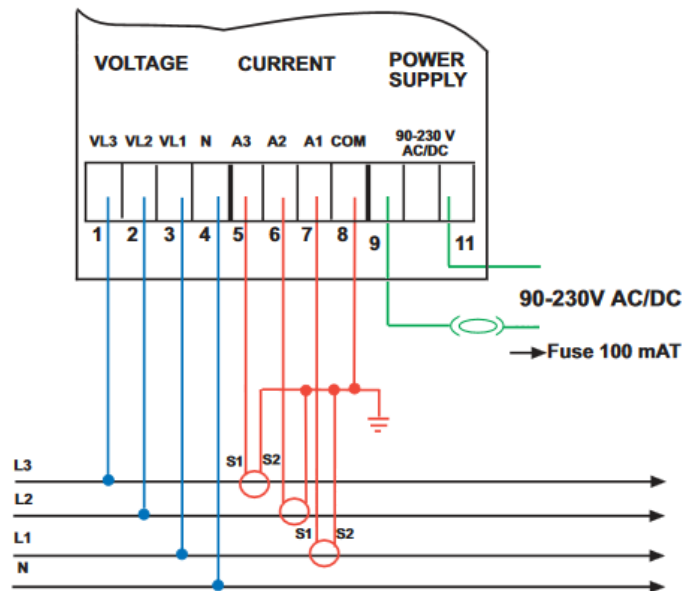


Figure 3.2: Grid-tied set-up configuration of the BESS

### 3.1.3. STAR3 Measurement Meter

Two units of STAR3 HARMO Energy & Harmonics Analyser, manufactured by Elcontrol® Energy Net are used in this research, to measure the power flows imported from the utility to the University building at KA lower ground floor (LG), ground floor (G) and mezzanine floor (M). The meter measures the voltage, current, frequency, power factor, and harmonics of up to the 25<sup>th</sup> order. Measurements such as the apparent, the active and the reactive power

and energy are also included. The sampling frequency is 2.5 kHz and its sensitivity is 20mA current and 10V voltage. Shown in Figure 3.3, the measurement meter is setup and configured as 3PH-N to the LV network. The meter is connected to a power source of 230V<sub>ac</sub>. Three units of current transformer (CT) with 5A secondary side are also used for each of the Star3, to step-down the current measurements on the LV network. Besides that, four units of voltage probes are also used for each of the Star3, to tape the line and neutral voltage of the LV network.



**Figure 3.3: 3PH-N set-up configuration of the measurement meter**

### 3.1.4. Control Unit

A Dell Precision T3600, mid-range workstation with window 7 professional license operating system is used in this research as the control unit. The control units, containing the computer programs, store the data, perform the necessary computations and make the appropriate control to the BESS

remotely. The computer programs or the virtual instruments (VIs) are developed in LabVIEW. Discussed in Section 3.4, the SI8.0H bi-directional power converters are supervised by the control unit via the TCP/IP network of Speedwire Ethernet. The power flow measurements, acquired by the Star3 measurement meters are then transmitted to the control unit through the RS485 serial line.

### 3.1.5. The Set-up of the Battery-based Energy Storage System

The set-up of the BESS with the control unit is shown in Figure 3.4. The installation of the measurement meters on the three-phase power supply riser at G and M floor is displayed in Figure 3.5.

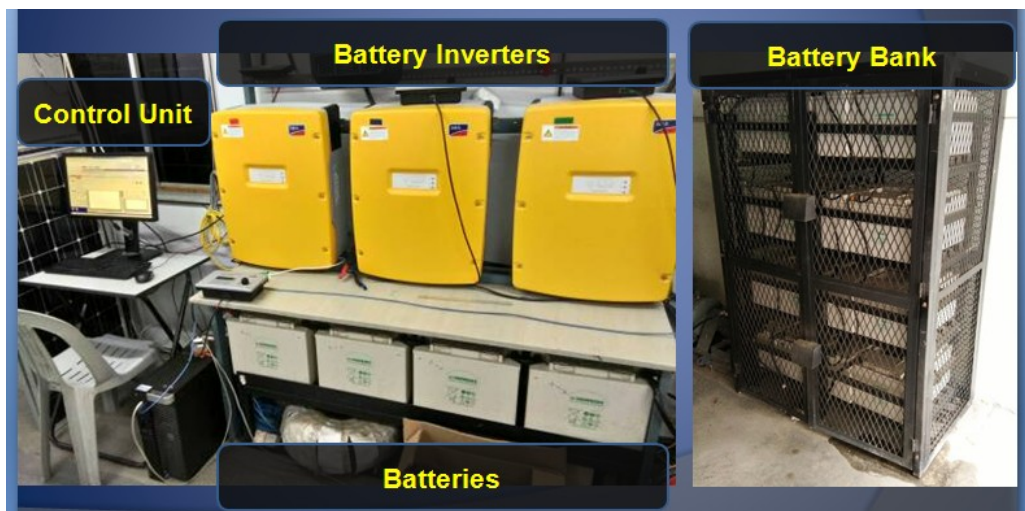


**Figure 3.4: The battery-based energy storage system and the control unit**



**Figure 3.5: The measurement meters installed at G and M floor**

### **3.2. Modbus**

Irrespective of the transmission medium, Modbus is a messaging protocol that defines the rules and structures for organizing and interpreting a data transmission message. Two transmission modes are commonly available, namely the RTU and the TCP. These transmission modes determine the way in which the Modbus messages are coded. Modbus RTU employs a Master–Slave communication model and the devices are communicated through the serial line such as RS232, RS411 or RS485. On the other hand, Modbus TCP adopts a Client–Server communication model and the devices are communicated through the TCP/IP Ethernet networks such as an ‘Intranet’ or the ‘Internet’ environment. The differences between the two types of messaging model are summarized in Table 3.1.

**Table 3.1: The Modbus messaging mode for RTU and TCP**

	<b>Modbus RTU</b>	<b>Modbus TCP</b>
<b>Messaging Protocol</b>	MODBUS	MODBUS
<b>Transport Protocol</b>	RTU	TCP/IP
<b>Transmission Medium</b>	Serial Line: RS232, RS485	Ethernet Networks: LAN, WAN

Each transmission modes has its unique framing sequence, error checking mechanism, and the address interpretation. A slave (or server) can be any peripheral device such as a controller, a measuring device or a relay, while a master (or client) device is typically a computer that is hosting the program and the user interface. In this research, the control unit serves as the master (or the client) and the slaves (or the servers) are the measuring meters, Star3 and the battery inverters, SI8.0H. The communication with Star3 is established through the Modbus RTU, while the communication with SI8.0H is set up through the Modbus TCP. Gathered from the documentations (ACROMAG, 2005; Modbus-IDA, 2012, 2006a, 2006b; Modicon, 1996), the Modbus communication protocol is discussed briefly in this section. Unless it is specified, if not, the numerical value of 5 represents the decimal of 5, and the hexadecimal value is represented as 0x05, the binaries are represented as 0101 binary.

### **3.2.1. Modbus RTU**

Firstly, the Modbus Remote Terminal Unit (RTU) is a Master–Slave communication model, transacting Modbus messages over a serial line such as RS232 or RS485. The slave device listens for commands (called the ‘request’)

from the master and reply (called the ‘response’) by returning the requested data to the master and performs the action as instructed by the master. The slave does not initiate a transaction on their own, they simply just respond to the requests from the master. Slave device also does not communicate with other slaves. The master device on the other hand, initiates the transactions and interprets the respond from the slave devices. Only one master can be connected at a time, and the master may communicate with up to a maximum of 247 slave devices. Before a Modbus RTU transaction can be established, the serial port handshake parameters such as the type of serial medium, the COM address, the baud rate and the parity mode are required to be configured as per the settings specified in the slave device.

Figure 3.6 shows the Modbus frame of the RTU transactions, wherein the Protocol Data Unit (PDU) contains the function code and the data fields. The entire Modbus frame forms up the Application Data Unit (ADU) that is containing the slave address, the PDU, and the error check.

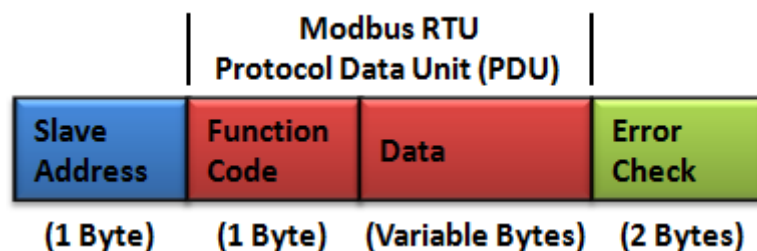


**Figure 3.6: Modbus RTU application data unit**

### **3.2.1.1. Slave Address (SA)**

The ‘Slave Address’ is 1-byte length, containing the unique address for the master to identify the slave in a Modbus transaction. The slave simply echoes its address in this field to allow the master to identify which slave is responding to the request.

### **3.2.1.2. Function Code (FC)**

The ‘Function Code’ is 1-byte length and it indicates to the slave what kind of action to be performed. This field is also used by the master to identify if an error-free or some kind of error called the exception response has occurred or not. In an error-free response, the slave will simply return the original function code back to the master. Only during an exception response, the slave will return a value that is equivalent to the original function code with the most significant bit (MSB) toggled to logic ‘1’. The different type of function code and the various type of exception response is discussed in Section 3.2.4.

### **3.2.1.3. Data Field**

The ‘Data Field’ is n-byte length. In the master’s request frame, the data field contains the information specifying to the slave the location of the register as well as how many register to read or write. In the slave’s response frame, if no error has occurred, the data field then contains the data requested by the master. If an error has occurred, the data field then contains a unique code that

the master can use to identify the kind of error that has occurred. A further detail of the different type of data in Modbus is discussed in Section 3.2.3.

#### 3.2.1.4. Error Check

The ‘Error Check’ is 2-byte length and it provides a method to validate the integrity of the Modbus message. In Modbus RTU, the error checking field is based on the Cyclical Redundancy Check (CRC). The CRC is computed by the transmitting device and it is appended to the end of the Modbus message. The receiving device then recalculates the CRC and compares with the one received. An error is detected if the two values are not matched. The computation of CRC can be found in the document Modbus-IDA (2006) under Appendix B.

**Table 3.2: Three possible types of event in a Modbus RTU transaction**

Events	Descriptions
Normal Response	The slave device receives the master request without error and a normal response is returned with the data requested.
No Response	No response is returned, the slave device did not receive the request due to a communication error. The incorrect bit parity or incorrect CRC checksum would also result in a ‘No Response’ event.
Exception Response	The slave device receives the request without error, but cannot handle the request and return an exception code (see Section 3.2.4) to inform the master device the nature of the error.

### 3.2.1.5. Modbus Events

Listed in Table 3.2, three possible types of event may occur in a Modbus RTU transaction. An example of a normal response is shown in Figure 3.7. ‘SA’ represents the slave unique address at 0x11 and ‘FC’ indicates the function code to be executed by the slave. In a normal response, the slave will simply echo its address and the function code. The slave will also handle the request and return the requested data. In this example, the function code of 0x01 is used. This command reads the discrete status of the slave’s output coils from starting address of 0x0013. A total of 36 (or 0x0025) output coils are requested by the master and the slave’s discrete status is 1100 1101 0110 1011 1011 0010 0000 1110 0001 1011 binary (or 0xCD6BB20E1B), where a binary 1 indicates an ON status and a binary 0 reflects an OFF status. The prefix of 0x05 in the data field of the slave’s response then represents the number of bytes to read before the data field ends.

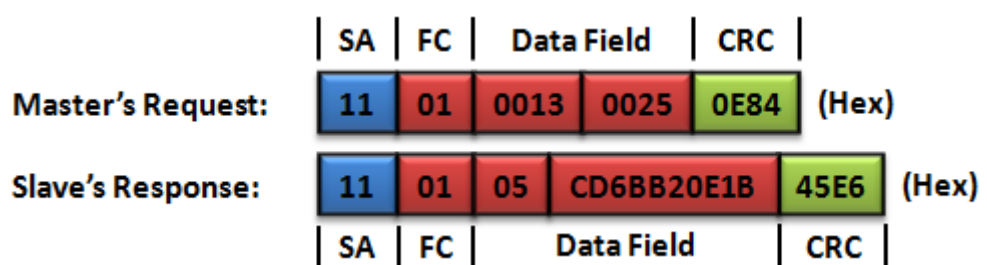


**Figure 3.7: An example of a normal Modbus RTU transaction**

Figure 3.8 then depicts an example of Modbus RTU transaction without a response due to the incorrect checksum of CRC in the request frame. The CRC supposed to be computed as 0x0E84, but 0x45E6 is received. Hence

a “No Response” occurred and the master will eventually carry out a timeout condition for this transaction.

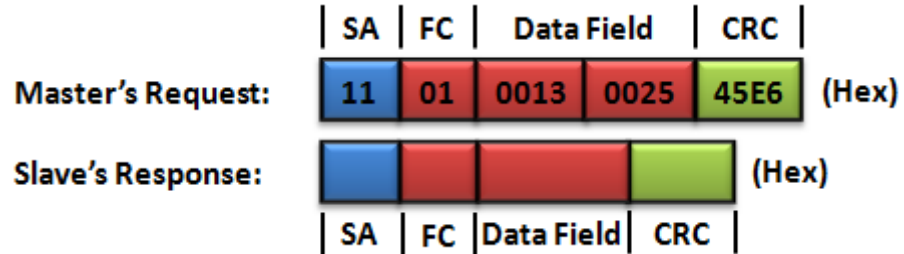


**Figure 3.8: An example of a Modbus RTU transaction without a response**

Apart from that, Figure 3.9 illustrates an example of a request with an exception response. In this example, the function code of 0x01 is used to communicate with the slave device of 0x11, to read 36 statuses (or 0x0025) of output coils from starting address of 0x04A1. The data address of 0x04A1 is, however, invalid and hence the slave return an invalid Modbus address with the exception code of 0x02 (see Section 3.2.4). The MSB of the function code in the slave's response is also set to logic '1' (or 0x81) to indicate an exception response.

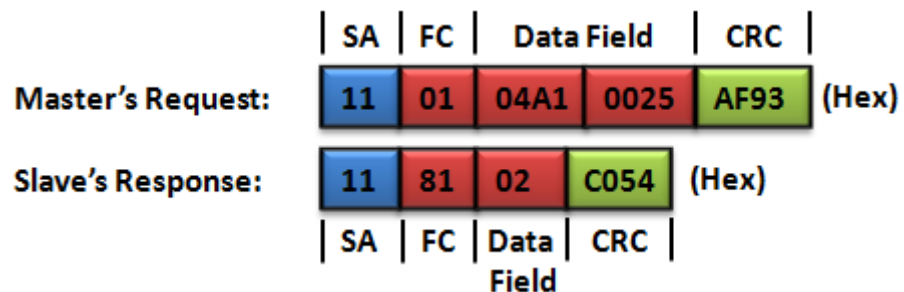


**Figure 3.9: An example of a Modbus RTU transaction with an exception response**

### 3.2.2. Modbus TCP

Moving on, the Modbus TCP is the Modbus RTU protocol with a TCP interface that is transmitted through the Ethernet. It follows the Client–Server communication model to transmit the Modbus message over TCP/IP. TCP/IP enables connection to be easily recognized at the protocol level, and a single connection can be carried by multiple independent transactions. Unlike the Modbus RTU, Modbus TCP utilizes the TCP/IP transmission protocol to allow a larger number of concurrent connections to be established. On the same TCP connection, several transactions with a remote server can be initiated by the client without having to wait or queue for a prior connection to complete the transaction.

All Modbus TCP transactions (‘Request’ or ‘Response’) are sent via TCP/IP to the registered port 502. When the client wants to send a Modbus TCP message to a server, the client requires to open a connection with the Modbus reserved port of 502 and deliver the TCP message to the designated server’s IPv4 address. As soon as a connection is established, the same connection can be used to exchange data between the client and the server. Several TCP/IP connections with multiple servers can also be established simultaneously.

Figure 3.10 shows the ADU of the Modbus TCP messaging structure. The ADU is embedded into the form of MBAP and PDU. The PDU; from the function code to the end of the data field have exactly the same layout and

meaning as the Modbus RTU. When Modbus message is carried over TCP/IP, the additional length of information is transmitted in the prefix, called the Modbus Application Protocol (MBAP), to allow the server to recognize the message even if the message had to be separated into multiple packets for transmission. Unlike the Modbus RTU, a server is addressed using its IP address and the device address is not needed. The ‘Error Check’ is also not needed in the Modbus TCP because the error-detection in TCP/IP is already provided by the Ethernet link layer checksum mechanisms.

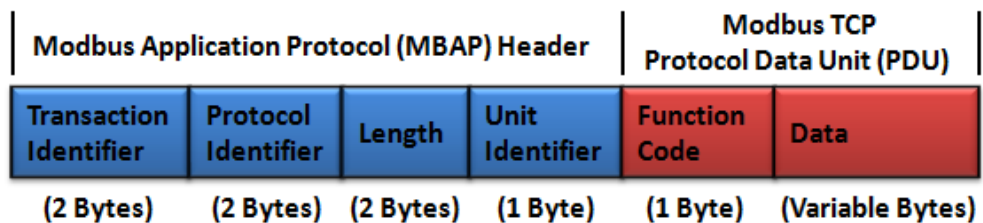


**Figure 3.10: Modbus TCP application data unit**

### 3.2.2.1. Transaction Identifier (TI)

The ‘Transaction Identifier’ is 2-byte length and it is used for transaction parsing when multiple Modbus transactions are transmitted on the same TCP connection by a client. In Modbus RTU, a master (similar role as a client) can only send a request at a time and must wait for the response before sending another request. However, in Modbus TCP, the client (similar role as a master) may send multiple requests to the same server without having to wait for the previous response to complete. For such instance, the transaction identifier is used to identify the future response with its originating request. The

transaction identifier is unique and it is usually a sequence number driven by a counter that is incremented by each request.

#### **3.2.2.2. Protocol Identifier (PI)**

The ‘Protocol Identifier’ is 2-byte length and it is used for intra-system multiplexing. The protocol identifier is always 0-bit for Modbus services. Other values are reserved for future extensions.

#### **3.2.2.3. Length Field**

The ‘Length Field’ is 2-byte length and it is used to count the remaining fields in the ‘Unit Identifier’ (1-byte), the ‘Function Code’ (1-byte) and the ‘Data Field’ (n-byte). It contains the information telling the server the start and how many subsequent bytes to read before the Modbus message ends.

#### **3.2.2.4. Unit Identifier (UI)**

The ‘Unit Identifier’ is 1-byte and it is used to facilitate intra-system communication. It is typically used to bridge a Modbus TCP client device with a remote Modbus RTU slave device through a gateway between the TCP/IP network and serial line. This field is specified by the client device in the ‘Request’ frame and it must be returned as the same value in the ‘Response’ frame. It is typically 0x00 or 0xFF for communication module in TCP/IP environment. The use of 0x00 or 0xFF causes the gateway device to block the

passage of the client message across the bridge. If the module is a traditional serial Modbus RTU, and it is being addressed through a gateway from an Ethernet Modbus TCP client, then this field is the traditional serial Modbus slave address.

### 3.2.2.5. Modbus Events

Similar to the Modbus RTU, there are also three types of event (see Table 3.2) in a Modbus TCP transaction. An example of a normal Modbus TCP response is shown in Figure 3.11. In a normal response, the server will simply echo the ‘TI’, ‘PI’, ‘UI’ and ‘FC’ back to the client, and handle the request and return the data requested. This example uses the function code of 0x01 to read the discrete status of the server’s output coils from starting address of 0x0013. A total of 36 (or 0x0025) output coils is requested. The server’s discrete status is returned as 1100 1101 0110 1011 1011 0010 0000 1110 0001 1011 binary (or 0xCD6BB20E1B). The prefix of 0x05 in the data field of the server’s response indicates the number of bytes to read before the data field ends. The length field of 0x0006 and 0x0008 for the client and the server then represents the number of byte counts from ‘UI’ to the end of the data field.

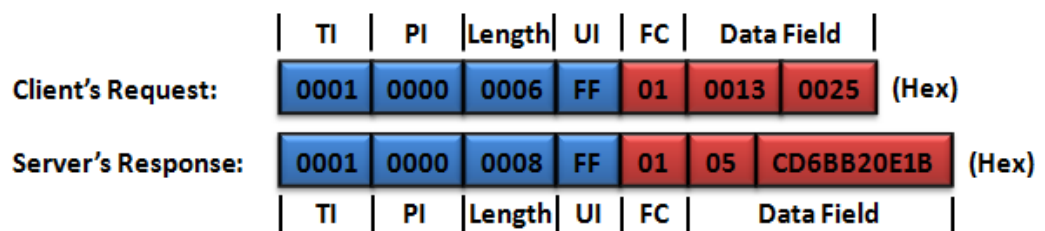


**Figure 3.11: An example of a normal Modbus TCP transaction**

Likewise to the Modbus RTU, the Modbus TCP event with “No Response” or “Exception Response” has the same description and concept as discussed in Section 3.2.1.

### 3.2.3. Modbus Profile

The Modbus profile can be thought as the addressing reference table of where the data are stored. It has a simple structure that is differentiated between four basic variations of data type such as output coil, discrete input, input register and holding register. These data type, such as listed in Table 3.3, are recorded in a register map uniquely defined for different slave device and can be identified by the leading value of the reference address of 0x, 2x, 3x or 4x.

**Table 3.3: The common type of Modbus profile**

Data Type	Reference	Description
Output Coil (1-bit)	0xxxx	A 1-bit, read or write, discrete output coil with address from 1 to 9999. It is used to set the output of a digital channel such as a solid-state relay.
Input Coil (1-bit)	1xxxx	A 1-bit, read only discrete input coil with address from 10001 to 19999. It is the ON or OFF status of a discrete input or contact, controlled by the corresponding digital input channel.
Input Register (2-byte)	3xxxx	A 2-byte, read-only input registers with address from 30001 to 39999. It usually contains the numerical data received from an external source such as an analog signal.
Holding Register (2-byte)	4xxxx	A 2-byte, read or write, output holding register with address from 40001 to 49999. It is used to store the numerical data or to send the data to an output channel.

The reference addresses are not a hard-coded memory addresses. Internally, all the Modbus devices employ a zero-based memory offset constructed from the reference address, wherein all data addresses in the Modbus messages are reference to zero. For instance, the coil #1 is addressed as coil 0x0000 in the data address field, whereas a holding register #40108 is addressed as 0x006B (or 107). Note that the reference address of 4x in the holding register #40108 is omitted from the specified address. This is because the leading number of the reference address is already indicated by the function code and thus it is usually omitted. However for some case, such as discussed in Section 3.4.2, the data address is not offset and the reference address is not omitted, and it follows the specification as given by the slave (or server) device.

**Table 3.4: List of function code in Modbus with data access and the respective data type that is involved**

Function Code	Code (Hex)	Data Type (Reference Address)	Data Access
Read Discrete Inputs	02 (0x02)	Physical Discrete Inputs (0xxxx)	1-bit
Read Coils	01 (0x01)	Internal Bits or	
Write Single Coil	05 (0x05)	Physical Coils (1xxxx)	
Write Multiple Coils	15 (0x0F)		
Read Input Register	04 (0x04)	Physical Input Registers (3xxxx)	2-byte or
Read Holding Registers	03 (0x03)	Internal Registers or	16-bit
Write Single Register	06 (0x06)	Physical Output	
Write Multiple Registers	16 (0x10)	Registers (4xxxx)	
Read/Write Multiple Registers	23 (0x17)		

### **3.2.4. Modbus Functions and Registers**

A function code represents the pointer in which the slave (or server) refers to identify the Modbus operation and action to be performed. It can be used for the purpose of data access, file record access, diagnostics or others. In this section, the function code with data access as listed in Table 3.4 will be discussed with the support of examples. The examples listed in this section however only contains the information specifies in the PDU frame and the other fields are not included. Readers are advised to refer to the examples discussed in Section 3.2.1 and Section 3.2.2 to have an overall idea of how the rest of the Modbus fields are transacted.

#### **3.2.4.1. Read Coils**

The 'Read Coils' command has a function code of 0x01, and it is used to read the state of the output coils with 0x reference addresses. The request PDU specifies the function code, the starting address and the number of output coils to request. The response PDU then returns the function code and the state of the output coils. The state of the output coils are packed as one bit per coil, where the output state is indicated as '1' for ON (or conducting current), and '0' for OFF (or not conducting). The least significant bit (LSB) of the data byte (8-bit) corresponds to the first state of the requested coil. The other states of the output coils then follow sequentially and move toward the high-order end of the byte. If the quantity of the returned output is not a multiple of eight,

the remaining bits in the final data byte will be padded with zeros toward the high-order end of the byte.

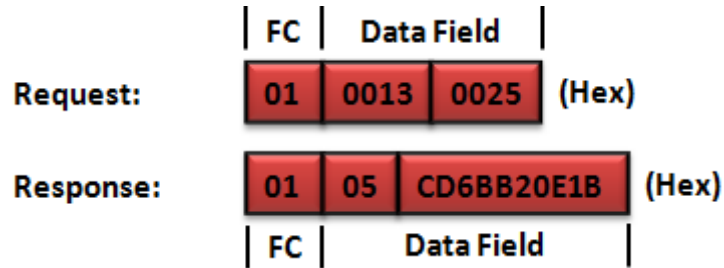


**Figure 3.12: An example of ‘Read Coils’ Modbus Function**

An example of reading the state of the output coils is shown in Figure 3.12. In this example, the discrete state of the output coils from #20 to #56 is requested. With starting address computed as  $20 - 1 = 19$  (0x0013), a total of  $56 - 20 + 1 = 37$  (0x0025) output coils status is requested. The data field of 0x05 in the response PDU indicates the number of data bytes to follow and the returned states of the output coils from #56 to #20 is indicated as 0xCD6BB20E1B, or binary 1100 1101 0110 1011 1011 0010 0000 1110 0001 1011.

Shown in Table 3.5: Breakdown of the data field in the responded frame in Figure 3.12, the first byte (0xCD) represents the status of the coils from #20 to #27, from right to left. The next byte (0x6B) then indicates the coils status from #28 to #35, from right to left. And so on. In the last byte, the state of coils #52 to #56 is shown as the byte value of 0x1B. Coil #56 is in the fourth-bit position from the left, and coil #52 is the LSB of this byte. Since the last byte only has 5 outputs, the remaining 3 bits of the data byte is therefore

padded with zero toward the unused high-order end of this byte. As a result, the last byte is binary of 0001 1011.

**Table 3.5: Breakdown of the data field in the responded frame in Figure**

**3.12**

	1 <sup>st</sup> Byte		2 <sup>nd</sup> Byte		3 <sup>rd</sup> Byte		4 <sup>th</sup> Byte		5 <sup>th</sup> Byte	
(Hex)	C	D	6	B	B	2	0	E	1	B
(Bin)	1100	1101	0110	1011	1011	0010	0000	1110	0001	1011
Coils	#27 – #20		#35 – #28		#43 – #36		#51 – #44		#56 – #52	

Similar Modbus PDU format and concept are also given to the function code of 0x02 ‘Read Discrete Inputs’ and therefore it is not discussed here. Readers are advised to refer to the cited Modbus documents for the example of ‘Read Discrete Inputs’.

**3.2.4.2. Read Holding Registers**

The ‘Read Holding Registers’ command has a function code of 0x03, and it is used to read the contents of a nearby block of holding registers with 4x reference addresses. The request PDU defines the function code, the starting address and the number of holding registers to be read. The response PDU then return the function code and the content of the holding register. The contents are packed as 2-bytes per register and within each byte, the binary values are right justified. In each register, the first byte reserves the high-order bits and the second stores the low-order bits.

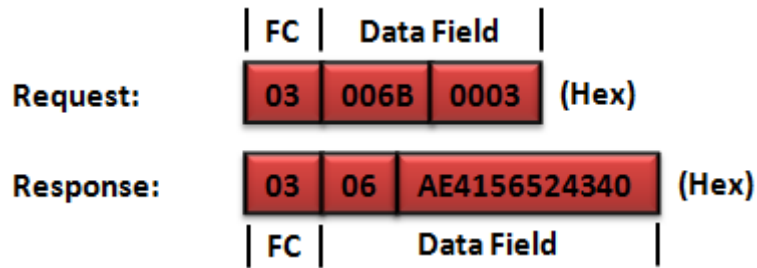


**Figure 3.13: An example of ‘Read Holding Registers’ Modbus Function**

An example of reading multiple holding registers simultaneously is shown in Figure 3.13. The breakdown of the data field in the responded frame is shown in Table 3.6. In this example, the content of the analog output holding registers from #40108 to #40110 is requested. With starting address computed as  $40108 - 40001 = 107$  (0x006B), a total of  $40110 - 40108 + 1 = 3$  (0x0003) holding registers are requested. The data field of 0x06 in the response PDU indicates the number of data bytes to follow and the content of the holding registers from #40108 to #40110 is returned with 0xAE4156524340, where 0xAE41 indicates the contents in register #40108, 0x5652 represents the data in register #40109 and 0x4340 reflects the values in register #40110.

**Table 3.6: Breakdown of the data field in the responded frame in Figure 3.13**

	First Byte		Second Byte		Third Byte		Fourth Byte		Fifth Byte		Sixth Byte	
(Hex)	A	E	4	1	5	6	5	2	4	3	4	0
(Dec)	44609				22098				17216			
Reg.	#40108				#40109				#40110			

Likewise, similar Modbus PDU format and concept are also given to the function code of 0x04 ‘Read Input Register’ and therefore it is not discussed here. Readers are also advised to refer to the cited Modbus documents for the example of the ‘Read Input Register’.

### 3.2.4.3. Write Single Coil

The ‘Write Single Coil’ command has a function code of 0x05, and it is used to write a single output coil with 0x reference addresses. The request PDU specifies the state (ON or OFF) and the address of the output coil to be written. A value of 0xFF00 requests the output coil to set to ON (or conducting current), whereas a value of 0x0000 requests it to be OFF (or not conducting). All other values are illegal and will not influence the output. In a normal response, the response PDU echoes (or copy) the request PDU and returned after the output coil has been written. An example of writing an output coil is shown in Figure 3.14. The discrete output coil #173 is set to ON, whereby the coil address is computed as  $173 - 1 = 172$  (0x00AC) and the ON state is written with the value of 0xFF00.

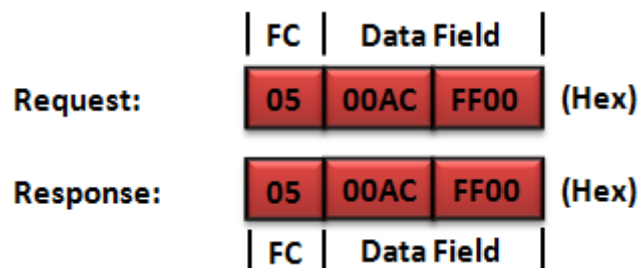


**Figure 3.14: An example of ‘Write Single Coil’ Modbus Function**

#### 3.2.4.4. Write Single Register

The 'Write Single Register' command has a function code of 0x06, and it is used to pre-set or writes a single holding register with 4x reference addresses. The request PDU specifies the function code, the address of the holding register, and the specific value to be written. The response PDU then return a copy of the request PDU. An example of writing a single holding register is shown in Figure 3.15. In this example, the holding register #40002 computed with  $40002 - 40001 = 1$  (0x0001) specified address, is written by a preset value of 0x0003, or 3.

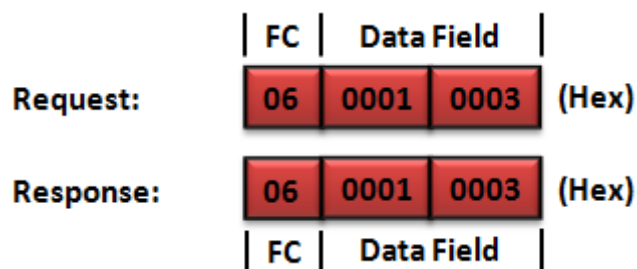


**Figure 3.15: An example of 'Write Single Register' Modbus Function**

#### 3.2.4.5. Write Multiple Coils

The 'Write Multiple Coils' command has a function code of 0x0F, and it is used to simultaneously write a series of output coils with 0x reference addresses. A '1' indicates ON (or conducting current), and '0' represents OFF (or not conducting). The request PDU specifies the function code, the starting address, the number of coils and the state (ON or OFF) of the coils to be written. The state of the output coils is packed as one bit per coil. In a normal

response, the response PDU echoes the function code, the starting address and the number of coils written. If the number of output coils is not a multiple of eight, then the remaining bits is required to be padded with zeros.

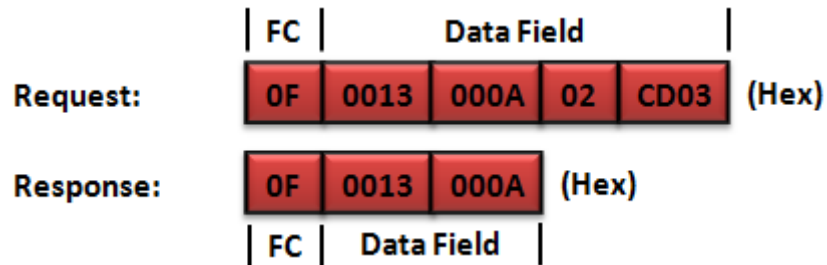


**Figure 3.16: An example of ‘Write Multiple Coils’ Modbus Function**

An example of writing a multiple of output coils simultaneously is shown in Figure 3.16. The breakdown of the data field in the requested frame is shown in Table 3.7. In this example, the state of the output coils in a series from #20 to #29 is written. With starting address computed as  $20 - 1 = 19$  (0x0013), a total of  $29 - 20 + 1 = 10$  (0x000A) output coils is written. The data field of 0x02 in the request PDU indicates the number of data bytes to follow and the state of the output coils is set to 0xCD03, or binary of 1100 1101 0000 0011. The bits in the first byte (0xCD) force the output coils from #20 to #27, with the least significant bit (LSB) addressing the output coil #20. The next byte transmitted (0x03) then set the output coils from #28 to #29, with the LSB addressing the output coils #28. Since the second byte only holds the state of 2 output coils, the remaining 6 bits of the data byte is, therefore zero-filled. The response PDU then returns a copy of the function code (0x0F), the starting address (0x0013) and the number of coils written (0x000A).

**Table 3.7: Breakdown of the data field in the requested frame in Figure**

**3.16**

1st Byte								
(Hex)	C				D			
(Bin)	1	1	0	0	1	1	0	1
Coils	#27	#26	#25	#24	#23	#22	#21	#20

2nd Byte								
(Hex)	0				3			
(Bin)	0	0	0	0	0	0	1	1
Coils	X	X	X	X	X	X	#29	#28

### 3.2.4.6. Write Multiple Registers

The ‘Write Multiple Registers’ command has a function code of 0x10, and it is used to write or pre-set a block of contiguous holding registers with 4x reference addresses. The request PDU specifies the function code, the starting address, the number of holding registers and the contents of the holding registers to be written. The contents are packed as 2-bytes per holding register. In a normal response, the response PDU return the function code, the starting address and the number of holding registers written, returned after the holding registers have been pre-set.

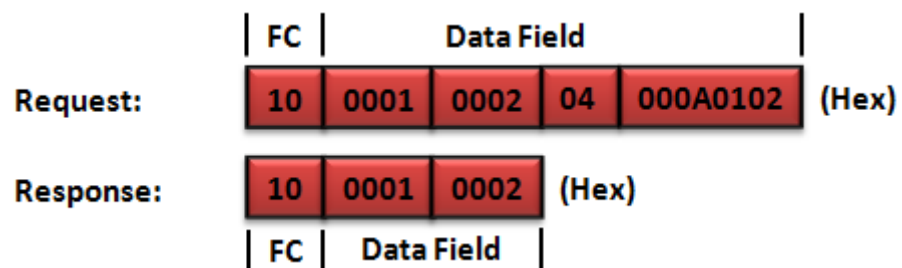


**Figure 3.17: An example of ‘Write Multiple Registers’ Modbus Function**

An example of writing a multiple of holding registers simultaneously is shown in Figure 3.17. The breakdown of the data field in the requested frame is shown in Table 3.8. In this example, the holding registers of #40002 and #40003 are written. With starting address computed as  $40002 - 40001 = 1$  (0x0001), a total of  $40003 - 40002 + 1 = 2$  (0x0002) holding registers are written. The data field of 0x04 in the request PDU indicates the number of data bytes to follow and the holding registers are set to 0x000A and 0x0102 respectively. The response PDU then returns a copy of the function code (0x10), the starting address (0x0001) and the number of holding registers written (0x0002).

**Table 3.8: Breakdown of the data field in the requested frame in Figure 3.17**

	1st Byte		2nd Byte		3rd Byte		4th Byte	
(Hex)	0	0	0	A	0	1	0	2
(Dec)	10				258			
Reg.	#40002				#40003			

#### 3.2.4.7. Read/Write Multiple Registers

The ‘Read/Write Multiple Registers’ command has a function code of 0x17, and it is used to perform a combination of one read and one write operations of the holding registers with 4x reference addresses in a single Modbus transaction. The request PDU specifies the starting address and the number of holding registers to be read as well as the starting address, the number of holding registers, and the data to be written. The write operation is performed first followed by the read operation. In a normal response, the response PDU

echoes the function code and the contents of the holding registers that were requested.



**Figure 3.18: An example of ‘Read/Write Multiple Registers’ Modbus Function**

An example of write and read multiple of holding registers is shown in Figure 3.18. The breakdown of the data field in the requested frame and the responded frame is shown in Table 3.9: Breakdown of the data field in the requested frame in Figure 3.18 and Table 3.10. In this example, the holding registers from #40015 to #40017 are written. With starting address computed as  $40015 - 40001 = 14$  (0x000E), a total of  $40017 - 40015 + 1 = 3$  (0x0003) holding registers is written. The data field of 0x06 in the request PDU indicates the number of data bytes to follow and the holding registers from #40015 to #40017 are set to 0x00FF.

**Table 3.9: Breakdown of the data field in the requested frame in Figure 3.18**

	1st Byte		2nd Byte		3rd Byte		4th Byte		5th Byte		6th Byte	
(Hex)	0	0	F	F	0	0	F	F	0	0	F	F
(Dec)	255				255				255			
Reg.	#40015				#40016				#40017			

Apart from that, the contents of the holding registers from #40004 to #40009 are also requested. With starting address computed as  $40004 - 40001 = 3$  (0x0003), a total of  $40009 - 40004 + 1 = 6$  (0x0006) holding registers is requested. The data field of 0x0C in the response PDU indicates the number of data bytes to follow and the content of the holding registers from #40004 to #40009 is returned with 0x00FE0ACD00010003000D00FF, where 0x00FE indicates the contents in register #40004, 0x0ACD represents the data in register #40005 and so on until 0x00FF which reflects the values in register #40009.

**Table 3.10: Breakdown of the data field in the responded frame in Figure**

**3.18**

	1st Byte		2nd Byte		3rd Byte		4th Byte		5th Byte		6th Byte	
(Hex)	0	0	F	E	0	A	C	D	0	0	0	1
(Dec)	254				2765				1			
Reg.	#40004				#40005				#40006			

	7th Byte		8th Byte		9th Byte		10th Byte		11th Byte		12th Byte	
(Hex)	0	0	0	3	0	0	0	D	0	0	F	F
(Dec)	3				13				255			
Reg.	#40007				#40008				#40009			

**3.2.5. Modbus Exception Response**

In a normal (or error-free) response, the slave (or server) echoes the function code of the original request and return a response containing the data

requested by the master (or client). The slave only returns an exception message if an error related to the requested function has occurred. The function code is modified to reflect an error response, and the data field then contains the unique code which tells the master what kind of error has occurred or the reason for the exception. That is, the function code is set equal to the request function code plus 0x80 and the PDU becomes the exception code which is of 1-byte length.

Figure 3.19 illustrates an example of a request with an exception response. In this example, the function code of 0x01 is used to read 36 statuses (or 0x0025) of output coils from starting address of 0x04A1. The data address of 0x04A1 is, however invalid and hence the slave returns an exception code of 0x02 which specifies an invalid (or illegal) data address for the slave. The MSB of the function code in the slave's response then set to logic '1' (or 0x81) to indicate an exception response.

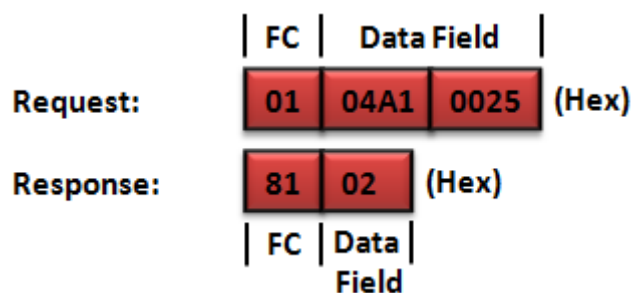


**Figure 3.19: An example of Modbus exception response**

There is a defined set of exception codes to be returned by the slave in the event of exceptions (or problems in processing the master request). For instance, if a master requested an unsupported service or an invalid function

code, then the slave will return the exception code of 0x01 in the data field to specify an illegal function, while if a holding register is written with an invalid value, then the exception code of 0x03, which specify an illegal data value will be returned in the data field. Table 3.11 lists some of the common exception codes in Modbus.

**Table 3.11: A list of exception codes**

<b>Exception codes</b>	<b>Definition of exceptions</b>
Illegal Function (0x01)	The function code received by the slave (or the server) is not an allowable action. This may be the function code is not implemented on the requested device (the slave or server) but only applicable to the other devices.
Illegal Data Address (0x02)	The data address received by the slave is not an allowable address. This may be the data address is incorrect, and the slave could not identify the register requested by the master (or client).
Illegal Data Value (0x03)	The data value contained in the master's request frame is not an allowable value for the requested device. This may indicate a fault in the structure of a complex request and the implied length is incorrect.
Device Failure (0x04)	An unrecoverable error occurred while the slave was attempting to perform the requested action and caused the slave failed to execute the request during the execution.
Acknowledge (0x05)	This response is echoed to prevent a timeout error on the master device. The slave has accepted the request but the service requires a relatively longer time to execute. An acknowledgment is therefore returned first to indicate that the service is still ongoing.
Device Busy (0x06)	The slave was unable to accept or process the master's request because it is occupied in processing a long duration command.

### **3.3. Star3 Communication System**

Followed by, the communication system of a Star3 measurement meter is implemented based on the Modbus RTU, encoded in binary coded decimal (BCD). The Modbus message is transmitted through the RS485 serial line. There are five types of Modbus functions in Star3 namely the 'Read Input Register', the 'Read Holding Register', the 'Read Output Status', the 'Preset Single Register' and the 'Force Single Coil'. The interpretation and decoding of the stated functions are discussed in this section. The RTU messaging structure is however not repeated here and readers are advised to refer to Section 3.2.1. Readers are also recommended to refer to the document (Elcontrol, 2006) for all the Modbus registers that are available in Star3.

#### **3.3.1. Star3 Modbus Function and Data**

##### **3.3.1.1. Read Input Register**

The 'Read Input Register' with a function code of 0x04, is a function used to read the Star3's parameters such as the measurements, the counters, and the device serial number. There are more than 100 input registers available in Star3. The line voltage (register #40029 and #40030), the line current (register #40035 and #40036) or the active energy counters (register #40021, #40022 and #40023) are some of the parameters stored in the input registers. The majority of the parameters are stored as floating value, encoded in BCD and it

is stored in 2 distinctive input registers. The counters floating value are however encapsulated in BCD and it is stored in 3 distinctive input registers.

The parameter in which is stored at 2 distinctive input registers carries the mantissa BCD and the exponent BCD. The mantissa BCD, which is located at the input register with a prior address, represents the sign and integer of the floating value. The most significant bit (MSB) of the mantissa BCD determines the sign of the floating value, where ‘0’ refers to a positive and ‘1’ reflects a negative. The rest of the binaries in the mantissa BCD then represent the integer of the floating value. On the other hand, the exponent BCD represents the number of decimal points of the floating value. Shown in Table 3.12, if the floating value is stored at input registers #40001 and #40002, then #40001 would hold the mantissa BCD and #40002 would carry the exponent BCD. If the mantissa BCD is 0x1248 or binary of 1001001001000, the MSB of ‘1’ then implies a negative value and the rest of the binary, 001001001000 or 0x248 represents the integer of the floating value. If the exponent BCD is 0x0003 (or 3), the floating value is then equal to value of -0.248.

**Table 3.12: An example of Star3’s measurements**

	<b>First Input Register</b>	<b>Second Input Register</b>
Address	#40001	#40002
Format	Mantissa BCD	Exponent BCD
Carry (Hex.)	0x1248	0x0003
(Binary)	1   001001001000	
(Hexadecimal)	-   0x0248	
Represent (Dec.)	-248	3 decimal points

Likewise, the counters in which is stored at 3 distinctive input registers also store the floating value as the mantissa BCD. The decimal points are however not represented by the exponent BCD but interpreted as the mantissa BCD itself stored at the third input register. For instance, as shown in Table 3.13, if the floating value of a counter is stored at input registers #40003, #40004 and #40005, then #40005 would hold the decimals of the floating value. The MSB of #40003 determines the sign, the rest of the binaries in #40003 and #40004 represent the integer. If #40003 holds 0x0111, #40004 carries 0x2222 and #40005 has 0x3333, the floating value would then equal to +111 2222.3333.

**Table 3.13: An example of Star3’s counters**

	<b>First Input Register</b>	<b>Second Input Register</b>	<b>Third Input Register</b>
Address	#40003	#40004	#40005
Format	Mantissa BCD	Mantissa BCD	Mantissa BCD
Carry (Hex.)	0x0111	0x2222	0x3333
(Binary)	0   00100010001		
(Hex.)	+   0x0111		
Represent (Dec.)	+111 2222		.3333

### 3.3.1.2. Read Holding Register

The ‘Read Holding Register’ with a function code of 0x03, is a function used to read the Star3 programmable settings such as the current transformer ratio (CTratio) in register #30001, the voltage transformer ratio (VTratio) in register #30002 and the demand integration time in register #30003. The settings are encoded in BCD and are stored as integer value at a distinctive holding register. If the value in the holding register is 0x000A, the setting is then

equaled to 10. Similarly, if the value in the holding register is 0x0010, the setting of the programming operation is then 16.

### 3.3.1.3. Read Output Status

The ‘Read Output Status’ (or ‘Read Coils’) with a function code of 0x01, is a function used to read the status of Star3’s digital output coils such as the ‘Reset all energy counters?’ (at register #00005), the ‘General reset of the meter?’ (at register #00006) and the ‘Reset maximum power demand?’ (at register #00007). The coils statuses are encoded in BCD and are packed as one bit per coil. Bit ‘0’ indicates an ‘OFF’ state and bit ‘1’ an ‘ON’ state. The coils statuses are interpreted by looking at each of the bit in a byte, where the LSB correspond to the status of the first coil, the next bit then correspond to the status of the next coil and so forth. For instance, as shown in Table 3.14, if 10 coils statuses are requested and 0x030F or binary of 0000 0011 0000 1111 is returned, then the coil #1, #2, #3, #4, #9 and #10 are ‘ON’ and the rest from coil #5 to #8 are ‘OFF’. The higher end bits are ignored because only 10 coils statuses are requested.

**Table 3.14: An example of Star3’s digital output**

	1st Byte								2nd Byte							
(Hex)	0				3				0				F			
(Bin)	0	0	0	0	0	0	1	1	0	0	0	0	1	1	1	1
Coil	X	X	X	X	X	X	#10	#9	#8	#7	#6	#5	#4	#3	#2	#1

#### 3.3.1.4. Preset Single Register

The 'Preset Single Register' (or 'Write Single Register') with a function code of 0x06, is a function used to program (or pre-set) the Star3's settings that are stored in distinctive holding registers. The value of the setting is BCD and it is packed as 2-byte per register. If the setting is required to be updated to 1234, then the upper-byte would contain the first datum of 0x12 and the lower-byte would carry the second datum of 0x34.

Programmatically, the settings of CTratio (in register #30001) and VTratio (in register #30002) can only be updated and cannot be overwritten. This is because Star3 only allowed the user to update the ratio and does not have the feature to modify the transformer's primary or secondary value. However, as long as the Star3 is powered ON or the on-panel setting (PAG.+SEL.) buttons are not pressed, the updated setting will remain. Once any of the two conditions is not satisfied, the setting will revert back to the ratio specified by the transformer's primary and secondary values that are configured on the meter. For instance, the primary and secondary voltage transformer values are 100/100, or equivalent to VTratio of 1. If the turn ratio is set programmatically to 10, the VTratio will be updated to 10, but the setting of voltage transformer values at the primary and secondary side are still 100/100. The VTratio will remain as 10 as long as Star3 is still powered ON or its' on-panel setting buttons are not pressed. If either of the conditions is not satisfied, the VTratio will revert to 1.

### **3.3.1.5. Force Single Coil**

The 'Force Single Coil' (or 'Write Single Coil') with a function code of 0x05, is a function used to program (or force) a single Star3's output coil. A value of 0xFF00 requests the output coil to be ON (or conducting current), whereas a value of 0x0000 requests it to be OFF (or not conducting). All other values are invalid and will not change the output.

### **3.3.2. Star3 Communication System in LabVIEW**

The program or the virtual instrument (VI) of the Star3 communication system is implemented in LabVIEW. LabVIEW is an interface to write higher level coding using graphical programming language. LabVIEW allow the user to develop a user-friendly graphical user interfaces (GUI) and contains built-in library functions for various data acquisition and measurement applications. It contains a front panel and block diagrams, where the GUI is displayed on the front panel and the graphical program called the virtual instrument (VI) is written in the block diagram. LabVIEW is chosen because of its ease of hardware and software integration. LabVIEW also provides the convenience of software customization and visualization for ease of troubleshooting and programming. As a result, LabVIEW provides a shorter time of system integration and development compared to other programming languages such as C, Python and Java.

The flow diagram of the VI, stored in the control unit is shown in Figure 3.20. The corresponding functions of the VIs are described in Table 3.15 and Table 3.16. In this research, two units of Star3 measurement meters are installed, one at KA ground floor and the other at KA mezzanine floor. Respectively, the device address of the meters is 0x01 and 0x02.

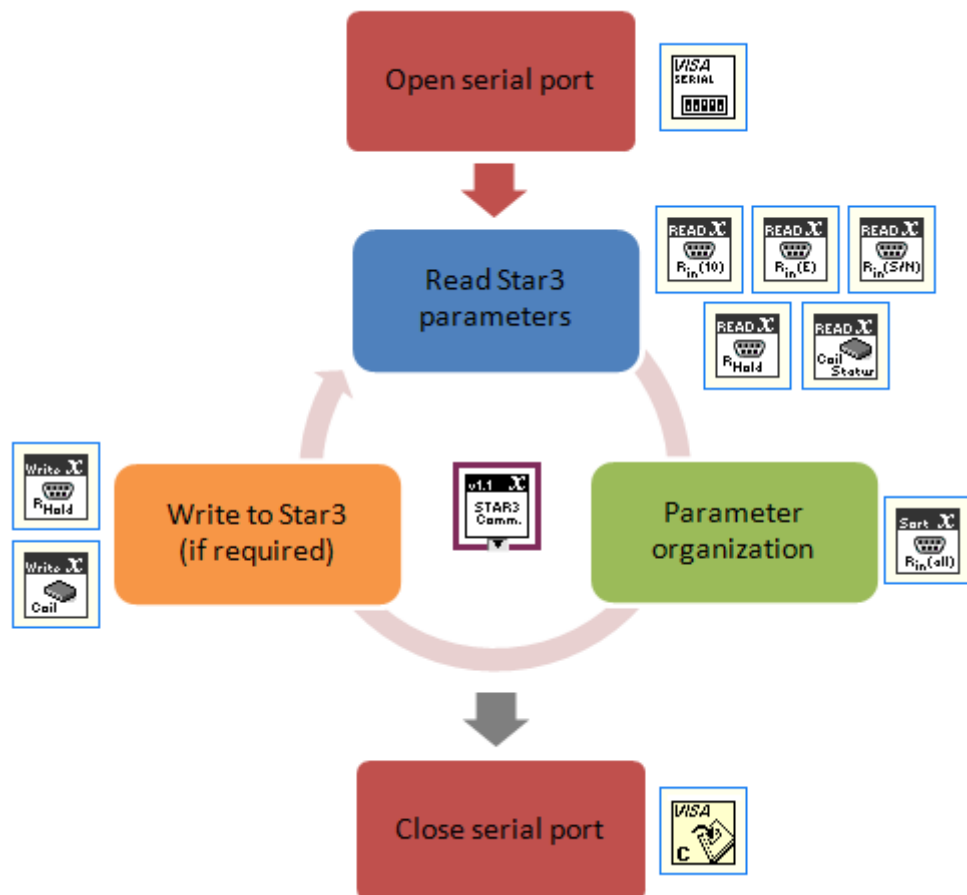


**Figure 3.20: Flow diagram of the Star3 communication system**

The communication between the control unit (the master) and Star3 (the slave) begins by opening the serial port, in which the Star3 is laid on, and initialize the serial port to the specified handshake settings of COM6 port number, baud rate of 19200, 8-bit of data bits, 0-bit of parity bit and 1-bit of stop bits. Once the handshake is established, the VI then moved on to a loop

consisting of the read and write operations. In every loop, the VI performs a read operation to collect the parameters from Star3 such as the measurements, the counters, the coils statuses and others. After that, the acquired data are then sorted and organized into groups for better data presentation. If writing is required to program the meter settings or trigger an output coil, the VI then initiate a write function before the loop is repeated. The communication with Star3 repeats until an error occurred and the VI closes the serial port, display the error message and stop the VI.

#### **3.3.2.1. The Read Function VI**

The VI of the read operation is depicted in Figure 3.21. The master's ADU or the master's request frame is constructed first by concatenating the Star3's device address, the PDU and the CRC. The ADU is then transmitted serially to Star3 to request for the specified data. A wait block is inserted in between to provide sufficient time for Star3 to process the request and acquire the data. After that, Star3 then response with a slave's ADU to acknowledge the actions has been performed. The slave's ADU then goes into an error-check function to verify the credibility of the message. If no error is found, the slave's ADU is then decoded into the respective data requested. If an error is detected, the VI will skip the decoding process and report the error.

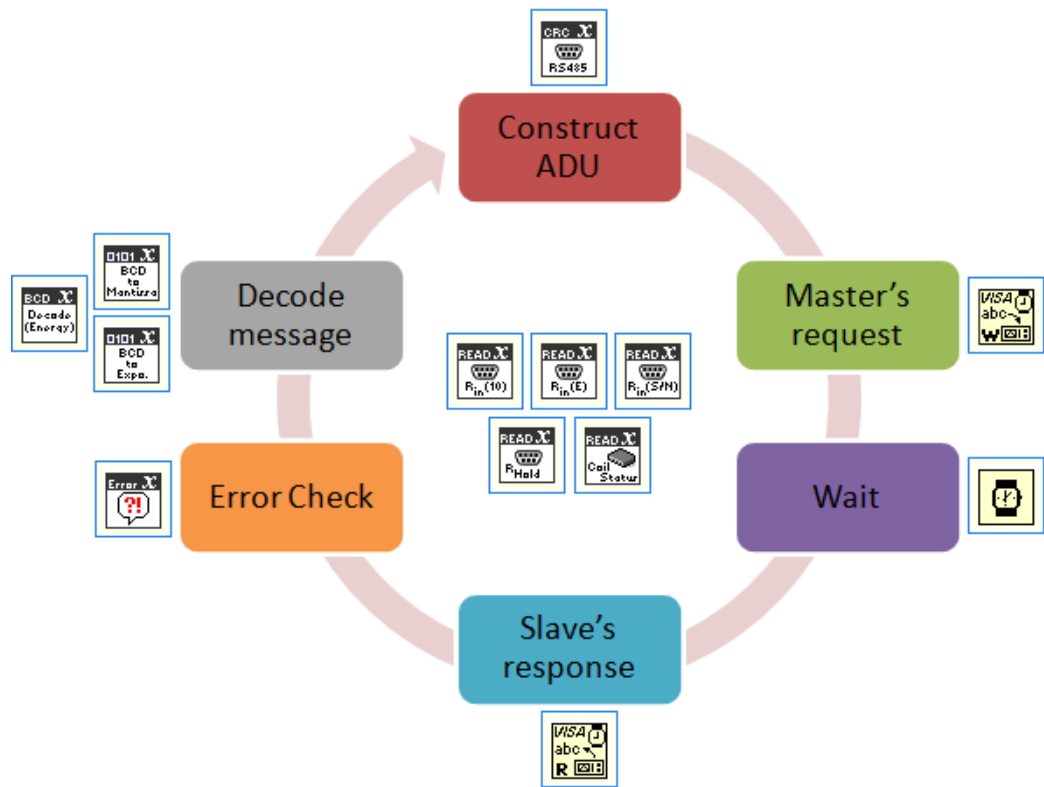


**Figure 3.21: Flow diagram of the Star3 read function**

### 3.3.2.2. The Write Function VI

The VI of the write operation is displayed in Figure 3.22. Likewise to the read operation, the write operation constructs the master's ADU first and then transmit the write function serially to program the specific settings or status of the output coils in Star3. A wait block is also inserted to provide sufficient time for Star3 to update the settings or the output coils statuses. Star3 then response with a slave's ADU when the update has been made and the slave's ADU is diagnosed by the error-check function. A success in writing to Star3 is indicated when no error is found. If an error is detected, the VI will reinitiate another write on the next loop. If the error persists, the VI then skip the operation and report the error.

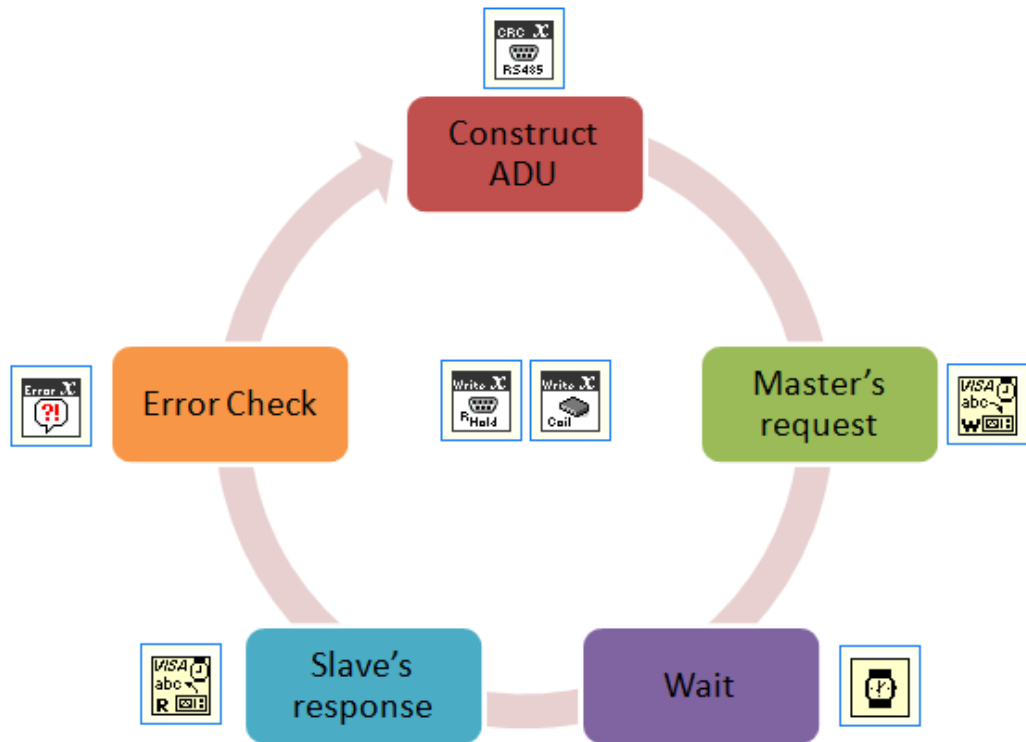


**Figure 3.22: Flow diagram of the Star3 write function**

### 3.3.2.3. The Error Check VI

The Error Check VI consists of three layers of error verification. Before the verification, the slave's ADU is first being partitioned into the respective field consisting of the slave address, the function code, the data and the CRC. The first layer then checks if the slave's ADU is from the specified slave queried. The error will be reported if the slave's address encoded in the ADU is not from the requested slave. The second layer then conducts a test to verify if the CRC framed in the slave's ADU is tallied or not. An error will be reported if the CRC encoded in the ADU is incorrect. Lastly, the third layer then analyzes the function code in the slave's ADU. The function code of the slave's ADU should be the same as the master's ADU. If the function code is not the same,

then the slave's ADU returns an invalid function code and error will be reported.

**Table 3.15: List of Star3 communication systems' main VIs**

Virtual Instruments	Functions of the Virtual Instruments
 (a)  (b)  (c)	<p>These VIs perform the function code of 0x04 to read the input registers in Star 3. (a) Retrieve the measurements data, (b) collect the counters value and (c) fetch the device serial number.</p>
	<p>This VI performs the function code of 0x03 to read the holding registers, wherein the Star3 settings are stored.</p>
	<p>This VI performs the function code of 0x01 to read the status of the digital output coils in Star3.</p>
	<p>This VI performs the function code of 0x06 to program (or pre-set) the settings of Star3 in which are stored at different holding registers.</p>
	<p>This VI performs the function code of 0x05 to program (or force) the digital output coils in Star3.</p>
	<p>This VI organizes the data of input registers for better data presentation. The data includes the measurements, the counters, and the device serial number.</p>
	<p>This VI set-up the serial connection with Star3 at the designated COM port and the specified handshake parameters such as the baud rate, the parity bit and others.</p>
	<p>This VI closes the serial connection with Star3.</p>

**Table 3.16: List of Star3 communication systems' subVIs**

Virtual Instruments	Functions of the Virtual Instruments
	This VI read the measurements' mantissa BCD and decodes (or interprets) the data into the integer of the measurements' floating value.
	This VI read the measurements' exponent BCD and decodes (or interprets) the data into the number of decimal points of the measurements' floating value. The measurements' floating value is also constructed in this VI.
	This VI read the counters' mantissa BCD and decodes the data into the counters' floating value.
	This VI reads the Star3 device address, the PDU, computes the CRC and produces the ADU.
	This VI performs the error check on the slave's response frame.
	This VI writes the master's ADU or requesting frame to Star3.
	This VI reads the slave's ADU or responding frame from Star3.
	This VI waits for the specified number of milliseconds.

### **3.4. SI8.0H Communication System**

The communication system of the SI8.0H bi-directional power converter is implemented based on the messaging structure of Modbus TCP (see Section 3.2.2) and the Modbus message is transmitted through the Local Area Network (LAN) connected with Speedwire Ethernet. There is a total of five types of Modbus functions available in SI8.0H, namely the ‘Read Holding Registers’, the ‘Read Input Register’, the ‘Write Single Register’, the ‘Write Multiple Registers’, and the ‘Read Write Multiple Registers’. The operation of the function code is the same as described in Section 3.2.4 and it is not repeated here.

Readers are advised to refer to the technical documents (SMA, 2016, 2015a, 2015b) for all the Modbus registers (or Modbus profile) that are available in SI8.0H. Readers are also to take note that the writable Modbus registers that can be changed (or modified) are intended for long-term storage and cyclical changing (or writing) of the register may lead to damage of the flash memory in SI8.0H. Special attention is hence needed when changing the writable Modbus registers, especially those that are labeled as non-cyclic type (or the device parameters that are programmable). Apart from that, the communication with SI8.0H is also only possible after its Modbus interface is activated. The Modbus interface (or the TCP server) is deactivated by default and can be activated by means of setting the Modbus server via the SI8.0H Sunny Remote Control or with SMA Sunny Explorer (see document SMA, 2015a section 4).

### **3.4.1. SI8.0H SMA Data Type and Format**

The data interpretation process in SI8.0H follows the specific data type and format that is defined by SMA. There are a total of 13 kinds of data formats in SI8.0H, namely the 'Duration', the 'DT', the 'ENUM' & 'FUNCTION\_SEC', the 'FIX', the 'FW' & 'HW', the 'IP4' & 'UTF8', the 'REV', the 'RAW', the 'TEMP' and the 'TM'. Each of the data formats can be represented with data type of a 16-bit signed word (S16), a 32-bit signed double word (S32), a 32-byte data field in UTF8 format (STR32), a 16-bit unsigned word (U16), a 32-bit unsigned double word (U32), or a 64-bit unsigned quadruple word (U64).

#### **3.4.1.1. Data with format of 'Duration'**

The data format of 'Duration' represents the time elapse in the form of Day, Hour, Minute and Second. It is stored in seconds with the data type of U32. For a data 'Duration' of 0x00008750 (or 34640) seconds, the time elapse (or duration) would be interpreted as 0 Day 9 Hour 37 Minute 20 Seconds. Shown in Table 3.17, the Day is computed as the quotient when the data of 34640 seconds is divided by 86400 seconds/day. The remainder is then used to calculate the Hour and the Minute respectively by dividing the remainder with 3600 seconds/hour and 60 seconds/minute. And the remaining is the Second.

**Table 3.17: An example of SI8.0H data with format of ‘Duration’**

<b>Dividend</b>	<b>Divisor</b>	<b>Remainder</b>	<b>Quotient, unit</b>
34640	86400	34640	0, day
34640	3600	2240	9, hour
2240	60	20	37, minute
20	1	0	20, second

### **3.4.1.2. Data with format of ‘DT’**

The data format of ‘DT’ represents the date in the form of Day, Month and Year. It is stored in seconds with a data type of U32, computed since the baseline of 01-01-1970. For ‘DT’ data of 0x572E8180 (or 1462665600) seconds, the date would be interpreted as Day 7 Month 5 Year 2016 (or 07-05-2016). Shown in Table 3.18, the number of days is first obtained by dividing the data of 1462665600 seconds with 86400 seconds/day. The number of days is then divided by 1461 days/leap cycle to obtain the quotient as the number of leaped years (in cycle) since the baseline of 01-01-1970. The remainder of 857 days is then divided by 365 days/year to calculate the additional number of years after the leap cycled years. The remaining of 127 days is then used to compute the date from day 1 month 1. In this example, the number of leap cycle since 01-01-1970 is 11 cycles (or 44 years) and there are additional 2 years after the leap cycled years. The year since 1970 is thus 2016 (1970 + 44 + 2) and because 2016 is a leap year, 127 days from 01-01-2016 hence result in the date of 07-05-2016.

**Table 3.18: An example of SI8.0H data with format of ‘DT’**

<b>Dividend</b>	<b>Divisor</b>	<b>Remainder</b>	<b>Quotient, the representation</b>
1462665600	86400	0	16929, days since 01-01-1970
16929	1461	857	11, cycles of leaped years since 1970 (or 44 years since 1970)
857	365	127	2, years addition to the 44 years since 1970 (or 46 years since 1970)
127	1	0	127, days from day 1 month 1

### 3.4.1.3. Data with format of ‘ENUM’ or ‘FUNCTION\_SEC’

The data format of ‘ENUM’ represents the annotation of a specific message that is stored as numerical values with the data type of U32. It formats the message in the form of numerical values and it is interpreted based on a specific list specified in the designated Modbus register in the SMA Modbus profile assignment table. Using the list as shown in Table 3.19, for ‘ENUM’ data of 0x00001F40 (or 8000), the message would be interpreted as “All devices”, while 0x00001F80 (or 8064) would be interpreted as “Sensor technology general” and so forth. Alike the data format of ‘ENUM’, the data format of ‘FUNCTION\_SEC’ is also formatted and interpreted in a similar fashion.

**Table 3.19: An example of SI8.0H data with format of ‘ENUM’**

<b>Hexadecimal</b>	<b>Decimal</b>	<b>Defined as</b>
0x00001F40	8000	All devices
0x00001F41	8001	PV inverter
0x00001F42	8002	Wind power inverter
0x00001F47	8007	Battery inverter
0x00001F61	8033	Load
0x00001F80	8064	Sensor technology general

#### 3.4.1.4. Data with format of ‘FIX’

The data format of ‘FIX’ represents the floating value stored as the data type of S16, S32, U16, U32 or U64. The floating value is formatted as a rounded decimal number without a decimal place (FIX0) or with one (FIX1), two (FIX2) or three (FIX3) decimal places. Shown in Table 3.20 are the examples of SI8.0H data with format of ‘FIX’. For ‘FIX3’ data of 0xA111 (or +41233), the floating value would be interpreted as 41.233. The same floating value is also obtained for U32 of 0x0000A111, U64 of 0x000000000000A111 and S32 of 0x0000A111. However, for S16 data of 0xA111 (or -24303), the floating value is interpreted as -24.303. This is because S16 is signed and the data is two’s complemented before it is interpreted. Prior to the data interpretation, the two’s complement process is also applied to the data type of S32.

**Table 3.20: An example of SI8.0H data with format of ‘FIX’**

	Floating Value			
	FIX0	FIX1	FIX2	FIX3
U16 of 0xA111	+41233	+4123.3	+412.33	+41.233
U32 of 0x0000A111				
U64 of 0x000000000000A111				
S16 of 0xA111	-24303	-2430.3	-243.03	-24.303
S32 of 0x0000A111	+41233	+4123.3	+412.33	+41.233

#### 3.4.1.5. Data with format of ‘FW’ or ‘HW’

The data format of ‘FW’ and ‘HW’ represents the firmware and hardware version in the form of the Major, the Minor, the Build and the Release Type. It is stored in the data type of U32 and each of the prefixes is 1-byte length. The

Major, the Minor, and the Release Type are coded in BCD, while the Build is not BCD coded. Shown in Table 3.21, for ‘FW’ data of 0x01100C04, the data would be interpreted as FW (or HW) version of Major 01 (0x01), Minor 10 (0x10), Build 12 (0x0C) and Release Type 04 (0x04).

**Table 3.21: An example of SI8.0H data with format of ‘FW’**

	<b>1st Byte</b>	<b>2nd Byte</b>	<b>3rd Byte</b>	<b>4th Byte</b>
Data Received	0x01	0x10	0x0C	0x04
Represents	Major 01	Minor 10	Build 12	Release Type 04
BCD coded?	YES	YES	NO	YES

#### **3.4.1.6. Data with format of ‘IP4’ or ‘UTF8’**

The data format of ‘IP4’ represents the internet protocol address (IPv4) in the form of AAA.BBB.CCC.DDD and it is stored as the data type of STR32. It is coded in ASCII and for ‘IP4’ data of 0x3136392E3235342E3139302E3537, the data would be interpreted as IPv4 of 169.254.190.57. Shown in Table 3.22, the first byte on the left, 0x31 represents the character of ‘1’ in ASCII, The subsequent byte, 0x36 then represents the character of ‘6’, 0x39 represents the character of ‘9’, 0x2E represents the character of ‘.’ and so forth. Alike the data format of ‘IP4’, the data format of ‘UTF8’ is also interpreted in a similar fashion.

**Table 3.22: An example of SI8.0H data with format of ‘IP4’**

	<b>1st Byte</b>	<b>2nd Byte</b>	<b>3rd Byte</b>	<b>4th Byte</b>	<b>5th Byte</b>	<b>6th Byte</b>	<b>7th Byte</b>
(Hex)	0x31	0x36	0x39	0x2E	0x32	0x35	0x34
(ASCII)	‘1’	‘6’	‘9’	‘.’	‘2’	‘5’	‘4’

	<b>8th Byte</b>	<b>9th Byte</b>	<b>10th Byte</b>	<b>11th Byte</b>	<b>12th Byte</b>	<b>13th Byte</b>	<b>14th Byte</b>
(Hex)	0x2E	0x31	0x39	0x30	0x2E	0x35	0x37
(ASCII)	‘.’	‘1’	‘9’	‘0’	‘.’	‘5’	‘7’

#### **3.4.1.7. Data with format of ‘REV’**

The data format of ‘REV’ represents the revision number in the form of A.B.C.D, stored as the data type of U32. Unlike the data format of ‘FW’ & ‘HW’, the data format of ‘REV’ is entirely coded in BCD. For U32 data of 0x03041507, the data would be interpreted as revision number of 03.04.15.07.

#### **3.4.1.8. Data with format of ‘RAW’**

The data format of ‘RAW’ represents the serial number (or ID) stored in the data type of U32. Alike the data format of ‘FIX0’, the serial number is formatted as a numerical value with no separation indicators (or no decimal place). For U32 data of 0x4B29A1DF, the data would be interpreted as a serial number of 1261019615.

#### **3.4.1.9. Data with format of ‘TEMP’**

The data format of ‘TEMP’ represents the temperature values stored in the data type of S32. Alike the data format of ‘FIX1’, the temperature data is formatted as a floating value with one decimal place. For S32 data of 0x00000113 (or +275), the data would be interpreted as the temperature of +27.5 °C. If the S32 data is 0xFFFFF9C (or -100), the temperature is then -10.0 °C.

#### **3.4.1.10. Data with format of ‘TM’**

The data format of ‘TM’ represents the UTC time in the form of Hour, Minute and Second. It is stored in seconds with a data type of U32. Alike the data format of ‘Duration’, the Hour is computed by dividing the ‘TM’ data with 3600 seconds/hour. The remainder is then divided by 60 seconds/ minute to obtain the Minute. The remaining then represents the Second. For ‘TM’ data of 0x00008750 (or 34640), the UTC time would be interpreted as Hour 9 Minute 37 and Second 20 (or 09:37:20).

### 3.4.2. SI8.0H Communication System in LabVIEW

The program (or the VI) of the SI8.0H communication system is implemented in LabVIEW. The flow diagram of the VI, stored in the control unit is shown in Figure 3.23 and the corresponding functions of the VIs are described in Table 3.30 and Table 3.31.

The VI begins by opening the TCP/IP connection on the Modbus reserved port of 502, with the SI8.0H specified by the IPv4 addresses of 169.254.190.2, 169.254.190.3 and 169.254.190.4. The VI then moved on to initialize the SI8.0H by activating the Grid Guard mode, enabling the system control and configuring the feed-in limits.

Once the initialization process is completed, the VI then proceeds to a loop consisting of the 'read', the 'update', the 'write' and the 'reinitialize' states. The 'read' state retrieves the battery measurements, the inverter measurements and the device statuses for supervision and control purposes. The 'update' state then check the device settings and if required, the VI will update the settings to the specified value. Followed by, the 'write' state then initiate the control command to the SI8.0H. Before the loop is repeated, if the Grid Guard mode or the feed-in mode is deactivated, the VI then reinitializes the SI8.0H at the 'reinitialize' state. After that, the loop repeats until an error occurs or a stop command is initiated. If an error occurs in between the operation, the VI will close the TCP/IP connection, display the error message and stops the VI.

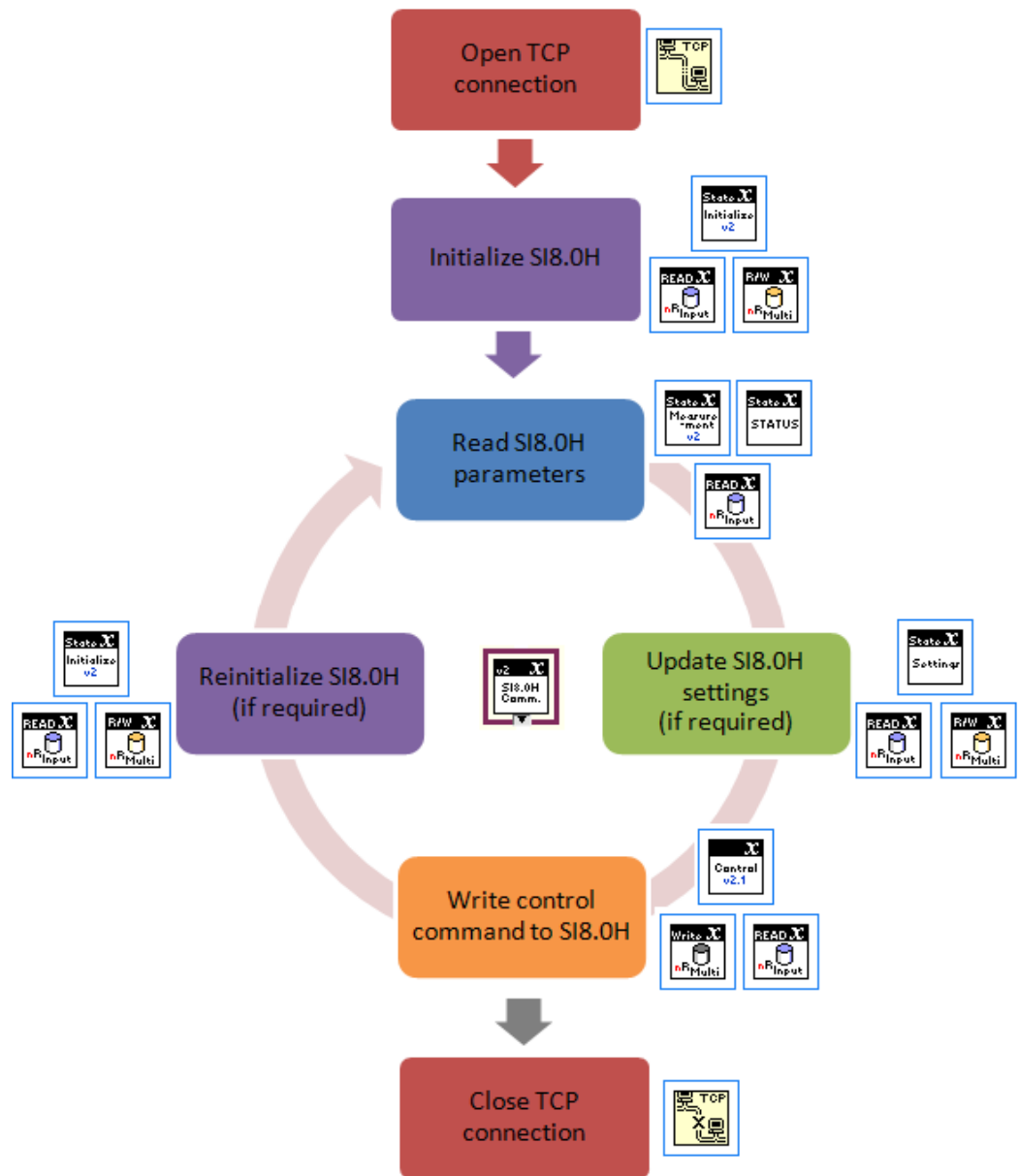


**Figure 3.23: Flow diagram of the SI8.0H communication system**

### 3.4.2.1. The Grid Guard Mode

Certain Modbus registers (see document SMA, 2015a section 5.3) in SI8.0H are password protected by the SMA Grid Guard code (GGC). Given in Table 3.23, to read or write to the Modbus registers that are protected, the Grid Guard mode must first be unlocked (or activated) by writing the unique GGC

to the register at Modbus register #43090. This register can be written cyclically without causing damage to the memory. A 1 would be returned if the SI8.0H is logged in with the GGC. If a 0 is received, this implies the SI8.0H is not logged in with the GGC and the GGC is required to be retransmitted. Reactivation of the Grid Guard mode is also necessary after a time lapsed of 30 minutes or if the SI8.0H is restarted. A manual (or explicit) log out from the Grid Guard mode is also possible by writing the register #43090 with 0.

**Table 3.23: The SI8.0H grid guard mode Modbus register**

<b>Register</b>	<b>Short description</b>	<b>Data Type</b>	<b>Data Format</b>	<b>Access</b>
#43090	SMA Grid Guard code	U32	FIX0	RW

#### **3.4.2.2. The System Control**

In SI8.0H, by default, the reactive power setting is disabled and the active power setting is automatic and it is determined based on the Battery Management System (BMS). The feed-in mode must first be activated before a system control of the SI8.0H power setting (active or reactive) can be initiated. Listed in Table 3.24, the feed-in mode can be unlocked by writing a value of 802 (or 0x00000322) to the register of #40151, which can be written cyclically without causing damage to the memory. A manual (or explicit) deactivation of the feed-in mode is also possible by writing the register #40151 with 803 (or 0x00000323). In addition, the state of the system control can be verified via the register #30825 and register #30835. If the system control is activated, the value of 1072 (or 0x00000430) should be returned

from the register #30825 and the value of 1079 (or 0x00000437) from the register #30835.

**Table 3.24: The SI8.0H system control Modbus registers**

<b>Register</b>	<b>Short Description</b>	<b>Data Type</b>	<b>Data Format</b>	<b>Access</b>
#40151	Eff./reac. pow. contr. via comm.	U32	ENUM	WO
#30825	Operating mode of the reactive power control	U32	ENUM	RO
#30835	Operating mode of active power limitation	U32	ENUM	RO

### **3.4.2.3. The Feed-in Limits**

A lower and upper feed-in limit is available in SI8.0H to protect the batteries from deep discharging. The lower feed-in limit specifies the lower SOC in which the SI8.0H can arrive before the inverter is locked (or stopped) from discharging further. That is, once the batteries' SOC is lower than the lower feed-in limit, the SI8.0H will be stopped from discharging, wherein the power output is clamped at zero, and only charging is possible. Consequently, after the SI8.0H is locked from the lower feed-in limit, the SI8.0H is only allowed (or permitted) to discharge again when the batteries' SOC is above the upper feed-in limit. Listed in Table 3.25, the lower feed-in limit and the upper feed-in limit can be set through the register #40705 and register #40707. These registers cannot be written cyclically. Repetitive changing of these limits should be avoided. In this research, the lower limit is set at 50% and the upper limit is set at 55%.

**Table 3.25: The SI8.0H feed-in limits Modbus registers**

<b>Register</b>	<b>Short description</b>	<b>Data Type</b>	<b>Data Format</b>	<b>Access</b>
#40705	Upper SOC for reactivating of grid feed-in (%)	U32	FIX0	RW
#40707	Lower SOC for locking grid feed-in (%)	U32	FIX0	RW

**3.4.2.4. The ‘Read’ State**

Listed in Table 3.26 are the Modbus registers used in the ‘Read’ state. This state retrieves the battery measurement parameters such as the battery current in register #30843 and battery state-of-charge in register #30845. This state also collects the inverter measurement parameters such as the inverter active power in register #30775 and inverter voltage in register #30783. Besides that, the SI8.0H statuses such as the device condition in register #30201 and the active battery charging mode in register #30853 are also acquired. If required, in this state, the VI can also retrieve the IP addresses such as the current Speedwire IP address in register #31017 and current Speedwire DNS server address in register #31041.

**Table 3.26: Modbus registers which are used in the ‘Read’ state**

<b>Register</b>	<b>Short Description</b>	<b>Data Type</b>	<b>Data Format</b>	<b>Access</b>
#30843	Battery current (A)	S32	FIX3	RO
#30845	Current battery state of charge (%)	U32	FIX0	RO
#30775	Active power (W)	S32	FIX0	RO
#30783	Grid voltage phase L1 (V)	U32	FIX2	RO
#30201	Status of the device	U32	ENUM	RO
#30853	Active battery charging mode	U32	ENUM	RO
#31017	Current Speedwire IP address	STR32	UTF8	RO
#31041	Current Speedwire DNS server address	STR32	UTF8	RO

### 3.4.2.5. The ‘Update’ State

Listed in Table 3.27 are the Modbus registers used in the ‘Update’ state. This state checks the device settings by first retrieving the settings such as the manual control of network connection in register #40527, the BMS operating mode in register #40236 and the manual equalization charge in register #40533, and if required, this operation will update the settings to the value specified by the user. These registers should not be written cyclically. Repetitive changing of these registers may damage the flash memory.

**Table 3.27: Modbus registers which are used in the ‘Update’ state**

<b>Register</b>	<b>Short Description</b>	<b>Data Type</b>	<b>Data Format</b>	<b>Access</b>
#40527	Manual control of network connection	U32	ENUM	RW
#40236	BMS operating mode	U32	ENUM	WO
#40533	Manual equalization charge	U32	ENUM	RW

### 3.4.2.6. The ‘Write’ State

Listed in Table 3.28 are the Modbus registers used in the ‘Write’ state. This state writes the control command to SI8.0H. Once the feed-in mode (#40151) is unlocked, the active power and the reactive power can be set via the register #40149 and register #40153. These registers can be written cyclically without causing damage to the memory and the time to reach the desired power after sending a power setting to SI8.0H is around 1kW/s (or 1kVAr/s). The power setting must be written repeatedly. A time out after 60 minutes would occur if the power setting gets no refresh. Subsequently, the feed-in mode will be

stopped and the register #40151 will change from 802 to 803 (or 0x00000323). This timeout feature is to ensure a defined fall-back behavior to take place in case the communication is interrupted. Furthermore, the active power and reactive power settings can be read from register #30775 and register #30805.

**Table 3.28: Modbus registers which are used in the ‘Write’ state**

<b>Register</b>	<b>Short Description</b>	<b>Data Type</b>	<b>Data Format</b>	<b>Access</b>
#40149	Active power setpoint (W)	S32	FIX0	WO
#40153	Reactive power setpoint (VAr)	S32	FIX0	WO
#30775	Active power (W)	S32	FIX0	RO
#30805	Reactive power (VAr)	S32	FIX0	RO

#### 3.4.2.7. The ‘Reinitialize’ State

If required, this state reinitializes the SI8.0H to reactivate the Grid Guard mode and enables the system control for feed-in operation. The Modbus registers that are involved in this state is listed in Table 3.29.

**Table 3.29: Modbus registers which are used in the ‘Reinitialize’ state**

<b>Register</b>	<b>Short Description</b>	<b>Data Type</b>	<b>Data Format</b>	<b>Access</b>
#43090	SMA Grid Guard code	U32	FIX0	RW
#40151	Eff./reac. pow. contr. via comm.	U32	ENUM	WO

#### 3.4.2.8. The Read Function VI

The VI of the read function such as the read holding registers (0x03), the read input registers (0x04) or the read and write multiple of input registers (0x17),

is shown in Figure 3.24. The control unit's ADU or the client's request frame is first constructed by concatenating the Transaction Identifier, the Protocol Identifier, the Length Field, the Unit Identifier, and the PDU. The ADU is then transmitted via the TCP/IP to the SI8.0H, to request for the specific data to be returned. The SI8.0H then response with a server's ADU, containing the data requested or the acknowledgement of the actions being performed. The server's ADU received by the control unit then goes into an error-check function to verify the credibility of the message. If no error is detected, the control unit then proceeds to decode the message (or server's ADU) from SI8.0H. If an error is detected, the VI will skip the decoding process and report the error status.

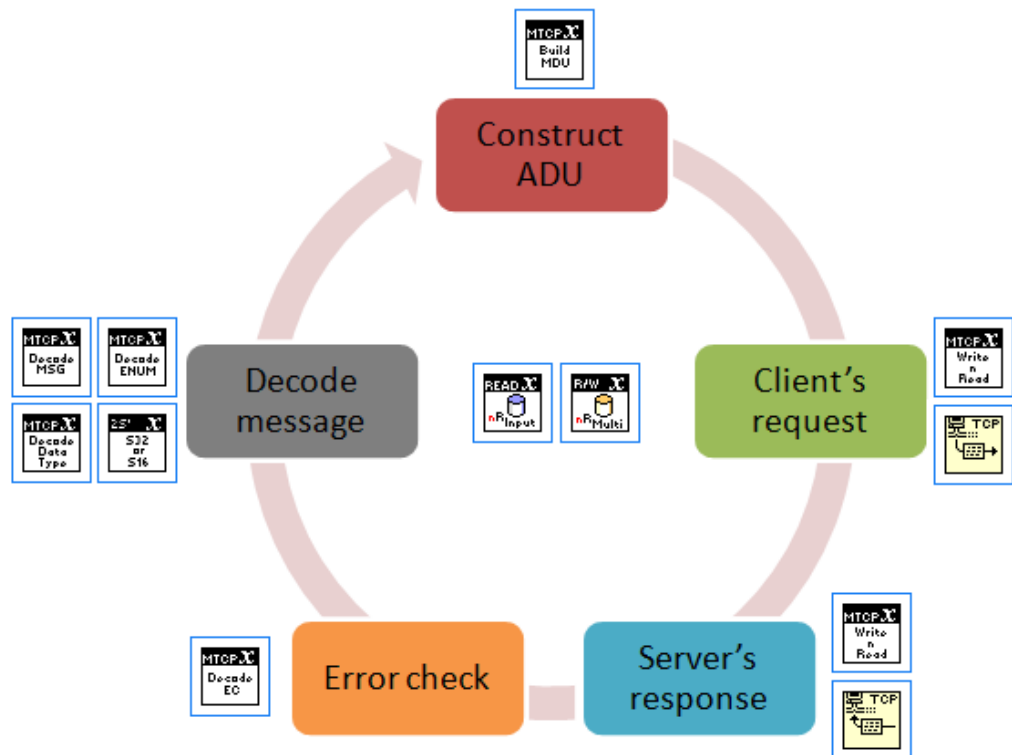


**Figure 3.24: Flow diagram of the SI8.0H read function**

### 3.4.2.9. The Write Function VI

The VI of the write function such as the write single register (0x06) and the write multiple registers (0x10), is shown in Figure 3.25. Likewise to the read function, the write function also construct the control unit's ADU first and then transmit the TCP message via TCP/IP to program the specific settings in SI8.0H. Once the SI8.0H processed the request, the SI8.0H then response with a server's ADU, to acknowledge the actions has being performed. The server's ADU then passes through the error-check function and if an error is detected, the VI will report the error status and reinitiate another write function on the next loop.

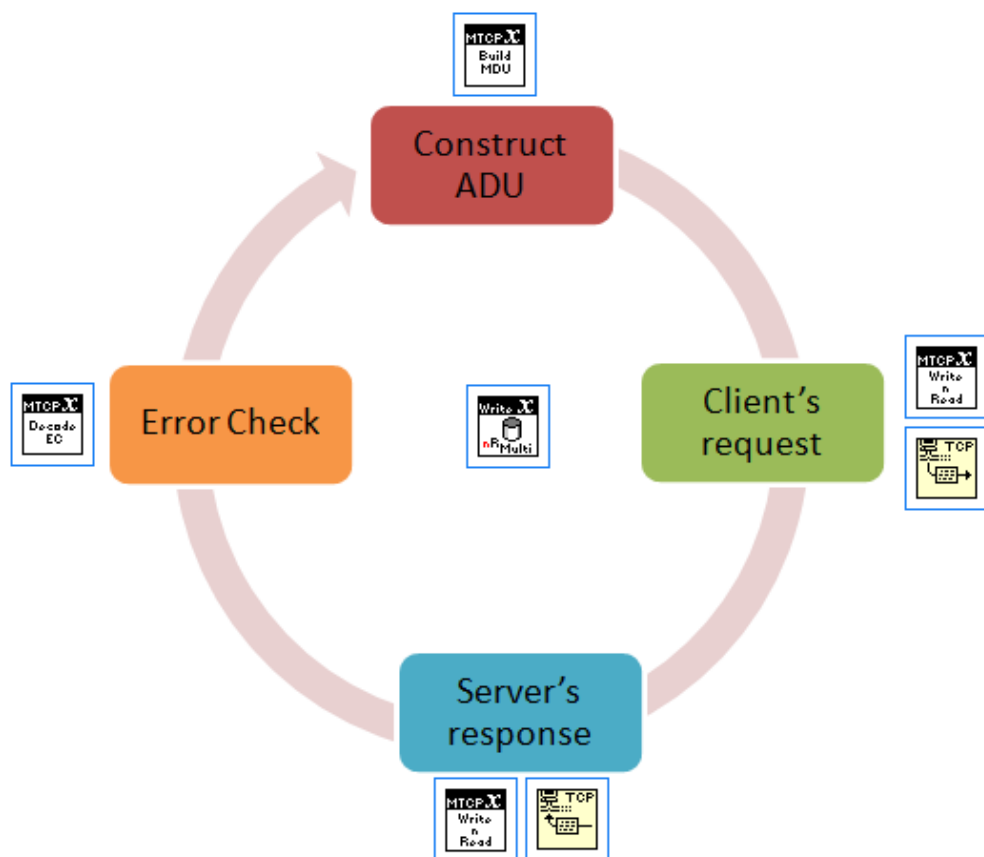


Figure 3.25: Flow diagram of the SI8.0H write function

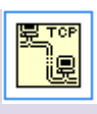
#### **3.4.2.10. The Error Check VI**

The error-check function is based on the exception response described in Section 3.2.4 and the decoding of the TCP message receipt from SI8.0H, followed the interpretation process listed in Section 3.4.1. In this research, the Transaction Identifier and the Protocol Identifier are set to 0x0000. The Unit Identifier, used to identify the server device of SI8.0H, is set to the SMA specified default value of 0x03. Unlike the standard addressing method described in Section 3.2.3, where the data address (part of the PDU field) is offset by 1 and the reference address is omitted, the Modbus registers in SI8.0H does not offset its address by 1 and the reference address is also retained. The SI8.0H addresses followed the specification specified by SMA and for Modbus register of #30057, the data address would be 0x7569 rather than 0x0038 (or 30056).

**Table 3.30: List of SI8.0H communication systems' main VIs**

Virtual Instruments	Functions of the Virtual Instruments
	<p>This VI initializes the SI8.0H by logging in (or re-log in) the Grid Guard mode at register #43090. This VI then activates (or reactivate) the system control at register #40151. If required, this VI can also write (or pre-set) the SI8.0H feed-in limits at register #40705 and register #40707.</p>
	<p>This VI reads the SI8.0H battery measurements (such as the battery current in register #30843 and battery state-of-charge in register #30845) and inverter measurements (such as the inverter active power in register #30775 and inverter voltage in register #30783).</p>
	<p>This VI reads the SI8.0H statuses such as the device condition in register #30201 and the active battery charging mode in register #30853. If required, this VI can also retrieve the IP addresses such as the current Speedwire IP address in register #31017 and current Speedwire DNS server address in register #31041.</p>
	<p>This VI reads the SI8.0H settings such as the manual control of network connection in register #40527 and the BMS operating mode in register #40236. If required, this VI can also be used to write (or pre-set) the settings.</p>
	<p>This VI writes the power setting to the SI8.0H at register #40149 for active power control and at address #40153 for reactive power control.</p>
	<p>This VI performs the function code of 0x03 to read the input registers in SI8.0H, where the battery measurements, inverter measurements and others are stored. This VI can also be used to perform the function code of 0x04, to read the holding registers in SI8.0H, where the device settings are stored.</p>

**(Table 3.30 Continued.)**

Virtual Instruments	Functions of the Virtual Instruments
	This VI performs the function code of 0x17 to write and read the holding registers in SI8.0H, where the device settings are stored.
	This VI performs the function code of 0x06 or 0x10 to program (or pre-set) the settings of SI8.0H in which are stored in different holding registers.
	This VI set-up the TCP/IP connection with SI8.0H at the designated IPv4 address and Modbus reserved port of 502.
	This VI closes the TCP/IP connection with SI8.0H.

**Table 3.31: List of SI8.0H communication systems' subVIs**

Virtual Instruments	Functions of the Virtual Instruments
	<p>This VI constructs the Modbus Data Unit (MDU) of the Modbus TCP message.</p>
	<p>These VIs are used to transmit and receive the Modbus TCP messages between the control unit (the client) and the SI8.0H (the server). (a) Is the VI containing the write and read function block, (b) writes the client's ADU or the request frame to SI8.0H, and (c) reads the server's ADU or the responding frame from SI8.0H.</p>
	
	
(a)	
(b)	
(c)	
	<p>This VI decode (or interpret) the Modbus TCP message based on the specification described in Section 3.4.1.</p>
	<p>This VI decode (or interpret) the Modbus TCP error message based on the exception codes listed in Table 3.11.</p>
	<p>This VI decode (or interpret) the data format of 'ENUM' (see Section 3.4.1).</p>
	<p>This VI decode (or interpret) the data type of S16, S32, STR32, U16, U32 or U64 (see Section 3.4.1).</p>
	<p>This VI two's compliments the signed data of S32 or S16.</p>

### **3.5. Summary**

In summary, the hardware components and the set-up of the battery-based energy storage system (BESS) have been overviewed. The fundamentals of the Modbus messaging protocol has been introduced as well. Besides that, the frameworks as well as the system implementations of the communication systems in the BESS have also been presented.

## CHAPTER 4

### ACTIVE CONTROL ALGORITHM IN ENERGY STORAGE FOR PEAK REDUCTION

The challenges associated with the battery-based energy storage system in reducing the peak demands are presented in this chapter, followed by the formulation and implementation of the active control algorithm. Next, the fundamental set-point control algorithm is elaborated before the simulation analysis is discussed. The fundamental set-point controller is to be used for comparison in the later chapter to assess how the active adjustment of the threshold can contribute to the peak reduction as well as highlight the importance of planning ahead while performing the peak reduction. The simulation analysis is also to be used in the later chapter as a benchmark to determine how far the experimental results are away from the best possible peak reduction and examine how the discrepancy between the forecasted and the actual loads can affect the ability of the BESS in peak reduction.

#### **4.1. Challenges of Reducing the Peak Demand with Battery-based Energy Storage System**

One of the main challenges in the peak reduction with the BESS is to predict the load profiles accurately. There are numerous load forecasting techniques that are available (Dudek, 2016; Hong and Fan, 2016; Zjavka and Snášel,

2016). However, their prediction results often contain some degrees of uncertainties. No single forecast is best at all intervals (Salis et al., 2014). The peaks of the load profiles can be unexpectedly higher or broader than that of the forecasted ones. Or they can happen much earlier or later than the expected time. For example, the forecasted load profile of a particular day is shown in Figure 4.1(a). With the available amount of energy in BESS ( $E_{\text{BESS}}$ ), the threshold is developed so that the BESS will supply the power to the load when the actual load demand exceeds the threshold. However, if the actual peak becomes broader than the forecasted one such as in Figure 4.1(b), then the peak may not be reduced at all even after all the energy of the BESS has been delivered to the load.

An active control strategy is therefore developed to persistently adjust the threshold throughout the day based on the latest information on the load demand. This approach can then reduce the peak of the actual load profile at the end of the day as shown in Figure 4.1(c). The threshold is computed such that the energy amount above equals to the remaining battery capacity that is available in the BESS. By doing so, the highest peak reduction for every day can be attained.

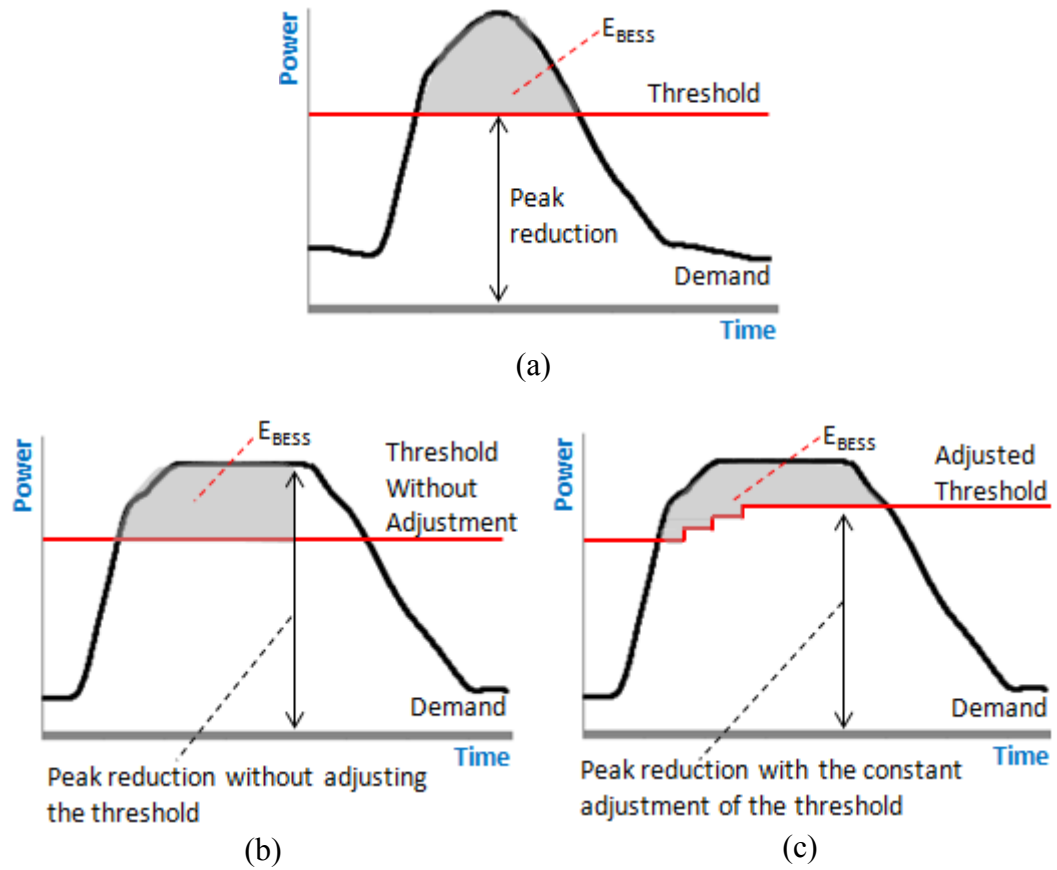


**Figure 4.1: (a) Forecasted load profile with the scheduled threshold, (b) Unsatisfactory peak reduction in the actual load profile with a broad peak and (c) Peak reduction achieved with the active adjustment of the threshold**

## 4.2. Active Control Strategy

The algorithm presented in this section is about how the threshold is constantly adjusted based on the latest information on the load demand. The overview of the active control strategy is described in Figure 4.2. The control strategy begins by forecasting the load profile ( $\mathbf{P}_{Load}^{For}$ ) of the next day ( $d + 1$ ). Based on the forecasted load profile, the control strategy will calculate the amount of the energy (kWh) required from the BESS to supply to the load on the next day and hence determine the threshold ( $\mathbf{P}_{Th}$ ) whereby the BESS is

scheduled to supply the power ( $\mathbf{P}_{\text{BESS}}^{\text{Sch}}$ ) when the demand exceeds the threshold. On the actual day ( $d$ ) of peak reduction, the control algorithm will begin with the supply of the power output from the BESS ( $\mathbf{P}_{\text{BESS}}^{\text{Act}}$ ) which is same as the scheduled power output ( $\mathbf{P}_{\text{BESS}}^{\text{Sch}}$ ) for  $t = 0$ . Then, the real-time load demand ( $\mathbf{P}_{\text{Load}}^{\text{Act}}$ ) is measured and then used to determine the discrepancy ( $\alpha$ ) between  $\mathbf{P}_{\text{Load}}^{\text{Act}}$  and  $\mathbf{P}_{\text{Load}}^{\text{For}}$ , before the new threshold for the next interval ( $t + 1$ ) is determined. As a result, a new schedule is generated for BESS to supply power for the next interval. This new schedule is then used to refine the power output ( $\mathbf{P}_{\text{BESS}}^{\text{Act}}$ ) of the BESS for the next interval. The minimum and maximum power outputs (kW) and storage capacity (kWh) of the BESS are defined in Equation (4.1) and (4.2).

$$-\mathbf{P}_{\text{BESS}}^{\text{max}} \leq \mathbf{P}_{\text{BESS}}^{\text{Act}}(d, t) \leq \mathbf{P}_{\text{BESS}}^{\text{max}} \quad (4.1)$$

$$0 \leq \mathbf{E}_{\text{BESS}}^{\text{Act}}(d, t) \leq \mathbf{E}_{\text{BESS}}^{\text{max}} \quad \equiv \quad 50\% \leq \text{SOC}(d, t) \leq 100\% \quad (4.2)$$

Where,  $\mathbf{P}_{\text{BESS}}^{\text{max}}$  is the power rating (kW) of the BESS,  $\mathbf{P}_{\text{BESS}}$ ;  $\mathbf{E}_{\text{BESS}}^{\text{max}}$  is the energy storage capacity (kWh) of the BESS,  $\mathbf{E}_{\text{BESS}}$ ; and  $\text{SOC}$  is the battery state-of-charge (%).

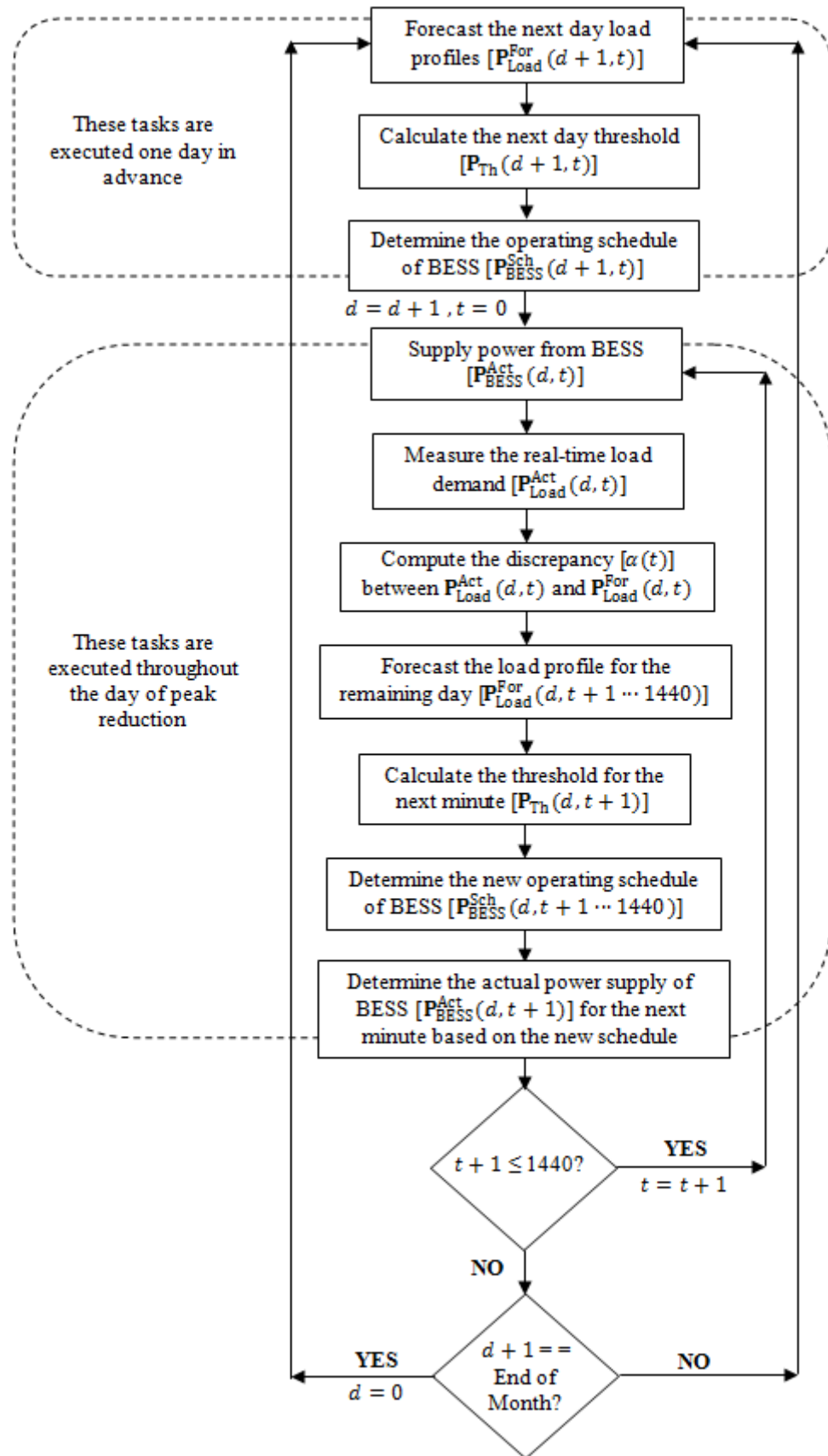


Figure 4.2: The flow chart of the active control strategy

#### **4.2.1. Activities before the Actual Peak Reduction: Calculating the Threshold Using the Forecasted Load Profile**

As shown in Figure 4.2, the active control strategy carries out the forecasting activities one day in advance. The use of forecasts is advantageous because it enables the proposed strategy to establish the demand threshold and BESS dispatch schedule, two which are not altogether if forecasting is not used. Under-forecasting of the load introduces conservatism and leaves unrealized the full potential for peak demand reduction. If accounted in real-time, the battery will discharge little energy when in fact greater demand reduction would be possible. Conversely, over-forecasting of load causes the battery to discharge more than anticipated, creating an ambitious dispatch schedule and potentially causing battery failure and unmitigated load spike (Hanna et al., 2014). An accurate forecast is therefore crucial. The further ahead the future demand is known, the more efficiently the storage devices can be operated. The function of this part of the algorithm is therefore to forecast a baseline load profile and determine the initial demand threshold and BESS dispatch schedule for the subsequent day of operation.

A series of Nth historical 24 hour weekdays load profiles ( $\mathbf{P}_{\text{Load}}^{\text{His}}$ ) are first retrieved in order to determine the envelope of the historical load profiles. The maximum ( $\mathbf{P}_{\text{Load}}^{\text{His(max)}}$ ) and minimum ( $\mathbf{P}_{\text{Load}}^{\text{His(min)}}$ ) boundaries of the envelope are used to calculate the forecasted load profile for the next day, where weekends and holidays are not considered because the peak demands are usually low compared to the weekdays.

$$\mathbf{P}_{\text{Load}}^{\text{His(max)}}(d, t) = \text{MAX}_{\forall n} \mathbf{P}_{\text{Load}}^{\text{His}}(d - n, t) \quad (4.3)$$

$$\mathbf{P}_{\text{Load}}^{\text{His(min)}}(d, t) = \text{MIN}_{\forall n} \mathbf{P}_{\text{Load}}^{\text{His}}(d - n, t) \quad (4.4)$$

where,  $n$  is the number of historical load profiles.  $n \in \{1, 2, 3, \dots, N\}$ ;  $t$  is the time of the day (minutes).  $t \in \{0, 1, 2, \dots, 1440\}$ ; and  $d$  is the date.  $d \in \{0, 1, 2, \dots, \text{End of Month}\}$ .

The forecasted load profile ( $\mathbf{P}_{\text{Load}}^{\text{For}}$ ) for the next day ( $d + 1$ ) is then determined using the mean ( $\mu$ ) of the envelope of the historical load demands with the time interval of 1 minute.

$$\mathbf{P}_{\text{Load}}^{\text{For}}(d + 1, t) = \mathbf{P}_{\text{Load}}^{\text{His(max)}}(d, t) - \mu(t) \left[ \mathbf{P}_{\text{Load}}^{\text{His(max)}}(d, t) - \mathbf{P}_{\text{Load}}^{\text{His(min)}}(d, t) \right] \quad (4.5)$$

$$\mu(t) = \text{AVG}_{\forall n} \left[ \frac{\mathbf{P}_{\text{Load}}^{\text{His(max)}}(d, t) - \mathbf{P}_{\text{Load}}^{\text{His}}(d - n, t)}{\mathbf{P}_{\text{Load}}^{\text{His(max)}}(d, t) - \mathbf{P}_{\text{Load}}^{\text{His(min)}}(d, t)} \right] \quad (4.6)$$

Once the forecasted load profile ( $\mathbf{P}_{\text{Load}}^{\text{For}}$ ) of the next day ( $d + 1$ ) is determined, the control algorithm will calculate the threshold ( $\mathbf{P}_{\text{Th}}$ ) by using the remaining battery capacity of the BESS ( $\mathbf{E}_{\text{BESS}}^{\text{Act}}$ ) or the power rating of the BESS ( $\mathbf{P}_{\text{BESS}}$ ) as shown in Equation (4.7).

$$\mathbf{P}_{\text{Th}}(d + 1, t \dots 1440) = \text{MAX} \left[ \begin{array}{l} \mathbf{P}_{\text{Th}} \mid \mathbf{P}_{\text{BESS}} \\ \mathbf{P}_{\text{Th}} \mid \mathbf{E}_{\text{BESS}}^{\text{Act}} \end{array} \right] \forall t \quad (4.7)$$

The threshold should be made as low as possible in order to achieve the maximum peak reduction, whereby the lowest threshold ( $P_{Th} | P_{BESS}$ ) is  $P_{Load}^{For(max)} - P_{BESS}$  as shown in Figure 4.3(a). However, the maximum peak reduction is only achievable if the peak is narrow enough for the total stored energy (kWh) to reduce the peak. If the stored energy is not sufficient because the peak load demand is broad, the algorithm then iteratively increase the threshold until the peak demand can be covered by the remaining energy ( $E_{BESS}^{Act}$ ) by the BESS. The threshold ( $P_{Th} | E_{BESS}^{Act}$ ) is computed as the difference between  $P_{Load}^{For(max)}$  and  $P_{Reduction}$ , where  $P_{Reduction}$  is the peak reduction achieved after the remaining energy in the BESS has been delivered to the load as illustrated in Figure 4.3(b). In addition, the peak periods are determined as  $t_s$  and  $t_e$ , when  $P_{Load}^{For}$  is above the threshold.

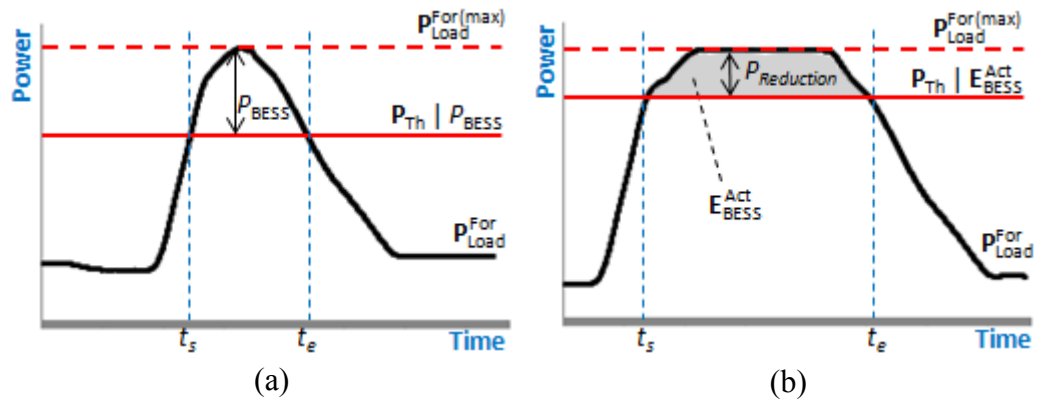


**Figure 4.3: The threshold level for scenario of (a) Narrow peak load demand and (b) Wide peak load demand**

Based on  $P_{Load}^{For}$  and  $P_{Th}$ , the schedule for the BESS ( $P_{BESS}^{Sch}$ ) to supply and absorb power is then generated as described in Equation (4.8). The BESS is scheduled to supply power during the peak period from  $t_s$  to  $t_e$ , when the

forecasted load demand ( $\mathbf{P}_{\text{Load}}^{\text{For}}$ ) exceeds the threshold ( $\mathbf{P}_{\text{Th}}$ ). The BESS is then scheduled to absorb power during the off-peak period from  $t_{Q2}$  to  $t_{Q1}$ .

$$\mathbf{P}_{\text{BESS}}^{\text{Sch}}(d+1, t) = \begin{cases} \mathbf{P}_{\text{Load}}^{\text{For}}(d+1, t) - \mathbf{P}_{\text{Th}}(d+1, t) & t_s \leq t \leq t_e \\ -\mathbf{P}_{\text{BESS}} & t_{Q2} \leq t \leq t_{Q1} \\ 0 & \text{Otherwise} \end{cases} \quad (4.8)$$

#### 4.2.2. Activities during the Day of Peak Reduction: Actively Adjusting the Threshold and Updating the Operating Schedule of BESS Using the Latest Load Demand

There are two types of BESS scheduling failure that are associated with the volatility of the load forecast (Bennett et al., 2015). The first relates to the misalignment between the BESS schedules ( $\mathbf{P}_{\text{BESS}}^{\text{Sch}}$ ) and the real-time load demand ( $\mathbf{P}_{\text{Load}}^{\text{Act}}$ ), and the second relates to the BESS battery being prematurely depleted during the reductions process and resulting in an unmitigated peak. The function of this part of the algorithm is therefore to measure the real-time load demand, compare it against the forecasted load demand, update the threshold and revise the BESS schedule in a way to minimize these two failures.

On the actual day ( $d$ ) of the peak reduction, at  $t = 0$ , the control algorithm will output power as  $\mathbf{P}_{\text{BESS}}^{\text{Act}}(d, 0) = \mathbf{P}_{\text{BESS}}^{\text{Sch}}(d, 0)$ . At the same time, the real-time load demand ( $\mathbf{P}_{\text{Load}}^{\text{Act}}$ ) is measured in order to determine the discrepancy ( $\alpha$ ). The discrepancy is calculated as the weighted difference between  $\mathbf{P}_{\text{Load}}^{\text{Act}}$  and  $\mathbf{P}_{\text{Load}}^{\text{For}}$  over the past 60 minutes to highlight the longer-term

response of the forecast results instead of the short-term fluctuations captured when there is a large mismatch between  $\mathbf{P}_{\text{Load}}^{\text{Act}}$  and  $\mathbf{P}_{\text{Load}}^{\text{For}}$ .

$$\alpha(t) = \sum_t^{t-59} \frac{\mathbf{P}_{\text{Load}}^{\text{Act}}(d, t) - \mathbf{P}_{\text{Load}}^{\text{For}}(d, t)}{60} \quad (4.9)$$

Higher battery capacity facilitates higher reduction of the peak demand. However limited capacity is often the situation due to the economical constraint. When the battery capacity of the BESS is relatively low, the less likely the peak demand can be reduced successfully. Hence, the control algorithm persistently adjusts the threshold ( $\mathbf{P}_{\text{Th}}$ ) in response to the change of the load demand ( $\mathbf{P}_{\text{Load}}^{\text{Act}}$ ), in hope to cut down the peak to the lowest possible level with the remaining energy in the BESS. With the use of the latest discrepancy, the forecasted load profile ( $\mathbf{P}_{\text{Load}}^{\text{For}}$  for the remaining day ( $t + 1, \dots, 1440$  minutes) is then updated and the threshold ( $\mathbf{P}_{\text{Th}}$ ) for the next interval is also adjusted based on the remaining capacity ( $\mathbf{E}_{\text{BESS}}^{\text{Act}}$ ) in the BESS. The  $\mathbf{P}_{\text{Load}}^{\text{For}}$  for the remaining day is updated as described in Equation (4.10) to (4.13), whereby the  $\mathbf{P}_{\text{Load}}^{\text{For}}$  up to present time ( $0, 1, \dots, t$  minute), with the least discrepancy is updated by approaching the real-time demand ( $\mathbf{P}_{\text{Load}}^{\text{Act}}$ ) measured at present time  $t$ . Followed by, the  $\mathbf{P}_{\text{Th}}$  is then updated as per Equation (4.7).

$$\mathbf{P}_{\text{Load}}^{\text{For}}(d, t + 1) = \alpha(t) \left[ \mathbf{P}_{\text{Load}}^{\text{For}(\ast)}(d, t) - \mathbf{P}_{\text{Load}}^{\text{Act}}(d, t) \right] + \mathbf{P}_{\text{Load}}^{\text{Act}}(d, t) \quad (4.10)$$

$$\mathbf{P}_{\text{Load}}^{\text{For}(\ast)}(d, t) = \text{MIN}_{\alpha(t)} \left[ \mathbf{P}_{\text{Load}}^{\text{For}}(d, 0), \mathbf{P}_{\text{Load}}^{\text{For}}(d, 1), \dots, \mathbf{P}_{\text{Load}}^{\text{For}}(d, t) \right] \quad (4.11)$$

$$\mathbf{P}_{\text{Load}}^{\text{For}}(d, t) = \mathbf{P}_{\text{Load}}^{\text{His(max)}}(d, t) - T(t) \left[ \mathbf{P}_{\text{Load}}^{\text{His(max)}}(d, t) - \mathbf{P}_{\text{Load}}^{\text{His(min)}}(d, t) \right] \quad (4.12)$$

$$T(t) = \frac{\mathbf{P}_{\text{Load}}^{\text{His(max)}}[d, t] - \mathbf{P}_{\text{Load}}^{\text{Act}}[d, t]}{\mathbf{P}_{\text{Load}}^{\text{His(max)}}[d, t] - \mathbf{P}_{\text{Load}}^{\text{His(min)}}[d, t]} \quad (4.13)$$

where,  $\mathbf{P}_{\text{Load}}^{\text{For}(\ast)}$  is the forecasted load profile with the least discrepancy from  $t = 0$  to  $t = 1440$ ; and  $T$  is the temporary variable to store the computation results.

The new operating schedule ( $\mathbf{P}_{\text{BESS}}^{\text{Sch}}$ ) for the remaining day starting from  $t + 1$  until the end of the day ( $t = 1440$  minutes) is then determined. As illustrated in Figure 4.4, the operating schedule of the BESS ( $\mathbf{P}_{\text{BESS}}^{\text{Sch}}$ ) encompasses six operating modes of the BESS namely, (i) Charging mode during off-peak periods, (ii) Charging mode during on-peak periods, (iii) Constant discharging mode, (iv) Discharging mode over the rising demand, (v) Discharging mode over the decreasing demand, and (vi) Standby mode. The BESS will carry out each of the operating modes when several specific conditions are fulfilled. The details of the operating modes and the corresponding conditions are described in the following.

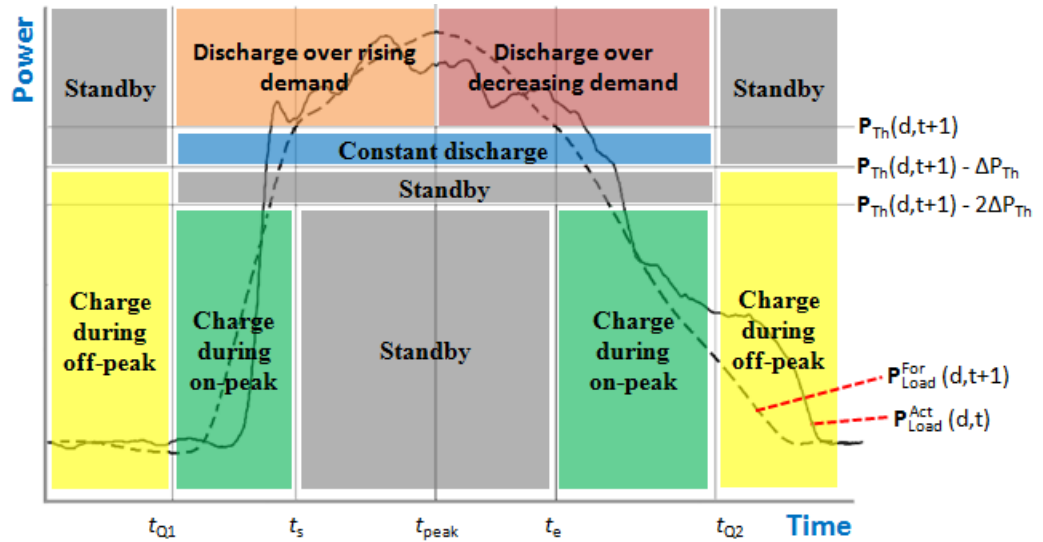


**Figure 4.4: The graphical representation of the six operating modes of the BESS**

#### 4.2.2.1. Charging mode during off-peak periods

This mode of operation is carried out during off-peak periods to ensure that the BESS is fully charged and ready to supply power in the coming operation. The BESS is charged at the specified value determined by the BESS internal battery management system (SMA, 2014) when the conditions in Table 4.1 are fulfilled:

**Table 4.1: Activation conditions for the charging mode during off-peak periods**

Conditions	Explanations
$t_{Q2} \leq t \leq t_{Q1}$	This condition represents the off-peak periods from $t_{Q2}$ to $t_{Q1}$ .
$\mathbf{P}_{\text{Load}}^{\text{For}}(d, t + 1) \leq \mathbf{P}_{\text{Th}}(d, t + 1) - \Delta\mathbf{P}_{\text{Th}}$	This condition ensures the BESS is not charged above the adjusted threshold. As soon as the forecasted load demand ( $\mathbf{P}_{\text{Load}}^{\text{For}}$ ) for the next interval ( $t + 1$ ) is above the adjusted threshold ( $\mathbf{P}_{\text{Th}}$ ) minus the specified permitted fluctuation margin ( $\Delta\mathbf{P}_{\text{Th}}$ ), the BESS will stop charging. $\Delta\mathbf{P}_{\text{Th}}$ is the user-specified permitted fluctuation margin along the adjusted threshold. It is a limit, added to monitor the peak demand reductions oscillation.
$\mathbf{E}_{\text{BESS}}^{\text{Act}}(d, t) \leq \mathbf{E}_{\text{BESS}}$	This condition is to ensure that the remaining energy ( $\mathbf{E}_{\text{BESS}}^{\text{Act}}$ ) in the BESS is not less than the energy stored in the BESS ( $\mathbf{E}_{\text{BESS}}$ ) at the depth-of-discharge of 50%.

#### 4.2.2.2. Charging mode during on-peak periods

The BESS is charged at the reduced rate as calculated using Equation (4.14). This mode of operation is for storing extra energy in the BESS in order to improve the possibility of reducing the incoming peak. The charging rate is reduced because it can avoid any significant increase in the load demand which may lead to the change in the operating schedule of the BESS.

$$\begin{aligned}
\mathbf{P}_{\text{BESS}}^{\text{Sch}}(d, t + 1) = & \alpha(t) \{ \mathbf{P}_{\text{Load}}^{\text{For}}(d, t + 1) - \mathbf{P}_{\text{Th}}(d, t + 1) \\
& - [ \mathbf{P}_{\text{Load}}^{\text{Act}}(d, t) - \mathbf{P}_{\text{Th}}(d, t + 1) ] \} \\
& + [ \mathbf{P}_{\text{Load}}^{\text{Act}}(d, t) - \mathbf{P}_{\text{Th}}(d, t + 1) ]
\end{aligned} \tag{4.14}$$

where,  $\mathbf{P}_{\text{Load}}^{\text{For}}(d, t + 1) - \mathbf{P}_{\text{Th}}(d, t + 1)$  is the absorption computed with the forecasted demand ( $\mathbf{P}_{\text{Load}}^{\text{For}}$ ) for the next interval ( $t + 1$ ); and  $\mathbf{P}_{\text{Load}}^{\text{Act}}(d, t) - \mathbf{P}_{\text{Th}}(d, t + 1)$  is the absorption determined based on the real-time load demand ( $\mathbf{P}_{\text{Load}}^{\text{Act}}$ ) measured at present time ( $t$ ).

This mode will be carried if the conditions in Table 4.2 are fulfilled.

**Table 4.2: Activation conditions for the charging mode during on-peak periods**

Conditions	Explanations
$t_{Q1} \leq t \leq t_s$ or $t_e \leq t \leq t_{Q2}$	This condition represents the on-peak periods from $t_{Q1}$ to $t_s$ and $t_e$ to $t_{Q2}$ , where the BESS is allowed to be charged.
$\mathbf{P}_{\text{Grid}}^{\text{Act}}(d, t) \leq \mathbf{P}_{\text{Th}}(d, t + 1) - 2\Delta\mathbf{P}_{\text{Th}}$	This condition is to ensure that the BESS is not charged above the adjusted threshold. As the BESS charge, the real-time supply from the utility ( $\mathbf{P}_{\text{Grid}}^{\text{Act}}$ ) at present time ( $t$ ) will increase. As soon as $\mathbf{P}_{\text{Grid}}^{\text{Act}}$ is above the adjusted threshold ( $\mathbf{P}_{\text{Th}}$ ) minus the double of the specified permitted fluctuation margin ( $\Delta\mathbf{P}_{\text{Th}}$ ), the BESS will stop charging.
$\mathbf{E}_{\text{BESS}}^{\text{Act}}(d, t) \leq \mathbf{E}_{\text{BESS}}$	This condition is to ensure that the BESS will continue to be charged if the remaining energy ( $\mathbf{E}_{\text{BESS}}^{\text{Act}}$ ) in the BESS is not less than the energy stored in the BESS ( $\mathbf{E}_{\text{BESS}}$ ) at the depth-of-discharge of 50%.

### 4.2.2.3. Constant discharging mode

Referring to Figure 4.4, this operating mode happens before and after the peak demand. In this mode of operation, the BESS will supply power at the minimum value of  $P_{\text{BESS}}^{\text{Act}(\text{min}+)}$ . Before the peak demand, the BESS will discharge at  $P_{\text{BESS}}^{\text{Act}(\text{min}+)}$ , in the anticipation of the incoming peak. After the peak demand, the BESS will discharge at  $P_{\text{BESS}}^{\text{Act}(\text{min}+)}$ , in anticipation of another incoming peaks. This is to ensure that the peak demand is reduced and minimize the fluctuations within the threshold of  $P_{\text{Th}} \pm \Delta P_{\text{Th}}$ . This also stops the BESS from the unnecessary reduction of the non-relevant peaks by preventing the BESS from reducing the peaks further than  $P_{\text{BESS}}^{\text{Act}(\text{min}+)}$ . This mode of operation will be carried out when the conditions in Table 4.3 are met.

**Table 4.3: Activation conditions for the constant discharging mode**

Conditions	Explanations
$t_{Q1} \leq t \leq t_{Q2}$	This condition represents the on-peak periods from $t_{Q1}$ to $t_{Q2}$ .
$P_{\text{Th}}(d, t + 1) - \Delta P_{\text{Th}} \geq P_{\text{Grid}}^{\text{Act}}(d, t) \geq P_{\text{Th}}(d, t + 1)$	This condition is to ensure that the peak demand is reduced and maintained within $P_{\text{Th}} \pm \Delta P_{\text{Th}}$ . As the BESS discharges, the real-time supply from the utility ( $P_{\text{Grid}}^{\text{Act}}$ ) at present time ( $t$ ) will be reduced. As the $P_{\text{Grid}}^{\text{Act}}$ is reduced lower than $P_{\text{Th}}$ , the BESS will supply power at the minimum value of $P_{\text{BESS}}^{\text{Act}(\text{min}+)}$ and the BESS will only stop discharging when the $P_{\text{Grid}}^{\text{Act}}$ is reduced lower than $P_{\text{Th}} - \Delta P_{\text{Th}}$ .

#### 4.2.2.4. Discharging mode over the rising demand

In this mode of operation, the BESS will discharge its power to the load in order to reduce the peak demand from the grid. The discharging power is calculated in Equation (4.15).

$$\begin{aligned} \mathbf{P}_{\text{BESS}}^{\text{Sch}}(d, t + 1) = & \alpha(t)[\mathbf{P}_{\text{Load}}^{\text{For}}(d, t + 1) - \mathbf{P}_{\text{Th}}(d, t + 1) \\ & - \text{MAX}\{\mathbf{P}_{\text{BESS}}^{\text{Act}(\text{min}+)}, \mathbf{P}_{\text{Load}}^{\text{Act}}(d, t) - \mathbf{P}_{\text{Th}}(d, t + 1)\}] \quad (4.15) \\ & + \text{MAX}\{\mathbf{P}_{\text{BESS}}^{\text{Act}(\text{min}+)}, \mathbf{P}_{\text{Load}}^{\text{Act}}(d, t) - \mathbf{P}_{\text{Th}}(d, t + 1)\} \end{aligned}$$

where,  $\mathbf{P}_{\text{Load}}^{\text{For}}(d, t + 1) - \mathbf{P}_{\text{Th}}(d, t + 1)$  is the peak demand reduction computed with the forecasted demand ( $\mathbf{P}_{\text{Load}}^{\text{For}}$ ) for the next interval ( $t + 1$ ); and  $\text{MAX}\{\mathbf{P}_{\text{BESS}}^{\text{Act}(\text{min}+)}, \mathbf{P}_{\text{Load}}^{\text{Act}}(d, t) - \mathbf{P}_{\text{Th}}(d, t + 1)\}$  is the peak demand reduction determined based on the real-time load demand ( $\mathbf{P}_{\text{Load}}^{\text{Act}}$ ) measured at present time ( $t$ ).

This process is carried out when the conditions in Table 4.4 are fulfilled.

**Table 4.4: Activation conditions for the discharging mode over the rising demand**

Conditions	Explanations
$t_{Q1} \leq t \leq t_{peak}$	This condition represents the rising peak periods from $t_{Q1}$ to $t_{peak}$ .
$\mathbf{P}_{Load}^{For}(d, t + 1) \geq \mathbf{P}_{Load}^{Act}(d, t)$	This condition indicates that the load demand is rising because the forecasted load demand ( $\mathbf{P}_{Load}^{For}$ ) for the next minute ( $t + 1$ ) is greater than the actual load demand ( $\mathbf{P}_{Load}^{Act}$ ) at present time ( $t$ ).
$\mathbf{P}_{Grid}^{Act}(d, t) \geq \mathbf{P}_{Th}(d, t + 1) - \Delta P_{Th}$	This condition is to ensure that the BESS is not over discharged. As the BESS discharge, the real-time supply from the utility ( $\mathbf{P}_{Grid}^{Act}$ ) at present time ( $t$ ) will decrease. As soon as $\mathbf{P}_{Grid}^{Act}$ is less than the adjusted threshold ( $\mathbf{P}_{Th}$ ) minus the specified permitted fluctuation margin ( $\Delta P_{Th}$ ), the BESS will stop discharging its power.

#### 4.2.2.5. Discharging mode over the decreasing demand

The BESS is discharged to reduce the peak over the decreasing load demand using Equation (4.14). This mode of operation is carried out once the conditions in Table 4.5 are fulfilled.

**Table 4.5: Activation conditions for the discharging mode over the decreasing demand**

Conditions	Explanations
$t_{peak} \leq t \leq t_{Q2}$	This condition represents the decreasing peak periods from $t_{peak}$ to $t_{Q2}$ .
$\mathbf{P}_{Load}^{For}(d, t + 1) < \mathbf{P}_{Load}^{Act}(d, t)$	This condition indicates that the load demand is decreasing because the forecasted load demand ( $\mathbf{P}_{Load}^{For}$ ) for the next minute ( $t + 1$ ) is less than the real-time load demand ( $\mathbf{P}_{Load}^{Act}$ ) at present time ( $t$ ).
$\mathbf{P}_{Grid}^{Act}(d, t) \geq \mathbf{P}_{Th}(d, t + 1) - \Delta P_{Th}$	This condition is to ensure that the BESS is not over discharged. As the BESS discharge, the real-time supply from the utility ( $\mathbf{P}_{Grid}^{Act}$ ) at present time ( $t$ ) will decrease. As soon as $\mathbf{P}_{Grid}^{Act}$ is less than the adjusted threshold ( $\mathbf{P}_{Th}$ ) minus the specified permitted fluctuation margin ( $\Delta P_{Th}$ ), the BESS will stop discharging its power.

#### 4.2.2.6. Standby mode

The BESS will be idle or standby with  $\mathbf{P}_{BESS}^{Sch}(d, t + 1) = 0$  if all the modes of operations as mentioned are not carried out.

The actual output of BESS for the next minute ( $\mathbf{P}_{BESS}^{Act}$ ) is then calculated based on the new operating schedule ( $\mathbf{P}_{BESS}^{Sch}$ ). Because the monthly maximum demand (MD) is charged over the highest level of load demand recorded by the utility during a 30 minute interval, many literatures developed and applied the peak demand reductions in an operational framework using 30 minute averaged load and assumed that the battery can discharge instantaneously all the requisite energy to shave the demand in the 30 minute interval. The use of 30 minutes resolution data however precludes the practical

real-time control of the BESS. The proposed strategy hence runs in an operational setting of 1-minute resolution data and to eliminate the unnecessary load demand transient as well as to ensure the battery can discharge instantaneously in an operational framework using 30 minute averaged load,  $\mathbf{P}_{\text{BESS}}^{\text{Act}}$  is computed as the aggregated power supplied by the BESS in the past 15 minutes. By trial and error, 15 minutes is selected because it has a good compromise between the 30 minutes resolution reductions deficient, and 1 minute resolution load demands that are fluctuating excessively.

$$\mathbf{P}_{\text{BESS}}^{\text{Act}}(d, t + 1) = 15 \times \mathbf{P}_{\text{BESS}}^{\text{Sch}}(d, t + 1) - \sum_{t-14}^{t-1} \mathbf{P}_{\text{BESS}}^{\text{Act}}(d, t) \quad (4.16)$$

where,  $\sum_{t-14}^{t-1} \mathbf{P}_{\text{BESS}}^{\text{Act}}(d, t)$  is the sum of the output supply from the BESS in the past 15 minutes, from previous intervals of  $t - 14$  up to  $t - 1$ .

Once the next interval  $\mathbf{P}_{\text{BESS}}^{\text{Act}}$  is determined, the BESS then proceed to supply power for the next minute and the process repeats until the end of the day, where  $t = 1440$ . Instead of retaining and carrying over to the next day, the end-of-day highest threshold ( $\mathbf{P}_{\text{Th}}^{\text{max}}$ ) is recalculated on every new day ( $d + 1$ ) to evaluate the robustness and peak reduction capability of the active control technique.

### 4.2.3. Implementation of the Active Control Strategy in LabVIEW

The program or the virtual instruments (VI) of the active control strategy are implemented in LabVIEW. The flow diagram of the VI is as shown in Figure 4.2. Listed in Table 4.6 are the VIs associated with the activities before the actual peak reduction discussed in Section 4.2.1 and in Table 4.7 are the VIs associated with the activities during the day of peak reductions described in Section 4.2.2.

**Table 4.6: List of VIs associated with the activities before the actual peak reduction**

Virtual Instruments	Functions
 (a)  (b)  (c)	<p>These VIs forecast the next day load profiles [<math>\mathbf{P}_{Load}^{For}(d + 1, t)</math>]. (a) Retrieve the historical load profiles, (b) compute the maximum and minimum boundaries of the historical load profiles envelop based on Equation (4.3) and (4.4), and (c) determine the forecasted load profile for the next day using Equation (4.5).</p>
 (a)  (b)	<p>These VIs calculates the next day threshold [<math>\mathbf{P}_{Th}(d + 1, t)</math>]. (a) Read the remaining battery capacity of the BESS and (b) compute the next day threshold based on the remaining battery capacity and the power rating of the BESS as defined in Equation (4.7).</p>
	<p>This VI determines the next day operating schedule of the BESS [<math>\mathbf{P}_{BESS}^{Sch}(d + 1, t)</math>] following Equation (4.8).</p>

**Table 4.7: List of VIs associated with the activities during the day of peak reduction**

Virtual Instruments	Functions
	<p>This VI controls the BESS to supply or absorb power [<math>\mathbf{P}_{\text{BESS}}^{\text{Act}}(d, t)</math>]. This VI also measures the state of the BESS. Further details of the VI are discussed in Chapter 3 Section 3.4.2.</p>
	<p>This VI measures the real-time load demands [<math>\mathbf{P}_{\text{Load}}^{\text{Act}}(d, t)</math>]. Further details of the VI are discussed in Chapter 3 Section 3.3.2.</p>
	<p>This VI computes the discrepancy between <math>\mathbf{P}_{\text{Load}}^{\text{Act}}(d, t)</math> and <math>\mathbf{P}_{\text{Load}}^{\text{For}}(d, t)</math> based on Equation (4.9), and forecast the load profile for the remaining day [<math>\mathbf{P}_{\text{Load}}^{\text{For}}(d, t + 1 \dots 1440)</math>] following Equation (4.10).</p>
	<p>This VI calculates the threshold for the next minute [<math>\mathbf{P}_{\text{Th}}(d, t + 1)</math>] based on the remaining battery capacity and the power rating of the BESS described in Equation (4.7).</p>
 <p>(a)</p>  <p>(b)</p>  <p>(c)</p>  <p>(d)</p>  <p>(e)</p>	<p>This VIs determines the new operating schedule of the BESS [<math>\mathbf{P}_{\text{BESS}}^{\text{Sch}}(d, t + 1 \dots 1440)</math>]. Referring to Figure 4.4, (a) represent the operating modes between the period from <math>t_{Q2}</math> to <math>t_{Q2}</math>, (b) represent the operating modes between <math>t_{Q1}</math> and <math>t_s</math>, (c) represent the operating modes between <math>t_s</math> and <math>t_{peak}</math>, (d) represent the operating modes between <math>t_{peak}</math> and <math>t_e</math>, and (e) represent the operating modes between <math>t_e</math> and <math>t_{Q2}</math>.</p>

**(Table 4.7 Continued.)**

Virtual Instruments	Functions
 A small square icon with a blue border. Inside, there is a black square with the text '03:3' in white, and below it, the text 'BESS Schedule.' in black on a white background.	This VI determines the actual power supply of BESS for the next time [ $P_{\text{BESS}}^{\text{Act}}(d, t + 1)$ ] based on the new schedule. The $P_{\text{BESS}}^{\text{Act}}(d, t + 1)$ is computed as per described in Equation (4.16).

### 4.3. Fundamental Control Strategy

The performance of the active control algorithm is compared to that of the fundamental controller in order to understand how the active adjustment of the threshold can contribute to the peak reduction.

Planning ahead is vital when performing peak demand reductions. To highlight this point, the performance of the active controller is compared to a fundamental set-point controller, where the threshold is found from historical load profiles and it is maintained throughout the day of operation. The BESS will deliver the power when the actual load demand exceeds the threshold and charges the batteries during off-peak periods (Leadbetter and Swan, 2012; Levron and Shmilovitz, 2012; Rowe et al., 2013). Following the same power and energy constraints defined in Equation (4.1) and (4.2), the structure of the fundamental control strategy is described in Figure 4.5.

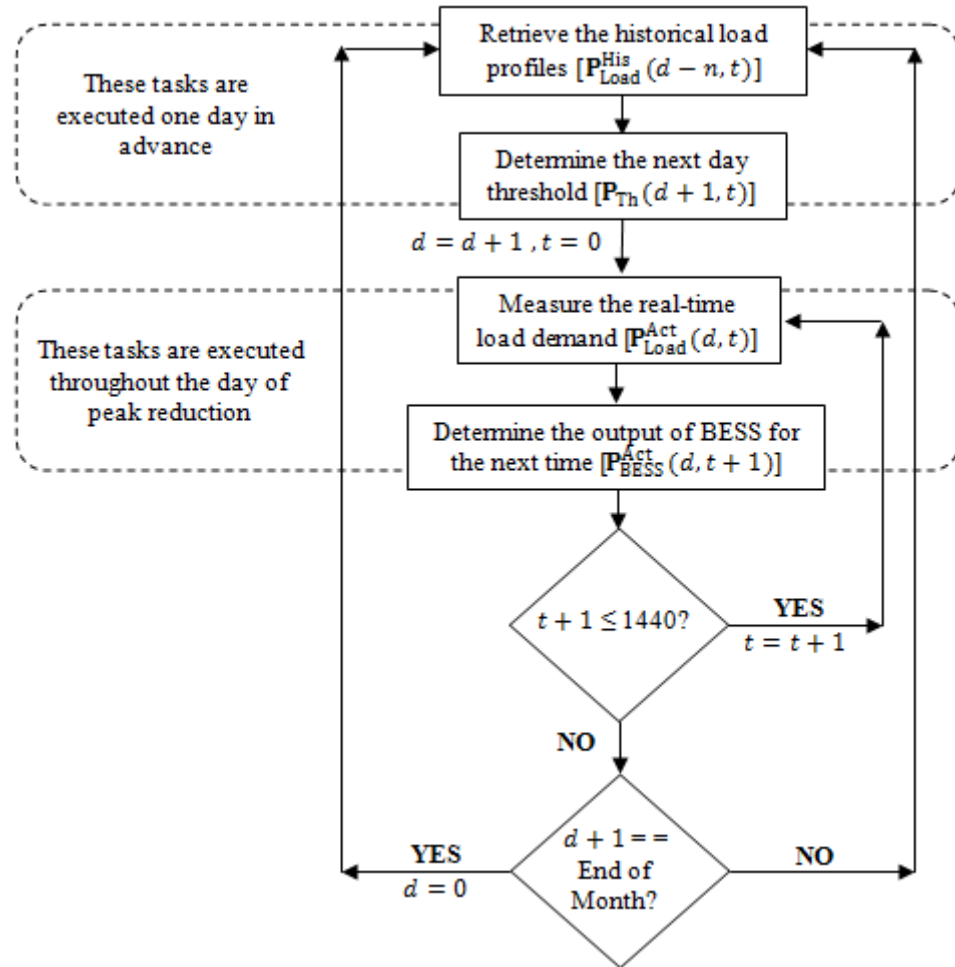


**Figure 4.5: The flowchart of the fundamental control strategy**

Prior to the day of peak reduction, the fundamental control strategy begins by retrieving a series of  $N^{\text{th}}$  historical 24 hours weekdays load profiles ( $\mathbf{P}_{\text{Load}}^{\text{His}}$ ), where weekends and holidays are not considered because the peak demands are usually low compared to the weekdays. The optimum threshold ( $\mathbf{P}_{\text{Th}}^{\text{opt}}$ ) for each of the historical load profiles are then computed following Equation (4.7) and the next day ( $d + 1$ ) threshold ( $\mathbf{P}_{\text{Th}}$ ) is determined as the frequently occurred threshold defined by Equation (4.17) to (4.19). The frequently occurred threshold is selected because it has a higher probability of recurring compared to other threshold levels.

$$\mathbf{P}_{Th}(d + 1, t) = k \mid \text{MAX} [f_{Th}(k, n)] \quad (4.17)$$

$$f_{Th}(k, n) = \sum_{n=0}^N \text{IF}[T(n) == k] \quad (4.18)$$

$$T(n) = \text{ROUND}[\mathbf{P}_{Th}^{\text{opt}}(d - n, t), 0] \quad (4.19)$$

where,  $k$  is the computation regions of  $\mathbf{P}_{Th}$ .  $k \in \{1, 2, 3, \dots, \mathbf{P}_{Load}^{\text{His(max)}}\}$ ;  $n$  is the number of historical load profiles.  $n \in \{1, 2, 3, \dots, N\}$ ;  $f_{Th}$  is the frequency of occurrence of the  $\mathbf{P}_{Th}^{\text{opt}}$ ; and  $T$  is the temporary variable storing the rounded to the closest integer value of  $\mathbf{P}_{Th}^{\text{opt}}$ .

On the actual day ( $d$ ) of the peak reduction, the fundamental control strategy then measures the real-time load demand ( $\mathbf{P}_{Load}^{\text{Act}}$ ) and used it to determine the output of the BESS for the next interval ( $\mathbf{P}_{BESS}^{\text{Act}}$ ). If the current demand is below the predetermined threshold ( $\mathbf{P}_{Th}$ ), the BESS will charge until the battery capacity is full ( $\mathbf{E}_{BESS}^{\text{Act}} = \mathbf{E}_{BESS}^{\text{max}} \equiv 100\% \text{ SOC}$ ); whereas if the current demand is above the predetermined threshold, the BESS will discharge at  $\mathbf{P}_{Load}^{\text{Act}} - \mathbf{P}_{Th}$  or  $\mathbf{P}_{BESS}^{\text{max}}$ , until the battery capacity is empty ( $\mathbf{E}_{BESS}^{\text{Act}} = 0 \equiv 50\% \text{ SOC}$ ) or the demand goes below the predetermined threshold.

Once the next interval  $\mathbf{P}_{BESS}^{\text{Act}}$  is determined, the BESS then proceed to supply power for the next minute and the process repeats until the end of the day, where  $t = 1440$ . Conversely, similar to the active control technique, instead of retaining and carrying over to the next day, the predetermined

threshold is recalculated on every new day ( $d + 1$ ) to evaluate the robustness and compare the peak reduction capability with the active control technique.

#### 4.4. Simulation Analysis: Ideal Peak Demand Reductions

Apart from that, to understand how the discrepancy between the forecasted and the actual loads can affect the ability of the BESS in peak reduction, the peak demand reductions of the active control technique are also benchmark to the ideal reductions when the discrepancy is zero, wherein the forecasted load profile is exactly the same as the actual load profile. The ideal reductions, obtained post experiment, provides a benchmark of how far the experimental results are away from the best possible demand reductions, in which the BESS can achieve for a given known load profile and remaining battery capacity.

The computation of the ideal peak demand reduction begins by retrieving the post-experiment real-time load profile [ $\mathbf{P}_{\text{Load}}^{\text{Act}}(d, t)$ ] and the remaining energy at the beginning of the experiment day [ $\mathbf{E}_{\text{BESS}}^{\text{Act}}(d, 0)$ ]. The best possible demand reduction is computed as  $\mathbf{P}_{\text{Load}}^{\text{Act}(\text{max})} - \mathbf{P}_{\text{Th}}^{\text{Opt}}$ , where an optimum threshold ( $\mathbf{P}_{\text{Th}}^{\text{Opt}}$ ) is determined, above which the BESS is discharged to reduce the peak demand and below which the battery is charged to prepare for later reductions. The  $\mathbf{P}_{\text{Th}}^{\text{Opt}}$  is determined in a way the energy amount above the threshold and below  $\mathbf{P}_{\text{Load}}^{\text{Act}}$  is equal to the usage of the battery capacity for the day [ $\mathbf{E}_{\text{BESS}}^{\text{Sim}}(d, 0 \dots 1440)$ ]. Following the constraints as

defined in Equation (4.1) and (4.2), the  $\mathbf{E}_{\text{BESS}}^{\text{Sim}}(d, 0 \dots 1440)$  is simulated based on a linearized ideal BESS power flow model as shown in Equation (4.20).

$$\mathbf{E}_{\text{BESS}}^{\text{Sim}}(d, t) = \mathbf{E}_{\text{BESS}}^{\text{Sim}}(d, t - 1) - \frac{\mathbf{P}_{\text{Load}}^{\text{Act}}(d, t)}{60} \quad (4.20)$$

where,  $\mathbf{E}_{\text{BESS}}^{\text{Sim}}$  is the simulated BESS battery usage (kWh).  $\mathbf{E}_{\text{BESS}}^{\text{Sim}}(d, 0) = \mathbf{E}_{\text{BESS}}^{\text{Act}}(d, 0)$ ; and  $t$  is the simulation time from  $t = 0$  to  $t = 1440$ minutes.

#### 4.5. Summary

The formulation of the active controller, the components in the active controller, as well as the implementation of the active controller has been elaborated. The framework of the fundamental control strategy in peak demand reductions has been outlined as well. The structure of the simulation analysis, used to compute the ideal peak demand reduction, has also been described.

## CHAPTER 5

### RESULTS AND DISCUSSIONS

The load profiles on the experimental site of the battery-based energy storage system (BESS) are presented in this chapter, followed by the technical evaluation of the active controller with experimental peak demand reductions. The active controller will be compared to the fundamental controller and benchmarked against the simulation results. The active controller will also be compared to the other literature experimental results before the financial evaluation is carried out. A financial analysis is also included at the end of this chapter to provide a financial foresight of what would have been achieved if the savings by the active controller is improved or the price of the BESS is reduced.

#### 5.1. Experimental Site

The performance of the active control strategy has been evaluated experimentally on a battery-based energy storage system (BESS) setup at the Universiti Tunku Abdul Rahman campus in Sungai Long KA Block. Summed up to the power rating ( $P_{\text{BESS}}$ ) of 18kW, the BESS consists of three units of 6kW bi-directional power converter, each connected to a  $4 \times 4$  matrix configuration battery bank formed by 16 pieces of 12V<sub>dc</sub>, 111Ah, valve-regulated lead-acid (VRLA) batteries. Each string of batteries has an energy

capacity of about 21.32kWh and a total energy capacity of up to 64kWh is available. To prolong the lifespan of the batteries, the amount of energy ( $E_{\text{BESS}}$ ) that can be used is however only about 27kWh or the depth-of-discharge (*DoD*) of up to 50%.

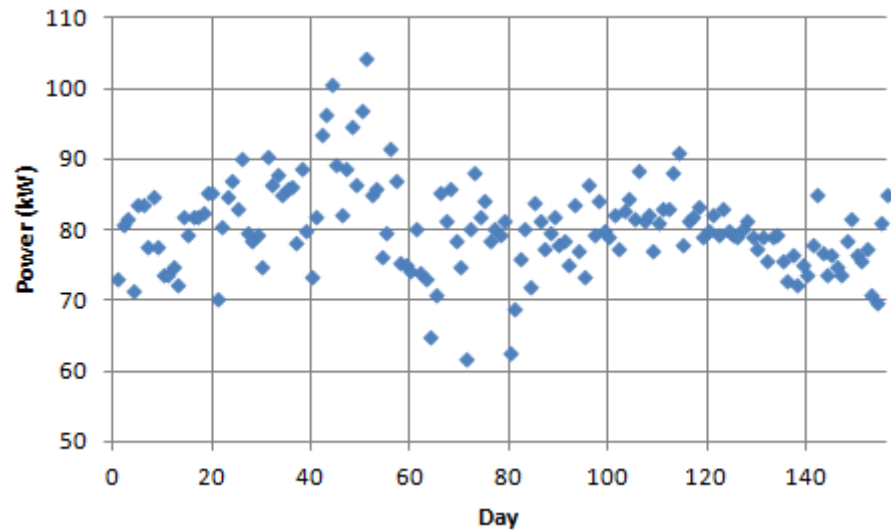


**Figure 5.1: The peak demands on the test site over a period of 156 weekdays**

The BESS is integrated on the low voltage (LV) line at the distribution board of NSM/GN that has about 114.6kW of connected load. On the same LV line, the electrical distributions are also supplied to the distribution board of NSM/M, which has about 110.2kW of connected load. The maximum load consumption (or herein the peak demand) on the LV line recorded over a period of 156 weekdays are shown in Figure 5.1. The peak demand recorded at one time was 104.33kW and the minimum was 61.82kW. The peak demand concentrates around the band from 70kW to 90kW, and is 80.59kW, on average, with the standard deviation of 6.36%. A sample week of load profiles

in Figure 5.2 showed that the load profiles on the experimental site are generally wide in distribution, peak starting from 7:00 am to 4:40 pm, and have peaks that can happen several times in a day.

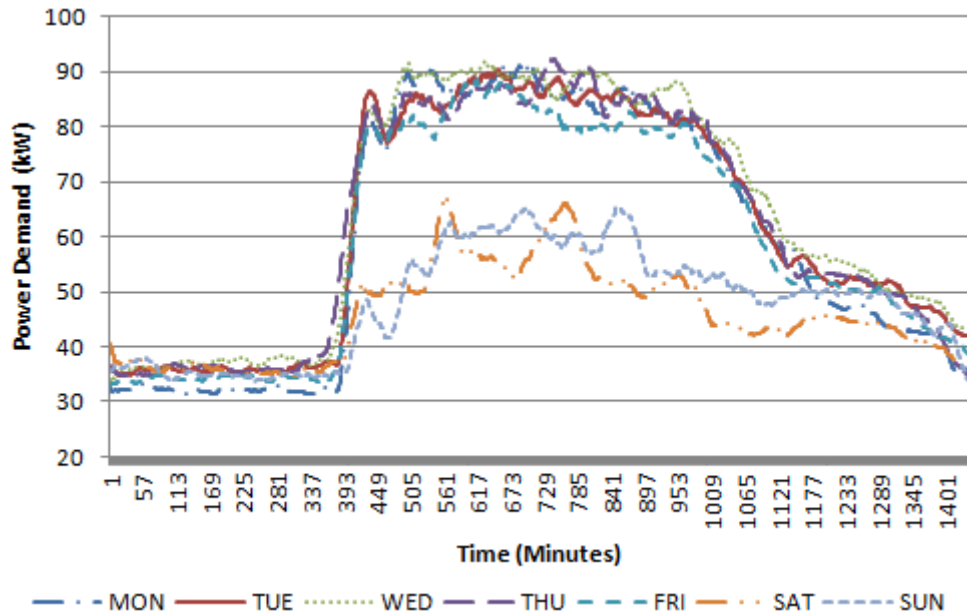


**Figure 5.2: A sample historical load profiles on the experimental site from Monday to Sunday**

A demand analysis is conducted to estimate the energy required to reduce the peak demand by 1kW, 2kW, 3kW and up to 21kW. A total of 156 weekdays is used to generate the result displayed in Figure 5.3. The energy required to reduce the peak demand by 18kW ( $P_{BESS}$ ) is estimated to be approximately 71.75kWh. With the available energy of 27kWh ( $E_{BESS}$ ), the maximum achievable reduction in the peak demand is however only about 11kW. A number of case studies presented in this chapter are therefore carried out to investigate the performance of the active controller in reducing the peak demands in spite of the limited capacity. Additional case studies are also

carried out to understand how the active adjustment of the threshold can improve the performance in peak reduction.

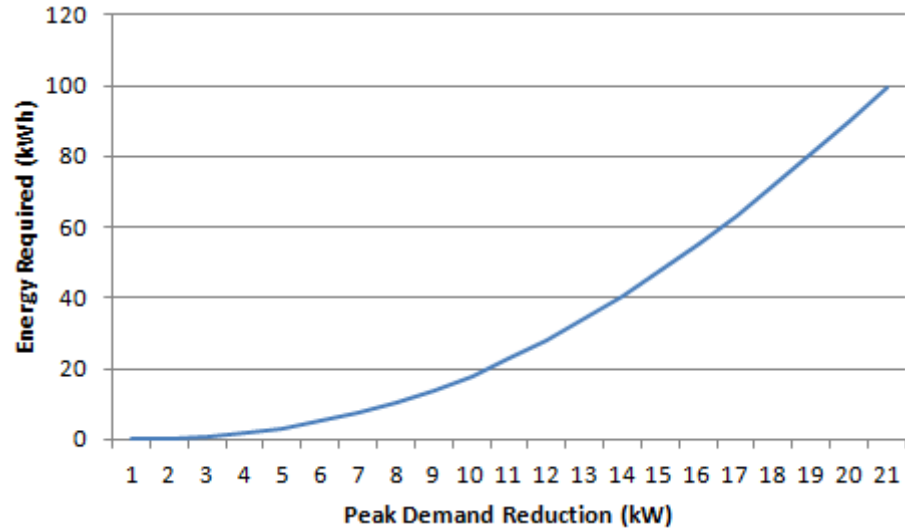


**Figure 5.3: The estimated energy required for peak demand reductions from 1kW to 21kW**

## 5.2. Technical Evaluations

Firstly, the performance of the active control strategy (see Chapter 4 Section 4.2) is compared to the fundamental controller (see Chapter 4 Section 4.3) in order to understand how the active adjustment of the threshold can contribute to the peak reduction. The experimental results of the active controller are also compared with the simulation studies (see Chapter 4 Section 4.4) in which the forecasted load is exactly the same as the actual load demand to understand how the discrepancy between the forecasted and the actual loads can affect the ability of the BESS in peak reduction. In this section, the results of the fundamental controller are first being reviewed in Section 5.2.1 and followed by with the results of the active controller in Section 5.2.2. Next, the

experimental results are then assessed based on the evaluation indexes described in Section 5.2.3. Besides that, in Section 5.2.4, the experimental results are also extended to compare with the other literature experimental results.

In total, 62 days of experimental peak reductions have been conducted and each control strategy was experimented for 31 days. The input parameters for the controllers are listed in Table 5.1. Appendix C and Appendix D enumerates the peak demand for the metered load ( $P_{Load}^{Act(max)}$ ), the net load ( $P_{Grid}^{Act(max)}$ ), the post peak demand reductions ( $P_{Reduction}^{Act}$ ) and the simulated peak demand reductions ( $P_{Reduction}^{Sim}$ ) for each day of the experiment. Throughout the analysis in this chapter, the weekends and holidays are ignored because those days do not contain an elevated daytime load or a conspicuous daytime load spike. In other words, the peaks are lower than the threshold and hence contain no peak to be reduced.

**Table 5.1: The controller’s input parameters**

Parameter	Description	Rating
$P_{BESS}$	BESS power rating	18 kW
$E_{BESS}$	BESS usable capacity at <i>DoD</i> of 50%	27 kWh
$\Delta P_{Th}$	Tolerance of threshold or fluctuation margin	$\pm 1$ kW
$P_{BESS}^{Act(min+)}$	Minimum positive supply from BESS	3 kW
$t_{Q1}$	Morning charging time	8 AM
$t_{Q2}$	Night charging time	10 PM

### **5.2.1. Results of the Peak Reductions using the Fundamental Controller**

The performance of the active control algorithm is first compared to that of the fundamental controller in order to understand how the active adjustment of the threshold can contribute to the peak reduction. Planning ahead is vital when performing peak demand reductions and to highlight this point, the performance of the active controller is compared to a fundamental set-point controller, where the threshold is found from historical load profiles and it is maintained throughout the day of operation. The BESS deliver the power when the actual load demand exceeds the threshold and charges the batteries during off-peak periods.

The setting of the threshold is important to determine the highest peak reduction that can be attained. Over-setting of the threshold may result in unnecessary usage of the BESS. Illustrates in Figure 5.4, such scenario can occur with the fundamental controller. When the threshold level ( $P_{Th}$ ) is over set, peak reduction is not necessary and the usage of the BESS is wasteful.

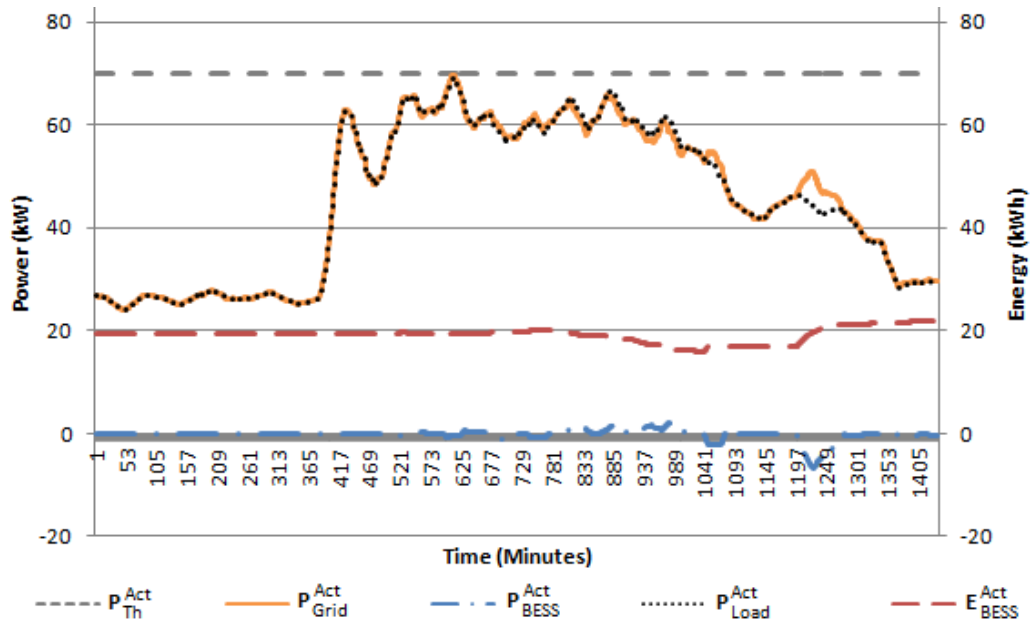


**Figure 5.4: The experimental result of a sample day without peak reduction by the fundamental controller due to the peak is lower than the threshold**

Note: This day is referred to day 27 in Appendix C. The peak ( $P_{Load}^{Act(max)}$ ) was lower than the threshold ( $P_{Th}^{Act}$ ) and hence, peak reduction was not performed on this day. The  $P_{Th}^{Act}$  was 70kW and the optimum threshold ( $P_{Th}^{Opt}$ ) simulated after the experiment is 61.6kW. The same scenario had happened on day 13 also.

On the other hand, under-setting the threshold may result in insufficient capacity of BESS to perform the targeted peak reduction. Shown in Figure 5.5, such scenario can also occur with the fundamental controller. When the threshold level ( $P_{Th}$ ) is under set, the target peak reduction ( $P_{Grid} = P_{Th}$ ) cannot be achieved because the capacity of the BESS is insufficient. At time when the state-of-charge (*SoC*) or the remaining energy in the battery ( $E_{BESS}$ ) of the BESS system is low, the demand ( $P_{Load}$ ) will overtake back and this result an incomplete peak reduction. This is observed at the later part of the peak in Figure 5.5. However, despite the threshold of the fundamental controller is under-set, there are still times when the fundamental controller

managed to reduce the peak demand partially such as the experimental result shown in Figure 5.6.

The effectiveness of the fundamental controller thus depends on whether the battery capacity surpasses the energy requirement of the peak demand or not. The entire peak demand can be shaved if the battery capacity is greater than the energy required to meet the peak demand. However, if the battery capacity is less than the energy requirement of the peak demand, the battery capacity may be depleted before the peak demand is reduced.

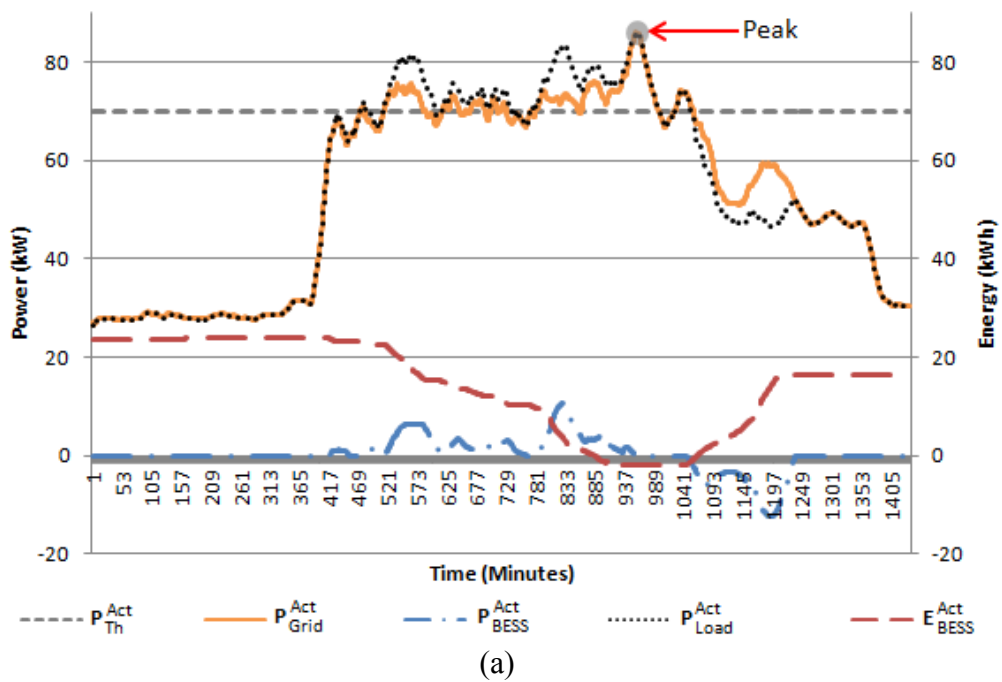


**Figure 5.5: (a) The experimental result of a sample day with the unsuccessful peak reduction by the fundamental controller**

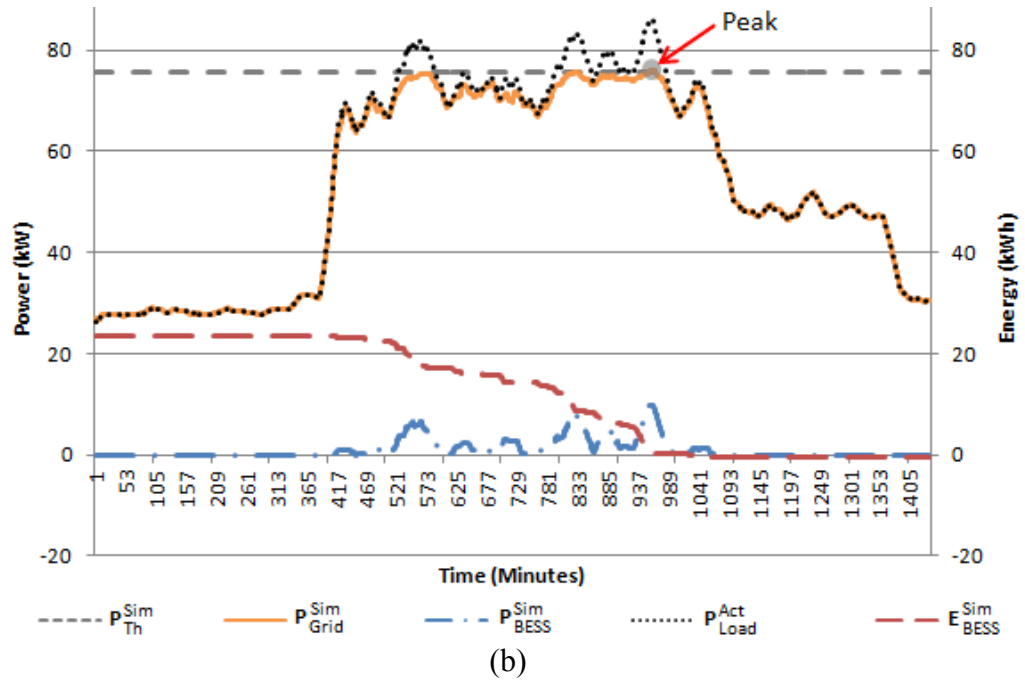


**Figure 5.5: (b) The simulated result of a sample day with the unsuccessful peak reduction by the fundamental controller**

Note: This day is referred to day 8 in Appendix C. The peak was the same, before ( $P_{Load}^{Act(max)}$ ) and after ( $P_{Grid}^{Act(max)}$ ) the peak reduction. The BESS battery protection mechanism was activated when  $E_{BESS}^{Act}$  is below zero, stopping the BESS from any operation and causing the BESS to be unable to reduce the peak demand at the later part. The  $P_{Th}^{Act}$  was 70kW and the optimum threshold ( $P_{Th}^{Opt}$ ) simulated after the experiment is 75.5kW. The same scenario has happened on day 6, 9, 14, 15, 16 and 22 also.

Recorded in Appendix C, there are two days in which the fundamental controller over-set the threshold and ten days the controller under-set the threshold, seven of which the peak demands is not reduced. It is, therefore, difficult to find a threshold that can achieve the best possible demand reduction with the fundamental controller. Most of the time, the fundamental controller is not able to reduce the wide peak supplied by the grid ( $P_{Grid}^{Act}$ ) as the threshold is always fixed throughout the day. The fundamental controller is

also unable to maintain the peak ( $P_{\text{Grid}}^{\text{Act(max)}}$ ) within the fluctuation margin of the threshold. The fundamental control is hence simple to implement, but it is fundamentally limited.

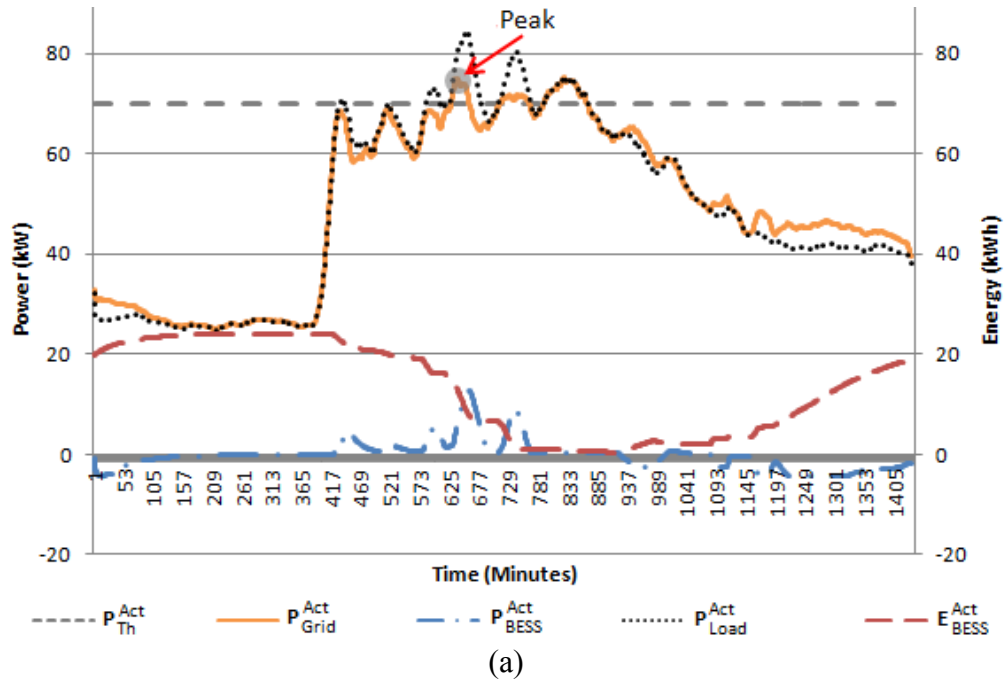


**Figure 5.6: (a) The experimental result of a sample day with the peak reduction achieved by the fundamental controller**

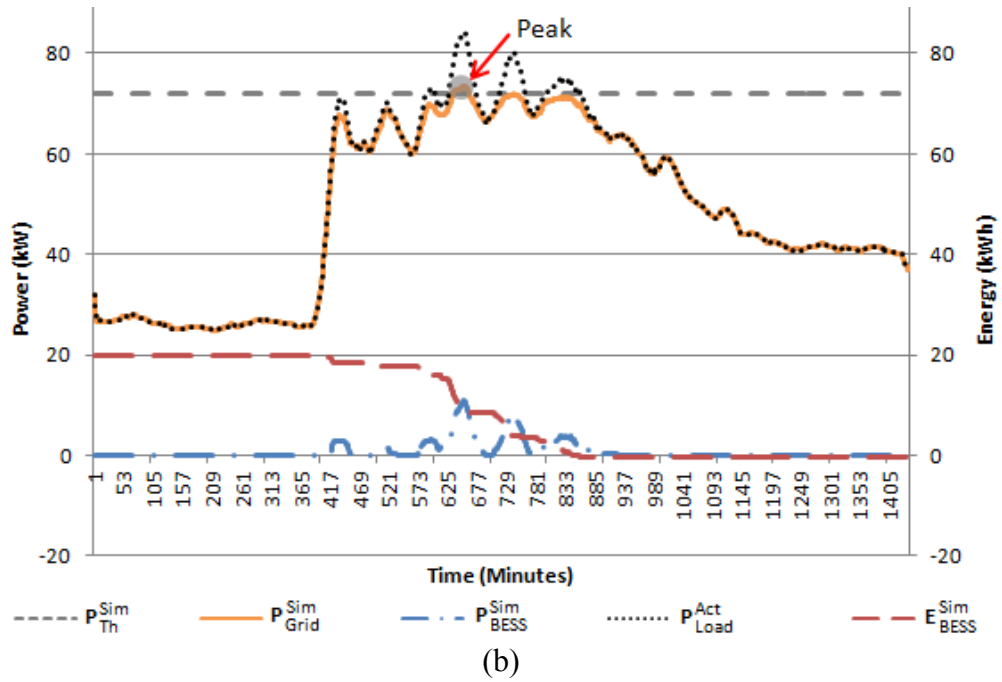


**Figure 5.6: (b) The simulated result of a sample day with the peak reduction achieved by the fundamental controller**

Note: This day is referred to day 17 in Appendix C. The peak ( $P_{Load}^{Act(max)}$ ) was partially reduced to  $P_{Grid}^{Act(max)}$  in spite of battery depletion at the later part of the peak. The BESS battery protection mechanism was activated when  $E_{BESS}^{Act}$  is below zero, thus, stopping the BESS from any operation at the later part of the peak. The  $P_{Th}^{Act}$  was 70kW and the optimum threshold ( $P_{Th}^{Opt}$ ) simulated after the experiment is 72.1kW. The same scenario has happened on day 1 and 31 also.

### 5.2.2. Results of the Peak Reductions using the Active Controller

Moving on, pure peak reduction method attempts to keep the peak demands as flat as possible to the threshold, but most of the time, the fundamental controller is unable to fulfil this requirement. The fundamental controller is susceptible to over and under-setting of the threshold. It is inconsistent when the battery does not have sufficient energy to cut down the whole peak.

Moreover, once the threshold is determined, it will not be adjusted anymore. As a result, the BESS can often fail to reduce the peak. An active controller with short-term load forecasting is therefore developed to persistently adjust the threshold throughout the day based on the latest information on the load demand. The threshold is determined in a way that the energy amount above the threshold equals to the battery capacity that is available in the BESS. By doing so, the highest peak demand reduction for every day can be attained.

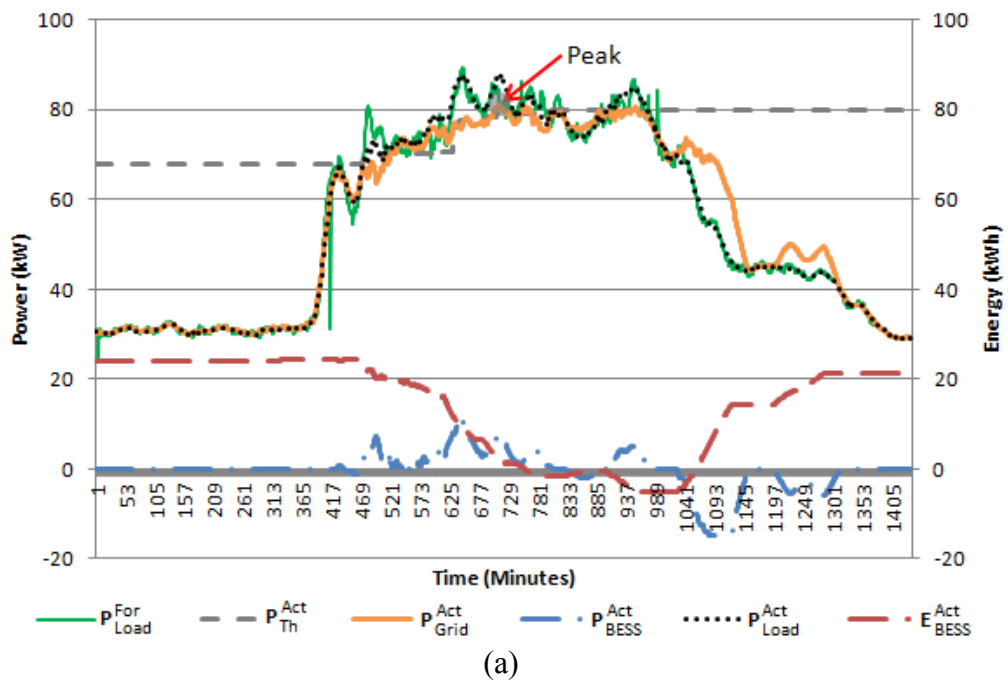


**Figure 5.7: (a) The experimental result of a sample day with the peak reduction achieved by the active controller**

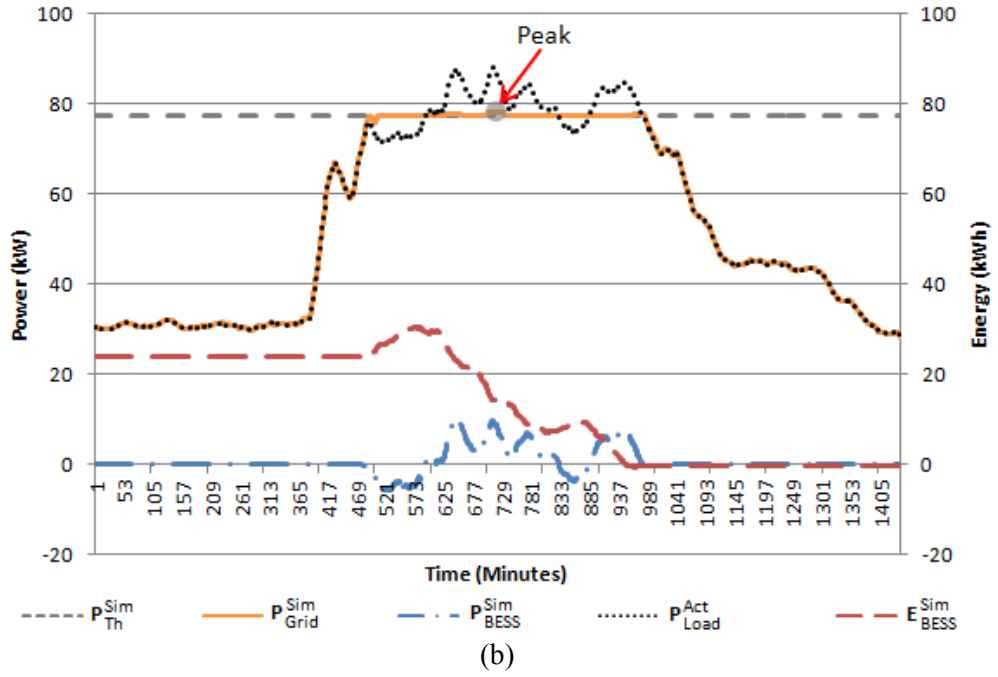


**Figure 5.7: (b) The simulated result of a sample day with the peak reduction achieved by the active controller**

Note: This day is referred to day 30 in Appendix D. The peak ( $P_{Load}^{Act(max)}$ ) was reduced to  $P_{Grid}^{Act(max)}$ . Despite the remaining energy in the BESS ( $E_{BESS}^{Act}$ ) is below zero, the BESS was able to continue discharge the battery by a margin of up to -5kWh without triggering the internal battery protection mechanism. The initial threshold ( $P_{Th}^{Act}$ ) was 68kW and it is adjusted to 79.9kW. The optimum threshold ( $P_{Th}^{Opt}$ ) simulated after the experiment is 77.3kW. The forecasted load profile ( $P_{Load}^{For}$ ) has mean absolute percentage error (*MAPE*) of 2.08%, with a standard deviation of 2.38%. The same scenario has happened on day 17, 23 and 24 also.

As shown in Figure 5.7, the active controller is able to reduce the wide peak because the threshold is actively being adjusted throughout the day. The use of the short-term load forecasting provides the dynamics foresight of the peak demand for the active controller to pre-estimate the energy requirement and hence preserving the stored energy to the end of the peak is possible. Despite the battery capacity ( $E_{BESS}^{Act}$ ) is depleted before the peak ends, the active controller is still able to reduce the peak as flat as possible to the

threshold ( $P_{Grid}^{Act} \cong P_{Th}^{Act}$ ) and able to maintain below the fluctuation margin of the threshold ( $P_{Th}^{Act} + \Delta P_{Th}$ ). Illustrated in Figure 5.8, there are also times when the remaining battery capacity ( $E_{BESS}^{Act}$ ) in the BESS is sufficient to meet the whole peak and the threshold is not adjusted while still managed to reduce the peak demand in spite the battery being depleted before the peak ends.

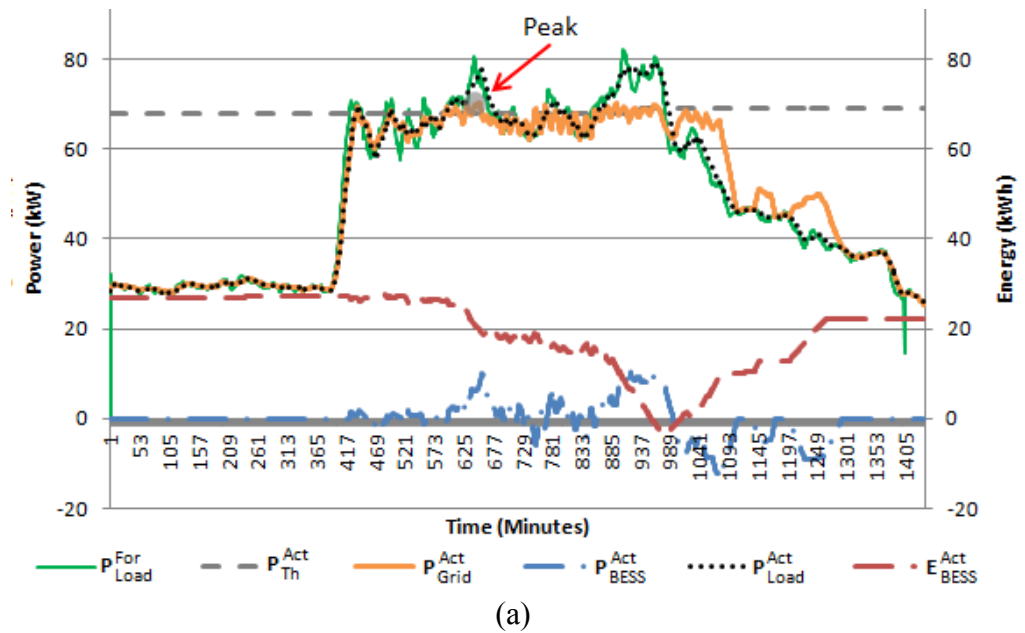


**Figure 5.8: (a) The experimental result of a sample day with the peak reduction achieved by the active controller without adjusting the threshold**

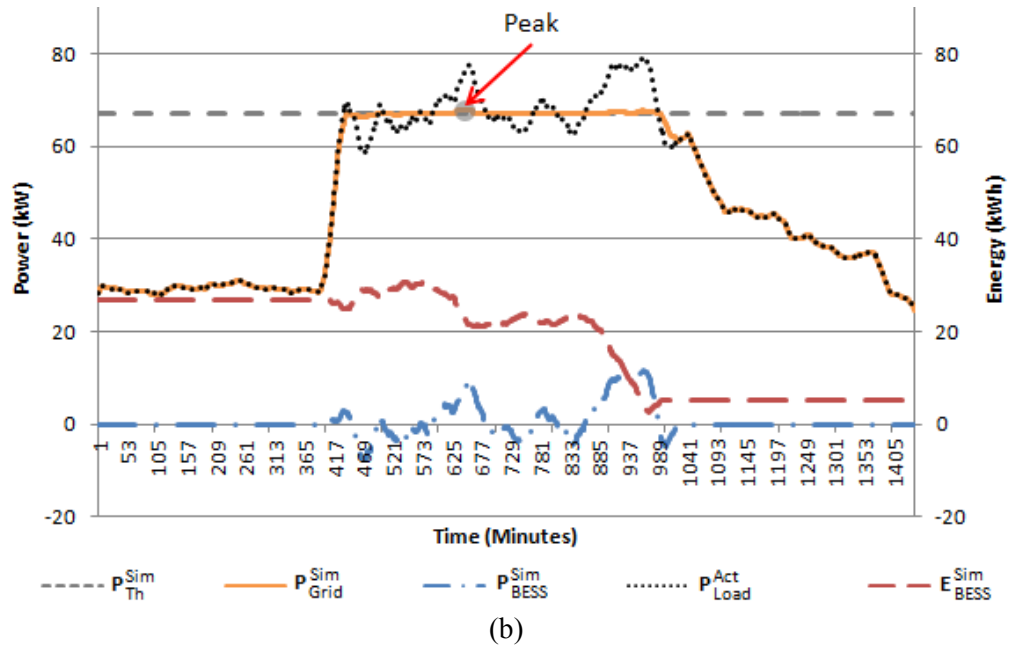
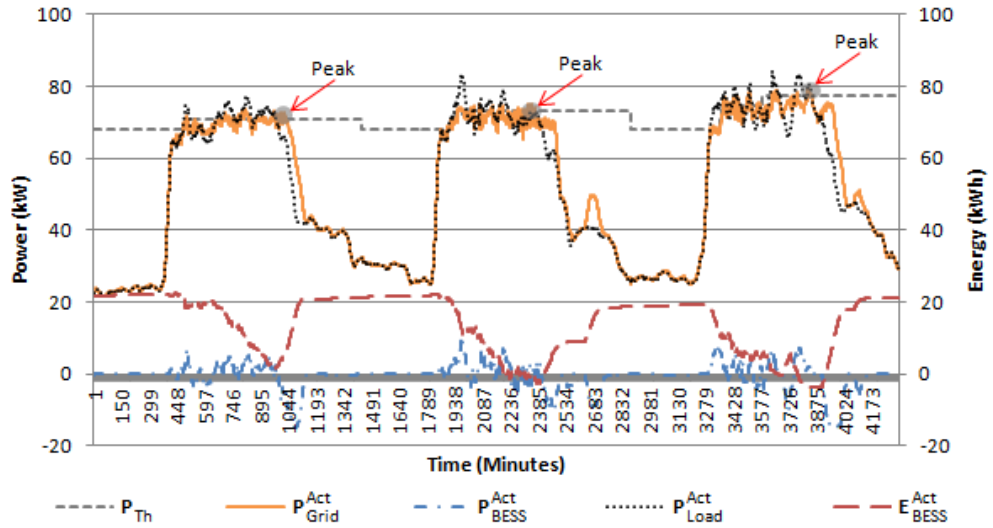


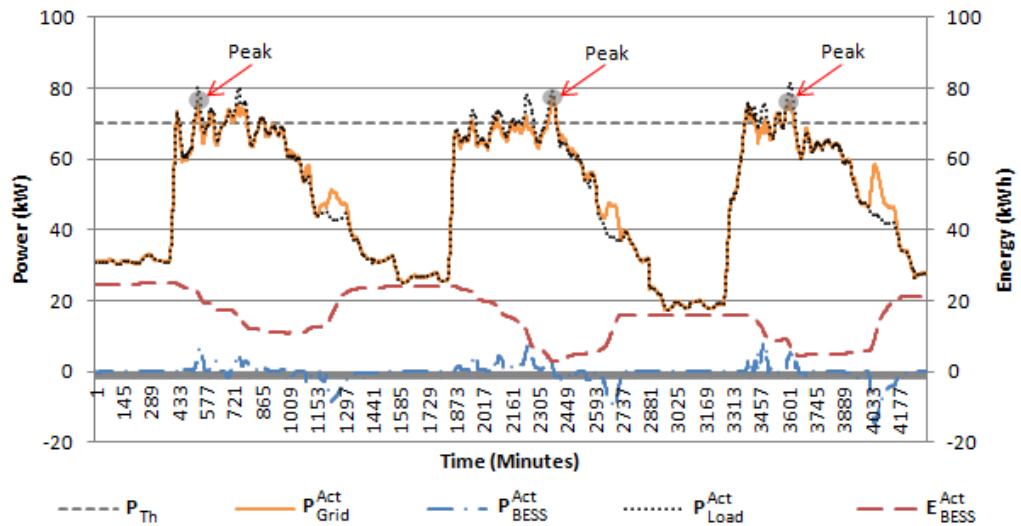
**Figure 5.8: (b) The simulated result of a sample day with the peak reduction achieved by the active controller without adjusting the threshold**

---

Note: This day is referred to day 11 in Appendix D. The peak ( $P_{Load}^{Act(max)}$ ) was reduced to  $P_{Grid}^{Act(max)}$ . Despite the remaining energy ( $E_{BESS}^{Act}$ ) have reached zero, the BESS was able to continue discharge the battery without triggering the internal battery protection mechanism. The threshold ( $P_{Th}^{Act}$ ) is unchanged at 68kW and the optimum threshold ( $P_{Th}^{Opt}$ ) simulated after the experiment is 67kW. The forecasted load profile ( $P_{Load}^{For}$ ) has mean absolute percentage error (*MAPE*) of 2.49%, with a standard deviation of 4.58%. The same scenario had happened on day 14 also.



(a)



(b)

**Figure 5.9: Three consecutive days of peak reduction carried out by (a) the active controller<sup>1</sup> and (b) the fundamental controller<sup>2</sup>**

Note: <sup>1</sup>The three days of results are referred to day 15, 16 and 17 in Appendix D. The peak ( $P_{Load}^{Act(max)}$ ) was reduced to  $P_{Grid}^{Act(max)}$  for all the three days. <sup>2</sup>The three days of results are referred to day 21, 22 and 23 in Appendix C. The peak ( $P_{Load}^{Act(max)}$ ) was reduced to  $P_{Grid}^{Act(max)}$  for day 21 and 23, however failed to reduce the peak on day 22 due to depletion of the battery. The BESS internal battery protection mechanism was activated on day 22.

Shown in Figure 5.9(a), the experimental results of the active controller are expanded to three consecutive days. Compared to the results of peak reduction using the fundamental controller shown in Figure 5.9(b), the results showed that the active controller is consistent and able to maintain the new peak below the fluctuation margin of the threshold ( $P_{Th}^{Act} + \Delta P_{Th}$ ). Indicated by 'b' in Appendix D, six days was recorded by the active controller that is in spite the battery was depleted before the peak is shaved, the active control is able to still reduce the peak for all the days.

### 5.2.3. Evaluation Indexes – $R$ and $A$

Next, two indexes, namely the demand reduction ( $R$ ) and the peak reduction factor ( $A$ ) or  $K_{ps}$  that is described in the literature (Chua, 2016), are used to assess; i) The contribution of the active adjustment of the threshold to the peak reduction, and ii) The effect of the discrepancy on the peak reduction. Equation (5.1) and Equation (5.2) show the definition of  $R$  and  $A$  in percentage.

$$R(d) = \frac{\mathbf{P}_{\text{Reduction}}^{\text{Act}}(d)}{\mathbf{P}_{\text{Load}}^{\text{Act(max)}}(d)} * 100\% \quad (5.1)$$

$$A(d) = \frac{\mathbf{P}_{\text{Reduction}}^{\text{Act}}(d)}{\mathbf{P}_{\text{Reduction}}^{\text{Sim}}(d)} * 100\% \quad (5.2)$$

where,  $\mathbf{P}_{\text{Reduction}}^{\text{Act}}$  is the experimental daily peak demand reduction  $\mathbf{P}_{\text{Load}}^{\text{Act(max)}} - \mathbf{P}_{\text{Grid}}^{\text{Act(max)}}$ ; and  $\mathbf{P}_{\text{Reduction}}^{\text{Sim}}$  is the simulated daily peak demand reduction  $\mathbf{P}_{\text{Load}}^{\text{Act(max)}} - \mathbf{P}_{\text{Grid}}^{\text{Sim(max)}}$ . This is the perfect reduction, a value that could have been achieved if the perfect model of the load profile had been used.

The index  $R$  is an indicator to represent how well the controller has performed in terms of the peak demand reductions. A high  $R$  indicates a good reductions and low  $R$  reflects a poor reductions. And shown in Figure 5.10, from the experimental results, the active controller has demonstrated a higher  $R$  as compared to the fundamental controller. The height of the box plot on the other hand then indicates the variance of  $R$ . A wide vertical box plot implies a large variation between the results, whereas a narrow vertical box plot reflects a more consistent and less variant results. And from the experimental results, the active controller has demonstrated a narrower vertical box plot as compared to the fundamental controller. Besides that, the experimental  $R$  of the active controller is also closer to the  $R$  simulated after the experiment. This implies that the experimental  $R$  achieved by the active controller is close to the perfect (or highest) reduction that can be achieved by the controller.

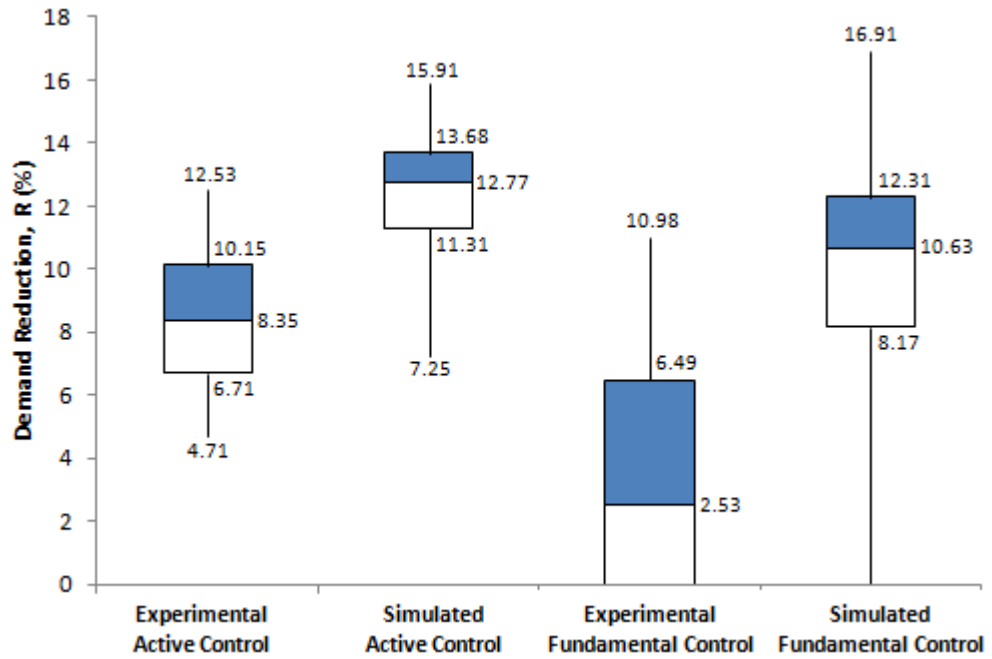


**Figure 5.10: The box plot of  $R$  achieved by the fundamental controller and the active controller from experiment and in simulation**

The box plot of  $A$  achieved by both the controllers is then plotted in Figure 5.11. A high  $A$  shows that the BESS has been effectively used for the peak reduction. A low  $A$  on the other hand reveals the BESS being under-utilized and the BESS is not operated at the optimal. The results showed that the values of  $A$  achieved by the active controller, on average, are higher than the fundamental controller. The median of  $A$  measured by the active controller is 68.82% as compared to 29.38% by the fundamental controller. The active controller also has narrower vertical box plot with a standard deviation of 13.76% as compared to the fundamental controller with a standard deviation of 29.01%.

From the evaluation indexes, the active controller has portrayed superiority over the fundamental controller. Despite the capacity of the BESS

being limited, the active control strategy however showed adaptability in adjusting the threshold in respond to the real-time demand. The active controller also minimises the BESS from failing to reduce the peak demand due to depletion failure. The demonstrated efficacy of the active controller is also consistent and can be maintained.

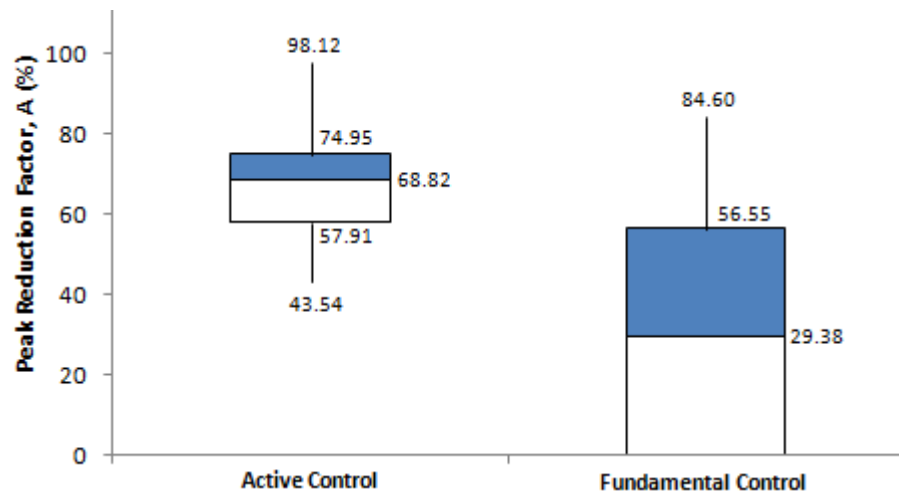


**Figure 5.11: The box plot of  $A$  achieved by the fundamental controller and the active controller**

#### **5.2.4. Comparison with the Other Literature Experimental Results**

Moving on, the active control strategy is also compared to the other literature experimental results. Of the three literature listed in Table 5.2, Chua (2016) has provided a more comprehensive analysis as compared to the others. The size of the ESS in (Chua, 2016) experiment is also comparable to the size of the BESS in this research. Chua (2016) experimental results, therefore, form the basis for the comparison in this section.

**Table 5.2: The experimental peak demand reductions from different literature**

Source	Controller	No. Supporting Results <sup>a</sup>	Size of BESS		Scenario A <sup>b</sup>		Scenario B <sup>c</sup>		
			P <sub>ESS</sub> (kW)	E <sub>ESS</sub> (kWh)	P <sub>Load</sub> <sup>Act(max)</sup> (kW)	P <sub>Reduc.</sub> <sup>Act(max)</sup> (kW)	MAX[P <sub>Load</sub> <sup>Act(max)</sup> ] (kW)	P <sub>Reduc.</sub> <sup>Act(eff.)</sup> (kW)	K <sub>ps</sub> <sup>d</sup> ( )
This dissertation	Fix-Threshold Control	31 days	18	64	84.45	9.28	85.89	0	0.37
	Active Control	31 days	18	64	79.96	10.02	91.13	7.58	0.68
Chua (2016)	Fix-Threshold Control	4 days	15	64	88.87	11.41	97.82	0.61	0.52
	Adaptive-Threshold Control	5 days	15	64	88.1	11.9	90.2	7.42	0.61
	Fuzzy Control	5 days	15	64	100.5	12.1	100.5	12.1	0.65
Reihani et al. (2016)	Real-Time Control	1 day	1,000	1,100	1,700	400	NIL <sup>e</sup>	NIL <sup>e</sup>	NIL <sup>f</sup>
Koller et al. (2015)	Model Predictive Control	4 days	1,000	580	113	30	115	10	NIL <sup>f</sup>

- The total number of peak reduction results recorded or listed in the literature.
- Represents the highest peak reduction ( $P_{Reduc.}^{Act(Max)}$ ) of the peak demand ( $P_{Load}^{Act(Max)}$ ) in a group of results.
- Represents the effective peak reduction ( $P_{Reduc.}^{Act(Eff.)}$ ) of the highest peak demand ( $MAX[P_{Load}^{Act(Max)}]$ ) in a group of results.
- Represents the peak reduction factor ( $K_{ps}$ ) described in Chua (2016). It has the same definition as  $A$  that is defined in Equation (5.2).
- Only one result is demonstrated in the literature and it is, therefore, insufficient for the benchmark.
- Unable to compute the peak reduction factor ( $K_{ps}$ ) because the maximum achievable peak deduction on the particular day of the experiment is not provided.

As tabulated in Table 5.2, the fuzzy controller has achieved a higher peak reduction in both the scenarios. However, the number of results supported by the literature is insufficient. It is unknown whether the demonstrated peak reductions can be maintained over an extended period of example 31 days. The highest minimization of the daily peak demands described in Scenario A also does not necessarily correspond to a maximisation of effective peak reductions defined in Scenario B. Furthermore, the minimization of the daily peak demands is also heavily depends on the type of peak, narrow or wide peak. The evaluation based on the peak reductions is hence insufficient when the experimented load profile is different. The assessment with the literature is therefore compared based on the peak reduction factor ( $A$  or  $K_{ps}$ ). The peak reduction factor sought to examine the consistency and accuracy of the controllers irrespective of the type of peak and load profile.

Even though the peak reductions ( $R$ ) demonstrated by the active controller is not the highest among the other controllers, when the experimental results are evaluated as a whole of all the data that are available in the literature, the active controller has achieved the highest peak reduction factor ( $A$ ) of 0.68 compared to the other controllers. This implies that the BESS controlled by the active controller has been effective for the application of peak reduction compared to the other controllers.

### 5.3. Economic Evaluations

In the previous section, the daily minimization of the non-coincident peak demand was examined and it sought to evaluate the robustness and peak reduction capability of the active controller. The scope of this research is however not solely on attempting to reduce the daily peak demands but also to investigate the savings as well as the financial feasibility of reducing the monthly maximum demand charge. This section thus shows the financial feasibility of using the BESS for maximum demand reductions with the active controller. A financial analysis is included at the end of this chapter to provide an estimated foresight of what would have been achieved if the savings by the active controller is improved or the price of the BESS is reduced.

In Malaysia, the monthly maximum demand charge is applicable to customers using the voltage level of 6.6kV and above. The monthly maximum demand charge is measured in price per kilowatts (RM/kW). Following the definition of the maximum demand charge given by the TNB (Tenaga Nasional Berhad, 2016), the saving from the reduction of the monthly maximum demand charge ( $S_{MD}$ ) is calculated using Equation (5.3). The introduction of BESS also brings saving in the electricity bill ( $S_{TR}$ ), whereby the BESS can be charged at time of low tariff and discharged at the time of high tariff price for peak demand reductions.

$$S_{MD} = U_{MD}[\mathbf{P}_{\text{Reduction}}^{\text{Act}}(d)] \quad (5.3)$$

$$S_{TR} = \sum_{d=0}^{\text{End of month}} \left( U_{\text{off}} * \Delta \mathbf{E}_{\text{BESS}}^{\text{Act}}(d)|_{\text{off-peak}} \right) - \left( U_{\text{on}} * \Delta \mathbf{E}_{\text{BESS}}^{\text{Act}}(d)|_{\text{on-peak}} \right) \quad (5.4)$$

where,  $d$  is the date with subsets of  $\{0, 1, 2, \dots, \text{End of month}\}$  ;  $\Delta \mathbf{E}_{\text{BESS}}^{\text{Act}}(d)|_{\text{off-peak}}$  is the energy (kWh) consumption during off-peak period;  $\Delta \mathbf{E}_{\text{BESS}}^{\text{Act}}(d)|_{\text{on-peak}}$  is the energy (kWh) consumption during on-peak period;  $U_{MD}$  is the unit price (RM/kW) for the monthly maximum demand charge;  $U_{\text{off}}$  is the unit price (RM/kWh) for energy consumption during the off-peak period; and  $U_{\text{on}}$  is the unit price (RM/kWh) for energy consumption during the on-peak period.

### 5.3.1. Evaluation Indexes – $T_{\text{payback}}$ and $NPV$

The type of capital budgeting techniques used in this study is the payback period ( $T_{\text{payback}}$ ) and the net present value ( $NPV$ ). This evaluation method investigates the economic viability of the active controller, by assessing the revenue of the peak reductions compared to the capital and operating costs over the BESS service life. The payback period is the number of years that is required to break-even the finances expended for the BESS investment. Shown in Equation (5.5), the payback period is determined when the saving from peak reduction (*Saving*) and the cost of BESS (*Cost*) are equals. Short payback period indicates a short duration to recoup the investment, whereas long payback period implies an undesirable, longer duration to break-even the initial capitals.

$$\sum_{i=1}^{T_{\text{payback}}} \frac{\text{Saving}(i)}{(1+r)^i} = \sum_{i=1}^{T_{\text{payback}}} \frac{\text{Cost}(i)}{(1+r)^i} \quad (5.5)$$

where,  $i$  is the year with subsets of  $\{1, 2, 3, \dots, Y_{\text{service}}\}$ ;  $Y_{\text{service}}$  is the projected service life of the BESS; and  $r$  is the discount rate.

The net present value, on the other hand, compares the current value of the investment to the value of investment in the future by taking inflation rate and the rate of returns of a time series of cash flows into account, to appraise the peak reduction project with BESS based on the time value of money. A positive  $NPV$  indicates the investment is adding monetary value into the project and a negative  $NPV$  is undesirable because it does not bring monetary gain into the project.

$$NPV = \sum_{i=1}^{Y_{\text{service}}} \frac{\text{Saving}(i) - \text{Cost}(i)}{(1+r)^i} \quad (5.6)$$

The *Saving* is computed by summing the avoided monthly maximum demand charge ( $S_{\text{MD}}$ ) and the saving in the electricity bill from taking the advantage of the on-peak and off-peak tariffs ( $S_{\text{TR}}$ ). The *Cost*, on the other hand, is calculated by adding the initial capital of  $C_{\text{PCU}} + C_{\text{ESC}}$  along with the replacement cost ( $C_{\text{Replacement}}$ ), operating and the maintenance cost ( $C_{\text{O\&M}}$ ) over the project period. Since the replacement cost of the BESS is already considered, the operating and maintenance cost is hence expected to be minimal and almost negligible ( $C_{\text{O\&M}} \cong 0$ ).

$$Saving(i) = S_{MD}^i(1 + g)^i + S_{TR}^i \quad (5.7)$$

$$Cost(i) = [C_{Capital}^0 + C_{Replacement}^{11}] - [C_{O\&M}^i(1 + r)^i] \quad (5.8)$$

where,  $i$  is the year with subsets of  $\{1, 2, 3, \dots, Y_{service}\}$ ;  $S_{MD}^i$  is the total yearly saving (RM) from maximum demand reductions;  $S_{TR}^i$  is the total yearly saving (RM) from electricity bill;  $C_{Capital}^0 = C_{PCU} + C_{ESC}$  is the capital cost (RM) of the BESS at year  $i = 0$ ;  $C_{Replacement}^{11} = C_{ESC}$  is the replacement cost (RM) of the BESS incur at year  $i = 11$ ;  $C_{O\&M}^i$  is the yearly operating and maintenance cost (RM) of the BESS; and  $g$  is the increment rate of tariff projected in Table 5.3.

**Table 5.3: The electricity tariff rate from 2006 to 2034**

Year	$U_{MD}$ (RM/kW)	$U_{on}$ (RM/kWh)	$U_{off}$ (RM/kWh)
2006 <sup>a</sup>	29.00	0.234	0.144
2009 <sup>b</sup>	35.60	0.288	0.177
2011 <sup>c</sup>	38.60	0.312	0.192
2014 <sup>d</sup>	45.10	0.365	0.224
2018 <sup>e</sup>	49.90	0.404	0.248
2022 <sup>e</sup>	55.03	0.446	0.273
2026 <sup>e</sup>	60.16	0.487	0.299
2030 <sup>e</sup>	65.29	0.529	0.324
2034 <sup>e</sup>	70.42	0.571	0.350

a. Retrieved from [https://www.tnb.com.my/assets/files/Tariff\\_booklet.pdf](https://www.tnb.com.my/assets/files/Tariff_booklet.pdf).

b. Retrieved from [https://www.tnb.com.my/assets/files/Tariff\\_Rate\\_Final\\_1.March.2009.pdf](https://www.tnb.com.my/assets/files/Tariff_Rate_Final_1.March.2009.pdf).

c. Retrieved from [https://www.tnb.com.my/assets/files/Tariff\\_Rate\\_Final\\_1.June.2011.pdf](https://www.tnb.com.my/assets/files/Tariff_Rate_Final_1.June.2011.pdf).

d. Retrieved from [https://www.tnb.com.my/assets/files/Tariff\\_Rate\\_Final\\_01.Jan.2014.pdf](https://www.tnb.com.my/assets/files/Tariff_Rate_Final_01.Jan.2014.pdf).

e. Extrapolated with the data recorded from 2006 to 2016.

The input parameters for the economic evaluation are listed in Table 5.4. According to the local price, the unit cost of the power conversion unit is RM 1942.50/kW, whereas the unit cost of lead-acid batteries is RM 425.50/kWh. The capital cost of BESS is computed as per Equation (5.9) and Equation (5.10). By taking into account the Malaysia national holidays of 13 days per year, the BESS is expected to operate 248 days in a year and the resultant battery service life is estimated to be 11 years at *DoD* of 50%. The utility tariff rates of C2 for the medium voltage peak-off-peak commercial customers are considered and the discount rate of 3% a year is applied.

$$C_{PCU} = U_{PCU} \times P_{BESS} \quad (5.9)$$

$$C_{ESC} = \frac{U_{ESC} \times E_{BESS}}{SoC^{max} - SoC^{min}} \quad (5.10)$$

where,  $C_{PCU}$  is the cost (RM) of the power conversion unit;  $C_{ESC}$  is the cost (RM) of energy storage capacity;  $U_{PCU}$  is the unit price (RM/kW) of the power conversion unit;  $U_{ESC}$  is the unit price (RM/kWh) of the energy storage capacity;  $SoC^{max}$  is the maximum BESS's battery state-of-charge (%);  $SoC^{min}$  is the minimum BESS's battery state-of-charge (%).

**Table 5.4: The input parameters for the economical analysis**

Description	Value	Unit
Size of the BESS's power rating ( $P_{\text{BESS}}$ )	18	kW
Size of the BESS's energy capacity ( $E_{\text{BESS}}$ )	64	kWh
The maximum BESS's battery state-of-charge ( $\text{SoC}^{\text{max}}$ )	100	%
The minimum BESS's battery state-of-charge ( $\text{SoC}^{\text{min}}$ )	50	%
Projected period of BESS operation ( $Y_{\text{service}}$ )	21	Years
Unit price of the power conversion unit ( $U_{\text{PCU}}$ )	1942.50 <sup>a</sup>	RM/kW
Unit price of the energy storage capacity ( $U_{\text{ESC}}$ )	425.50 <sup>a</sup>	RM/kWh
Battery inverter life	21 <sup>a</sup>	Years
Battery life	11 <sup>a</sup>	Years
Maximum demand charge ( $U_{\text{MD}}$ )	45.1 <sup>b</sup>	RM/kW
On-peak tariff ( $U_{\text{on}}$ )	0.365 <sup>b</sup>	RM/kWh
Off-peak tariff ( $U_{\text{off}}$ )	0.224 <sup>b</sup>	RM/kWh
Discount rate ( $r$ )	3 <sup>c</sup>	%

a. Retrieved from Chua et al. 2015.

b. Retrieved from [https://www.tnb.com.my/assets/files/Tariff\\_Rate\\_Final\\_01.Jan.2014.pdf](https://www.tnb.com.my/assets/files/Tariff_Rate_Final_01.Jan.2014.pdf).

c. Retrieved from <http://www.tradingeconomics.com/malaysia/interest-rate> on 21/12/2016.

### 5.3.2. Results of the Monthly Maximum Demand Reductions

From the results listed in Appendix C, battery depletion failure caused by the overly aggressive discharge of the BESS or under-set of the threshold can dramatically decrease the maximum demand charge savings. A single failure can cause a significant spike in the post peak demand reductions, erasing a large percentage of maximum demand charge savings for the month. The fundamental control technique only achieves the savings of 0.79% from the peak reductions with the incentive gain of RM 32.45 from utilising the on-

peak and off-peak tariff differences. If a perfect model of the load profile had been used, a maximum demand reduction of 8.25kW or about RM 372 addition would have been achieved by the fundamental controller. For a project period of 21 years, the fundamental control strategy is projected to have more than 21 years of payback period with the net present value of –RM 73,770. This implies that the peak reduction carried out by the fundamental controller is inefficient and may not be financially viable because the recouping of the capital cost is slow.

On contrary, listed in Appendix D, the active control technique achieves an overall savings of 9.07% or RM 341.86 from the avoided maximum demand of 7.58kW and incentive gain of RM 30.88 from utilising the differences between the on-peak and off-peak tariffs. The active controller is projected to have payback period of about 19.59 years with the net present value of +RM 5,930. Though the payback period is long and the incentive gain at the end of the project is minimal, the active controller has demonstrated a feasible financial as compared to the fundamental controller.

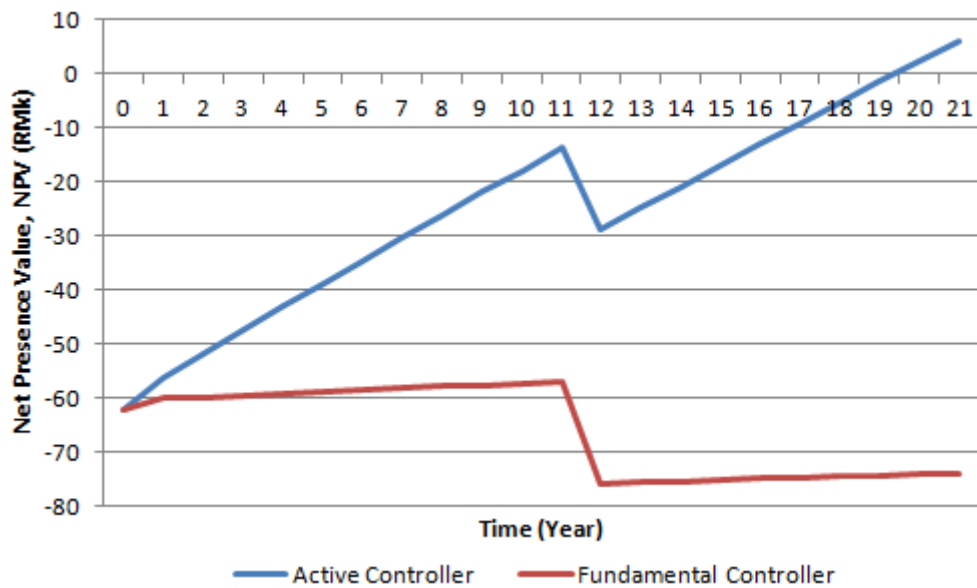


**Figure 5.12: The breakdown of the net presence value achieved by the fundamental controller and the active controller**

Note: At the 11<sup>th</sup> year, there is a replacement of all the batteries and therefore a drop is observed.

Next, based on the load profile analysis discussed in Section 5.1, with the current BESS battery capacity of about 27kWh or depth-of-discharge of 50%, the achievable maximum demand reduction on average is about 11kW. If every month, the avoided maximum demand is 11kW, the payback period would be 12.73 years with a net present value of +RM 41,900 by the end of the 21 years.

Listed in Table 5.5, every increment by 5% of the maximum demand reduction per month, from 7.58kW, would result on average an increase of 1.12% of net presence value and a payback period of 0.97% drop. To achieve a payback period of below 11 years and net presence value of above RM

65,000, the maximum demand reduction (MDR) per month is required to be improved to 13.3kW and above.

**Table 5.5: Results of the financial analysis if the maximum demand reduction per month is improved by 5%–step of the present active controller’s performance**

MDR (kW)	$T_{payback}$ (Year)	NPV (k RM)		MDR (kW)	$T_{payback}$ (Year)	NPV (k RM)
7.58	19.59	5.93	(Continued.)	12.89	11.32	61.73
7.96	18.73	9.93		13.27	11.02	65.71
8.34	17.94	13.93		13.64	10.73	69.70
8.72	16.87	17.89		14.02	10.11	73.68
9.10	16.22	21.88		14.40	9.86	77.67
9.48	15.61	25.86		14.78	9.62	81.66
9.85	14.90	29.85		15.16	9.39	85.64
10.23	14.38	33.83		15.54	9.17	89.63
10.61	13.90	37.82		15.92	8.96	93.61
10.99	13.45	41.80		16.30	8.76	97.60
11.37	12.89	45.79		16.68	8.57	101.58
11.75	12.49	49.77		17.06	8.38	105.57
12.13	12.12	53.76		17.43	8.21	109.55
12.51	11.77	57.74		17.81	8.04	113.54

Apart from that, every decrement by 5% of the total investment cost of the BESS listed in Table 5.6 would result on average an increase of 1.18% of net present value and a payback period of 0.91% drop. To achieve a payback period of below 11 years and net present value of above RM 37,000, the total

investment cost for the BESS is required to be reduced or discounted by 60% and above.

**Table 5.6: Results of the financial analysis if the total investment cost of the BESS is reduced by 5%–step of the current BESS price**

Discount (%)	$T_{payback}$ (Year)	$NPV$ (k RM)	Discount (%)	$T_{payback}$ (Year)	$NPV$ (k RM)
0	19.59	5.93	40	11.28	37.73
5	18.61	9.91	45	10.34	41.70
10	17.63	13.88	50	9.30	45.68
15	16.31	17.86	55	8.37	49.65
20	15.36	21.83	60	7.44	53.62
25	14.40	25.80	65	6.51	57.60
30	13.16	29.78	70	5.58	61.57
35	12.22	33.75	75	4.65	65.66

(Continued.)

#### 5.4. Summary

In summary, the load demands, the load characteristic and the energy consumption on the experimental site have been analyzed. The experimental peak demand reduction results of the active controller have also been technically evaluated with the fundamental controller. From the evaluation indexes ( $R$  and  $A$ ), the active control strategy portrayed superiority over the fundamental control strategy. Despite the capacity of the BESS being limited, the active control strategy somehow showed adaptability in adjusting the threshold in respond to the real-time demand. The demonstrated efficacy of the active controller is also consistent and can be maintained throughout.

Apart from that, the active control strategy was also compared to the other literatures of similar topics of research interest and of similar sizes of the BESS. Even though the peak reductions ( $R$ ) demonstrated by the active controller was not the highest among the other controllers, when the experimental results were evaluated as a whole, the active controller has achieved the highest peak reduction factor ( $A$ ) of 0.68. This implies that the BESS controlled by the active controller has been effective for the application of peak reduction compared to the other controllers.

Not only that, the active control strategy also managed to reduce the monthly maximum demand charge of the building by 9.07% as compared to 0.79% by the fundamental set-point control strategy. For a project period of 21 years, the fundamental control strategy is projected to have more than 21 years of payback period with the net present value of -RM 73,770. This implies that the peak reduction carried out by the fundamental controller is inefficient and may not be financially viable because the recouping of the capital cost is slow. On the other hand, the active controller is projected to have the payback period of about 19.59 years with the net present value of +RM 5,930. Though the payback period is long and the incentive gain at the end of the project is minimal, the active controller has demonstrated a feasible financial as compared to the fundamental controller.

## CHAPTER 6

### CONCLUSIONS AND FUTURE WORKS

#### 6.1. Conclusions

A battery-based energy storage system (BESS) has been designed and setup at the Universiti Tunku Abdul Rahman (UTAR) campus in Sungai Long. The BESS is coupled to the low voltage (LV) distribution network interconnected with the loads located at KA block LG, G and M floors. The BESS have a total power rating of 18kW and total energy capacity of up to 64kWh. To prolong the lifespan of the batteries, the amount of energy that can be used is however only about 27kWh. Multiple of measuring meters have been set up to measure the supplies imported from the utility. Communication system between the BESS as well as the measuring meters has been established with a central control unit. A user interface, displaying the measurements and the controls has also been implemented in LabVIEW.

An active control strategy has been developed to reduce the daily peak demands for cutting down the monthly maximum demand charges. The active control strategy with real-time threshold adjuster, day-ahead and next minute load forecasting has been developed, tested and evaluated on the BESS setup at the university. It improved the fundamental control strategy by incorporating a short-term load forecast, accompanied by the real-time BESS

schedule and a persistence strategy to adjust the threshold continuously based on the discrepancy between the forecasted and the real-time load demands. The performance of the active control strategy was thoroughly evaluated experimentally. From the evaluation indexes, the active control strategy portrayed superiority over the fundamental control strategy. Despite the capacity of the BESS being limited, the active control strategy showed adaptability in adjusting the threshold in respond to the real-time demand. The demonstrated efficacy of the active controller is also consistent and can be maintained.

The active control strategy was also compared to the other literature of similar topics of research interest and of similar sizes of the BESS. Even though the peak reductions ( $R$ ) demonstrated by the active controller was not the highest among the other controllers, when the experimental results were evaluated as a whole of all the experimental data, the active controller has achieved the highest peak reduction factor ( $A$ ) of 0.68. This implies that the BESS controlled by the active controller has been effective for the application of peak reduction compared to the other controllers.

Not only that, the active control strategy also managed to reduce the monthly maximum demand charge of the building by 9.07% as compared to 0.79% by the fundamental control strategy. For a project period of 21 years, the fundamental control strategy is projected to have more than 21 years of payback period with the net present value of –RM 73,770. This implies that the peak reduction carried out by the fundamental controller is inefficient and

may not be financially viable because the recouping of the capital cost is slow. On the other hand, the active controller is projected to have the payback period of about 19.59 years with the net present value of +RM 5,930. Though the payback period is long and the incentive gain at the end of the project is minimal, the active controller has demonstrated a feasible financial as compared to the fundamental controller.

In summary, the contributions of this research work are as listed:

1. A new and improved performance peak reduction control strategy has been developed for the BESS. The controller has demonstrated its efficacy over the fundamental control strategy as well as the other controllers that are presented in the literature of the similar topics of research interest and of similar sizes of the BESS.
2. Besides that, compared to the other literature with supports of only a handful of peak demand reduction experimental results, this research demonstrated a persistent reduction of the daily peak demands up to a month of experimental results. This research also presented the monthly maximum demand reduction carried out by the active controller.
3. Apart from that, the BESS has also been successfully integrated with an actual 415V LV network for more than a year with no power stability issue so far.

4. Not only that, the BESS as well as the active control strategy were also designed in a way that they are modular and scalable for future expansion and improvement. The interface developed for the BESS is also commercializable.
5. In addition, the research findings have also been published in international peer review journals such as the one listed in the list of publications.

## **6.2. Future Work**

Compared to the fundamental control strategy as well as the other controllers that are presented in the literatures of the similar topic of interest and of similar size of the BESS, although the active control strategy presented in this research has demonstrated the efficacy in reducing the peak demands, there are still room for the active control strategy to improve the peak reduction factor of 0.68 to 1.00, where a peak reduction factor of 1.00 implies that the control strategy have effectively used all the energy that is available in the BESS for peak demand reduction. The following thus elaborates the future work that can be introduced to improve the active control strategy.

Firstly, the further ahead the future demands are known, the more efficiently the BESS can be operated. The load forecasting method derived in this research is however only accurate, less than 5% prediction error, up to the demands prediction for the next minute interval. Further than that, the

prediction error would increase. Future work therefore can explore and introduce intelligent forecasting method (such as expert systems, fuzzy logic methods, and neural network methods) to improve the prediction accuracy of the load profile. Apart from predicting the peak demands of the daily load profile, the forecasting target can also be expanded to predict the monthly maximum demands. Having known the maximum demand, the controller would be able to operate the BESS effectively, by performing the peak reduction only on those days that are contributing to the maximum demand and avoid wastage of supply on days that are not.

However, forecasting often contains some degrees of uncertainties. No single forecast is best at all intervals. To handle the forecast uncertainties, this research work proposed to persistently adjust the threshold throughout the day based on the latest information on the load demand. Future work can thus look into and introduce optimization algorithms (such as evolutionary algorithm, particle swarm optimization approach and simulated annealing technique) to fine tune the control parameters and enhance the adjustment of the threshold such that the energy capacity that is available in the BESS is efficiently used for the peak reduction.

## LIST OF PUBLICATIONS

Hau, L. C. and Lim, Y. S., 2016. A Real-Time Active Peak Demand Reduction for Battery Energy Storage with Limited Capacity. *Journal of Communications*. 11(9), pp. 841-847.

Hau, L. C., Lim, Y. S. and Chua, K. H., 2017. Active Control Strategy of Energy Storage System for Reducing Maximum Demand Charges under Limited Storage Capacity. *Journal of Energy Engineering*. pp. 04017010.

# A Real-Time Active Peak Demand Reduction for Battery Energy Storage with Limited Capacity

Lee Cheun Hau and Yun Seng Lim

Lee Kong Chian Faculty of Engineering and Science, Universiti Tunku Abdul Rahman

Jalan Sungai Long, Bandar Sungai Long, Cheras 43000, Kajang, Selangor

Email: alveyhau@gmail.com; yslim@utar.edu.my

**Abstract**—Battery-based energy storage (BESS) has found to have potential and interest in reducing the peak demand. Over the years, a number of control strategies have been developed for BESS to reduce the peak demand. The control strategies are however complex and confined to simulation evaluation only. The control strategies are also not tested in BESS set-up with limited capacity. A simple and yet comprehensive real-time active peak demand reduction control has therefore been developed and presented in this paper. The real-time active control has been evaluated experimentally using the university building as the site. The performance of the real-time control has been evaluated as compared to the fundamental control as well as the ideal reduction in simulation. Even though the capacity is limited, the results showed superiority and adoptability of the real-time active control as compared to the fundamental control, with peak demand reduction of about 8.64% as compared to 4.24%. The real-time active control also showed higher accuracy of 70.52% towards the ideal reduction result as compared to the fundamental control with only 35.25%.

**Index Terms**—Peak demand reduction, energy storage system, bess, limited capacity, control system

## I. INTRODUCTION

Every month, the industrial and commercial consumers are charged by the utility company on the peak demand contribution as well as the electricity used. To meet and supply peak demand, utility company require to set up peak load power plants which operate to cover 20% of the total power demand and on average only 55% of the installed capacity are used [1]. Such power plants only operate for about 6 to 8 hours a day. To recover the capital cost as well as the operating and maintenance cost within the lifespan of the power plant, utility company therefore require to charged higher cost of energy consumption to consumer who contributes to the peak demand. In Malaysia, Tenaga Nasional Berhad charges the peak demand through maximum demand charge [2]. Such charges often contribute as high as 30% of the total electricity costs [3]. Reduction of peak demand therefore brings monetary savings to industrial and commercial consumers. A number of approaches have thus been

introduced and battery-based energy storage system (BESS) has found to have potential and interest [4]–[6]. BESS store energy during low demand period and supply power during peak demand period to lighten the power supply from the utility and mitigate peak demand on the customer site.

### A. Fundamental BESS Peak Reduction Control

Present there are two fundamental controls for BESS. The first operates BESS using a fixed scheduled pattern that is pre-determined from historical demand [7]–[9] and the second is a load following control with real time monitoring of power network, mitigates peak demand when the consumption exceeds a set threshold [10]–[12]. The first control has advantage of removing the need of monitoring the power network. The peak demand is however reduced uniformly and operates without any knowledge of the energy demand. Stored energy might be wasted during non-peak period if misalignment occurred between the schedule and actual demand. On contrary, the second control has the control flexibility but also operates without any knowledge of energy demand. If threshold is set too high, the maximum demand reduction might not be achieved. If the threshold is set too low, the stored energy might become exhausted and latter part of peak might not be reduced. Both the controls thus have the tendency to run into failure of storage shortage or unnecessary peak demand reduction.

### B. Advance BESS Peak Reduction Control

It has been studied that if demand can be anticipated, BESS can be off-line scheduled optimally and set-point can be determined optimally. Due to the inherently stochastic nature of demand, forecast error is however unavoidable. If anticipated demand can be optimized in real-time, the forecast error can hence be minimized as real-time demand is available. Failure such as shortage of energy or unnecessary peak demand reduction during day of low demand can thus be minimized. Adopting from this, a number of complex BESS peak reduction control strategies have thus been proposed [13]–[15]. The literatures are however limited to examine only the variability effect of demand forecast and neglected the nonlinear nature of battery such as the battery degradation, which also has an effect to the overall respond of BESS when compared to a real-case scenario. Though a number of complex BESS control strategies has been proposed, the

---

Manuscript received June 11, 2016; revised September 26, 2016.

This work was supported by the CREST R&D Grant under Grant No. P01C1-14.

Corresponding author email: alveyhau@utar.my.

doi:10.12720/jcm.11.9.841-847

analysis are however confined to simulation and only a few literatures are supported with limited number of actual experimental results [16], [17]. Besides that, the

control strategies are also not tested in BESS set-up with limited capacity, which happened often in the real-case scenario because of economic constraints.

Nomenclature		Subscript	
$P$	power (kW)	$start$	starting condition
$E$	energy (kWh)	$stop$	stopping condition
$d$	day ( )	$eLoad$	estimated load demand
$t$	time (minutes)	$fLoad$	forecasted load demand
$T$	current time (minutes)	$hLoad$	historical load demand
$SoC$	battery state-of-charge (%)	$sBESS$	scheduled supply from BESS
$a$	approximate factor ( )	$aBESS$	real-time supply from BESS
<u>Superscript</u>		$fBESS$	forecasted supply from BESS
$0$	initial value	$aGrid$	real-time supply from utility
$max$	maximum value	$fTh$	forecasted threshold
$min$	minimum value	$req$	minimum required value
$freq$	frequent occurred value	$aPD$	experimental peak demand reduction
$m$	Mth forecasted index	$sPD$	simulated peak demand reduction
$k$	Kth step index	$Bat$	BESS energy capacity
$adj$	fine tuned value	$Inv$	BESS power rating

C. Outline of Content

The scope of this paper therefore aims to look into the literatures' limitations and derive a simple yet comprehensive control strategy for BESS to reduce peak demand with limited capacity. Experimental evaluation is carried out using the university building as the site. Case study such as the comparison of the proposed control

strategy with the fundamental control strategy as well as the ideal reduction in simulation is also conducted. The remainders of this paper structured with the framework of the proposed control strategy in Section II, followed by the experimental validation and evaluation in Section III and lastly the conclusion in Section IV.

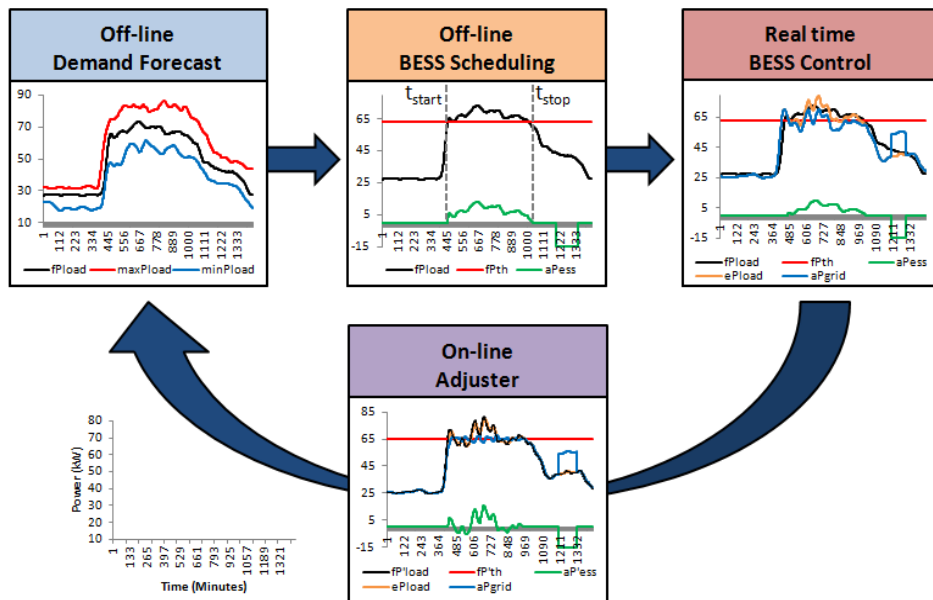


Fig. 1. Real-time active peak demand reduction framework

II. REAL-TIME ACTIVE PEAK DEMAND REDUCTION FRAMEWORK

A simple yet comprehensive real-time active peak demand reduction control strategy ( $\alpha$ PDR), depicted in Fig. 1, consisting of an off-line demand forecast, an off-line BESS scheduling, a real-time BESS control and an

on-line adjuster is developed. The equations described in this section are subjected to the technical constrained defined in Eq. (1) and (2). Where Eq. (1) defined the power output range and Eq. (2) defined the energy level of the BESS.

$$-P_{Inv} \leq P_{BESS}(t) \leq P_{Inv} \tag{1}$$

$$\text{SoC}^{\min} \leq \text{SoC}(t) \leq \text{SoC}^{\max} \quad (2)$$

#### A. Off-Line Framework

The off-line framework consists of a demand forecast and a BESS scheduling. Prior to peak demand reduction, on present day ( $d$ ), an off-line demand analysis is first being carried out to compute the necessary initial parameters for the subsequent day,  $d + 1$ . A series of historical demand are first being retrieved, the maximum and minimum bands of the historical demands are then deduced. The baseline forecast of the subsequent day 24 hours demand ( $\mathbf{P}_{\text{fLoad}}^0$ ) is computed as per a statistical approach listed in Eq. (3), locating the frequently occurred demand ( $\mathbf{P}_{\text{hLoad}}^{\text{freq}}$ ) compared over the maximum ( $\mathbf{P}_{\text{hLoad}}^{\max}$ ) and minimum ( $\mathbf{P}_{\text{hLoad}}^{\min}$ ) bands at every instant of 1 minute.

$$\mathbf{P}_{\text{fLoad}}^0(d+1) = \mathbf{P}_{\text{hLoad}}^{\max}(d) - \mathbf{P}_{\text{hLoad}}^{\text{freq}}(d) \quad (3)$$

$$[\mathbf{P}_{\text{hLoad}}^{\max}(d) - \mathbf{P}_{\text{hLoad}}^{\min}(d)]$$

Once a baseline forecast is obtained, the  $\alpha$ PDR then locate the subsequent day threshold ( $\mathbf{P}_{\text{fTh}}^0$ ) as per Eq. (4) to (6), sweeping from the maximum power of the forecasted demand ( $\mathbf{P}_{\text{fLoad}}^0$ ) down until the highest threshold when the power rating ( $\mathbf{P}_{\text{fTh1}}^0$ ) or the capacity ( $\mathbf{P}_{\text{fTh2}}^0$ ) limits of BESS is reached. The  $\alpha$ PDR then derive a schedule profile based on Eq. (7), to prepare the BESS such that it has enough capacity to reduce the peak demand for the subsequent day. Where the BESS will supply the difference between the forecasted demand and threshold at time of forecasted peak period ( $t_{\text{start}}^0$  to  $t_{\text{stop}}^0$ ), and charge with the maximum power ( $\mathbf{P}_{\text{Inv}}$ ) at time of non-peak period ( $t_{\text{Q2}}$  to  $t_{\text{Q1}}$ ).

$$\mathbf{P}_{\text{fTh}}^0(d+1) = \max[\mathbf{P}_{\text{fTh1}}^0, \mathbf{P}_{\text{fTh2}}^0] \quad (4)$$

$$\mathbf{P}_{\text{fTh1}}^0 = \max_{\forall t} [\mathbf{P}_{\text{fLoad}}^0(d+1)] - \mathbf{P}_{\text{Inv}} \quad (5)$$

$$\mathbf{P}_{\text{fTh2}}^0 = \mathbf{P}_{\text{fTh1}}^0 | E^{\text{req}}(k-1) > E_{\text{bat}} \quad (6)$$

$$\mathbf{P}_{\text{sBESS}}^0(d+1) = \mathbf{P}_{\text{fLoad}}^0(d+1) - \mathbf{P}_{\text{fTh}}^0(d+1) \quad (7)$$

$$\text{if } t_{\text{start}}^0 \leq t \leq t_{\text{stop}}^0$$

$$= -\mathbf{P}_{\text{Inv}}$$

$$\text{if } t \leq t_{\text{Q1}}$$

$$\text{or } t \geq t_{\text{Q2}}$$

$$= 0 \text{ otherwise}$$

#### B. On-Line Framework

The on-line framework consists of two parts, a real-time control and an on-line adjuster. On the operation day, the  $\alpha$ PDR then proceed to perform peak reduction in real-time, continuously monitor the real-time demand ( $\mathbf{P}_{\text{eLoad}}$ ) and actively perform peak demand reduction based on Eq. (8) and a set of heuristic rules displayed in Fig. 2. Eq. (8) defines the required supply from BESS ( $\mathbf{P}_{\text{aBESS}}^{\text{req}}$ ) for the

next interval ( $t + 1$ ), in which to reduce the mean absolute percentage error (MAPE), it is computed by bringing the scheduled profile towards the forecasted supply ( $\mathbf{P}_{\text{fBESS}}$ ) by an approximate factor ( $\alpha$ ), determined from the current MAPE at time  $T$ .

The forecasted supply is determined from the present demand location on the heuristic map depicted in Fig. 2. Briefly, the heuristic rules on the map in Fig. 2 are categorized into 6 zones, namely A, B, C, D, E and F, with 4 possible types of operations *Charge*, *Discharge*, *Standby* and *Idle*. *Charge* represents the period when BESS is given to replenish the battery energy, whereas *Discharge* is the period when BESS is supplying power to reduce the peak demand. *Idle* then indicate the occasion when BESS is unused and *Standby* is the portion when BESS is boost supplying for the operation of *Discharge*, added to kick start the BESS and address the delay of supply when demand is analyzed in consecutive average of different resolutions.

$$\mathbf{P}_{\text{aBESS}}^{\text{req}}(t+1) = \alpha(t) [\mathbf{P}_{\text{sBESS}}^{\text{adj}}(t+1) - \mathbf{P}_{\text{fBESS}}(t+1)] + \mathbf{P}_{\text{fBESS}}(t+1) \quad (8)$$

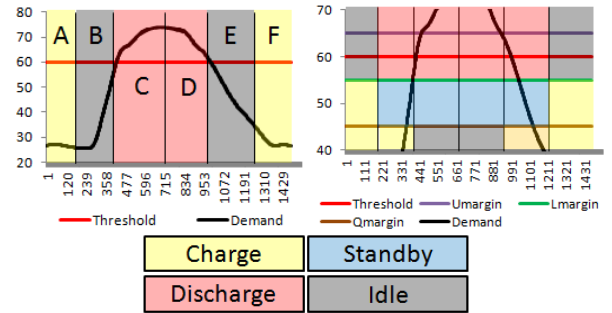


Fig. 2. The heuristic map control for BESS

Next, the  $\alpha$ PDR then actively perform appropriate adjustment to fine-tune the off-line parameters, and as such the forecasted and present demand misalignment is reduced, fluctuation along the threshold is minimized and ultimately the BESS energy is conserved and utilized only at interval of potential peak demand. Eq. (9) defines the adjustment on the demand forecast ( $\mathbf{P}_{\text{fLoad}}^{\text{adj}}$ ), by bringing the forecasted demand with the least MAPE ( $\mathbf{P}_{\text{fLoad}}^{\text{m}}$ ) up until time  $T$ , towards the demand measured in real-time ( $\mathbf{P}_{\text{eLoad}}$ ).

Eq. (10) then defines the BESS schedule adjustment, in which the future schedule ( $\mathbf{P}_{\text{sBESS}}^{\text{adj}}$ ) prepare the BESS by charging with  $\mathbf{P}_{\text{Q}}$ ; a charging mechanism determine by the BESS power conversion unit, at time of non-peak period and perform peak demand reduction at time of potential peak ( $t_{\text{start}}^{\text{adj}}$  to  $t_{\text{stop}}^{\text{adj}}$ ), with supply of the difference between the adjusted demand forecast ( $\mathbf{P}_{\text{fLoad}}^{\text{adj}}$ ) and the adjusted future threshold ( $\mathbf{P}_{\text{fTh}}^{\text{adj}}$ ). The future threshold is determined following Eq. (11), by locating the maximum between the highest threshold setting at time  $T$  with the least MAPE ( $\mathbf{P}_{\text{fTh}}^{\text{m}}$ ) and the highest

reduction achieved up until  $T$ ; which is the measured grid supply ( $P_{aGrid}$ ) deducts the permitted fluctuation margin,  $\Delta P_{Th}$ .

Once the appropriate adjustment is performed on the off-line parameters, the  $\alpha$ PDR then proceed back to perform peak reduction in real-time with Eq. (8) and Eq. (12). Eq. (12) is added to first eliminate the unnecessary demand transient or noise, and second is to reduce the delay of supply when demand is analyzed in consecutive average of different resolutions, by supplying power at a magnitude computed over the past 15 minutes instead of supplying with the power amount defined in Eq. (8).

$$P_{fLoad}^{adj}(t+1) = \alpha(t)[P_{fLoad}^m(t) - P_{eLoad}(t)] + P_{eLoad}(t) \quad (9)$$

$$P_{sBESS}^{adj}(t+1) = P_Q(t+1) \text{ if } t \leq t_{Q1} \text{ or } t \geq t_{Q2} \quad (10)$$

$$= P_{fLoad}^{adj}(t+1) - P_{fTh}^{adj}(t+1)$$

$$\text{if } t_{start}^{adj} \leq t \leq t_{stop}^{adj}$$

$$= 0 \text{ otherwise}$$

$$P_{fTh}^{adj}(t+1) = \max_{\forall t} \left\{ \begin{array}{l} \max_{m=0 \rightarrow M} [P_{fTh}^m(t)], \\ \max_{\forall t} [P_{aGrid}(t) - \Delta P_{Th}] \end{array} \right\} \quad (11)$$

$$(t+1) = \text{mov avg}_{t=T-15 \rightarrow T} [P_{aBESS}^{req}(t+1)] \quad (12)$$

$$- \sum_{T-15}^T [P_{aBESS}^{adj}(t)]$$

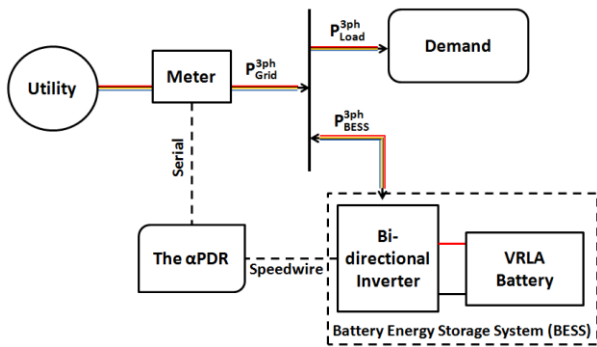


Fig. 3. The experimental set-up

### III. EXPERIMENTAL EVALUATION

A course of 32 days of experimental evaluation is carried out on a low-voltage system installed at Universiti Tunku Abdul Rahman, Malaysia. The system is set up as depicted in Fig. 3, with BESS consisting of 18kW bi-directional inverter and a bank of valve-regulated lead-acid (VRLA) battery with total capacity of about 64kWh. To preserve the life span of battery, the BESS however only have usable capacity of about 27kWh, deduced empirically, at depth-of-discharge of 50%. Compared to the average energy required to reduce peak demand of 18kW, obtained from demand analysis displayed in Fig. 4,

the usable capacity is however insufficient and about 62.37% lesser. To evaluate the performance of the control strategy under such scenario; limited capacity, a new evaluation method is therefore introduced and is elaborated in this section. Evaluation of the  $\alpha$ PDR with the fundamental control as well as the ideal reduction in simulation is also discussed. The assessment of the controls' performance is reviewed based on the overall percentage of peak demand reduction and also the overall percentage difference as compared to the ideal reduction simulated when forecast error is zero.

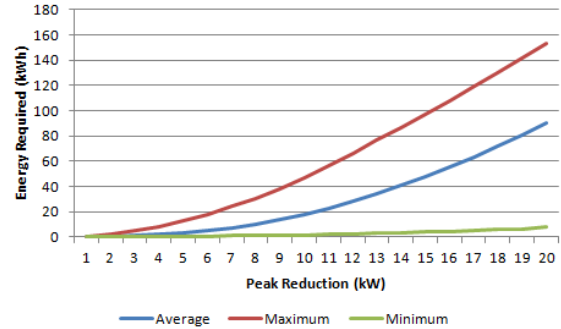


Fig. 4. The estimated energy required to reduce the peak demand at the experiment site

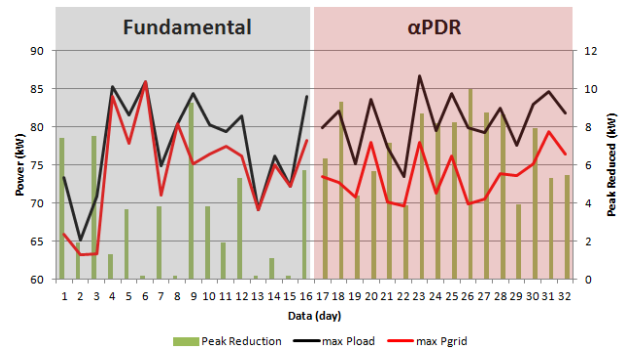


Fig. 5. Peak demand reduction of the fundamental and  $\alpha$ PDR control strategy

#### A. Experimental Results

Fig. 5 illustrates the peak demand reduction achieved over the course of 32 days, with 16 days each for the fundamental control and the  $\alpha$ PDR. Even though the highest peak demand reduced over the 16 days for both the controls are comparable, where for fundamental control is 9.28kW and for  $\alpha$ PDR is 10.02kW, the overall reduction observed through the 16 days are however uniform for  $\alpha$ PDR.

From the results, some depicted in Fig. 6, day 4, 6, 8, 11, 13, 14, 15, 18, 27 and 31 are the days when failures occurred. Day 4, 6, 8, 11, 14 and 15 were the failures due to under setting of threshold by the fundamental control. Day 13 on the other hand failed due to over setting of threshold; whereby the peak demand is below the threshold and demand reduction was not performed. Besides that, the fundamental control also projected delay of supply when demand is analyzed in consecutive average of 30 minutes resolutions; standard computation period for peak demand in Malaysia [2]. Referring to Fig.

6(a), the delay of BESS supply is observed at every beginning of BESS supply, such as at 511 minute, 613 minute and 783 minute. The BESS was trying to reduce

the demand, but a delay in coping with the increase in demand occurred with the fundamental control.

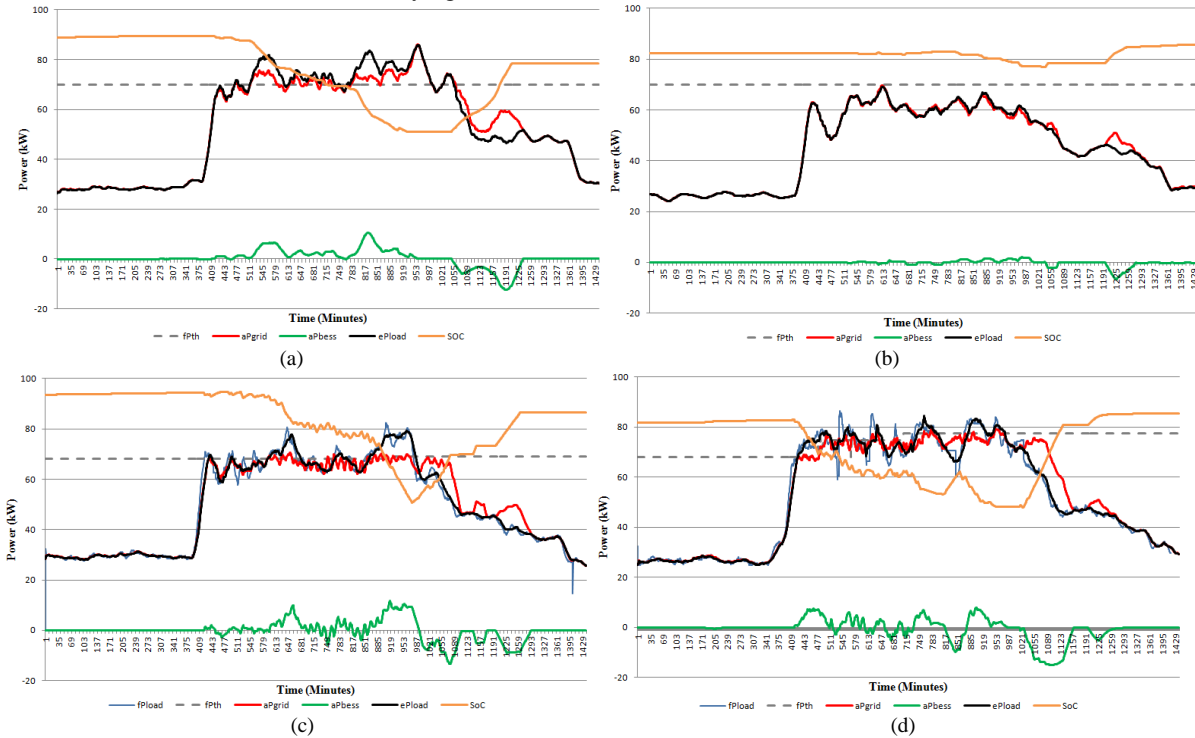


Fig. 6. Experimental results on (a) Day 6 (b) Day 13, (c) Day 27 and (d) Day 31

On contrary, although failures have occurred on day 18, 27 and 31, the  $\alpha$ PDR however still managed to reduce the peak demand. Observed on both Fig. 6(c) and 6(d) results, the delay of BESS supply is also reduced greatly with the  $\alpha$ PDR. The fundamental control hence depicted weakness of over or under setting of threshold such as had happened on day 4, 6, 8, 11, 14 and 15 as a results of depletion failure due to under setting of threshold and day 13 as a result of over setting of threshold, whereby the demand on day 13 is lower than the set threshold and no reduction of peak was performed. As compared to  $\alpha$ PDR, although depletion failure occurred, the proposed control however still managed to reduce the peak despite the limited capacity of battery. In addition, delay of supply is also mitigated greatly by the proposed  $\alpha$ PDR.

**B. Performance Evaluation**

Fig. 7 then illustrates the percentage of peak demand reduced (%R) by the fundamental control and  $\alpha$ PDR. A

percentage difference (%D) between the experimental result and the ideal reduction simulated with no forecast error is also included in Fig. 7 to provide a benchmark of how far the experimental result is away from the simulated, best achievable result with no forecast error. A new parameter, the percentage of performance (%P) is also proposed to provide a more holistic review of BESS control with limited capacity. The percentages of performance not only account the peak reduction differences compared to the ideal reduction, but also consider the energy density ratio ( $W_{peak}$ ) required to reduce the peak. The proposed evaluation methods are comprehensive and can be serves as a rule-of-thumb assessment for any other peak reduction control. All the evaluation methods discussed are calculated as per Eq (13) to (15) and the results are listed in Table I.

$$\%R(d) = \frac{\max_{\forall t} P_{eLoad}(d) - \max_{\forall t} P_{aGrid}(d)}{\max_{\forall t} P_{eLoad}(d)} \times 100 \quad (13)$$

TABLE I: THE EXPERIMENTAL AND SIMULATED RESULTS

Day	$P_{eLoad}^{max}$ (kW)	$P_{aGrid}^{max}$ (kW)	$P_{aPD}$ (kW)	$P_{siPD}$ (kW)	$E_{aBESS}^0$ (kWh)	$E_{aBESS}^Q$ (kWh)	$E_{siBESS}^{req}$ (kWh)	$W_{peak}$ ( )	%R (%)	%D (%)	%P (%)
1	73.30	65.88	7.42	10.10	25.00	0.00	40.74	1.63	10.12	26.56	83.70
2	65.08	63.18	1.90	5.56	9.38	0.00	5.00	0.53	2.92	65.79	34.21
3	70.92	63.38	7.54	10.15	11.91	0.00	10.26	0.86	10.63	25.71	74.29
4	85.33	84.04	1.29	7.69	20.39	0.00	29.07	1.43	1.52	83.16	41.68
5	81.57	77.88	3.69	6.43	22.30	0.00	15.84	0.71	4.52	42.59	57.41
6	85.89	85.89	0.00	9.91	23.49	0.00	51.05	2.17	0.00	100.00	53.99
7	74.91	71.08	3.82	9.71	18.41	0.00	17.11	0.93	5.10	60.61	39.39
8	80.36	80.36	0.00	3.30	13.73	0.00	43.25	3.15	0.00	100.00	68.26
9	84.45	75.17	9.28	10.96	19.86	0.00	25.66	1.29	10.98	15.40	88.08
10	80.32	76.48	3.84	9.21	24.47	0.00	23.62	0.97	4.78	58.27	41.73

11	79.42	77.51	1.91	8.64	23.57	0.00	19.16	0.81	2.40	77.94	22.06
12	81.49	76.20	5.29	9.50	15.83	0.00	17.98	1.14	6.49	44.30	61.00
13	69.10	69.10	0.00	1.76	19.06	0.00	0.18	0.01	0.00	100.00	0.00
14	76.18	75.06	1.12	6.44	21.44	0.00	14.74	0.69	1.47	82.66	17.34
15	72.21	72.21	0.00	3.26	20.54	0.00	3.37	0.16	0.00	100.00	0.00
16	83.97	78.24	5.73	12.21	20.59	0.00	19.40	0.94	6.82	53.08	46.92
17	79.86	73.52	6.34	8.93	25.52	2.18	25.77	0.93	7.93	29.04	70.96
18	82.08	72.74	9.34	10.47	14.81	0.79	20.89	1.34	11.38	10.80	91.94
19	75.20	70.82	4.38	6.37	21.11	7.36	18.88	0.66	5.83	31.18	68.82
20	83.65	78.00	5.65	10.70	21.82	5.86	55.82	2.02	6.76	47.18	76.60
21	77.31	70.16	7.15	9.10	21.18	3.84	20.84	0.83	9.25	21.43	78.57
22	73.54	69.66	3.88	5.33	22.33	1.09	14.06	0.60	5.27	27.25	72.75
23	86.66	77.94	8.72	13.79	22.65	8.67	37.82	1.21	10.06	36.76	69.56
24	79.50	71.31	8.19	9.93	22.43	2.87	25.93	1.02	10.30	17.53	82.89
25	84.42	76.17	8.25	12.44	17.94	14.98	29.83	0.91	9.77	33.67	66.33
26	79.96	69.94	10.02	10.21	26.52	8.67	15.16	0.43	12.53	1.88	98.12
27	79.24	70.48	8.76	10.43	26.67	0.66	26.60	0.97	11.06	16.01	83.99
28	82.49	73.84	8.65	11.25	21.95	1.96	40.21	1.68	10.49	23.13	86.24
29	77.55	73.60	3.95	8.02	21.75	4.26	36.69	1.41	5.09	50.78	64.00
30	83.05	75.12	7.93	11.12	21.39	1.30	50.47	2.22	9.55	28.68	87.11
31	84.67	79.34	5.32	9.43	18.69	4.12	84.71	3.71	6.29	43.54	88.27
32	81.85	76.39	5.46	11.59	21.20	13.77	22.92	0.66	6.67	52.90	47.10

$$\%D(d) = \frac{P_{aPD}(d) - P_{siPD}(d)}{P_{siPD}(d)} \times 100 \quad (14)$$

$$\%P(d) = \frac{\%D(d)}{W_{peak}(d)} \quad (15)$$

$$W_{peak}(d) = \left[ \frac{E_{siBESS}^{req}(d)}{E_{aBESS}^0 + E_{aBESS}^Q(d)} \right]$$

#### IV. CONCLUSION

A simple yet comprehensive real-time active peak demand reduction control strategy has been developed, consisting of an off-line demand forecast, an off-line BESS scheduling, a real-time BESS control and an on-line adjuster. Performance validation and evaluation of the control strategy has been carried out experimentally using the university building as the site. The evaluation compared the peak reduction of the real-time active control strategy with the fundamental control strategy as well as examines the percentage of peak reduction and percentage of difference compared to the ideal reduction simulated with no forecast error. A new performance evaluation parameter is also proposed to provide a more holistic review of the peak demand reduction control when the capacity is limited. Overall, the results showed superiority and adoptability of the proposed control. Where the real-time active control strategy achieved percentage reduction of up to 8.64%, with accuracy of 70.52% or percentage difference of 29.48% away from the ideal reduction and has percentage performance of 77.08% in achieving the peak demand reduction.

#### ACKNOWLEDGMENT

The authors wish to thank SMA Australia for their help and support with the setup of the battery inverters. This work was supported in part by CREST R&D Grant P01C1-14 between Collaborative Research in Engineering, Science and Technology centre (CREST), Universiti Tunku Abdul Rahman (UTAR) and ERS Energy Sdn Bhd.

#### REFERENCES

- [1] M. T. Lawder, B. Suthar, P. W. C. Northrop, S. De, C. M. Hoff, O. Leitermann, M. L. Crow, S. Santhanagopalan, and V. R. Subramanian, "Battery Energy Storage System (BESS) and Battery Management System (BMS) for grid-

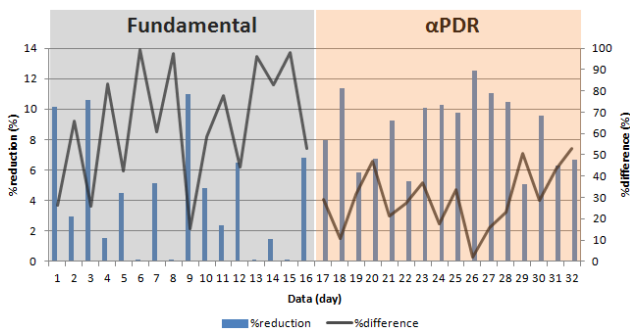


Fig. 7. Percentage of peak demand reduction for the fundamental and  $\alpha$ PDR control strategy

Overall, the real-time active control has a higher percentage of reduction of 8.64% as compared to the fundamental control with 4.24%. The proposed control also has an overall lower percentage difference of 29.48% as compared to the fundamental control with 64.75%. Apart from that, the real-time active control also has higher percentage of peak reduction performance of 77.08% as compared to the fundamental control with only 45.63%. As a whole, the results portrayed superiority of the real-time active control over the fundamental control, with higher percentage of peak reduction performance, higher percentage of peak demand reduction and lower percentage of difference as compared to the ideal reduction. Moreover the proposed control also has the adoptability to adjust (Fig. 6(d)) and minimize the chances of falling into the depletion failure or oversetting of threshold when the capacity of battery is limited.

- scale applications,” *Proc. IEEE*, vol. 102, no. 6, pp. 1014–1030, Jun. 2014.
- [2] TNB Better. Brighter. *TNB Better. Brighter.* [Online]. Available: <https://www.tnb.com.my/commercial-industrial/maximum-demand>
- [3] K. H. Chua, Y. S. Lim, and S. Morris, “Cost-benefit assessment of energy storage for utility and customers: A case study in Malaysia,” *Energy Convers. Manag.*, vol. 106, pp. 1071–1081, Dec. 2015.
- [4] X. Han, T. Ji, Z. Zhao, and H. Zhang, “Economic evaluation of batteries planning in energy storage power stations for load shifting,” *Renew. Energy*, vol. 78, pp. 643–647, Jun. 2015.
- [5] K. Qian, Z. Li, C. Zhou, and Y. Yuan, “Benefits of energy storage in power systems with high level of intermittent generation,” in *Proc. 20th International Conference and Exhibition on Electricity Distribution - Part 1*, 2009, pp. 1–4.
- [6] J. Leadbetter and L. Swan, “Battery storage system for residential electricity peak demand shaving,” *Energy Build.*, vol. 55, pp. 685–692, Dec. 2012.
- [7] A. Purvins, I. T. Papaioannou, and L. Debarberis, “Application of battery-based storage systems in household-demand smoothening in electricity-distribution grids,” *Energy Convers. Manag.*, vol. 65, pp. 272–284, Jan. 2013.
- [8] K. A. Joshi and N. M. Pindoriya, “Day-ahead dispatch of Battery Energy Storage System for peak load shaving and load leveling in low voltage unbalance distribution networks,” in *Proc. IEEE Power Energy Society General Meeting*, 2015, pp. 1–5.
- [9] K. Mattern, A. Ellis, S. E. Williams, C. Edwards, A. Nourai, and D. Porter, “Application of inverter-based systems for peak shaving and reactive power management,” in *Proc. Transmission and Distribution Conference and Exposition*, 2008, pp. 1–4.
- [10] M. Rowe, W. Holderbaum, and B. Potter, “Control methodologies: Peak reduction algorithms for DNO owned storage devices on the low voltage network,” in *Proc. 4th Innovative Smart Grid Technologies Europe*, 2013, pp. 1–5.
- [11] M. Koller, T. Borsche, A. Ulbig, and G. Andersson, “Defining a degradation cost function for optimal control of a battery energy storage system,” in *Proc. IEEE Grenoble Power Tech*, 2013, pp. 1–6.
- [12] Y. Levron and D. Shmilovitz, “Power systems’ optimal peak-shaving applying secondary storage,” *Electr. Power Syst. Res.*, vol. 89, pp. 80–84, Aug. 2012.
- [13] C. J. Bennett, R. A. Stewart, and J. W. Lu, “Development of a three-phase battery energy storage scheduling and operation system for low voltage distribution networks,” *Appl. Energy*, vol. 146, pp. 122–134, May 2015.
- [14] M. Rowe, T. Yunusov, S. Haben, W. Holderbaum, and B. Potter, “The real-time optimisation of DNO owned storage devices on the LV network for peak reduction,” *Energies*, vol. 7, no. 6, pp. 3537–3560, May 2014.
- [15] G. Bao, C. Lu, Z. Yuan, and Z. Lu, “Battery energy storage system load shifting control based on real time load forecast and dynamic programming,” in *Proc. IEEE International Conference on Automation Science and Engineering*, 2012, pp. 815–820.
- [16] M. Koller, T. Borsche, A. Ulbig, and G. Andersson, “Review of grid applications with the Zurich 1 MW battery energy storage system,” *Electr. Power Syst. Res.*, vol. 120, pp. 128–135, Mar. 2015.
- [17] E. Reihani, S. Sepasi, L. R. Roose, and M. Matsuura, “Energy management at the distribution grid using a Battery Energy Storage System (BESS),” *Int. J. Electr. Power Energy Syst.*, vol. 77, pp. 337–344, May 2016.



**Lee Cheun Hau** received his B. Eng. degree in electrical and electronics from Universiti Tunku Abdul Rahman (UTAR), Malaysia, in 2014, and is currently pursuing the M. Eng. degree in engineering science at UTAR. He is a graduate member of BEM, graduate member of IEM and student member of IEEE.



**Yun Seng Lim** received his PhD at University of Manchester Institute of Science and Technology (UMIST), United Kingdom, in the area of power system from September 1998 to September 2001. In 2002, he worked as a postdoctoral research assistant at UMIST in the area of renewable energy. In 2003, he joined Econnect Ltd, United Kingdom as an R&D Engineer specialising in research on the integration of renewable energy sources with the power system networks. Dr. Lim started his academic career at Universiti Tunku Abdul Rahman (UTAR) in 2005. He is the Professional Engineer with Practising Certificate and CEng registered with Board of Engineer Malaysia and UK Engineering Council respectively. He is the full member of IET, IEM and also the senior member of IEEE. He is also the Fellow of ASEAN Academy of Engineering and Technology (AAET).

# Active Control Strategy of Energy Storage System for Reducing Maximum Demand Charges under Limited Storage Capacity

Lee Cheun Hau<sup>1</sup>; Yun Seng Lim, Ph.D.<sup>2</sup>; and Kein Huat Chua, Ph.D.<sup>3</sup>

**Abstract:** Commercial and industrial customers are subject to monthly maximum demand charges, which can be as high as 30% of the total electricity bill. A battery-based energy storage system (BESS) can be used to reduce the monthly maximum demand charges. A number of control strategies have been developed for the BESS to reduce the daily peak demands. However, the existing control strategies may fail to reduce the peaks on some occasions because the energy of the BESS runs out during the process of peak reduction. Therefore, a new active control strategy for the BESS is developed and presented in this paper. This strategy is able to reduce the peaks even though the peaks are different from the forecasted ones. This strategy is able to reduce the monthly maximum demands by 9% when the BESS capacity is reduced to 37% of the full capacity due to financial constraints. Hence, the customers can achieve the payback period of 11 years over the project lifespan of 21 years with the reduced capacity of the BESS. DOI: 10.1061/(ASCE)EY.1943-7897.0000440. © 2017 American Society of Civil Engineers.

**Author keywords:** Maximum demand charge; Peak demand reduction; Battery energy storage; Limited capacity.

## Introduction

Commercial and industrial customers are subject to high maximum demand charges every month, which can be as high as 30% of the total electricity bill (Chua et al. 2015). Therefore, commercial and industrial customers have the urge to reduce their monthly maximum demand charges through the minimization of all the daily peak demands of each month. Demand-side management (DSM), demand response (DR), distributed generation (DG), and energy storage system (ESS) are possible solutions for peak reductions. Demand-side management is a long-term program aimed at encouraging customers to be energy efficient. Programs such as investment on energy-saving devices (Luo et al. 2010) and scheduling the usage of loads (Logenthiran et al. 2012) are forms of DSM. Demand response is a short-term program for customers to make their demand reductions in response to online electricity tariffs or the instructions sent by the grid operators (Salies 2013; He and Zhang 2015). Some customers, however, may not be able to participate in DSM or DR because of their daily business and manufacturing activities. Distributed generation and ESS, on the other hand, do not have such an issue. Distributed generation is on-site generation that can assist in the peak reductions (Rüther et al. 2008; Hanna et al. 2014). However, DG often fails to reduce

every peak of each month because the power outputs of DG are not in phase with the peaks on some occasions. Conversely, ESS can be used to reduce the daily peaks without interrupting the daily activities of the customers. It can also be designed to supply its power in phase with the peaks and then recover its energy during off-peak hours (Oudalov et al. 2006; Han et al. 2015).

Energy storage system reduces the daily peak demands if it is placed after the utility's meter as shown in Fig. 1. The power rating (kW) and the storage capacity of the energy storage system (kWh) play an important role in the effective minimization of the daily peak demands. The power rating (kW) of any power conversion unit determines the highest power demand that can be reduced from the grid as shown in Fig. 2(a). However, the peak demand can only be effectively reduced if the ESS has sufficient energy storage capacity (kWh) to supply the power to the load across the specified width of the peak as shown in Fig. 2(b). Numerous research efforts have been conducted to derive the optimum sizes of a battery-based ESS (BESS) designed based on the largest daily peak demands from the historical load data (Oudalov et al. 2007; Lu et al. 2014; Chauhan and Saini 2014; ElNozahy et al. 2015). The storage capacity is, however, often limited due to financial constraints. The energy of the BESS can run out quickly during the process of peak reductions. Therefore, a control strategy has to be used together with a load forecasting technique in order to establish the schedule of power supply from the BESS for improving the success rate of peak reductions.

At present, there are two fundamental control strategies for the BESS. The first is known as the fixed-scheduled pattern whereby historical load data are used to determine the times for the BESS to deliver power as well as to charge the batteries (Mattern et al. 2008; Purvins et al. 2013; Joshi and Pindoriya 2015). The second strategy is a load-following approach whereby a threshold is determined based on the historical load data so that the BESS will deliver the power when the actual load demand exceeds the threshold and charges the batteries during the off-peak periods (Levron and Shmilovitz 2012; Leadbetter and Swan 2012; Rowe et al. 2013). Although the first control strategy has the advantage of performing the function without any monitoring system, the daily

<sup>1</sup>Researcher, Lee Kong Chian Faculty of Engineering and Science, Universiti Tunku Abdul Rahman, Jalan Sungai Long, Selangor 43000, Malaysia (corresponding author). E-mail: alveyhau@gmail.com

<sup>2</sup>Professor, Lee Kong Chian Faculty of Engineering and Science, Universiti Tunku Abdul Rahman, Jalan Sungai Long, Selangor 43000, Malaysia. E-mail: yslim@utar.edu.my

<sup>3</sup>Assistant Professor, Lee Kong Chian Faculty of Engineering and Science, Universiti Tunku Abdul Rahman, Jalan Sungai Long, Selangor 43000, Malaysia. E-mail: chuakh@utar.edu.my

Note. This manuscript was submitted on September 9, 2016; approved on November 23, 2016; published online on February 25, 2017. Discussion period open until July 25, 2017; separate discussions must be submitted for individual papers. This paper is part of the *Journal of Energy Engineering*, © ASCE, ISSN 0733-9402.

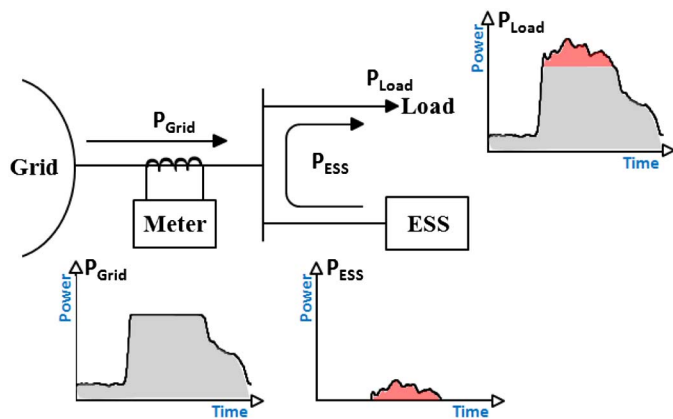


**Fig. 1.** Power flow diagram when ESS supplies power to the load

peak demand reduction is not always successful. This is because the actual load demand is different from the forecasted result. On the other hand, the second control strategy has the ability to control the power supply of BESS based on the real-time load demand. However, the BESS may still fail to reduce some daily peak demands, especially if the discrepancy between the real-time and the forecasted load demands is very significant.

There are additional control strategies, coupled with the forecasting and optimization techniques, being developed as presented in Bao et al. (2012), Rowe et al. (2014), Bennett et al. (2015), and Reihani et al. (2016a). The analyses are, however, confined to simulation evaluation. Only a few papers have shown the experimental works (Koller et al. 2015; Reihani et al. 2016b), but the evaluation was only based on a few experimental results and the reduction of the maximum demand charge was not assessed. It is, therefore, unknown whether the demonstrated efficacy can be maintained or has economic benefit. The majority of the control strategies are also not tested when the capacity of the BESS is limited, which is often the case in the actual BESS setup due to financial constraint.

Therefore, this paper presents a new control strategy for the BESS to reduce the monthly maximum demand under a limited storage capacity. In contrast to the previous preliminary work discussed in Hau and Lim (2016), which only validates the control strategy based on selected days of daily peak demand reductions, this paper is an extended version of the research work, including the economic aspect of the proposed control strategy based on a month of continuous and persistent reduction of the daily peak demands. Using a university building as the test site, with a usable capacity of approximately 26 kWh storage capacity and 18 kW power rating, the monthly maximum demand charge (\$) of the building is

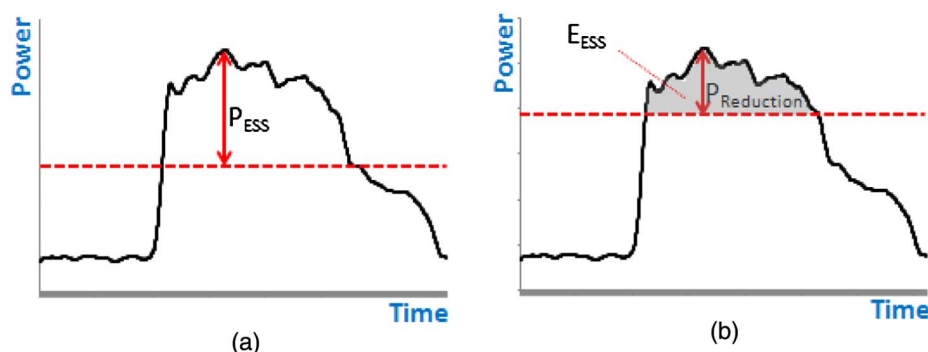


**Fig. 2.** Highest peak demand reduction for scenario of BESS (a) constrained by the power rating (kW); (b) limited by the energy storage capacity (kWh)

reduced by 9.07% as compared with 0.79% by the fundamental control strategy based on the load-following approach. The layout of this paper begins with the framework of the new active control algorithm in “Active Control Framework,” followed by the setup of the test site in “Experimental Setup” and the validation in “Experimental Evaluation” and “Economic Evaluation.”

## Active Control Framework

One of the main challenges in the peak reduction with the BESS is to predict the load profiles accurately. There are numerous load-forecasting techniques such as those discussed in Hong and Fan (2016), Dudek (2016), and Zjavka and Snašel (2016). However, their prediction results often contain some degrees of uncertainties. The peaks of the load profiles can be unexpectedly higher or broader than those of the forecasted ones. Or they can happen much earlier or later than the expected time. For example, the forecasted load profile of a particular day is shown in Fig. 3(a). With the available amount of energy in BESS ( $E_{BESS}$ ), the threshold is developed so that the BESS will supply the power to the load when the actual load demand exceeds the threshold. However, if the actual peak becomes broader than the forecasted one such as in Fig. 3(b), then the peak may not be reduced at all even after all the energy of the BESS has been delivered to the load. Therefore, an active control algorithm is developed to constantly adjust the threshold throughout the day based on the latest information on the load demand. This approach can then reduce the peak of the actual load profile at the end of the day as shown in Fig. 3(c).

The algorithm presented in this section is about how the threshold is constantly adjusted based on the latest information on the load demand. The overview of the active control strategy is described in Fig. 4. The control strategy begins by forecasting the load profile ( $P_{Load}^{For}$ ) of the next day ( $d + 1$ ). Based on the forecasted load profile, the control strategy will calculate the amount of the energy (kWh) required from the BESS to supply to the load on the next day and hence determine the threshold ( $P_{Th}$ ) whereby the BESS is scheduled to supply the power ( $P_{BESS}^{Sch}$ ) when the demand exceeds the threshold. On the actual day ( $d$ ) of peak reduction, the control algorithm will begin with the supply of the power output from the BESS ( $P_{BESS}^{Act}$ ), which is the same as the scheduled power output ( $P_{BESS}^{Sch}$ ) for  $t = 0$ . Then, the real-time load demand ( $P_{Load}^{Act}$ ) is measured and used to determine the discrepancy ( $\alpha$ ) between  $P_{Load}^{Act}$  and  $P_{Load}^{For}$  before the new threshold for the next interval ( $t + 1$ ) is determined. As a result, a new schedule is generated for BESS to supply power for the next interval. This new schedule is then used to refine the power output ( $P_{BESS}^{Act}$ ) of the BESS for the next interval. The minimum and maximum power outputs (kW) and storage capacity (kWh) of the BESS are defined in Eqs. (1) and (2)

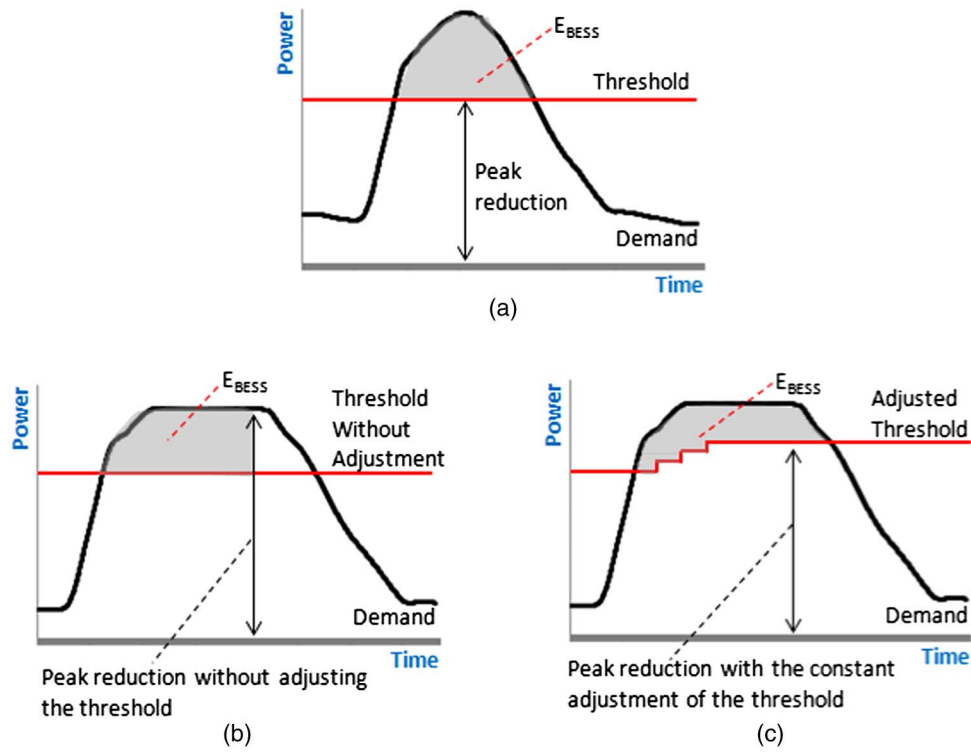


**Fig. 3.** (a) Forecasted load profile with the scheduled threshold; (b) unsatisfactory peak reduction in the actual load profile with a broad peak; (c) peak reduction achieved with the active adjustment of the threshold

$$-P_{BESS}^{max} \leq \mathbf{P}_{BESS}^{Act}(d, t) \leq P_{BESS}^{max} \quad (1)$$

$$0 \leq \mathbf{E}_{BESS}^{Act}(d, t) \leq E_{BESS}^{max} \quad (2)$$

**Activities before the Actual Peak Reduction: Calculating the Threshold Using the Forecasted Load Profile**

As shown in Fig. 4, the control algorithm will carry out the forecasting activities 1 day in advance. A series of  $N$ th historical load profiles ( $\mathbf{P}_{Load}^{His}$ ) are first retrieved in order to determine the envelope of the historical load profiles. The maximum ( $\mathbf{P}_{Load}^{His(max)}$ ) and minimum ( $\mathbf{P}_{Load}^{His(min)}$ ) boundaries of the envelope are used to calculate the forecasted load profile for the next day

$$\mathbf{P}_{Load}^{His(max)}(d, t) = \max_{\forall n} \mathbf{P}_{Load}^{His}(d - n, t) \quad (3)$$

$$\mathbf{P}_{Load}^{His(min)}(d, t) = \min_{\forall n} \mathbf{P}_{Load}^{His}(d - n, t) \quad (4)$$

The forecasted load profile ( $\mathbf{P}_{Load}^{For}$ ) for the next day ( $d + 1$ ) is then determined using the mean ( $\mu$ ) of the envelope of the historical load demands with the time interval of 1 min

$$\mathbf{P}_{Load}^{For}(d + 1, t) = \mathbf{P}_{Load}^{His(max)}(d, t) - \mu(t) [\mathbf{P}_{Load}^{His(max)}(d, t) - \mathbf{P}_{Load}^{His(min)}(d, t)] \quad (5)$$

$$\mu(t) = \text{AVG}_{\forall n} \left[ \frac{\mathbf{P}_{Load}^{His(max)}(d, t) - \mathbf{P}_{Load}^{His}(d - n, t)}{\mathbf{P}_{Load}^{His(max)}(d, t) - \mathbf{P}_{Load}^{His(min)}(d, t)} \right] \quad (6)$$

Once the forecasted load profile ( $\mathbf{P}_{Load}^{For}$ ) of the next day ( $d + 1$ ) is determined, the control algorithm will calculate the threshold

( $\mathbf{P}_{Th}$ ) by using the remaining energy capacity in the BESS ( $\mathbf{E}_{BESS}^{Act}$ ) or the power rating of the BESS ( $P_{BESS}$ ) as shown in Eq. (7)

$$\mathbf{P}_{Th}(d + 1, t, \dots, 1,440) = \max \left[ \begin{matrix} \mathbf{P}_{Th} | P_{BESS} \\ \mathbf{P}_{Th} | \mathbf{E}_{BESS}^{Act} \end{matrix} \right] \quad \forall t \quad (7)$$

The threshold should be made as low as possible in order to achieve the maximum peak reduction, whereby the lowest threshold ( $\mathbf{P}_{Th} | P_{BESS}$ ) is  $\mathbf{P}_{Load}^{For(max)} - P_{BESS}$  as shown in Fig. 5(a). However, the maximum peak reduction is only achievable if the peak is narrow enough for the total stored energy (kWh) to reduce the peak. If the stored energy is not sufficient because the peak load demand is broad, the threshold ( $\mathbf{P}_{Th} | \mathbf{E}_{BESS}^{Act}$ ) is then computed as the difference between  $\mathbf{P}_{Load}^{For(max)}$  and  $P_{Reduction}$ , where  $P_{Reduction}$  is the peak reduction achieved after the remaining energy ( $\mathbf{E}_{BESS}^{Act}$ ) in the BESS has been delivered to the load as illustrated in Fig. 5(b).

The schedule for the BESS ( $\mathbf{P}_{BESS}^{Sch}$ ) to supply and absorb power is then computed as described in Eq. (8). The BESS is scheduled to supply power during the period from  $t_s$  to  $t_e$ , when the forecasted load demand exceeds the threshold. The BESS is then scheduled to absorb power during the off-peak period from  $t_{Q2}$  to  $t_{Q1}$

$$\mathbf{P}_{BESS}^{Sch}(d + 1, t) = \begin{cases} \mathbf{P}_{Load}^{For}(d + 1, t) - \mathbf{P}_{Th}(d + 1, t) & t_s \leq t \leq t_e \\ -P_{BESS} & t_{Q2} \leq t \leq t_{Q1} \\ 0 & \text{Otherwise} \end{cases} \quad (8)$$

**Activities during the Day of Peak Reduction: Actively Adjusting the Threshold and Updating the Operating Schedule of BESS Using the Latest Load Demand**

On the actual day ( $d$ ) of the peak reduction, at  $t = 0$ , the control algorithm will output power as  $\mathbf{P}_{BESS}^{Act}(d, 0) = \mathbf{P}_{BESS}^{Sch}(d, 0)$ . At the

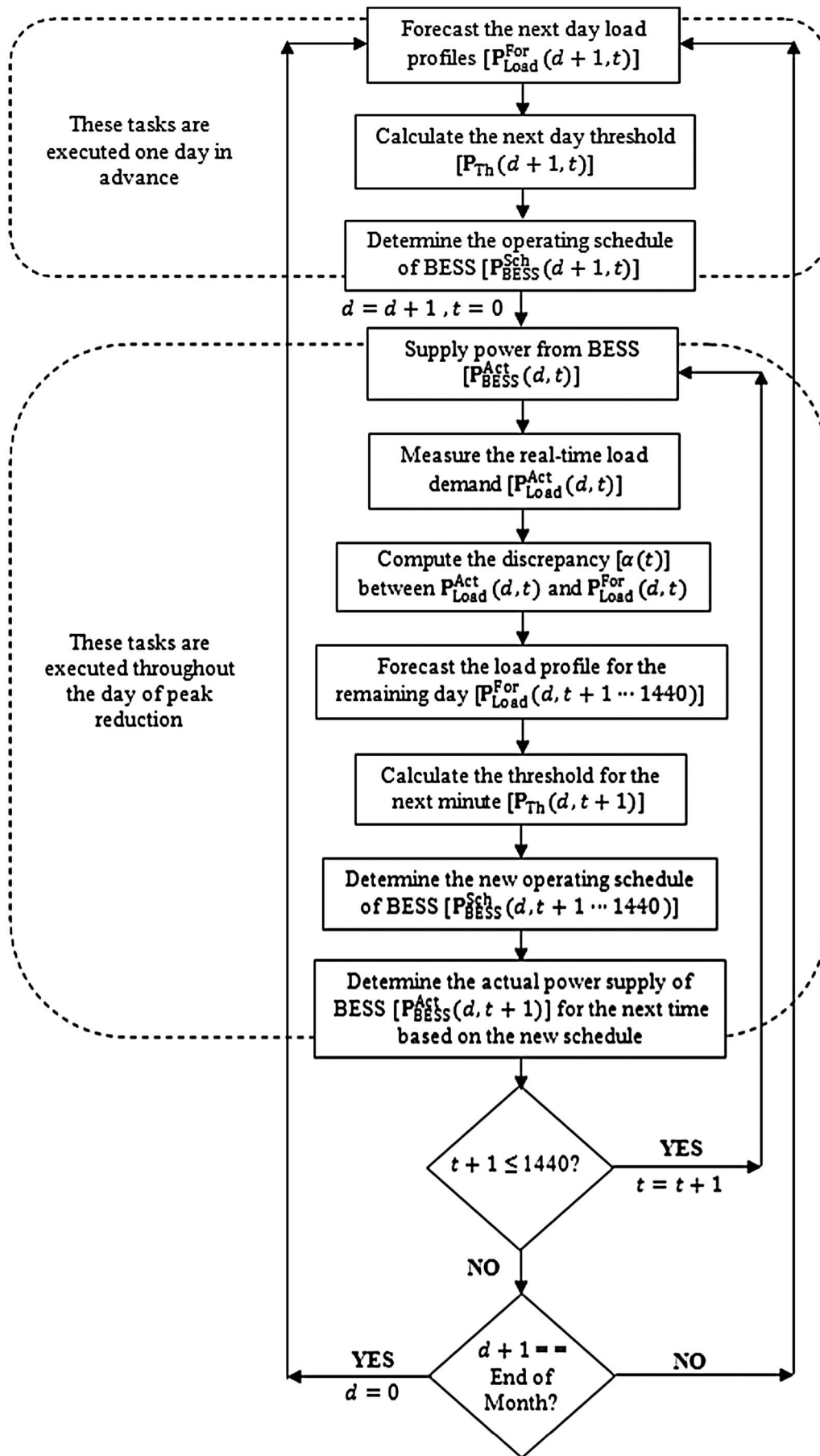
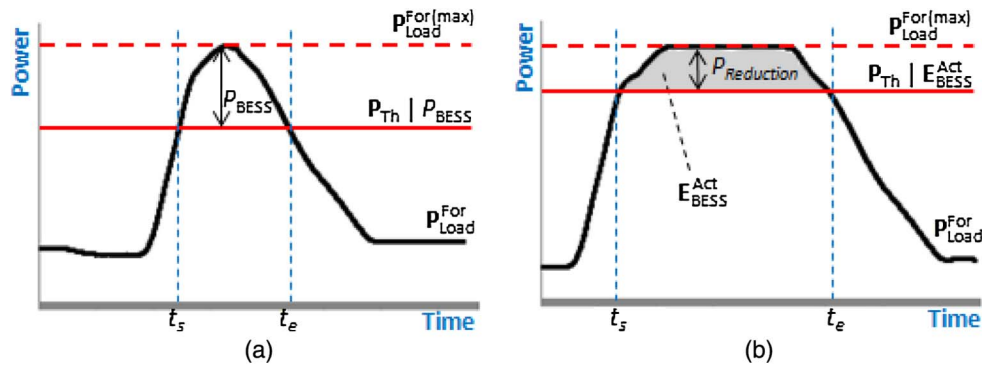


Fig. 4. Flowchart of the active control strategy



**Fig. 5.** Threshold level for scenario of (a) narrow peak load demand; (b) wide peak load demand

same time, the real-time load demand ( $\mathbf{P}_{Load}^{Act}$ ) is measured in order to determine the discrepancy ( $\alpha$ ). The discrepancy is calculated as the weighted difference between  $\mathbf{P}_{Load}^{Act}$  and  $\mathbf{P}_{Load}^{For}$  over the past 60 min to highlight the longer-term response of the forecast results instead of the short-term fluctuations captured when there is a large mismatch between  $\mathbf{P}_{Load}^{Act}$  and  $\mathbf{P}_{Load}^{For}$

$$\alpha(t) = \sum_t^{t-59} \frac{\mathbf{P}_{Load}^{Act}(d, t) - \mathbf{P}_{Load}^{For}(d, t)}{60} \quad (9)$$

With the use of the latest discrepancy, the forecasted load profile ( $\mathbf{P}_{Load}^{For}$ ) for the remaining day ( $t + 1, \dots, 1,440$  min) is then updated and the threshold ( $\mathbf{P}_{Th}$ ) for the next interval is also adjusted based on the remaining capacity ( $\mathbf{E}_{BESS}^{Act}$ ) in the BESS. The control algorithm adjusts the threshold ( $\mathbf{P}_{Th}$ ) in response to the change of the load demand in hopes of cutting down the peak to the lowest possible level with the remaining energy in the BESS.

The new operating schedule ( $\mathbf{P}_{BESS}^{Sch}$ ) for the remaining day starting from  $t + 1$  until the end of the day ( $t = 1,440$  min) is then determined. As illustrated in Fig. 6, the operating schedule of the BESS ( $\mathbf{P}_{BESS}^{Sch}$ ) encompasses six operating modes of the BESS, namely, (1) charging mode during off-peak periods, (2) charging mode during on-peak periods, (3) constant discharging mode, (4) discharging mode over the rising demand, (5) discharging mode over the decreasing demand, and (6) standby mode. The BESS will carry out each of the operating modes when several specific conditions are fulfilled. The details of the operating modes and the corresponding conditions are described in the following.

### Charging Mode during Off-Peak Periods

This mode of operation is carried out during off-peak periods to ensure that the BESS is fully charged and ready to supply power in the coming operation. The BESS is charged at the specified value determined by the BESS internal battery management system (SMA 2014) when the conditions in Table 1 are fulfilled.

### Charging Mode during On-Peak Periods

The BESS is charged at the reduced rate as calculated using Eq. (10). This mode of operation is for storing extra energy in the BESS in order to improve the possibility of reducing the incoming peak. The charging rate is reduced because it can avoid any significant increase in the load demand, which may lead to the change in the operating schedule of the BESS. This mode of operation will be carried out if the conditions in Table 2 are satisfied, where  $\mathbf{P}_{Load}^{For}(d, t + 1) - \mathbf{P}_{Th}(d, t + 1)$  is the absorption computed with the forecasted demand ( $\mathbf{P}_{Load}^{For}$ ) for the next interval ( $t + 1$ ) and  $\mathbf{P}_{Load}^{Act}(d, t) - \mathbf{P}_{Th}(d, t + 1)$  is the absorption determined based on the real-time load demand ( $\mathbf{P}_{Load}^{Act}$ ) measured at present time ( $t$ )

$$\begin{aligned} \mathbf{P}_{BESS}^{Sch}(d, t + 1) = & \alpha(t) \{ \mathbf{P}_{Load}^{For}(d, t + 1) - \mathbf{P}_{Th}(d, t + 1) \\ & - [\mathbf{P}_{Load}^{Act}(d, t) - \mathbf{P}_{Th}(d, t + 1)] \} + [\mathbf{P}_{Load}^{Act}(d, t) \\ & - \mathbf{P}_{Th}(d, t + 1)] \end{aligned} \quad (10)$$

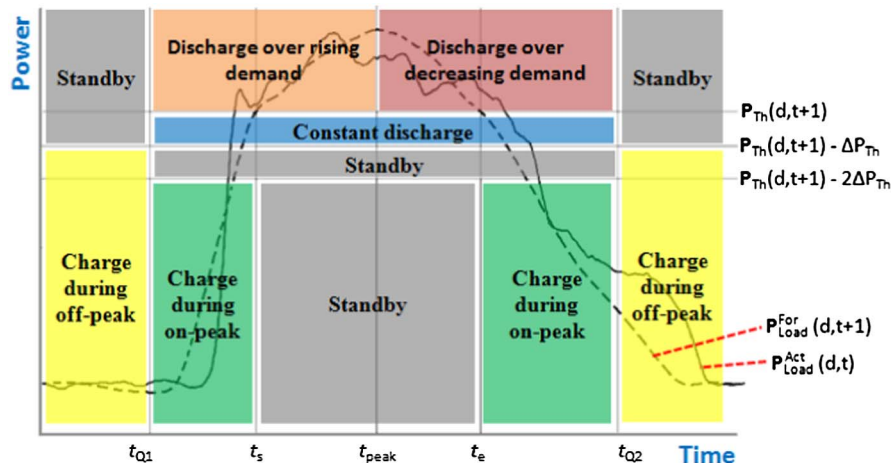


**Fig. 6.** Six operating modes of the BESS

**Table 1.** Activation Conditions of the Charging Mode during Off-Peak Periods

Conditions	Explanations
$t_{Q2} \leq t \leq t_{Q1}$ $\mathbf{P}_{\text{Load}}^{\text{For}}(d, t+1) \leq \mathbf{P}_{\text{Th}}(d, t+1) - \Delta P_{\text{Th}}$	Off-peak periods from $t_{Q2}$ to $t_{Q1}$ . Ensures the BESS is not charged above the adjusted threshold; as soon as the forecasted load demand ( $\mathbf{P}_{\text{Load}}^{\text{For}}$ ) for the next interval ( $t+1$ ) is above the adjusted threshold ( $\mathbf{P}_{\text{Th}}$ ) minus the specified permitted fluctuation margin ( $\Delta P_{\text{Th}}$ ), the BESS will stop charging; $\Delta P_{\text{Th}}$ is the user-specified permitted fluctuation margin along the adjusted threshold, it is a limit, added to monitor the peak demand reductions oscillation.
$\mathbf{E}_{\text{BESS}}^{\text{Act}}(d, t) \leq E_{\text{BESS}}$	Ensures that the remaining energy ( $\mathbf{E}_{\text{BESS}}^{\text{Act}}$ ) in the BESS is not less than the energy stored in the BESS ( $E_{\text{BESS}}$ ) at the depth of discharge of 50%.

**Table 2.** Activation Conditions of the Charging Mode during On-Peak Periods

Conditions	Explanations
$t_{Q1} \leq t \leq t_s$ or $t_e \leq t \leq t_{Q2}$ $\mathbf{P}_{\text{Grid}}^{\text{Act}}(d, t) \leq \mathbf{P}_{\text{Th}}(d, t+1) - 2\Delta P_{\text{Th}}$	On-peak periods from $t_{Q1}$ to $t_s$ and $t_e$ to $t_{Q2}$ , where the BESS is allowed to be charged. Ensures that the BESS is not charged above the adjusted threshold; as the BESS charges, the real-time supply from the utility ( $\mathbf{P}_{\text{Grid}}^{\text{Act}}$ ) at present time ( $t$ ) will increase; as soon as $\mathbf{P}_{\text{Grid}}^{\text{Act}}$ is above the adjusted threshold ( $\mathbf{P}_{\text{Th}}$ ) minus the double of the specified permitted fluctuation margin ( $\Delta P_{\text{Th}}$ ), the BESS will stop charging.
$\mathbf{E}_{\text{BESS}}^{\text{Act}}(d, t) \leq E_{\text{BESS}}$	Ensures that the BESS will continue to be charged if the remaining energy ( $\mathbf{E}_{\text{BESS}}^{\text{Act}}$ ) in the BESS is not less than the energy stored in the BESS ( $E_{\text{BESS}}$ ) at the depth of discharge of 50%.

### Constant Discharging Mode

Referring to Fig. 6, this operating mode happens before and after the peak demand. In this mode of operation, the BESS will supply power at the minimum value of  $\mathbf{P}_{\text{BESS}}^{\text{Act}(\text{min}+)}$ . Before the peak demand, the BESS will discharge at  $\mathbf{P}_{\text{BESS}}^{\text{Act}(\text{min}+)}$  in the anticipation of the incoming peak. After the peak demand, the BESS will discharge at  $\mathbf{P}_{\text{BESS}}^{\text{Act}(\text{min}+)}$  in anticipation of another incoming peak. This is to ensure that the peak demand is reduced and maintained within the threshold of  $\mathbf{P}_{\text{Th}} \pm \Delta P_{\text{Th}}$ . This mode of operation will be carried out when the conditions in Table 3 are met.

### Discharging Mode over the Rising Demand

In this mode of operation, the BESS will discharge its power to the load in order to reduce the peak demand from the grid. The discharging power is calculated in Eq. (11). This process is carried out when the conditions in Table 4 are satisfied, where  $\mathbf{P}_{\text{Load}}^{\text{For}}(d, t+1) - \mathbf{P}_{\text{Th}}(d, t+1)$  is the peak demand reduction

computed with the forecasted demand ( $\mathbf{P}_{\text{Load}}^{\text{For}}$ ) for the next interval ( $t+1$ ) and  $\max[\mathbf{P}_{\text{BESS}}^{\text{Act}(\text{min}+)}, \mathbf{P}_{\text{Load}}^{\text{Act}}(d, t) - \mathbf{P}_{\text{Th}}(d, t+1)]$  is the peak demand reduction determined based on the real-time load demand ( $\mathbf{P}_{\text{Load}}^{\text{Act}}$ ) measured at present time ( $t$ )

$$\begin{aligned} \mathbf{P}_{\text{BESS}}^{\text{Sch}}(d, t+1) = & \alpha(t) \left\{ \mathbf{P}_{\text{Load}}^{\text{For}}(d, t+1) - \mathbf{P}_{\text{Th}}(d, t+1) \right. \\ & \left. - \max \left[ \mathbf{P}_{\text{BESS}}^{\text{Act}(\text{min}+)}, \mathbf{P}_{\text{Load}}^{\text{Act}}(d, t) - \mathbf{P}_{\text{Th}}(d, t+1) \right] \right\} \\ & + \max \left[ \mathbf{P}_{\text{BESS}}^{\text{Act}(\text{min}+)}, \mathbf{P}_{\text{Load}}^{\text{Act}}(d, t) - \mathbf{P}_{\text{Th}}(d, t+1) \right] \end{aligned} \quad (11)$$

### Discharging Mode over the Decreasing Demand

The BESS is discharged to reduce the peak over the decreasing load demand using Eq. (10). This mode of operation is carried out once the conditions in Table 5 are met.

**Table 3.** Activation Conditions of the Constant Discharging Mode

Conditions	Explanations
$t_{Q1} \leq t \leq t_{Q2}$ $\mathbf{P}_{\text{Th}}(d, t+1) - \Delta P_{\text{Th}} \geq \mathbf{P}_{\text{Grid}}^{\text{Act}}(d, t) \geq \mathbf{P}_{\text{Th}}(d, t+1)$	On-peak periods from $t_{Q1}$ to $t_{Q2}$ . Ensures that the peak demand is reduced and maintained within $\mathbf{P}_{\text{Th}} \pm \Delta P_{\text{Th}}$ ; as the BESS discharges, the real-time supply from the utility ( $\mathbf{P}_{\text{Grid}}^{\text{Act}}$ ) at present time ( $t$ ) will be reduced; as $\mathbf{P}_{\text{Grid}}^{\text{Act}}$ is reduced lower than $\mathbf{P}_{\text{Th}}$ , the BESS will supply power at the minimum value of $\mathbf{P}_{\text{BESS}}^{\text{Act}(\text{min}+)}$ and the BESS will only stop discharging when the $\mathbf{P}_{\text{Grid}}^{\text{Act}}$ is reduced lower than $\mathbf{P}_{\text{Th}} - \Delta P_{\text{Th}}$ .

**Table 4.** Activation Conditions of the Discharging Mode over the Rising Demand

Conditions	Explanations
$t_{Q1} \leq t \leq t_{\text{peak}}$ $\mathbf{P}_{\text{Load}}^{\text{For}}(d, t+1) \geq \mathbf{P}_{\text{Load}}^{\text{Act}}(d, t)$	Rising peak periods from $t_{Q1}$ to $t_{\text{peak}}$ . Indicates that the load demand is rising because the forecasted load demand ( $\mathbf{P}_{\text{Load}}^{\text{For}}$ ) for the next minute ( $t+1$ ) is greater than the actual load demand ( $\mathbf{P}_{\text{Load}}^{\text{Act}}$ ) at present time ( $t$ ).
$\mathbf{P}_{\text{Grid}}^{\text{Act}}(d, t) \geq \mathbf{P}_{\text{Th}}(d, t+1) - \Delta P_{\text{Th}}$	Ensures that the BESS is not overdischarged; as the BESS discharges, the real-time supply from the utility ( $\mathbf{P}_{\text{Grid}}^{\text{Act}}$ ) at present time ( $t$ ) will decrease; as soon as $\mathbf{P}_{\text{Grid}}^{\text{Act}}$ is less than the adjusted threshold ( $\mathbf{P}_{\text{Th}}$ ) minus the specified permitted fluctuation margin ( $\Delta P_{\text{Th}}$ ), the BESS will stop discharging its power.

**Table 5.** Activation Conditions of the Discharging Mode over the Decreasing Demand

Conditions	Explanations
$t_{\text{peak}} \leq t \leq t_{Q2}$ $P_{\text{Load}}^{\text{For}}(d, t+1) < P_{\text{Load}}^{\text{Act}}(d, t)$	Decreasing peak periods from $t_{\text{peak}}$ to $t_{Q2}$ . Indicates that the load demand is decreasing because the forecasted load demand ( $P_{\text{Load}}^{\text{For}}$ ) for the next minute ( $t+1$ ) is less than the real-time load demand ( $P_{\text{Load}}^{\text{Act}}$ ) at present time ( $t$ ).
$P_{\text{Grid}}^{\text{Act}}(d, t) \geq P_{\text{Th}}(d, t+1) - \Delta P_{\text{Th}}$	Ensures that the BESS is not overdischarged; as the BESS discharges, the real-time supply from the utility ( $P_{\text{Grid}}^{\text{Act}}$ ) at present time ( $t$ ) will decrease; as soon as $P_{\text{Grid}}^{\text{Act}}$ is less than the adjusted threshold ( $P_{\text{Th}}$ ) minus the specified permitted fluctuation margin ( $\Delta P_{\text{Th}}$ ), the BESS will stop discharging its power.

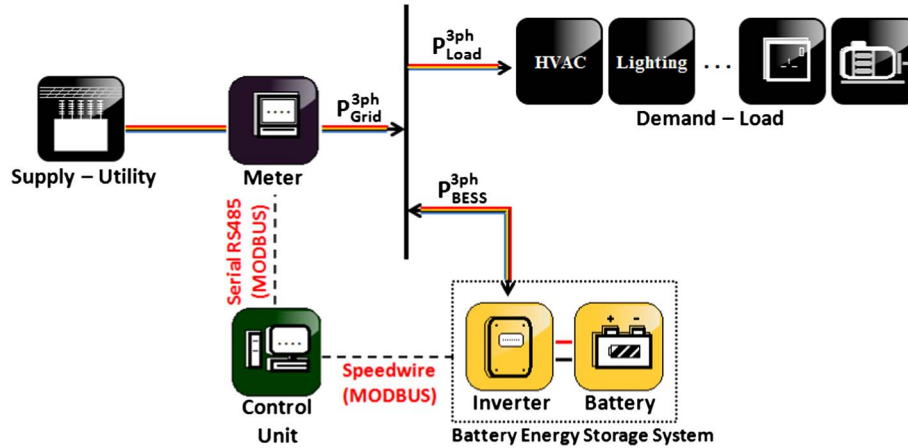


**Fig. 7.** Experimental equipment setup

**Standby Mode**

The BESS will be idle or standby with  $P_{\text{BESS}}^{\text{Sch}}(d, t+1) = 0$  if all the modes of operation as mentioned are not carried out.

Finally, the actual output of BESS for the next minute ( $P_{\text{BESS}}^{\text{Act}}$ ) is calculated based on the new operating schedule ( $P_{\text{BESS}}^{\text{Sch}}$ ). To eliminate the unnecessary load-demand transient,  $P_{\text{BESS}}^{\text{Act}}$  is computed as the aggregated power supplied by the BESS in the past 15 min, where  $\sum_{t-1}^{t-14} P_{\text{BESS}}^{\text{Act}}(d, t)$  is the sum of the output supply from the BESS in the past 15 min, from previous intervals of  $t-14$  up to  $t-1$

$$P_{\text{BESS}}^{\text{Act}}(d, t+1) = 15 \times P_{\text{BESS}}^{\text{Sch}}(d, t+1) - \sum_{t-14}^{t-1} P_{\text{BESS}}^{\text{Act}}(d, t) \quad (12)$$

The control algorithm will repeat its process until the end of the day where  $t = 1,440$ . After that, the control algorithm will forecast the load profile for the next day by using the historical load demand data again as mentioned previously.

**Experimental Setup**

The performance of the active control strategy has been evaluated experimentally. Using the low-voltage electrical network at the university building as a test site, Fig. 7 shows the setup of the BESS connected to the electrical network. The BESS has total power rating ( $P_{\text{BESS}}$ ) of 18 kW. It consists of three units of 6 kW bidirectional power converters. Each of the power converters is connected to a string of batteries formed by 16 pieces of 12 V, 111 Ah, valve-regulated lead acid batteries, connected in a  $4 \times 4$  matrix configuration. Each string of batteries has an energy capacity of 21.32 kWh forming the total energy capacity of up to 64 kWh. To prolong the lifespan of the batteries, the amount of energy ( $E_{\text{BESS}}$ ) that can be

used is only approximately 27 kWh, or the depth of discharge (DoD) is up to 50%. The power converters are supervised by control units that communicate with each other through the Speedwire Modbus (SI8.0H, SMA Solar Technology AG, Germany). The power flow of the electrical network is measured using the meter and the measurements are transmitted to the control unit through the RS485 Modbus (STAR3 Harmo, Elcontrol energy net, Italy). The control unit stores the historical data and performs the necessary computations for the control algorithm.

Fig. 8 shows the historical load profiles on the experimental site. The demand profiles have a wide peak starting from 7:00 a.m. until 4:40 p.m. The peaks are approximately 90 kW, which can happen several times in a day. The energy required to reduce the peak demand by 18 kW is estimated to be approximately 71.75 kWh. With the available energy of 27 kWh, the maximum achievable

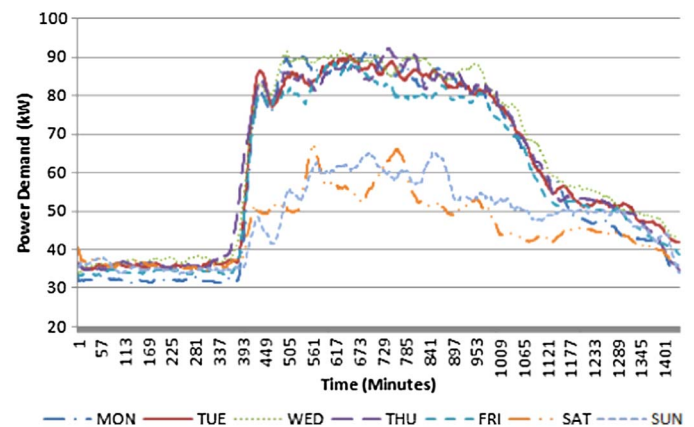


**Fig. 8.** Sample historical load demands on the experimental site from Monday to Sunday

Downloaded from ascelibrary.org by UNIVERSITI TUNKU ABDUL RAHMAN on 05/23/17. Copyright ASCE. For personal use only; all rights reserved.

reduction in the peak is only approximately 12 kW. A number of case studies are therefore carried out to investigate the performance of the proposed active controller on peak reduction in spite of the limited capacity. Additional case studies are also carried out to understand how the active adjustment of the threshold can improve the performance in peak reduction.

## Experimental Evaluation

### Experimental Results of the Fundamental and Active Control Strategies

The experimental results and the ideal reductions simulated after the experiment are listed in Appendixes I and II. Fig. 9 shows the experimental results of peak reduction carried out by the fundamental control strategy and the active control strategy. The input parameters for the experiment are listed in Table 6. Fig. 9(a), dated as Day 8 in Appendix I, shows that the fundamental controller is not able to

**Table 6.** Active Control Strategy Input Parameters

Parameter	Description	Rating
$P_{BESS}$	BESS power rating	18 kW
$E_{BESS}$	BESS usable capacity at DoD of 50%	27 kWh
$\Delta P_{Th}$	Tolerance of threshold or fluctuation margin	$\pm 1$ kW
$P_{BESS}^{Act(min+)}$	Minimum positive supply from BESS	3 kW
$t_{Q1}$	Morning charging time	8 a.m.
$t_{Q2}$	Night charging time	10 p.m.

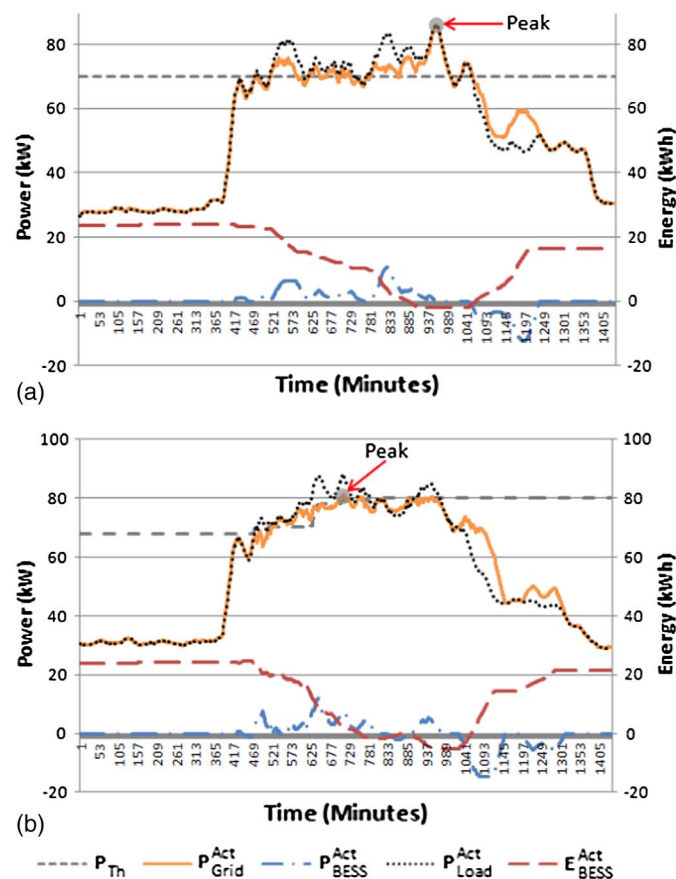


**Fig. 9.** Load profile of a sample day with the (a) unsuccessful peak reduction by the fundamental control approach; (b) peak reduction achieved by the active controller

reduce the wide peak supplied by the grid  $P_{Grid}^{Act}$  as the threshold is always fixed throughout the day. When the threshold level ( $P_{Th}$ ) is set too low, the target peak reduction ( $P_{Grid}^{Act(max)} = P_{Th}$ ) cannot be achieved because the capacity of the BESS is insufficient. Thus, when the remaining energy in the BESS is depleted ( $E_{BESS}^{Act} = 0$  kWh), the demand ( $P_{Load}^{Act}$ ) will overtake back and this result an incomplete peak reduction ( $P_{Grid}^{Act(max)} = P_{Load}^{Act(max)}$ ).

On the contrary, in Fig. 9(b), dated as Day 30 in Appendix II, the active controller is able to reduce the wide peak. The use of the short-term load forecasting provides the dynamics foresight of the peak demand for the active controller to pre-estimate the energy requirement. This enable the controller to actively adjust the threshold throughout the day and hence preserving the stored energy to the end of the peak is possible. Even though the remaining energy in the BESS is depleted, the active controller is still able to reduce the peak to the targeted level ( $P_{Grid}^{Act(max)} \cong P_{Th}$ ). Next, shown in Fig. 10(b), dated as Day 15, 16, and 17 in Appendix II, the experimental results of the active controller are extended to three consecutive days. Compared to the fundamental controller shown in Fig. 10(a), dated as Day 21, 22, and 23 in Appendix I, the results continue to show that the active controller is consistent and able to maintain the new peak below the fluctuation margin of  $P_{Th}^{Act} + \Delta P_{Th}$ .

### Ability of the Active Controller on Peak Reduction

The performance of the active controller is compared with the fundamental controller in order to understand how the active adjustment of the threshold can contribute to the peak reduction. The experimental results of the active controller are also compared with the simulation studies in which the forecasted load is exactly the same as the actual load demand. This comparison is to understand how the discrepancy between the forecasted and the actual loads can affect the ability of the BESS in peak reduction. Two indexes, namely  $R$  and  $A$ , are used to assess (1) contribution of the active adjustment of the threshold to the peak reduction, and (2) effect of

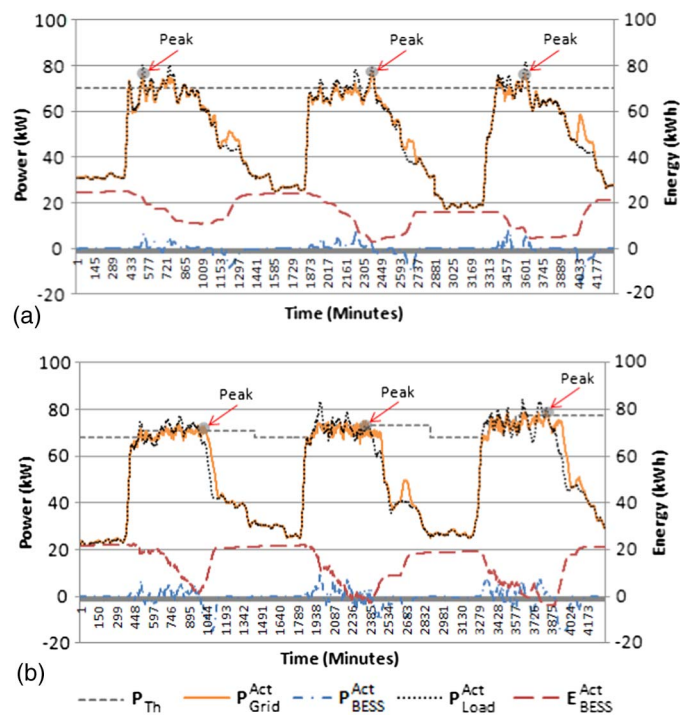


**Fig. 10.** Three consecutive days of peak reduction carried out by the (a) fundamental control strategy; (b) active control strategy

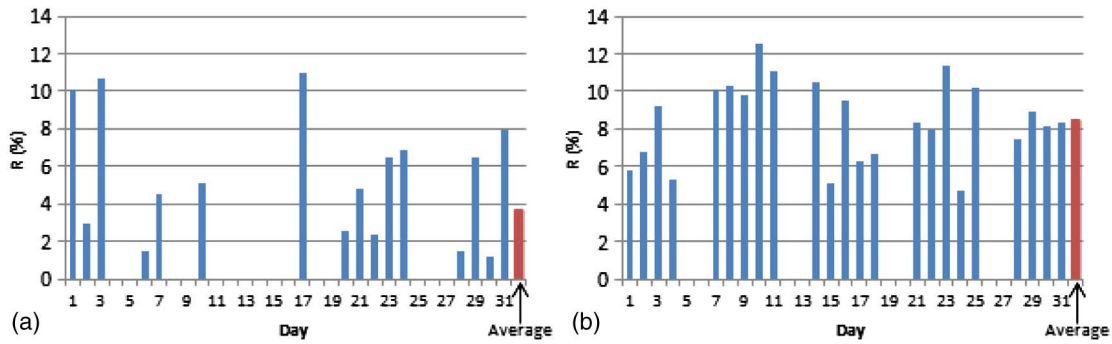


**Fig. 11.** Values of  $R$  achieved by the (a) fundamental control strategy; (b) active control strategy

the discrepancy on the peak reduction. Eqs. (13) and (14) show the definition of  $R$  and  $A$  in percentage

$$R(d) = \frac{P_{\text{Reduction}}^{\text{Act}}(d)}{P_{\text{Load}}^{\text{Act(max)}}(d)} \times 100 \quad (13)$$

$$A(d) = \frac{P_{\text{Reduction}}^{\text{Act}}(d)}{P_{\text{Reduction}}^{\text{Sim}}(d)} \times 100 \quad (14)$$

A high  $R$  reveals a high reduction of the peak demand. Fig. 11 shows the  $R$  achieved by the fundamental control strategy and the active control strategy. Day 4, 5, 11, 12, 18, 19, 25, and 26, displayed in Fig. 11(a) as well as tabulated in Appendix I, are the weekends in which the fundamental controller does not require to carry out peak reduction because the corresponding peaks on those days are lower than the threshold ( $P_{\text{Grid}}^{\text{Act(max)}} \ll P_{\text{Th}}$ ). Similarly the days on Day 5, 6, 12, 13, 19, 20, 26, and 27, that are presented in Fig. 11(b) as well as recorded in Appendix II, are the weekends in which the active controller does not require to perform the peak reduction and therefore 0% are observed on these days. On average, the  $R$  achieved by the active controller is higher than the fundamental controller, where 8.45% is achieved by the active controller and 3.73% is attained by the fundamental controller.

Fig. 12 then shows the values of the peak reduction factor ( $A$ ) achieved by both the controllers. A high  $A$  shows that the BESS has been effectively used for the peak reduction. A low  $A$  on the other hand reveals the BESS being under-utilized and the BESS is not operated at the optimal. Day 8, 9, 13, 14, 15, 16, and 27, displayed in Fig. 12(a) as well as tabulated in Appendix I, are the days in which the fundamental controller failed to reduce the peak demands due to the depletion of the BESS. On the contrary, the active controller manages to reduce the peak demands in spite of depletion on Day 11, 17, 23, 24, and 30. On average, the  $A$  achieved by the active controller is higher than the fundamental controller. The active

controller is also able to achieve perfect reductions or 100% of  $A$  more often than the fundamental controller.

From the evaluation indexes, the active controller hence portrayed strength over the fundamental controller. Despite the capacity of the BESS being limited, the active control strategy however showed adaptability in adjusting the threshold in respond to the real-time demand. The active controller also minimises the BESS from failing to reduce the peak demand due to depletion failure. The demonstrated efficacy of the active controller is also consistent and can be maintained.

### Economic Evaluation

This section shows the financial feasibility of using the BESS for maximum demand reductions. In Malaysia, the monthly maximum demand charge is applicable to customers using the voltage level of 6.6 kV and above. The monthly maximum demand charge is measured in price per kilowatts (\$/kW). The saving from the reduction of the monthly maximum demand charge ( $S_{\text{MD}}$ ) is calculated using Eq. (15). Introduction of BESS also brings saving in the electricity bill ( $S_{\text{TR}}$ ) by taking advantage of the on-peak and off-peak tariffs, whereby the BESS can be charged at times of low tariff and discharged at times of high tariff price for peak demand reductions

$$S_{\text{MD}} = U_{\text{MD}} [P_{\text{Load}}^{\text{Act(max)}}(d) - P_{\text{Grid}}^{\text{Act(max)}}(d)] \quad (15)$$

$$S_{\text{TR}} = \sum_{d=0}^{\text{End of month}} [U_{\text{off}} \times \Delta E_{\text{BESS}}^{\text{Act}}(d)|_{\text{off}}] - [U_{\text{on}} \times \Delta E_{\text{BESS}}^{\text{Act}}(d)|_{\text{on}}] \quad (16)$$

The net present value (NPV) and the payback period ( $T_{\text{payback}}$ ) are used in this study (Chen and Garcia 2016). The input parameters for the economic evaluation are listed in Table 7. According to the local price, the unit cost of the power conversion unit

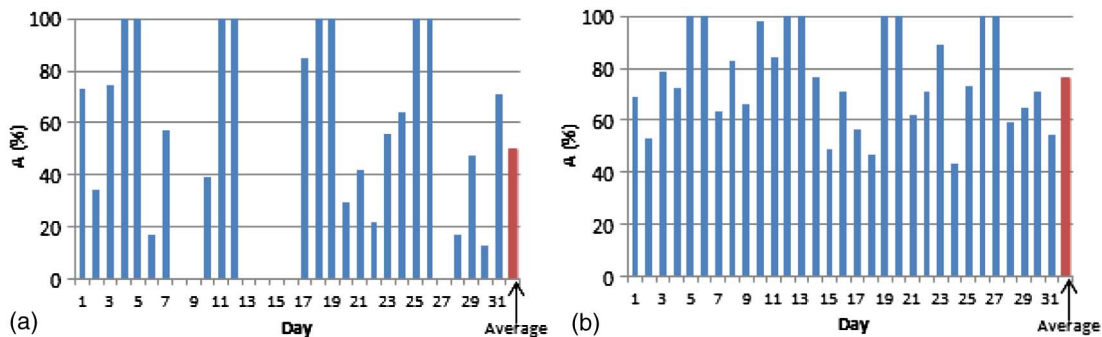


**Fig. 12.** Values of  $A$  achieved by the (a) fundamental control strategy; (b) active control strategy

**Table 7.** Input Parameters for the Economical Analysis

Description	Value	Unit
Projected period of BESS operation	21	years
Unit price of the power conversion unit ( $U_{PCU}$ )	1,942.50 <sup>a</sup>	RM/kW <sup>c</sup>
Unit price of the energy storage capacity ( $U_{ESC}$ )	425.50 <sup>a</sup>	RM/kWh <sup>c</sup>
Battery life	11 <sup>a</sup>	years
Maximum demand charge ( $U_{MD}$ )	45.1 <sup>b</sup>	RM/kW <sup>c</sup>
On-peak tariff ( $U_{on}$ )	0.365 <sup>b</sup>	RM/kWh <sup>c</sup>
Off-peak tariff ( $U_{off}$ )	0.224 <sup>b</sup>	RM/kWh <sup>c</sup>
Discount rate	6 <sup>a</sup>	%

<sup>a</sup>Obtained from Chua et al. (2015).

<sup>b</sup>Obtained from “Tenaga Nasional Berhad (TNB 2016) Better Brighter” 2016.

<sup>c</sup>The conversion rate of U.S. dollars to RM is 1:4.

is Ringgit Malaysia (RM) 1,942.50/kW (US\$485.62/kW), whereas the unit cost of lead-acid batteries is RM 425.50/kWh (US\$106.37/kWh). The capital cost of BESS is computed according to Eqs. (17) and (18). By taking into account the Malaysia national holidays of 13 days per year, the BESS is expected to operate 248 days in a year and the resultant battery service life is estimated to be 11 years at DoD of 50%. The utility tariff rates of C2 for the medium voltage peak–off-peak commercial customers are considered and the discount rate of 6% a year is applied

$$C_{PCU} = U_{PCU} \times P_{BESS} \quad (17)$$

$$C_{ESC} = \frac{U_{ESC} \times E_{BESS}}{SoC^{max} - SoC^{min}} \quad (18)$$

From the results listed in Appendix I, the fundamental control technique only achieves savings of 0.79% from the peak reductions with the incentive gain of RM 32.45 (US\$8.11) from utilizing the on-peak and off-peak tariff differences. The active control technique, on the other hand, achieves an overall savings of 9.07% or RM 341.86 (US\$85.46) from the monthly maximum demand charge reduction with the incentive gain of RM 30.88 (US \$7.72) from utilizing the differences between the on-peak and off-peak tariffs. The active control strategy is thus projected to achieve the payback period ( $T_{payback}$ ) of approximately 10.85 years with the NPV of RM 19,040 (US\$4,760) over the project period of 21 years. These values indicate that the BESS is a financially viable approach for reducing the peak demands for customers.

## Conclusion

An active control strategy has been developed to reduce the daily peak demands. This method instructs the BESS to supply power to the load by constantly adjusting the threshold based on the discrepancy between the forecasted and actual load demands. The details of the active controller have been described in this paper. This method has been used to reduce the daily peaks in a commercial building. Based on the experimental results, the active controller is able to reduce the peak effectively even though the peaks are broader than the forecasted ones. The results also show that the peak reductions achieved by the active controller are close to the simulation studies whereby the actual load demand is the same as the forecasted load demand. An economic analysis has been carried out to evaluate whether or not the BESS can bring any financial benefits to the customers. The net present value of the BESS is calculated to be RM 19,040 (US\$4,760) over the life-span of 21 years with the payback period of 10.85 years. These values indicate that the BESS is financially viable approach for reducing the peak demands of customers.

## Appendix I. Experimental and Simulation Results: Fundamental Control Strategy

Day	$P_{Load}^{Act(max)}$ (kW)	$P_{Reduction}^{Act}$ (kW)	$P_{Reduction}^{Sim}$ (kW)
1	73.30	7.42	10.10
2	65.08	1.90	5.56
3	70.92	7.54	10.15
4	50.67	0.00	0.00
5	60.02	0.00	0.00
6	85.33	1.29	7.69
7	81.57	3.69	6.43
8	85.89	0.00	9.91
9	78.65	0.00	4.86
10	74.91	3.82	9.71
11	54.38	0.00	0.00
12	56.50	0.00	0.00
13	61.82	0.00	0.00
14	80.36	0.00	3.30
15	80.32	0.00	3.26
16	72.21	0.00	12.21
17	84.45	9.28	10.96
18	49.70	0.00	0.00
19	61.05	0.00	0.00
20	78.67	1.99	6.76
21	80.32	3.84	9.21
22	79.42	1.91	8.64
23	81.49	5.29	9.50
24	83.97	5.73	8.93
25	47.83	0.00	0.00
26	56.73	0.00	0.00
27	69.10	0.00	1.76
28	76.18	1.12	6.44
29	81.49	5.29	11.06
30	77.47	0.90	6.89
31	79.86	6.34	8.93

## Appendix II. Experimental and Simulation Results: Active Control Strategy

Day	$P_{Load}^{Act(max)}$ (kW)	$P_{Reduction}^{Act}$ (kW)	$P_{Reduction}^{Sim}$ (kW)
1	75.20	4.38	6.37
2	83.65	5.65	10.70
3	77.31	7.15	9.10
4	73.54	3.88	5.33
5	46.23	0.00	0.00
6	60.01	0.00	0.00
7	86.66	8.72	13.79
8	79.50	8.19	9.93
9	84.42	8.25	12.44
10	79.96	10.02	10.21
11	79.24	8.76	10.43
12	42.17	0.00	0.00
13	53.99	0.00	0.00
14	82.49	8.65	11.25
15	77.55	3.95	8.02
16	83.05	7.93	11.12
17	84.67	5.32	9.43
18	81.85	5.46	11.59
19	44.98	0.00	0.00
20	63.19	0.00	0.00
21	88.64	7.41	11.96
22	79.86	6.34	8.93
23	82.08	9.34	10.47
24	77.38	3.64	8.37
25	81.10	8.30	11.37
26	45.53	0.00	0.00
27	51.62	0.00	0.00

## Appendix II (Continued.)

Day	$P_{Load}^{Act(max)}$ (kW)	$P_{Reduction}^{Act}$ (kW)	$P_{Reduction}^{Sim}$ (kW)
28	82.11	6.10	10.28
29	83.36	7.40	11.44
30	88.26	7.20	10.09
31	91.13	7.58	13.85

## Acknowledgments

This work is supported in part by CREST R&D Grant P01C1-14 between Collaborative Research in Engineering, Science and Technology Centre (CREST), Universiti Tunku Abdul Rahman (UTAR), and ERS Energy Sdn Bhd.

## Notation

The following symbols are used in this paper:

- $A$  = percentage of peak reduction factor;
- $C_{ESC}$  = cost of energy storage capacity (\$);
- $C_{PCU}$  = cost of power conversion unit (\$);
- $d$  = date with subsets of  $\{0, 1, 2, \dots, \text{end of month}\}$ ;
- $E_{BESS}^{Act}$  = real-time remaining energy capacity in the BESS (kWh);
- $E_{BESS}^{max}$  or  $E_{BESS}$  = energy storage capacity of the BESS (kWh);
- $n$  = number of historical load profiles with subsets of  $\{1, 2, 3, \dots, N\}$ ;
- $P_{Reduction}$  = peak reduction achieved by the BESS after the remaining energy has been delivered (kW);
- $P_{Th}$  = peak reduction threshold (kW);
- $P_{BESS}^{Act}$  = real-time BESS supply (kW);
- $P_{Grid}^{Act}$  = real-time supply from the electrical grid (kW);
- $P_{Load}^{Act}$  = real-time load profile (kW);
- $P_{Grid}^{Act(max)}$  = real-time peak demand after peak reduction (kW);
- $P_{Load}^{Act(max)}$  = real-time peak demand (kW);
- $P_{BESS}^{Act(min+)}$  = specified minimum positive output supply for the BESS (kW);
- $P_{Reduction}^{Act}$  = experimental peak demand reduction (kW) of  $P_{Load}^{Act(max)} - P_{Grid}^{Act(max)}$ ;
- $P_{Load}^{For}$  = forecasted load profile (kW);
- $P_{Load}^{For(max)}$  = forecasted peak demand (kW);
- $P_{Load}^{His}$  = historical load profile (kW);
- $P_{Load}^{His(max)}$  = maximum historical load profile (kW);
- $P_{Load}^{His(min)}$  = minimum historical load profile (kW);
- $P_{BESS}^{max}$  or  $P_{BESS}$  = power rating of the BESS (kW);
- $P_{Th}^{max}$  = maximum peak reduction threshold (kW);
- $P_{Th}^{opt}$  = optimum peak reduction threshold (kW);
- $P_{BESS}^{Sch}$  = BESS scheduled supply (kW);
- $P_{Grid}^{Sim(max)}$  = simulated peak demand after peak reduction (kW);
- $P_{Reduction}^{Sim}$  = simulated peak demand reduction (kW) of  $P_{Load}^{Act(max)} - P_{Grid}^{Sim(max)}$ ;
- $R$  = percentage of peak demand reduction;
- $S_{MD}$  = savings from the reduction of the monthly maximum demand charge (\$);
- $S_{TR}$  = savings in the electricity bill from utilizing the on-peak and off-peak tariff difference (\$);
- $SoC^{max}$  = maximum BESS's battery state of charge (%);

- $SoC^{min}$  = minimum BESS's battery state of charge (%);
- $t$  = time of the day with subsets of  $\{0, 1, 2, \dots, 1,440 \text{ min}\}$ ;
- $t_e$  = end time of the peak period (min);
- $T_{payback}$  = payback period (years);
- $t_{peak}$  = time of the peak demand (min);
- $t_s$  = start time of the peak period (min);
- $t_{Q1}$  = BESS charging end time (min);
- $t_{Q2}$  = BESS charging start time (min);
- $U_{ESC}$  = unit price of the energy storage capacity (\$/kWh);
- $U_{MD}$  = unit price for the monthly maximum demand charge (\$/kW);
- $U_{off}$  = unit price for energy consumption during the off-peak period (\$/kWh);
- $U_{on}$  = unit price for energy consumption during the on-peak period (\$/kWh);
- $U_{PCU}$  = unit price of the power conversion unit (\$/kW);
- $\alpha$  = discrepancy between  $P_{Load}^{Act}$  and  $P_{Load}^{For}$ ;
- $\Delta E_{BESS}^{Act}(d)|_{off}$  = energy consumption during the off-peak period (kWh);
- $\Delta E_{BESS}^{Act}(d)|_{on}$  = energy consumption during the on-peak period (kWh);
- $\Delta P_{Th}$  = specified permitted fluctuation margin (kW); and
- $\mu$  = mean of the historical load profile envelopes.

## References

- Bao, G., Lu, C., Yuan, Z., and Lu, Z. (2012). "Battery energy storage system load shifting control based on real time load forecast and dynamic programming." *2012 IEEE Int. Conf. on Automation Science and Engineering (CASE)*, Seoul, 815–820.
- Bennett, C. J., Stewart, R. A., and Lu, J. W. (2015). "Development of a three-phase battery energy storage scheduling and operation system for low voltage distribution networks." *Appl. Energy*, 146(1), 122–134.
- Chauhan, A., and Saini, R. P. (2014). "A review on integrated renewable energy system based power generation for stand-alone applications: Configurations, storage options, sizing methodologies and control." *Renewable Sustainable Energy Rev.*, 38(1), 99–120.
- Chen, J., and Garcia, H. E. (2016). "Economic optimization of operations for hybrid energy systems under variable markets." *Appl. Energy*, 177(1), 11–24.
- Chua, K. H., Lim, Y. S., and Morris, S. (2015). "Cost-benefit assessment of energy storage for utility and customers: A case study in Malaysia." *Energy Conversion Manage.*, 106(1), 1071–1081.
- Dudek, G. (2016). "Neural networks for pattern-based short-term load forecasting: A comparative study." *Neurocomputing*, 205(1), 64–74.
- ElNozahy, M. S., Abdel-Galil, T. K., and Salama, M. M. A. (2015). "Probabilistic ESS sizing and scheduling for improved integration of PHEVs and PV systems in residential distribution systems." *Electr. Power Syst. Res.*, 125(1), 55–66.
- Han, X., Ji, T., Zhao, Z., and Zhang, H. (2015). "Economic evaluation of batteries planning in energy storage power stations for load shifting." *Renewable Energy*, 78(1), 643–647.
- Hanna, R., Kleissl, J., Nottrott, A., and Ferry, M. (2014). "Energy dispatch schedule optimization for demand charge reduction using a photovoltaic-battery storage system with solar forecasting." *Solar Energy*, 103(1), 269–287.
- Hau, L. C., and Lim, Y. S. (2016). "A real-time active peak demand reduction for battery energy storage with limited capacity." *J. Commun.*, 11(9), 841–847.
- He, Y., and Zhang, J. (2015). "Real-time electricity pricing mechanism in China based on system dynamics." *Energy Convers. Manage.*, 94(1), 394–405.

- Hong, T., and Fan, S. (2016). "Probabilistic electric load forecasting: A tutorial review." *Int. J. Forecasting*, 32(3), 914–938.
- Joshi, K. A., and Pindoriya, N. M. (2015). "Day-ahead dispatch of battery energy storage system for peak load shaving and load leveling in low voltage unbalance distribution networks." *2015 IEEE Power and Energy Society General Meeting*, Denver, 1–5.
- Koller, M., Borsche, T., Ulbig, A., and Andersson, G. (2015). "Review of grid applications with the Zurich 1 MW battery energy storage system." *Electric Power Syst. Res.*, 120(1), 128–135.
- Leadbetter, J., and Swan, L. (2012). "Battery storage system for residential electricity peak demand shaving." *Energy Build.*, 55(1), 685–692.
- Levron, Y., and Shmilovitz, D. (2012). "Power systems' optimal peak-shaving applying secondary storage." *Electr. Power Syst. Res.*, 89(1), 80–84.
- Logenthiran, T., Srinivasan, D., and Shun, T. Z. (2012). "Demand side management in smart grid using heuristic optimization." *IEEE Trans. Smart Grid*, 3(3), 1244–1252.
- Lu, C., Xu, H., Pan, X., and Song, J. (2014). "Optimal sizing and control of battery energy storage system for peak load shaving." *Energies*, 7(12), 8396–8410.
- Luo, T., Ault, G., and Galloway, S. (2010). "Demand side management in a highly decentralized energy future." *45th Int. Universities Power Engineering Conf. (UPEC)*, Cardiff, Wales, U.K., 1–6.
- Mattern, K., Ellis, A., Williams, S. E., Edwards, C., Nourai, A., and Porter, D. (2008). "Application of inverter-based systems for peak shaving and reactive power management." *2008 IEEE/PES Transmission and Distribution Conf. and Exposition*, Chicago, 1–4.
- Oudalov, A., Chartouni, D., Ohler, C., and Linhofer, G. (2006). "Value analysis of battery energy storage applications in power systems." *2006 IEEE PES Power Systems Conf. and Exposition*, Atlanta, 2206–2211.
- Oudalov, A., Cherkaoui, R., and Beguin, A. (2007). "Sizing and optimal operation of battery energy storage system for peak shaving application." *2007 IEEE Lausanne Power Tech*, Lausanne, Switzerland, 621–625.
- Purvins, A., Papaioannou, I. T., and Debarberis, L. (2013). "Application of battery-based storage systems in household-demand smoothening in electricity-distribution grids." *Energy Convers. Manage.*, 65(1), 272–284.
- Reihani, E., Motalleb, M., Ghorbani, R., and Saoud, L. S. (2016). "Load peak shaving and power smoothing of a distribution grid with high renewable energy penetration." *Renewable Energy*, 86(1), 1372–1379.
- Reihani, E., Sepasi, S., Roose, L. R., and Matsuura, M. (2016). "Energy management at the distribution grid using a battery energy storage system (BESS)." *Int. J. Electr. Power Energy Syst.*, 77(1), 337–344.
- Rowe, M., Holderbaum, W., and Potter, B. (2013). "Control methodologies: Peak reduction algorithms for DNO owned storage devices on the low voltage network." *IEEE PES Innovative Smart Grid Technologies Europe 2013*, Lyngby, Denmark, 1–5.
- Rowe, M., Yunusov, T., Haben, S., Holderbaum, W., and Potter, B. (2014). "The real-time optimisation of DNO owned storage devices on the LV network for peak reduction." *Energies*, 7(6), 3537–3560.
- Rüther, R., Knob, P. J., da Silva Jardim, C., and Rebechi, S. H. (2008). "Potential of building integrated photovoltaic solar energy generators in assisting daytime peaking feeders in urban areas in Brazil." *Energy Convers. Manage.*, 49(5), 1074–1079.
- Salies, E. (2013). "Real-time pricing when some consumers resist in saving electricity." *Energy Policy*, 59(1), 843–849.
- SMA (Solar Technology AG). (2014). "Technical information—Battery management of the sunny island gentle charging control for lead-acid batteries based on current state of the battery." ([http://files.sma.de/dl/7910/SI\\_Batteriemanagement-TI-en-21.pdf](http://files.sma.de/dl/7910/SI_Batteriemanagement-TI-en-21.pdf)) (Jan. 16, 2014).
- TNB (Tenaga Nasional Berhad). (2016). "Pricing and tariffs for industrial and commercial consumers." (<https://www.tnb.com.my/commercial-industrial/pricing-tariffs1/>) (Mar. 16, 2016).
- Zjavka, L., and Snášel, V. (2016). "Short-term power load forecasting with ordinary differential equation substitutions of polynomial networks." *Electric Power Syst. Res.*, 137(1), 113–123.

## LIST OF REFERENCES

ACROMAG, 2005. BusWorks 900EN Series 10/100M Industrial Ethernet I/O Modules w/ Modbus Technical Reference - Modbus TCP/IP, 1st ed. USA: Acromag, Inc.

Akinyele, D.O. and Rayudu, R.K., 2014. Review of energy storage technologies for sustainable power networks. *Sustainable Energy Technologies Assessments*, 8, pp. 74–91.

Arnold, M. and Andersson, G., 2011. Model Predictive Control of Energy Storage including Uncertain Forecasts. *Proceedings of the 17th Power Systems Computation Conference*, Zurich, Switzerland.

Bao, G., Lu, C., Yuan, Z. and Lu, Z., 2012. Battery energy storage system load shifting control based on real time load forecast and dynamic programming. *Proceeding of the 2012 IEEE International Conference on Automation Science and Engineering*, Seoul, pp. 815–820.

Benetti, G., Caprino, D., Della Vedova, M.L. and Facchinetti, T., 2016. Electric load management approaches for peak load reduction: A systematic literature review and state of the art. *Sustainable Cities and Society*, 20, pp. 124–141.

Bennett, C.J., Stewart, R.A. and Lu, J.W., 2015. Development of a three-phase battery energy storage scheduling and operation system for low voltage distribution networks. *Applied Energy*, 146, pp. 122–134.

Bhuiyan, F.A. and Yazdani, A., 2012. Energy storage technologies for grid-connected and off-grid power system applications. *Proceedings of the 2012 IEEE Electrical Power and Energy Conference*, London, Ontario, pp. 303–310.

Chauhan, A. and Saini, R.P., 2014. A review on Integrated Renewable Energy System based power generation for stand-alone applications: Configurations, storage options, sizing methodologies and control. *Renewable and Sustainable Energy Reviews*, 38, pp. 99–120.

Chua, K.H., 2016. *Innovative Control Algorithms and Socioeconomic Benefits of Energy Storage System for Peak Reduction*. PhD thesis, Universiti Tunku Abdul Rahman, Malaysia.

Chua, K.H., Lim, Y.S. and Morris, S., 2015. Cost-benefit assessment of energy storage for utility and customers: A case study in Malaysia. *Energy Conversion Management*, 106, pp. 1071–1081.

Dudek, G., 2016. Neural networks for pattern-based short-term load forecasting: A comparative study. *Neurocomputing*, 205, pp. 64–74.

Dupont, G. and Baltus, P., 2009. Dimensioning and grid integration of mega battery energy storage system for system load leveling. *Proceedings of the 2009 IEEE Bucharest PowerTech*, Bucharest, pp. 1–6.

Elcontrol, 2006. *MODBUS RS485 SERIAL PROTOCOL for ED39DIN, DMM3, VIP39DIN, VIP396, SIRIO, STAR3 and STAR3din* [Online]. Available at: [http://www.elcontrol-energy.net/download/modbus\\_396\\_39din\\_dmm3\\_sirio\\_ed39din\\_star3\\_eng.pdf](http://www.elcontrol-energy.net/download/modbus_396_39din_dmm3_sirio_ed39din_star3_eng.pdf) [Accessed: 26 October 2016].

ElNozahy, M.S., Abdel-Galil, T.K. and Salama, M.M.A., 2015. Probabilistic ESS sizing and scheduling for improved integration of PHEVs and PV systems in residential distribution systems. *Electric Power Systems Research*, 125, pp. 55–66.

Energy Commission, 2016. *Peninsular Malaysia Electricity Supply Industry Outlook 2016* [Online]. Available at: <http://www.st.gov.my/index.php/en/download-page/category/106-outlook.html?download=591:peninsular-malaysia-electricity-supply-industry-outlook-2016> [Assessed: 12 November 2016].

Fathima, A.H. and Palanisamy, K., 2015. Optimization in microgrids with hybrid energy systems – A review. *Renewable and Sustainable Energy Reviews*. 45, pp. 431–446.

Haben, S., Ward, J., Vukadinovic Greetham, D., Singleton, C. and Grindrod, P., 2014. A new error measure for forecasts of household-level, high resolution electrical energy consumption. *International Journal of Forecasting*. 30, pp. 246–256.

Hanna, R., Kleissl, J., Nottrott, A. and Ferry, M., 2014. Energy dispatch schedule optimization for demand charge reduction using a photovoltaic-battery storage system with solar forecasting. *Solar Energy*. 103, pp. 269–287.

Han, X., Ji, T., Zhao, Z. and Zhang, H., 2015. Economic evaluation of batteries planning in energy storage power stations for load shifting. *Renewable Energy*. 78, pp. 643–647.

He, Y. and Zhang, J., 2015. Real-time electricity pricing mechanism in China based on system dynamics. *Energy Conversion and Management*. 94, pp. 394–405.

Hong, T. and Fan, S., 2016. Probabilistic electric load forecasting: A tutorial review. *International Journal of Forecasting*. 32(3), pp. 914–938.

Hussein, A.A., Kutkut, N., Shen, Z.J. and Batarseh, I., 2012. Distributed Battery Micro-Storage Systems Design and Operation in a Deregulated Electricity Market. *IEEE Transactions on Sustainable Energy*. 3, pp. 545–556.

Joshi, K.A. and Pindoriya, N.M., 2015. Day-ahead dispatch of Battery Energy Storage System for peak load shaving and load leveling in low voltage unbalance distribution networks. *Proceedings of the 2015 IEEE Power Energy Society General Meeting*, Denver, Colorado, pp. 1–5.

Khodaei, A., Shahidehpour, M. and Bahramirad, S., 2011. SCUC With Hourly Demand Response Considering Intertemporal Load Characteristics. *IEEE Transactions on Smart Grid*. 2(2), pp. 564–571.

Koller, M., Borsche, T., Ulbig, A. and Andersson, G., 2015. Review of grid applications with the Zurich 1 MW battery energy storage system. *Electric Power Systems Research*. 120, pp. 128–135.

Koller, M., Borsche, T., Ulbig, A. and Andersson, G., 2013. Defining a degradation cost function for optimal control of a battery energy storage system. *Proceedings of the 2013 IEEE Grenoble Conference*, Grenoble, pp. 1–6.

Lawder, M.T. et al., 2014. Battery Energy Storage System (BESS) and Battery Management System (BMS) for Grid-Scale Applications. *Proceedings of the IEEE*. 102(6), pp. 1014–1030.

Leadbetter, J. and Swan, L., 2012. Battery storage system for residential electricity peak demand shaving. *Energy and Buildings*. 55, pp. 685–692.

Levron, Y. and Shmilovitz, D., 2012. Power systems' optimal peak-shaving applying secondary storage. *Electric Power Systems Research*. 89, pp. 80–84.

Lim, K.Y., Lim, Y.S., Wong, J. and Chua, K.H., 2015. Distributed Energy Storage with Real and Reactive Power Controller for Power Quality Issues Caused by Renewable Energy and Electric Vehicles. *Journal of Energy Engineering*. 142(4), pp. 04015051:1-12.

Logenthiran, T., Srinivasan, D. and Shun, T.Z., 2012. Demand Side Management in Smart Grid Using Heuristic Optimization. *IEEE Transactions on Smart Grid*. 3, pp. 1244–1252.

Lu, C., Xu, H., Pan, X. and Song, J., 2014. Optimal Sizing and Control of Battery Energy Storage System for Peak Load Shaving. *Energies*. 7(12), pp. 8396–8410.

Luo, T., Ault, G. and Galloway, S., 2010. Demand Side Management in a highly decentralized energy future. *Proceedings of the 2010 45th International Universities Power Engineering Conference*, Cardiff, Wales, pp. 1–6.

Mattern, K. et al., 2008. Application of inverter-based systems for peak shaving and reactive power management. *Proceedings of the 2008 IEEE PES Transmission and Distribution Conference and Exposition*, Chicago, Illinois, pp. 1–4.

Modbus-IDA, 2012. MODBUS APPLICATION PROTOCOL SPECIFICATION, V1.1b3 ed.

Modbus-IDA, 2006a. MODBUS MESSAGING ON TCP/IP IMPLEMENTATION GUIDE, V1.0b ed.

Modbus-IDA, 2006b. MODBUS over Serial Line Specification and Implementation Guide, V1.02 ed.

Modicon, 1996. Modicon Modbus Protocol Reference Guide, Rev. J.

Oudalov, A., Chartouni, D., Ohler, C. and Linhofer, G., 2006. Value Analysis of Battery Energy Storage Applications in Power Systems. *Proceedings of the 2006 IEEE PES Power Systems Conference and Exposition*, Atlanta, Georgia, pp. 2206–2211.

Oudalov, A., Cherkaoui, R. and Beguin, A., 2007. Sizing and Optimal Operation of Battery Energy Storage System for Peak Shaving Application. *Proceedings of the 2007 IEEE Lausanne Power Tech*, Lausanne, pp. 621–625.

Palensky, P. and Dietrich, D., 2011. Demand Side Management: Demand Response, Intelligent Energy Systems, and Smart Loads. *IEEE Transactions on Industrial Informatics*. 7(3), pp. 381–388.

Pandiaraj, K., Fox, B., Morrow, D.J., Persaud, S. and Martin, J.P., 2002. Centralised control of diesel gen-sets for peak shaving and system support. *IEE Proceedings on Generation Transmission and Distribution*. 149(2), pp. 126.

Purvins, A., Papaioannou, I.T. and Debarberis, L., 2013. Application of battery-based storage systems in household-demand smoothening. *Energy Conversion and Management*. 65, pp. 272–284.

Reihani, E., Motalleb, M., Ghorbani, R. and Saad Saoud, L., 2016a. Load peak shaving and power smoothing of a distribution grid with high renewable energy penetration. *Renewable Energy*. 86, pp. 1372–1379.

Reihani, E., Sepasi, S., Roose, L.R. and Matsuura, M., 2016b. Energy management at the distribution grid using a Battery Energy Storage System (BESS). *International Journal of Electrical Power & Energy Systems*. 77, pp. 337–344.

Rowe, M., Holderbaum, W. and Potter, B., 2013. Control methodologies: Peak reduction algorithms for DNO owned storage devices on the Low Voltage network. *Proceedings of the 2013 IEEE PES 4th Innovative Smart Grid Technologies*, Europe, Lyngby, pp. 1–5.

Rowe, M., Yunusov, T., Haben, S., Holderbaum, W. and Potter, B., 2014a. The Real-Time Optimisation of DNO Owned Storage Devices on the LV Network for Peak Reduction. *Energies*. 7(6), pp. 3537–3560.

Rowe, M. et al., 2014. A Peak Reduction Scheduling Algorithm for Storage Devices on the Low Voltage Network. *IEEE Transactions on Smart Grid*. 5(4), pp. 2115–2124.

Rüther, R., Knob, P.J., da Silva Jardim, C. and Rebechi, S.H., 2008. Potential of building integrated photovoltaic solar energy generators in assisting daytime peaking feeders in urban areas in Brazil. *Energy Conversion and Management*. 49(5), pp. 1074–1079.

Salies, E., 2013. Real-time pricing when some consumers resist in saving electricity. *Energy Policy*. 59, pp. 843–849.

Salis, R.T. de, Clarke, A., Wang, Z., Moyne, J. and Tilbury, D.M., 2014. Energy storage control for peak shaving in a single building. *Proceedings of the 2014 IEEE PES General Meeting | Conference Exposition*, National Harbor, Maryland, pp. 1–5.

Shankar, R., Chatterjee, K. and Bhushan, R., 2016. Impact of energy storage system on load frequency control for diverse sources of interconnected power system in deregulated power environment. *International Journal of Electrical Power and Energy Systems*. 79, pp. 11–26.

SMA, 2016. *Technical Information - SMA Modbus Interface* [Online]. Available at: <http://www.sma.de/en/products/monitoring-control/modbus-protocol-interface.html> [Accessed: 15 September 2015].

SMA, 2015a. *Technical Description - SMA Modbus Interface* [Online]. Available at: <http://www.sma.de/en/products/monitoring-control/modbus-protocol-interface.html> [Accessed: 15 September 2015].

SMA, 2015b. *Operating Manual - SUNNY ISLAND 3.0M/ 4.4M/ 6.0H/ 8.0H - Sunny Remote Control* [Online]. Available at: <http://www.sma.de/en/products/battery-inverters/sunny-island-60h-80h.html> [Accessed: 15 September 2015].

SMA, 2014. *Technical Information - Battery Management of the Sunny Island Gentle charging control for lead-acid batteries based on current state of the battery* [Online]. Available at: <http://www.sma.de/en/products/battery-inverters/sunny-island-60h-80h.html> [Accessed: 15 September 2015].

Tenaga Nasional Berhad, 2016. *Pricing and Tariffs for Industrial and Commercial Consumers* [Online]. Available at: <https://www.tnb.com.my/commercial-industrial/maximum-demand> [Accessed: 3 July 2016].

Whittingham, M.S., 2012. History, Evolution, and Future Status of Energy Storage. *Proceedings of the IEEE*. 100, pp. 1518–1534.

Wong, J., Seng Lim, Y. and Morris, E., 2014. Distributed Energy Storage Systems with an Improved Fuzzy Controller for Mitigating Voltage Unbalance on Low-Voltage Networks. *Journal of Energy Engineering*. 142, pp. 04014058.

Yang, Y., Li, H., Aichhorn, A., Zheng, J. and Greenleaf, M., 2014. Sizing Strategy of Distributed Battery Storage System With High Penetration of Photovoltaic for Voltage Regulation and Peak Load Shaving. *IEEE Transactions on Smart Grid*. 5(2), pp. 982–991.

Yan, X., Zhang, X., Chen, H., Xu, Y. and Tan, C., 2014. Techno-economic and social analysis of energy storage for commercial buildings. *Energy Conversion and Management*. 78, pp. 125–136.

Zakeri, B. and Syri, S., 2015. Electrical energy storage systems: A comparative life cycle cost analysis. *Renewable and Sustainable Energy Reviews*. 42, pp. 569–596.

Zjavka, L. and Snášel, V., 2016. Short-term power load forecasting with ordinary differential equation substitutions of polynomial networks. *Electric Power Systems Research*. 137, pp. 113–123.

## APPENDIX A: LIST OF (SOME) ELECTRICITY TARIFFS AROUND THE WORLD

	MD (\$/kW)	RTP (\$/kWh)	TOU (\$/kWh)	References
Canada	–	–	Yes	<a href="http://www.ontarioenergyboard.ca/OEB/Consumers/Electricity/Electricity+Prices">http://www.ontarioenergyboard.ca/OEB/Consumers/Electricity/Electricity+Prices</a>
Mexico	–	–	Yes	<a href="http://www.pnm.com/regulatory/pdf_electricity/schedule_3_b.pdf">http://www.pnm.com/regulatory/pdf_electricity/schedule_3_b.pdf</a>
Brazil	Yes	Yes	Yes	<a href="http://www.aneel.gov.br/arquivos/PDF/Cartilha_INSIDETHEELECTRICBILL_PDF.pdf">http://www.aneel.gov.br/arquivos/PDF/Cartilha_INSIDETHEELECTRICBILL_PDF.pdf</a>
US	Yes	Yes	Yes	<a href="http://www.nationalgridus.com/niagaramohawk/non_html/eff_elec-demand.pdf">http://www.nationalgridus.com/niagaramohawk/non_html/eff_elec-demand.pdf</a>
Peru	Yes	–	Yes	<a href="http://www.peruutilities.com/ElectricRates.htm">http://www.peruutilities.com/ElectricRates.htm</a>
Venezuela	Yes	–	Yes	<a href="http://venezuelanalysis.com/news/6274">http://venezuelanalysis.com/news/6274</a>
Denmark	–	Yes	–	<a href="http://www.energinet.dk/EN/EI/Engrosmarked/Tariffer-og-priser/Sider/Aktuelle-tariffer-og-gebyrer.aspx">http://www.energinet.dk/EN/EI/Engrosmarked/Tariffer-og-priser/Sider/Aktuelle-tariffer-og-gebyrer.aspx</a>
Finland	Yes	–	Yes	<a href="http://www.fingrid.fi/en/news/announcements/Pages/New-prices-of-balance-service-as-of-1-October-2013.aspx">http://www.fingrid.fi/en/news/announcements/Pages/New-prices-of-balance-service-as-of-1-October-2013.aspx</a>
France	–	–	Yes	<a href="http://www.electriciansbrittany.com/electricity%20in%20france.htm">http://www.electriciansbrittany.com/electricity%20in%20france.htm</a>
Germany	Yes	Yes	Yes	<a href="http://www.swm.de/dms/swm/dokumente/m-strom/preise-strom-moosburg-03-2013.pdf">http://www.swm.de/dms/swm/dokumente/m-strom/preise-strom-moosburg-03-2013.pdf</a>
Italy	–	–	Yes	<a href="http://www.italiaelectricity.com/">http://www.italiaelectricity.com/</a>
Kazakhstan	Yes	–	Yes	<a href="http://www.almaty.kz/page.php?page_id=1918&amp;lang=2">http://www.almaty.kz/page.php?page_id=1918&amp;lang=2</a>
Netherlands	–	Yes	–	<a href="http://www.energievergelijken.nl/en/compare/pricelist/">http://www.energievergelijken.nl/en/compare/pricelist/</a>
Norway	Yes	–	Yes	<a href="http://www.statnett.no/en/Market-and-operations/Tariffs/Tariffs-2014/">http://www.statnett.no/en/Market-and-operations/Tariffs/Tariffs-2014/</a>

**(APPENDIX A Continued.)**

	<b>MD (\$/kW)</b>	<b>RTP (\$/kWh)</b>	<b>TOU (\$/kWh)</b>	<b>References</b>
Poland	Yes	–	Yes	<a href="http://www.pse.pl/uploads/kontener/tariff_of_pse_operator_2011.pdf">http://www.pse.pl/uploads/kontener/tariff_of_pse_operator_2011.pdf</a>
Romania	–	Yes	Yes	<a href="http://www.cez.cz/en/products-and-services/companies-and-businesses/electricity-2013.html">http://www.cez.cz/en/products-and-services/companies-and-businesses/electricity-2013.html</a>
Spain	Yes	–	Yes	<a href="https://www.iberdrola.es/customers/home/information/bill/electricity-bill#imagenBloque5">https://www.iberdrola.es/customers/home/information/bill/electricity-bill#imagenBloque5</a>
Sweden	Yes	–	Yes	<a href="http://www.svk.se/Start/English/Energy-Market/Electricity/National-Grid/Transmission-tariff/">http://www.svk.se/Start/English/Energy-Market/Electricity/National-Grid/Transmission-tariff/</a>
Turkey	–	–	Yes	<a href="http://www.tedas.gov.tr/en/Pages/FAQ.aspx">http://www.tedas.gov.tr/en/Pages/FAQ.aspx</a>
UK	Yes	Yes	Yes	<a href="http://en.wikipedia.org/wiki/National_Grid_%28Great_Britain%29#Demand_charges">http://en.wikipedia.org/wiki/National_Grid_%28Great_Britain%29#Demand_charges</a>
Saudi Arabia	–	Yes	Yes	<a href="http://www.se.com.sa/SEC/English/Menu/Customers/Consumption+bills/TarifAndTax.htm">http://www.se.com.sa/SEC/English/Menu/Customers/Consumption+bills/TarifAndTax.htm</a>
Africa	Yes	–	Yes	<a href="http://www.eskom.co.za/">http://www.eskom.co.za/</a>
Australia	–	–	Yes	<a href="http://www.energymadeeasy.gov.au/how-read-your-electricity-bill-page-2-0">http://www.energymadeeasy.gov.au/how-read-your-electricity-bill-page-2-0</a>
Hong Kong	Yes	–	Yes	<a href="https://www.clponline.com.hk/MyBusiness/CustomerService/TariffOverview/BulkTariff/Pages/Default.aspx">https://www.clponline.com.hk/MyBusiness/CustomerService/TariffOverview/BulkTariff/Pages/Default.aspx</a>
India	Yes	–	Yes	<a href="https://cp.tatapower.com/customer_care/apply-for-power-supply/pdf/schedule.pdf">https://cp.tatapower.com/customer_care/apply-for-power-supply/pdf/schedule.pdf</a>
Japan	Yes	Yes	Yes	<a href="http://www.chuden.co.jp/english/price/epri_mechanism/emec_electriccharges/eele_calculation/index.html">http://www.chuden.co.jp/english/price/epri_mechanism/emec_electriccharges/eele_calculation/index.html</a>
Malaysia	Yes	–	Yes	<a href="http://www.tnb.com.my/business/for-commercial/pricing-tariff.html">http://www.tnb.com.my/business/for-commercial/pricing-tariff.html</a>

**(APPENDIX A Continued.)**

	<b>MD (\$/kW)</b>	<b>RTP (\$/kWh)</b>	<b>TOU (\$/kWh)</b>	<b>References</b>
New Zealand	–	Yes	Yes	<a href="http://www.oriongroup.co.nz/downloads/PricingGuide_2010.pdf">http://www.oriongroup.co.nz/downloads/PricingGuide_2010.pdf</a>
Pakistan	Yes	Yes	Yes	<a href="http://www.lesco.gov.pk/CustomerServices/3000063.asp">http://www.lesco.gov.pk/CustomerServices/3000063.asp</a>
Philippines	Yes	–	Yes	<a href="http://www.vecocom.ph/page.html?main=clients&amp;sub1=your%20bill&amp;sub2=Oct%202013%20Ave%20Rate">http://www.vecocom.ph/page.html?main=clients&amp;sub1=your%20bill&amp;sub2=Oct%202013%20Ave%20Rate</a>
Singapore	–	–	Yes	<a href="http://www.singaporepower.com.sg/">http://www.singaporepower.com.sg/</a>
South Korea	Yes	–	Yes	<a href="http://cyber.kepco.co.kr/kepco/EN/F/htmlView/ENFBHP00103.do?menuCd=EN060201">http://cyber.kepco.co.kr/kepco/EN/F/htmlView/ENFBHP00103.do?menuCd=EN060201</a>
Taiwan	Yes	–	Yes	<a href="http://www.taipower.com.tw/e_content/content/household/household01-1.aspx?sid=7">http://www.taipower.com.tw/e_content/content/household/household01-1.aspx?sid=7</a>
Thailand	–	–	Yes	<a href="http://www.eria.org/events/Power%20Tariff%20Structure%20in%20Thailand.pdf">http://www.eria.org/events/Power%20Tariff%20Structure%20in%20Thailand.pdf</a>

## APPENDIX B: SUMMARY OF THE SIZE OF BESS AND ITS CONTROLLER FROM VARIOUS LITERATURES

Source	Experiment or Simulation (No. of Results <sup>a</sup> )	$P_{Load}^{Max(Max)}$	$P_{PCU}$	$E_{ESC}$	$P_{Load}^{Max}{}^b$	$P_{Reduc.}^{Max}{}^c$	Controller <sup>d</sup>
		(kW)	(kW)	(kWh)	(kW)	(kW)	
This dissertation	Experiment (62 days)	104.33	18	64	79.96	10.02	Active Control with Real-Time Threshold Adjuster, Day-Ahead and Next-Minute Load Forecasting
Chua (2016)	Experiment (14 days)	100.5	15	64	100.5	12.1	Fuzzy Control with Adaptive-Threshold Adjustment based on the BESS Battery's State-of-Charge
Reihani et al. (2016a)	Experiment (1 day)	1,700	1,000	1,100	1,700	400	Real-Time Control with Peak Smoothing Scheme and Series-Parallel Load Forecasting
Koller et al. (2015)	Experiment (4 days)	115	1,000	580	113	30	Model Predictive Control with Mixed-Integer Programming and Online Neural Network Load Forecasting
Bao et al. (2012)	Simulation (1 day)	44,000	5,000	20,000	44,000	4,000	Model Predictive Control with Dynamic Programming and Short-Term Load Forecasting

(APPENDIX B Continued.)

Source	Experiment or Simulation (No. of Results <sup>a</sup> )	$P_{Load}^{Max(Max)}$	$P_{PCU}$	$E_{ESC}$	$P_{Load}^{Max}{}^b$	$P_{Reduc.}^{Max}{}^c$	Controller <sup>d</sup>
		(kW)	(kW)	(kWh)	(kW)	(kW)	
Lu et al. (2014)	Simulation (15 days)	59,000	4,000	16,000	59,000	4,000	Mixed-Integer Programming Control with Day-Ahead Rolling Load Prediction
Rowe et al. (2014b)	Simulation (40 profiles)	- <sup>e</sup>	- <sup>e</sup>	- <sup>e</sup>	25	7.1	Stochastic Receding Horizon Control with Day-Ahead Load Characteristic Forecasting
Bennett et al. (2015)	Simulation (3 days)	181	40	100	174.5	28.5	Real-Time Operator Control with Day-Ahead Neural Network Load Forecasting

- The total number of peak reduction results recorded or listed in the literature.
- The peak load ( $P_{Load}^{Max}$ ) of the highest peak reduction ( $P_{Reduc.}^{Max}$ ) recorded in the literature.
- The highest peak reduction ( $P_{Reduc.}^{Max}$ ) demonstrated in the literature on a particular day.
- The controller in which demonstrated the highest peak reduction results in the literature.
- The size of the battery-based energy storage system is not specified in the literature.

**APPENDIX C: THE EXPERIMENTAL AND SIMULATION RESULTS  
OF A MONTH OF PEAK REDUCTIONS WITH THE  
FUNDAMENTAL CONTROL STRATEGY**

Day	$P_{Load}^{Act(max)}$	$P_{Reduction}^{Act}$	$P_{Reduction}^{Sim}$	$R$	$A$	$S_{MD}$	$S_{TR}$	$\sum S_{Total}$
	(kW)	(kW)	(kW)	(%)	(%)	(RM)	(RM)	(RM)
1 <sup>d</sup>	73.30	7.42	10.10	10.12	73.44	-	0.60	0.60
2	65.08	1.90	5.56	2.92	34.21	-	0.39	0.99
3	70.92	7.54	10.15	10.63	74.29	-	1.49	2.48
4 <sup>a</sup>	50.67	0.00	0.00	0.00	100.00	-	0.10	2.59
5 <sup>a</sup>	60.02	0.00	0.00	0.00	100.00	-	0.10	2.69
6 <sup>c</sup>	85.33	1.29	7.69	1.52	16.84	-	1.99	4.67
7	81.57	3.69	6.43	4.52	57.41	-	1.62	6.30
8 <sup>c</sup>	85.89	0.00	9.91	0.00	0.00	-	1.73	8.03
9 <sup>c</sup>	78.65	0.00	4.86	0.00	0.00	-	1.87	9.90
10	74.91	3.82	9.71	5.10	39.39	-	0.36	10.26
11 <sup>a</sup>	54.38	0.00	0.00	0.00	100.00	-	0.16	10.42
12 <sup>a</sup>	56.50	0.00	0.00	0.00	100.00	-	0.16	10.59
13 <sup>b</sup>	61.82	0.00	0.00	0.00	100.00	-	0.16	10.75
14 <sup>c</sup>	80.36	0.00	3.30	0.00	0.00	-	1.94	12.69
15 <sup>c</sup>	80.32	0.00	3.26	0.00	0.00	-	2.24	14.93
16 <sup>c</sup>	72.21	0.00	12.21	0.00	0.00	-	1.29	16.22
17 <sup>d</sup>	84.45	9.28	10.96	10.98	84.60	-	2.15	18.37
18 <sup>a</sup>	49.70	0.00	0.00	0.00	100.00	-	0.27	18.64
19 <sup>a</sup>	61.05	0.00	0.00	0.00	100.00	-	0.19	18.83
20	78.67	1.99	6.76	2.53	29.38	-	0.69	19.51
21	80.32	3.84	9.21	4.78	41.73	-	1.26	20.78
22 <sup>c</sup>	79.42	1.91	8.64	2.40	22.06	-	1.27	22.04
23	81.49	5.29	9.50	6.49	55.70	-	1.56	23.60

(APPENDIX C Continued.)

Day	$P_{Load}^{Act(max)}$	$P_{Reduction}^{Act}$	$P_{Reduction}^{Sim}$	$R$	$A$	$S_{MD}$	$S_{TR}$	$\sum S_{Total}$
	(kW)	(kW)	(kW)	(%)	(%)	(RM)	(RM)	(RM)
24	83.97	5.73	8.93	6.82	64.16	-	1.55	25.15
25 <sup>a</sup>	47.83	0.00	0.00	0.00	100.00	-	0.00	25.15
26 <sup>a</sup>	56.73	0.00	0.00	0.00	100.00	-	0.00	25.15
27 <sup>b</sup>	69.10	0.00	1.76	0.00	0.00	-	0.62	25.77
28	76.18	1.12	6.44	1.47	17.34	-	1.24	27.01
29	81.49	5.29	11.06	6.49	47.84	-	1.56	28.57
30	77.47	0.90	6.89	1.16	13.02	-	2.04	30.61
31 <sup>d</sup>	79.86	6.34	8.93	7.93	70.96	0.00	1.84	32.45

- a. These are the days on the weekends in which peak reductions were not performed because the peak is lower than the threshold.
- b. This is a weekday in which peak reductions were not performed because the peak is lower than the threshold.
- c. These are the days in which the control strategy failed to reduce the peak demand due to the depletion of the battery.
- d. These are the days in which the control strategy managed to reduce the peak demand in spite of the depletion of the battery.

**APPENDIX D: THE EXPERIMENTAL AND SIMULATION RESULTS  
OF A MONTH OF PEAK REDUCTIONS WITH THE ACTIVE  
CONTROL STRATEGY**

Day	$P_{Load}^{Act(max)}$	$P_{Reduc.}^{Act}$	$P_{Reduc.}^{Sim}$	MAPE	R	A	$S_{MD}$	$S_{TR}$	$\sum S_{Tot.}$
	(kW)	(kW)	(kW)	(%)	(%)	(%)	(RM)	(RM)	(RM)
1	75.20	4.38	6.37	4.49	5.83	68.82	-	1.43	1.43
2	83.65	5.65	10.70	2.69	6.76	52.82	-	1.06	2.48
3	77.31	7.15	9.10	8.13	9.25	78.57	-	1.68	4.17
4	73.54	3.88	5.33	2.39	5.27	72.75	-	0.86	5.03
5 <sup>a</sup>	46.23	0.00	0.00	1.50	0.00	100.00	-	0.12	5.15
6 <sup>a</sup>	60.01	0.00	0.00	1.78	0.00	100.00	-	0.13	5.28
7	86.66	8.72	13.79	3.22	10.06	63.24	-	1.01	6.29
8	79.50	8.19	9.93	3.42	10.30	82.47	-	1.26	7.55
9	84.42	8.25	12.44	3.09	9.77	66.33	-	1.59	9.14
10	79.96	10.02	10.21	2.29	12.53	98.12	-	1.31	10.45
11 <sup>b</sup>	79.24	8.76	10.43	2.49	11.06	82.99	-	1.71	12.16
12 <sup>a</sup>	42.17	0.00	0.00	1.36	0.00	100.00	-	0.00	12.16
13 <sup>a</sup>	53.99	0.00	0.00	0.00	0.00	100.00	-	0.00	12.16
14 <sup>b</sup>	82.49	8.65	11.25	3.30	10.49	76.87	-	1.45	13.60
15	77.55	3.95	8.02	2.51	5.09	49.22	-	1.41	15.01
16	83.05	7.93	11.12	2.70	9.55	71.32	-	1.54	16.55
17 <sup>b</sup>	84.67	5.32	9.43	2.86	6.29	56.46	-	2.04	18.59
18	81.85	5.46	11.59	2.44	6.67	47.10	-	1.25	19.84
19 <sup>a</sup>	44.98	0.00	0.00	1.55	0.00	100.00	-	0.00	19.84
20 <sup>a</sup>	63.19	0.00	0.00	2.23	0.00	100.00	-	0.00	19.84
21	88.64	7.41	11.96	2.85	8.35	61.90	-	0.90	20.74
22	79.86	6.34	8.93	3.39	7.94	71.01	-	1.28	22.02
23 <sup>b</sup>	82.08	9.34	10.47	4.27	11.38	89.22	-	1.51	23.53

(APPENDIX D Continued.)

Day	$P_{Load}^{Act(max)}$	$P_{Reduc.}^{Act}$	$P_{Reduc.}^{Sim}$	MAPE	R	A	$S_{MD}$	$S_{TR}$	$\sum S_{Tot.}$
	(kW)	(kW)	(kW)	(%)	(%)	(%)	(RM)	(RM)	(RM)
24 <sup>b</sup>	77.38	3.64	8.37	2.54	4.71	43.54	-	1.70	25.23
25	81.10	8.30	11.37	22.54 <sup>c</sup>	10.24	73.02	-	1.08	26.31
26 <sup>a</sup>	45.53	0.00	0.00	23.29 <sup>c</sup>	0.00	100.00	-	0.15	26.46
27 <sup>a</sup>	51.62	0.00	0.00	7.82	0.00	100.00	-	0.13	26.60
28	82.11	6.10	10.28	2.58	7.43	59.36	-	0.45	27.04
29	83.36	7.40	11.44	2.44	8.88	64.71	-	1.09	28.13
30 <sup>b</sup>	88.26	7.20	10.09	2.08	8.16	71.38	-	1.71	29.84
31	91.13	7.58	13.85	0.66 <sup>c</sup>	8.32	54.74	341.86	1.04	372.74

- a. These are the days on the weekends in which peak reductions were not performed because the peak is lower than the threshold.
- b. These are the days in which the control strategy managed to reduce the peak demand in spite of the depletion of the battery.
- c. These are the days in which an unexpected error has occurred in the load forecast. The experiment results on these days are however not affected, because the unexpected error is at later of the day, at the non-peak period.